THE HONG KONG
POLYTECHNIC UNIVERSITY
香港理工大學
Pao Yue-kong Library
包玉剛圖書館

Copyright Undertaking

This thesis is protected by copyright, with all rights reserved.

By reading and using the thesis, the reader understands and agrees to the following terms:

1. The reader will abide by the rules and legal ordinances governing copyright regarding the use of the thesis.
2. The reader will use the thesis for the purpose of research or private study only and not for distribution or further reproduction or any other purpose.
3. The reader agrees to indemnify and hold the University harmless from and against any loss, damage, cost, liability or expenses arising from copyright infringement or unauthorized usage.

IMPORTANT

If you have reasons to believe that any materials in this thesis are deemed not suitable to be distributed in this form, or a copyright owner having difficulty with the material being included in our database, please contact lbsys@polyu.edu.hk providing details. The Library will look into your claim and consider taking remedial action upon receipt of the written requests.

Pao Yue-kong Library, The Hong Kong Polytechnic University, Hung Hom, Kowloon, Hong Kong

http://www.lib.polyu.edu.hk

STRUCTURAL BEHAVIOUR

OF

SHEAR CONNECTIONS OF LARGE RESISTANCES

FOR

SIMPLE ON-SITE ASSEMBLY

OF

PREFABRICATED COMPOSITE BEAMS

DING YAN

PhD

The Hong Kong Polytechnic University

2025

The Hong Kong Polytechnic University

Department of Civil and Environmental Engineering

Structural Behaviour of Shear Connections of Large Resistances for Simple On-Site Assembly of Prefabricated Composite Beams

DING YAN

A thesis submitted in partial fulfilment of the requirements
for the degree of Doctor of Philosophy

August 2025

CERTIFICATE OF ORIGINALITY

I hereby declare that this thesis is my own work and that, to the best of my knowledge and belief, it reproduces no material previously published or written, nor material that has been accepted for the award of any other degree or diploma, except where due acknowledgement has been made in the text.

_____(Signed)

DING YAN (Name of student)

ABSTRACT

Since composite structures are highly effective in providing high stiffnesses and resistances under large applied loads, they are extensively used in high-rise buildings and long-span bridges. In composite beams, the performance of shear connectors is critical for an effective load-transfer between concrete slabs and steel members. Although many researchers have examined the deformation characteristics of various shear connectors with different configurations and concrete grades, there are only a limited number of investigations into bolted shear connections in precast concrete slabs. Among these investigations, many shear connections are shown to have low shear resistances and stiffnesses despite of their good ductility, and multiple use of these bolted shear connections is often needed in composite beams of road bridges. Hence, it is highly desirable to investigate and quantify the behaviour of high-strength bolted shear connections with high performance concrete in prefabricated composite beams for simple on-site assembly of road bridges.

This thesis presents a comprehensive investigation into the structural behaviour of a newly proposed shear connection incorporating a steel block and a pair of high-strength large-diameter steel bolts in conjunction with steel fibre reinforced concrete blocks. Both experimental and numerical investigations have been conducted to the proposed shear connection, and it is demonstrated that **the proposed shear connection acts effectively as a twin shear connection due to the provision of a steel connector fully embedded into an infilled concrete block, and three typical modes of failure are identified: a) concrete failure of the concrete block; b) shear failure of the bolts; and c) concrete failure of the precast concrete slabs.** The present study takes the following forms of investigations:

i) An investigation into connections with six types of shear connectors using **single-sided push-**

out tests was conducted to examine their structural performance in terms of resistance, stiffness, and ductility, and a suitable configuration of the proposed connection was identified, in which a steel block was pre-welded onto the beam flange to increase the initial stiffness, while steel fibres were added into the infilled concrete to improve their tensile strengths.

ii) An investigation into the proposed shear connection using large-scale **standard push-out tests and non-linear numerical simulations** was also conducted to examine typical failure modes, deformation characteristics as well as the internal force distributions within the shear connections. After extensive calibrations against test data of the present study and also reported in the literature, various damage parameters were incorporated to simulate concrete crushing and cracking.

iii) **A systematic parametric study** was then performed to identify load transfer mechanisms, and to formulate effective design rules for shear resistances and load-slippage curves of the connections for applications in prefabricated composite beams.

Key findings are summarised as follows:

a) Effective bolted shear connection

Based on data analyses and interpretation on the deformation characteristics of the shear connections described in this investigation, the use of a 30 mm thick steel block together with a pair of specially designed high strength bolts, each with a diameter of 30 mm, in the proposed shear connection is shown to have **a large stiffness (≥ 1,500 kN/mm), a large resistance (≥ 1,000 kN), and a large ductility (≥ 6 mm)**. Hence, the proposed shear connection is demonstrated to meet all the requirements for prefabricated composite beams in road bridges. With a proper design, only two different failure modes are identified in these tests, namely concrete failure (Mode CF), and shear fracture of bolts (Mode SFB).

b) Effects of various components

The results showed that the shear resistance of the proposed shear connection depends primarily on **the bearing area of the steel block**, and also **the pull-out resistances offered by the pair of steel bolts**. Increasing the thickness of the steel block from 30 to 50 mm offers only minimal benefits to the overall connection behaviour, and a reduction in its resistance at large deformations is also evident. As the concrete block acts as **a "concrete shear connector"**, it should be made of high performance concrete reinforced with steel fibre, and **the dimensions of the concrete block together with a properly designed arrangement of steel rebars** are shown to have considerable effects on the structural behaviour of the proposed shear connections in both ultimate and serviceability limit states.

c) Load transfer mechanisms

The non-linear finite element models are able to predict the structural responses of the proposed shear connections, and **the distributions of internal forces among the steel block, the pair of the steel bolts, the infilled concrete block, and also the precast concrete slabs are carefully established.** Ductile damages in the steel bolts and local damage in the concrete are readily quantified through data interpretation of the finite element results.

d) Design recommendations

Design rules for the shear resistances of the proposed bolted shear connections are proposed after calibration against both test and numerical data, and **the shear resistances of individual components** of the connections are readily predicted to a high level of accuracy. **Simplified load-slippage curves** of the connections are also proposed which are readily adopted for numerical modelling to simulate the structural behaviour of the composite beams.

Keywords: prefabricated composite beams; simple on-site assembly; twin shear connection; large-scale standard push out tests; non-linear numerical simulations; internal force distributions, shear resistances and load-slippage curves

PUBLICATIONS

Journal papers

Ding Y., Chung K.F., Tong C.C., Wang X.D., Zhou X.H., & Elghazouli A.Y. (2024). Behaviour of large-diameter high-strength bolted shear connections for prefabricated composite beams. Engineering Structures, 322, 119002.

Ding Y., Wang X.D., Shen M.H., Chung K.F., Zhou X.H., & Elghazouli A.Y. (2024). Deformation characteristics of ductile large resistance shear connections for practical composite beams. Engineering Structures, 320: 118838.

Ding Y., Chung K.F., Wang X.D., Shen M.H., Zhou X.H., & Elghazouli A.Y. Numerical simulations on high strength bolted shear connections for simple on-site assembly of composite beams. (under preparation)

Ding Y., Chung K.F., Wang X.D., Shen M.H., Zhou X.H., & Elghazouli A.Y. An investigation into high strength bolted shear connections with various fibre content of concrete block. (under preparation)

Ding Y., Chung K.F., Wang X.D., Zhou X.H., & Elghazouli A.Y. Structural behaviour of various types of shear connections with high resistances in prefabricated composite beams. (under preparation)

Conference papers

Ding Y. & Chung K.F. (2023). Standard push out tests on large diameter bolted shear connections in prefabricated composite beams. Proceedings of the 13th Pacific Structural Steel Conference, Chengdu, pp248-254.

Ding Y., Chung K.F., Tong C.C., & Wang X.D. (2023). Load-slippage characteristics of bolted and welded shear connections in prefabricated composite beams. Proceedings of Eleventh International Conference on Advances in Steel Structures, Malaysia, pp1349-1359.

Ding Y., Wang X.D., Shen M.H., & Chung K.F. (2024). Development of large resistance shear connections for simple on-site assembly of prefabricated composite beams. Proceedings of Thirteenth International Conference on Advances in Steel-Concrete Composite Structures, Hong Kong, pp535-538.

Tong C.C., **Ding Y.**, Chung K.F., & Wang X.D. (2024). Single-sided push out tests on high-strength bolted shear connections in prefabricated composite beams. Proceedings of Thirteenth International Conference on Advances in Steel-Concrete Composite Structures, Hong Kong, pp444-447.

ACKNOWLEDGEMENT

I would like to express my sincere gratitude to my supervisor, Prof. K.F. Chung, for his knowledge, expertise, patience, kindness, and precious guidance. Prof. Chung has provided valuable and professional instructions for my research project and greatly improved my presentation skills. His profound knowledge and expertise have consistently offered me constructive feedback and insightful guidance, which have been instrumental throughout my doctoral journey.

I would like to thank Dr. H.C. Ho, Dr. M.F. Hui, and Dr. Y.F. Hu for their encouragement and support in my academic research. I would also like to express my sincere thanks to Dr. X.D. Wang from Chongqing University for his valuable advice and meaningful suggestions on both the experimental and the numerical investigations. My heartfelt appreciation goes to Dr. P.F. Men for his generous help in both scientific research and laboratory experiments.

Special thanks to the laboratory technicians Mr. K.H. Wong, Mr. M.C. NG, and Mr. K.L. Cheung for their dedicated efforts and assistance in the experimental work. I am truly grateful to the Hong Kong Polytechnic University and Chinese National Engineering Research Centre for Steel Construction (Hong Kong Branch) for their financial support in my research. I also appreciate the facilities and resources provided by the university, the CNERC, and the Department of Civil and Environmental Engineering (CEE).

Last but not least, I would like to express my deep appreciation to my parents, my husband, and my friends for their unwavering support, understanding, and care. Their encouragement has been a constant source of strength and motivation, enabling me to complete my studies successfully.

CONTENTS

CERTIFICATE OF ORIGINALITY I

ABSTRACT III

PUBLICATIONS VII

ACKNOWLEDGEMENT IX

CONTENTS X

LIST OF FIGURES XVI

LIST OF TABLES XXV

LIST OF NOTATIONS XXVII

CHAPTER 1 INTRODUCTION 1

1.1 Shear connections in composite beams 1

1.2 Simple on-site assembly of composite beams 3

1.3 Structural requirements for shear connections 5

1.4 Objectives and scope of work 5

1.5 Overview of the thesis 8

CHAPTER 2 LITERATURE REVIEW 12

2.1 Introduction 12

2.2 Experimental investigation 13

2.2.1 Standard push-out tests on headed shear studs 13

2.2.2 Standard push-out tests on bolted shear connectors 20

2.2.3 Standard push-out tests on the other shear connectors 26

2.2.4 Beam tests 30

2.2.5 Summary 31

2.3 Numerical simulation 34

2.3.1 Numerical simulation on headed shear studs 34

2.3.2 Numerical simulation on bolted shear connectors 38

2.3.4 Summary 41

2.4 Design rule 44
2.4.1 Codified rules for headed shear studs 44
2.4.2 Codified rules for channel shear connectors 46
2.4.3 Design rules for block connectors 47
2.4.4 Design rules suggested in literature 47
2.4.5 Summary 48
2.5 Conclusions 49
CHAPTER 3 EXPERIMENTAL INVESTIGATIONS USING SINGLE-SIDED PUSH-OUT TESTS 51
3.1 Introduction 51
3.2 Experimental assessments 52
3.2.1 Test programme 52
3.2.2 Specimen preparation 56
3.2.3 Test setup and loading procedures 58
3.3 Test results 60
3.3.1 Material tests 60
3.3.2 Results of Tests A-C1 63
3.3.3 Results of Tests A-C0 67
3.3.4 Results of Tests B-C1-p 70
3.3.5 Results of Tests C-C1-p 71
3.3.6 Results of Tests SC, BC, and PC 72
3.4 Comparison of deformation characteristics 77
3.4.1 Effect of Connector type 77
3.4.2 Effect of fibre content 78
3.4.3 Effect of bolt diameter 80
3.5 Design method 81
3.5.1 Shear connections with large diameter high strength bolts 81
3.5.2 Shear connections with welded shear connectors 84
3.6 Conclusions 86

CHAPTER 4 EXPERIMENTAL INVESTIGATIONS USING STANDARD PUSH-OUT TESTS 89
4.1 Introduction 89
4.2 Test programme 90
4.3 Preparation of test specimens 94
4.4 Test setup and loading procedures 96
4.4.1 Test setup and instrumentation 96
4.4.2 Loading procedures 97
4.5 Material tests 98
4.5.1 Steel material test 98
4.5.2 Concrete material test 100
4.6 Results of the tests with Type A connections 102
4.6.1 Results of Test A-1-W 105
4.6.2 Results of Test A-1-N 108
4.6.3 Results of Test A-2-W 111
4.6.4 Results of Tests A-2-N 114
4.6.5 Results of Test A-3-W 117
4.7 Results of the tests with Type B connections 120
4.7.1 Results of Test B-1-W 122
4.7.2 Results of Test B-1-N 125
4.7.2 Results of Test B-3-W 128
4.8 Results of the tests with Type C connections 131
4.8.1 Results of Test C-0-W 132
4.9 Results of the tests with Type D connections 135
4.9.1 Results of Test D-0-W 136
4.10 Conclusions 139
CHAPTER 5 ANALYSIS OF THE RESULTS OF STANDARD PUSH-OUT TESTS 142
5.1 Introduction 142
5.2 Normalized shear resistances 143
5.3 Simplified load-slippage curves 144

5.4 Comparative deformation characteristics 149
5.4.1 Effect of connection configuration 150
5.4.2 Effect of steel block thickness 152
5.4.3 Effect of concrete block size 153
5.4.4 Effect of bolt diameter 155
5.4.5 Effect of strength of concrete block 156
5.5 Comparison with single-sided push-out tests 158
5.5.1 Tests with Type A connections 159
5.5.2 Tests with Type B connectors 159
5.6 Comparison with the tests reported in the literature 160
5.6.1 Comparison with the tests on stud / bolted shear connectors 160
5.6.2 Comparison with the tests on block shear connectors 162
5.6.3 Comparison with the tests on perfobond rib shear connectors 165
5.7 Design approach 167
5.8 Applicability 171
5.9 Conclusions 172

CHAPTER 6 NUMERICAL SIMULATIONS OF STANDARD PUSH-OUT TESTS 174
6.1 Introduction 174
6.2 Static analysis of the shear connections 175
6.3 Modelling procedures 176
6.3.1 Overall geometry 176
6.3.2 Element types 177
6.3.3 Boundary conditions and interactions 177
6.3.4 Material models for steel 179
6.3.5 Material models for concrete 181
6.3.6 Mesh convergence 184
6.4 Simulation results of Types A and B connections 186
6.4.1 Finite element modelling of Types A and B connections 186
6.4.2 Calibration against test results 188
6.4.3 Distributions of internal forces and concrete bearing forces 192

6.5 Simulation results of Type C connection 196
6.5.1 Finite element modelling of Type C connection 197
6.5.2 Calibration against test results 198
6.5.3 Distributions of internal forces and concrete bearing forces 200
6.6 Simulation results of Type D connection 201
6.6.1 Finite element modelling of Type D connection 202
6.6.2 Calibration against test results 202
6.6.3 Distributions of internal forces and concrete bearing forces 204
6.7 Conclusions 206
CHAPTER 7 PARAMETRIC STUDY AND DESIGN RULES 209
7.1 Introduction 209
7.2 Parametric studies on Connection RBN 210
7.2.1 Effect of bolt diameter 211
7.2.2 Effect of steel block thickness 215
7.2.3 Effect of concrete block width 218
7.2.4 Effect of concrete block strength 220
7.2.5 Effect of precast concrete slab strength 223
7.2.6 Effect of fibre content in concrete block 225
7.2.7 Effect of longitudinal spacing of shear connections 227
7.2.8 Key findings of parametric studies 229
7.3 Parametric studies on Connection R 232
7.3.1 Effect of bolt diameter 232
7.3.2 Effect of bolt strength 235
7.3.3 Effect of concrete block strength 237
7.3.4 Effect of concrete slab strength 239
7.3.5 Key findings of parametric studies 241
7.4 Load transfer mechanisms 243
7.5 Development of design method 245
7.5.1 Shear resistances 245
7.5.2 A work example for the shear resistance of a shear connection 249

7.5.3 Simplified load-slippage curves 251
7.6 Calibration of the simplified load-slippage curves 254
7.6.1 Brief introduction of the practical beam tests 255
7.6.2 Development of numerical models 258
7.6.3 Assessment of the simulation results 260
7.7 Conclusions and design recommendations 266
CHAPTER 8 CONCLUSIONS AND FUTURE WORK 269
8.1 Introduction 269
8.2 Experimental investigations 269
8.3 Numerical simulations 272
8.4 Design recommendations 276
8.5 Significance of the present study 277
8.6 Practical implications and limitations 279
8.7 Future work 280
REFERENCES 283

LIST OF FIGURES

Fig. 1.1 Various types of shear connections 2

Fig. 1.2 Prefabricated composite beams 4

Fig. 1.3 On-site assembly of bolted shear connections for composite beams 5

Fig. 2.1 Various types of shear connectors (Ding *et al.*, 2024) 13

Fig. 2.2 Load-transfer mechanisms within stud shear connections (Shen *et al*., 2023) 15

Fig. 2.3 Load-slippage curves of large diameter headed studs in HPC (Wang *et al.*, 2018) 20

Fig. 2.4 Comparison of load-slippage curves of headed studs and bolts (Pavlović *et al*., 2013) 21

Fig. 2.5 Details of the LNSC (He *et al.*, 2022) 23

Fig. 2.6 Detailed configuration of SYDBCs (Luo *et al.*, 2022) 24

Fig. 2.7 Tests on HSFGB shear connectors (Zhang *et al.*, 2019; 2020) 26

Fig. 2.8 Modelling of headed studs by Ellobody *et al.* (2006) 35

Fig. 2.9 Comparison of the measured and the simulated results (Nguyen *et al*., 2009) 36

Fig. 2.10 Comparison of the plastic strain contour (Luo *et al.*, 2016) 37

Fig. 2.11 Numerical simulations on headed studs and bolts (Pavlović *et al*., 2013) 39

Fig. 2.12 Numerical simulations on HSFGB (Ataei *et al*., 2021) 40

Fig. 2.13 Comparison of the simulated and the test results of HSFGB shear connectors 41

Fig. 2.14 Schematic diagram of a block connector (EC4, 1992) 47

Fig. 3.1 Arrangements of the proposed shear connectors 54

Fig. 3.2 Concrete and raw materials 55

Fig. 3.3 Detailed dimensions of the test specimens 56

Fig. 3.4 Fabrication procedures of test specimens 57

Fig. 3.5 Dimensions of steel coupons 58
Fig. 3.6 Material tests for concrete 58
Fig. 3.7 Test setup and instrumentation 59
Fig. 3.8 Concrete failure in Type A connections with concrete C100 and various fibre content 64
Fig. 3.9 Key results of Tests A-C1-p 65
Fig. 3.10 Key results of Tests A-C1-q 66
Fig. 3.11 Key results of Tests A-C1-r 66
Fig. 3.12 Key results of Tests A-C1-s 66
Fig. 3.13 Concrete failure in Type A connections with concrete C50 and various fibre content 67
Fig. 3.14 Key results of Tests A-C0-p 69
Fig. 3.15 Key results of Tests A-C0-q 69
Fig. 3.16 Key results of Tests A-C0-r 70
Fig. 3.17 Key results of Tests A-C0-s 70
Fig. 3.18 Concrete failure in connections with 24 mm diameter bolts 71
Fig. 3.19 Key results of Tests B-C1-p 71
Fig. 3.20 Shear fracture of steel bolts in connection with Connector R 72
Fig. 3.21 Results of Tests C-C1 72
Fig. 3.22 Typical failure modes in connections with Connectors SC, BC and PC 73
Fig. 3.23 Results of Tests SC 74
Fig. 3.24 Results of Tests BC 75
Fig. 3.25 Results of Tests PC 76
Fig. 3.26 Effect of connector type 77

Fig. 3.27 Effect of fibre content in shear connections with C100 concrete blocks 79
Fig. 3.28 Effect of fibre content in shear connections with C50 concrete blocks 80
Fig. 3.29 Effect of bolt diameter 81
Fig. 4.1 Arrangements of the proposed shear connectors 92
Fig. 4.2 General views on various types of shear connectors (before concreting) 93
Fig. 4.3 Detailed dimensions of test specimens 93
Fig. 4.4 Fabrication procedures of test specimens 95
Fig. 4.5 Dimensions of steel coupons 95
Fig. 4.6 Test setup and instrumentation 97
Fig. 4.7 Schematic presentation of loading procedures 98
Fig. 4.8 Material tests for steel 99
Fig. 4.9 Material tests for concrete 101
Fig. 4.10 Mode CF in tests with Type A connections 104
Fig. 4.11 Results of Tests A-1-W 105
Fig. 4.12 Measured curves of Test A-1-W-a 106
Fig. 4.13 Measured curves of Test A-1-W-b 107
Fig. 4.14 Results of Tests A-1-N 108
Fig. 4.15 Measured curves of Test A-1-N-a 109
Fig. 4.16 Measured curves of Test A-1-N-b 110
Fig. 4.17 Results of Tests A-2-W 111
Fig. 4.18 Measured curves of Test A-2-W-a 112
Fig. 4.19 Measured curves of Test A-2-W-b 113
Fig. 4.20 Results of Tests A-2-N 114
Fig. 4.21 Measured curves of Test A-2-N-a 116

Fig. 4.22 Load-slippage curves of Test A-2-N-b 117
Fig. 4.23 Results of Tests A-3-W 118
Fig. 4.24 Measured curves of Test A-3-W-a 119
Fig. 4.25 Measured curves of Test A-3-W-b 120
Fig. 4.26 Mode CF in tests with Type B connections 121
Fig. 4.27 Results of Tests B-1-W 123
Fig. 4.28 Measured curves of Test B-1-W-a 124
Fig. 4.29 Measured curves of Test B-1-W-b 125
Fig. 4.30 Results of Tests B-1-N 126
Fig. 4.31 Measured curves of Test B-1-N-a 127
Fig. 4.32 Measured curves of Test B-1-N-b 128
Fig. 4.33 Results of Tests B-3-W 129
Fig. 4.34 Measured curves of Test B-3-W-a 130
Fig. 4.35 Measured curves of Test B-3-W-b 131
Fig. 4.36 Mode SFB in tests with Type C connections 132
Fig. 4.37 Results of Tests C-0-W 133
Fig. 4.38 Measured curves of Test C-0-W-a 134
Fig. 4.39 Measured curves of Test C-0-W-b 135
Fig. 4.40 Mode CF in tests with Type D connections 136
Fig. 4.41 Results of Tests D-0-W 137
Fig. 4.42 Measured curves of Test D-0-W-a 138
Fig. 4.43 Measured curves of Test D-0-W-b 139
Fig. 5.1 Normalized load-slippage curves 147
Fig. 5.2 Validation of the simplified load slippage curves (Liu *et al*., 2023) 148

Fig. 5.3 Effect of connection configuration 151
Fig. 5.4 Effect of steel block thickness 153
Fig. 5.5 Effect of concrete block size 155
Fig. 5.6 Effect of bolt diameter 156
Fig. 5.7 Effect of strength of concrete block 158
Fig. 5.8 Comparison with single-sided push-out tests 159
Fig. 5.9 Comparison with stud / bolted shear connections 162
Fig. 5.10 Comparison with block shear connections 165
Fig. 5.11 Comparison with perfobond rib shear connections 167
Fig. 5.12 Schematic diagram of the design method 169
Fig. 6.1 Overall geometry of typical models 176
Fig. 6.2 Element types in three-dimensional finite element model 177
Fig. 6.3 Boundary conditions and interactions 178
Fig. 6.4 Constitutive model for bolt steel 180
Fig. 6.5 Stress-strain curves for concrete 184
Fig. 6.6 Damage models for concrete 184
Fig.6.7 Mesh sizes for the concrete blocks and the shear connectors 185
Fig. 6.8 Results of convergence study 185
Fig. 6.9 Finite element models of typical models with Types A and B connections 187
Fig. 6.10 Concrete failure of the concrete slabs in numerical models with Types A and B connections 189
Fig. 6.11 Failure of bolts in models with Types A and B connections 190
Fig. 6.12 Comparison of measured and simulated load-slippage curves of Types A and B connections 191

Fig. 6.13 Internal forces and moments within the bolts and steel blocks in models with Types A and B connections 195
Fig. 6.14 Concrete bearing forces in models with Types A and B connections 196
Fig. 6.15 Finite element model of Model C-0-W 197
Fig. 6.16 Concrete failure of the concrete blocks in Model C-0-W 199
Fig. 6.17 Failure of bolts in Model C-0-W 199
Fig. 6.18 Comparison of measured and simulated load-slippage curves of Model C-0-W 200
Fig. 6.19 Internal forces and moments within the bolts in Model C-0-W 201
Fig. 6.20 Concrete bearing forces of Model C-0-W 201
Fig. 6.21 Finite element model of Model D-0-W 202
Fig. 6.22 Concrete failure of the concrete slabs in Model D-0-W 203
Fig. 6.23 Comparison of measured and simulated load-slippage curves of Model D-0-W 204
Fig. 6.24 Internal forces and moments within the steel section in Model D-0-W 205
Fig. 6.25 Concrete bearing forces of Model D-0-W 206
Fig. 7.1 Models with Connection RBN and various bolt diameters 213
Fig. 7.2 Load-slippage curves of models with Connection RBN and various bolt diameters 213
Fig. 7.3 Damage in models with Connection RBN and various bolt diameters 214
Fig. 7.4 Internal force distributions in models with Connection RBN and various bolt diameters 214
Fig. 7.5 Models with Connection RBN and various steel block thicknesses 216
Fig. 7.6 Load-slippage curves of models with 217
Connection RBN and various steel block thicknesses 217
Fig. 7.7 Damage in models with Connection RBN and various steel block thicknesses 217
Fig. 7.8 Internal force distributions in models with 217

Connection RBN and various steel block thicknesses 217
Fig. 7.9 Models RBN with various concrete block widths 219
Fig. 7.10 Load-slippage curves of models with 219
Connection RBN and various concrete block widths.....219
Fig. 7.11 Damage in models with Connection RBN and various concrete block widths 220
Fig. 7.12 Internal force distributions in models with 220
Connection RBN and various concrete block widths.....220
Fig. 7.13 Load-slippage curves of models with 222
Connection RBN and various strengths of concrete blocks 222
Fig. 7.14 Damage in models with Connection RBN and various strengths of concrete blocks 222
Fig. 7.15 Internal force distributions in models with 222
Connection RBN and various strengths of concrete blocks 222
Fig. 7.16 Load-slippage curves of those models with.....224
Connection RBN and various strengths of concrete slabs 224
Fig. 7.17 Damage in those models with Connection RBN and various strengths of concrete slabs 224
Fig. 7.18 Internal force distributions in those models with.....224
Connection RBN and various strengths of concrete slabs 224
Fig. 7.19 Load-slippage curves of those models with Connection RBN and various fibre content 226
Fig. 7.20 Damage in models with Connection RBN and various fibre content 226
Fig. 7.21 Internal force distributions in models with Connection RBN and various fibre content 226
Fig. 7.22 Load-slippage curves of those models with.....228

Connection RBN and various longitudinal spacings.....228

Fig. 7.23 Damage in those models with Connection RBN and various longitudinal spacings 228

Fig. 7.24 Internal force distributions in those models with.....229

Connection RBN and various longitudinal spacings.....229

Fig. 7.25 Models with Connection R with various bolt diameters.....233

Fig. 7.26 Load-slippage curves of models with Connection R and various bolt diameters....234

Fig. 7.27 Damage in models with Connection R and various bolt diameters 234

Fig. 7.28 Internal force distributions in models with Connection R and various bolt diameters 234

Fig. 7.29 Load-slippage curves of models with Connection R and various bolt strengths.....236

Fig. 7.30 Damage in models with Connection R and various bolt strengths 236

Fig. 7.31 Internal force distributions in models with Connection R and various bolt strengths 236

Fig. 7.32 Load-slippage curves of models with Connection R and various strengths of concrete blocks.....238

Fig. 7.33 Damage in models with Connection R and various strengths of concrete blocks ...238

Fig. 7.34 Internal force distributions in models with 238

Connection R and various strengths of concrete blocks.....238

Fig. 7.35 Load-slippage curves of models with Connection R and various strengths of precast slabs 240

Fig. 7.36 Damage in models with Connection R and various strengths of precast slabs.....240

Fig. 7.37 Internal force distributions in models with 240

Connection R and various strengths of concrete slabs 240

Fig. 7.38 Load transfer mechanisms of Connections RBN and R 244

Fig. 7.39 Schematic diagram of the design method 247

Fig. 7.40 Evaluation of the proposed design method 249

Fig. 7.41 Comparison of simulated and simplified load-slippage curves 254

Fig. 7.42 Typical dimensions of Beams HSS-PCS 257

Fig. 7.43 Loading and support conditions of Beams HSS-PCS 257

Fig. 7.44 Load-deflection curves of the composite beams 257

Fig. 7.45 Three-dimensional numerical models of the composite beams 258

Fig. 7.46 Boundary conditions and interactions 259

Fig. 7.47 Non-linear behaviour of shear connections 260

Fig. 7.48 Three dimensional plots of “stress and strain” distributions 262

Fig. 7.49 Load-mid-span deflection curves of composite beams 263

Fig. 7.50 Load-slippage curves of shear connections at beam ends and mid-spans 265

Fig. 7.51 Load-deflection curves of shear connections at beam ends and mid-spans 266

Fig. 8.1 Load-slippage curves of connections with various configurations 272

Fig. 8.2 Distributions of internal forces and concrete bearing forces along the height of the shear connectors 274

Fig. 8.3 Load transfer mechanisms within shear connections of Connectors RBN and R 276

LIST OF TABLES

Table 2.1 Key deformation characteristics of various shear connectors 31

Table 2.2 Friction coefficients between various components 43

Table 2.3 The fracture strain and the displacement at failure for the steel connectors 43

Table 2.4 Design rules for shear resistances and load-slippage models of shear connectors 48

Table 3.1 Test programme of single-sided push-out tests 53

Table 3.2 Concrete mix proportion (kg / m^3) 56

Table 3.3 Mechanical properties of the steel 60

Table 3.4 Mechanical properties of the concrete with various fibre content 61

Table 3.5 Key results of single-sided push-out tests 62

Table 3.6 Comparison of test results 77

Table 3.7 Values of γ_{cb} in shear connections with various concrete grades and fibre content 82

Table 3.8 Comparison on measured and design shear resistances of Types A to C connections 83

Table 3.9 Comparison on measured and design shear resistances of Types SC, BC, and PC connections 86

Table 4.1 Test programme of standard push-out tests 92

Table 4.2 Proportional mix of SFRC with a fibre content of 1.5% (kg / m^3) 92

Table 4.3 Mechanical properties of the steel 99

Table 4.4 Measured data of the mechanical properties of concrete 101

Table 4.5 Key results of tests with Type A connections 103

Table 4.6 Measured curves for Tests A-1-W-a and -b 105

Table 4.7 Measured curves for Tests A-1-N-a and -b 108

Table 4.8 Measured curves for Tests A-2-W-a and -b. 111

Table 4.9 Measured curves for Tests A-2-N-a and -b 115
Table 4.10 Measured curves for Tests A-3-W-a and -b 117
Table 4.11 Key results of tests with Type B connections 122
Table 4.12 Measured curves for Tests B-1-W-a and -b. 122
Table 4.13 Measured curves for Tests B-1-N-a and -b. 125
Table 4.14 Measured curves for Tests B-3-W-a and -b. 128
Table 4.15 Key results of tests with Type C connections 132
Table 4.16 Key results of tests with Type D connections 136
Table 5.1 Normalized results of the standard push out tests 144
Table 5.2 Simplified load-slippage curves of the shear connections 149
Table 5.3 Comparison of the test results 150
Table 5.4 Comparison with stud / bolted shear connectors in the literature 162
Table 5.5 Comparison with block shear connectors in the literature 164
Table 5.6 Comparison with perfobond shear connectors in the literature 166
Table 5.7 Calibration of the proposed design method 170
Table 6.1 Plastic parameters in CDP models 183
Table 6.2 Comparison between the measured and the simulated results 192
Table 7.1 Parameters and their values in parametric studies on Connection RBN 211
Table 7.2 Key results of the models with Connection RBN 230
Table 7.3 Parameters and their values in parametric studies on Connection R 232
Table 7.4 Key results of the models with Connection R 242
Table 7.5 Comparison of the design and the measured shear resistances 248
Table 7.6 Test programme of the beam tests 256
Table 7.7 Comparison of the measured and the predicted results 264

LIST OF NOTATIONS

A_s	Cross-sectional area of a stud shear connector
A_t	Cross-sectional area of grout-infilled tube
A_b	Cross-sectional area of a bolt
A_{cl}	Bearing area of the concrete in the vicinity of a connector
A_{cp1}	Projected area of the concrete in the direction of loading
A_{c2}	Bearing area of the concrete in the vicinity of a bolt
A_{cp2}	Projected area of the concrete in the direction of loading
A_r	Cross sectional area of steel rebars
A and B	Parameters for the ascending and the descending segments of the curve
D	Concrete damage variable
E_c	Elastic modulus of concrete
E_s	Elastic modulus of steel
$E_{c,HK}$	Elastic modulus of concrete blocks according to the Hong Kong Concrete Code
E_{cp}	Elastic modulus of precast concrete slabs
E_{ci}	Elastic modulus of concrete blocks
$E_{c,EC2}$	Elastic modulus of concrete blocks according to Eurocode 2
$E_{c,GB}$	Elastic modulus of concrete blocks according to Chinese code GB50010-2010
F_{vi}	Internal shear force
F_{ti}	Internal tensile force
F_{bi}	Concrete bearing force
$F_{v,max}$	Maximum internal shear force
F_{bs}	Concrete bearing force acting onto the steel block
F	Bending load
K	Initial stiffness of a shear connection
K_r	Flexural rigidity of the beam
L_T	Transverse welding length
L_L	Longitudinal welding length

L_s	Longitudinal spacing of shear connections
M_i	Internal moment
M	Moment resistance
Q_m	Shear resistance a shear connection
Q	Applied load at a slippage of s
$Q_{0.5}$	Applied load at a slippage of 0.5 mm
Q_{cbs}	Concrete bearing resistance against the steel block
Q_{cbb}	Concrete bearing resistance against the two bolts
Q_{sfb}	Steel shear resistance against shear fracture of bolts
Q_{Rt}	Measure shear resistance of a shear connection
Q_{Rd}	Design shear resistance of a shear connection
Q_w	Resistance of a weldment
Q_{sfs}	Shear resistance of a steel connector
Q_a	Maximum applied load on shear connections
$Q_{6.0}$	Applied load at a slippage of 6.0 mm
Q_n	Normalized shear resistance of a shear connection
Q_1	Shear resistance of the connections in single-sided push-out tests
Q_{c1}	Concrete bearing resistance against the steel block
Q_{c2}	Concrete bearing resistance against the two bolts
Q_{c3}	Concrete bearing resistance against precast concrete slab
T_b	Thickness of steel block
V_f	Volumetric percentage of steel fibre
W_ε	Strain energy density of damaged material
W_0	Strain energy density of undamaged material
W_c	Width of concrete block
a_w	Throat size of the weld
a, b, and c	Coefficients related to shear resistances of steel block shear connectors
d	Diameter of a stud or bolt
d_{ref}	Reference bolt diameter
d_{tf}	Coefficient for the tensile damage evolution
d_t	Damage variable

d_f	Diameter of steel fibre
e_1	Distance between the steel block and the concrete block
e_2	Distance between the steel bolt and the concrete block
f_c	Compressive strength of concrete
f_{ck}	Characteristic compressive strength of concrete
f_{ck1}	Characteristic compressive strength of the concrete block
f_{ck2}	Characteristic compressive strength of the precast concrete slab
f_t	Tensile strength of concrete
f_y	Yield strength of steel
f_u	Tensile strength of steel
$f_{cu,28}$	Measured cube strengths of concrete blocks at 28 days
$f_{cu,test}$	Measured cube strengths of concrete blocks on the testing days
$f_{cy,test}$	Measured cylinder strengths of concrete blocks on the testing days
f_{ct}	Measured tensile strengths of concrete blocks at 28 days
$f_{cup,28}$	Measured cube strengths of precast concrete slabs at 28 days
$f_{cup,test}$	Measured cube strengths of precast concrete slabs on the testing days
$f_{cyp,test}$	Measured cylinder strengths of precast concrete slabs on the testing days
$f_{cu,150}$	Measured compressive strength of a concrete cube
f_{ub}	Tensile strength of the bolt steel
f_{usc}	Tensile strength of a steel connector
f_{b0} / f_{c0}	Ratio of biaxial to uniaxial compressive strength
f_{tf}	Tensile strength of steel fibre reinforced concrete
$f_{cu,k}$	Cube compressive strength of normal concrete
f_{ci}	Infilled concrete block strength
f_{cp}	Precast concrete slab strength
f_{cu}	Cube compressive strength of the precast concrete slab
$f_{cu,f}$	Cube compressive strength of steel fibre reinforced concrete
f_{cf}	Characteristic cylinder compressive strength of steel fibre reinforced concrete
h_b	Height of a bolted shear connector
h_{slab}	Thickness of a concrete slab

h	Height of the bearing plate
h_s	Height of the steel block
h_{sb}	Height of the steel bolt
h_{sc}	Nominal height of a stud
k	Slope of the descending part of the simplified load-slippage curve
l	Length of the bearing plate
l_a	Length of a channel section
l_s	Length of the steel block
l_{sb}	Length of the steel bolt
l_f	Length of steel fibre
p_w	Yield strength of the weld
s	Slippage of a shear connection
s_u	Ultimate slippage of a shear connection
t	Thickness of a steel plate in a material test
t_f	Thickness of the channel flange
t_w	Thickness of the channel web
$\bar{u}^{pl}$	Equivalent plastic displacement
w	Fibre content in concrete block
Δ	Deflection of a composite beam
Δ_m	Mid-span deflection at peak load
Θ	Limiting value of the proposed relationship through a regression analysis
α_v	Reduction factor for a bolted shear connector
α_{tf}	Shape parameter of the descending part of the tensile stress-strain curve
α and β	Coefficients depending on the connection type
α_b and β	Coefficients for LNSC connector
γ_v	Partial factor
γ_{cs}	Reduction factor considering the influence of fibre content on the concrete bearing resistance against the steel block
γ_{cb}	Reduction factor considering the influence of fibre content on mobilization of the shear resistances of bolts

ε	Flow potential eccentricity of concrete
ε_{us}	Ultimate strain of steel
ε_t	True strain of steel
ε_e	Engineering strain of steel
ε_n^{pl}	Uniaxial plastic strain at the onset of necking
ε_{tf}	Peak tensile strain of steel fibre reinforced concrete
$\bar{\varepsilon}_0^{pl}$	Equivalent plastic strain at the onset of damage
η	Ratio of the measured to the design shear resistance
η_n	Reduction factor for normalizing shear resistance
η_1	Factor considering the effect of concrete block strength
η_2	Factor considering the effect of precast concrete strength
η_b	Factor considering the effective bolt length for bearing against the surrounding concrete
η_3	Factor considering the effect of precast concrete strength on the resistance against the precast concrete slab failure
θ	Stress triaxiality
λ_f	Characteristic parameter for steel fibre content
λ	Proportion of shear force taken by the steel block
σ_{us}	Ultimate stress of steel
σ_t	True stress of steel
σ_e	Engineering stress of steel
σ_m	Hydrostatic stress of steel
σ_{eq}	von Mises equivalent stress
φ	Factor for headed shear studs
ψ	Dilation angle of concrete

CHAPTER 1

INTRODUCTION

1.1 Shear connections in composite beams

Composite members comprise of concrete and steel sections are widely used in bridges and buildings owing to their large load-carrying capacities, high rigidities and excellent inherent fire resistance. In order to mobilize efficiently the high resistance of composite beams, mechanical locking devices, namely shear connectors, are provided to ensure that both the steel sections and the concrete slabs can work together, i.e. the full tensile resistance of the steel section is fully mobilized, and that they are balanced with the compressive resistance of the concrete slab through an effective shear connection (Ernst, 2006). Hence, the structural behaviour of composite beams is always superior to that of steel sections alone. It should also be noted that in-situ concreting is generally labour intensive and time consuming in bridge construction, and hence, any means to minimize site activities are highly desirable.

Three different types of shear connectors, namely, headed shear studs, bolted shear connectors, and perfobond ribs are widely used in bridge construction, as shown in Fig. 1.1. The construction details and the structural behaviour of these shear connectors are outlined as follows:

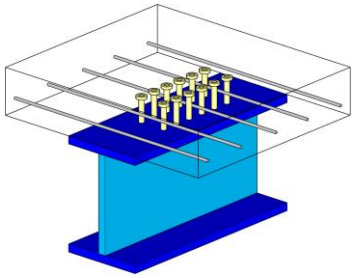

a) Headed studs

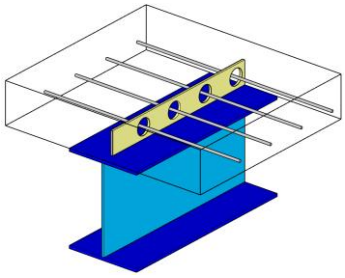

b) Perfobond rib

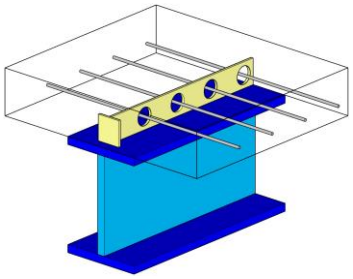

c) Modified Perfobond rib

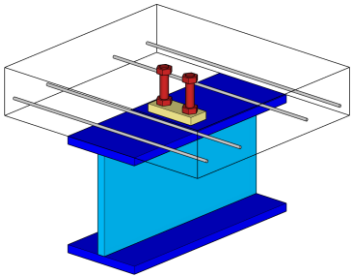

d) Bolts with a steel block: Connection RBN

Fig. 1.1 Various types of shear connections

a) Headed shear studs

In building constructions, the most widely used shear connector is a headed shear stud. Many studies have focused on the behaviour of these connectors in terms of their deformation characteristics and failure modes (Ollgaard *et al*., 1971; Shen *et al*., 2017a; 2017b; 2020; 2023; Hu *et al*., 2021; Xue *et al*., 2008; Spremic *et al*., 2013; 2017; Luo *et al*., 2016). Stud fracture and concrete failure due to dowel action are two failure modes commonly found in these forms, and associated design rules can be found in various codes, e.g. BS EN 1994-1-1 (EC4, 2004). It is worth noting that the diameter and the tensile strength of these studs and the strength of the surrounding concrete are key factors that affect the shear resistance. Fig. 1.1a) illustrates the use of headed shear studs in a composite beam of a bridge under construction, requiring large number of such connectors, often causing problems in reinforcement fixing and concreting.

b) Bolted shear connectors

Black bolts are often used in prefabricated composite beams owing to their availability in various sizes and grades. Comparison of the deformation characteristics of bolted shear connections and stud shear connections of similar diameters and grades indicate that the shear resistance of a bolted connection is typically about 95% of that of the stud connection. However, its stiffness is roughly 50% of that of the stud shear connection due to the presence of the tolerance in the bolt hole (Pavlović *et al*., 2013). To address this, some researchers suggested

the insertion of grouting materials into the gap between the bolt shank and the steel plate, or to machine the bolt nut into a conical shape to improve interlocking with the steel plate (Lee *et al*., 2013). There are also possible variants to standard black bolts, such as high-strength friction-grip bolts (HSFGB) (Zhao *et al*., 2020; Fang *et al*., 2021; Zhang *et al*., 2019; 2020). HSFGB can be used as well in bolted shear connections in prefabricated composite beams, as their shear resistances can be comparable to those with cast in-situ concrete slabs despite their lower stiffness (Fang *et al*., 2021).

c) Perfobond ribs

In order to develop a shear connection with large stiffness and resistance, a perfobond rib was proposed as a shear connector, as shown in Fig. 1.1b) (Vianna *et al*., 2008; 2009; 2013). It consists of a perforated steel plate welded longitudinally onto the flange of a steel beam, and steel reinforcements are placed through its perforated holes for improved resistances against both shear and uplift forces. Since the shear resistance of the perfobond rib depends also on the bearing area against the surrounding concrete, a bearing plate can be provided at the end of the rib to increase its shear resistance, i.e. a modified perfobond rib, as shown in Fig. 1.1c). It should be noted that the geometries of these perfobond ribs are readily modified to increase their stiffnesses and resistances correspondingly. However, the ductility of these shear connections is relatively limited.

1.2 Simple on-site assembly of composite beams

Since prefabricated construction is environmentally friendly and sustainable, this form has been extensively investigated in many countries (US Dept. of Trans., 2011). Fig. 1.2 illustrates typical configurations of prefabricated composite beams in bridges. For such structures, it is generally highly desirable to develop effective prefabrication using high strength materials. To this end,

the authors have in recent years, conducted a series of research projects to investigate the structural behaviour of headed shear studs and large diameter bolts in shear connections for composite beams, involving a wide range deformation characteristic and construction methods (Shen *et al*., 2017; 2020; 2023; Wang *et al*., 2022). In this research project, a newly proposed type of bolted shear connection is investigated through single-sided push-out tests and large-scale standard push-out tests, and the connection configuration is shown in Fig. 1.1d).

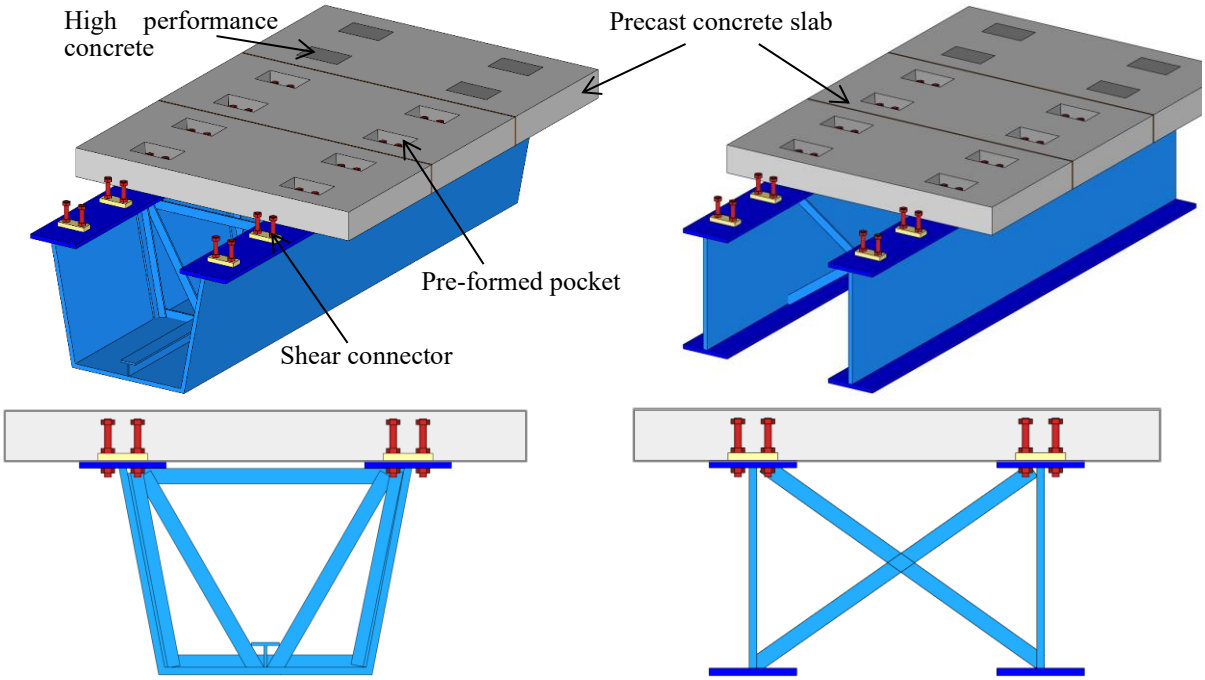

Fig. 1.2 Prefabricated composite beams

Fig. 1.3 shows a typical on-site assembly of a prefabricated composite beam with a bolted shear connection provided by the authors (Wang *et al*., 2022; Ding *et al*., 2024). Small steel blocks are welded onto the top surfaces of the flanges of the steel beams in a fabrication yard, and the high strength bolts are installed with a pre-determined tension force in each of the bolt shanks. After erection of these steel beams on site, the precast concrete slabs with preformed holes are then placed onto the steel beams. Finally, high performance concrete is cast into the

preformed holes of the concrete slabs, and hence, the high strength bolts are fully encased by the high performance concrete (HPC) to form a strong and stiff shear connection between the steel beam and the concrete slab.

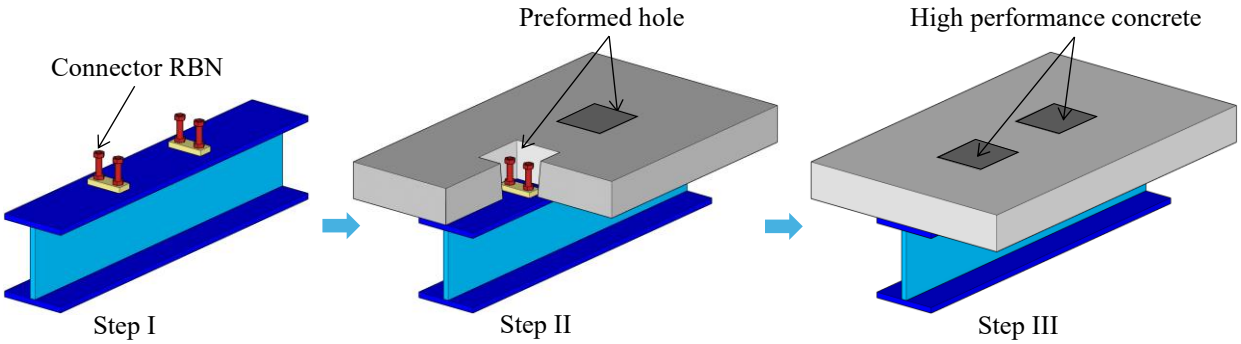

Fig. 1.3 On-site assembly of bolted shear connections for composite beams

1.3 Structural requirements for shear connections

In order to develop shear connections with adequate stiffness, resistance and ductility for prefabricated composite beams, the following requirements should be satisfied (Ding *et al.*, 2024):

i) a shear resistance $Q_m \geq 1{,}000$ kN;

ii) a stiffness in the linear elastic range, $K \geq 1{,}500$ kN/mm; and

iii) a slippage at failure $s_u \geq 6.0$ mm.

It is also necessary for the shear connections to provide a high level of resistance against pull-out forces, and to distribute the stresses effectively within the concrete in the proximity of the shear connectors to alleviate concrete cracking and crushing at large deformations.

1.4 Objectives and scope of work

In order to promote wide application of prefabricated composite beams in highway bridges, there is a pressing need to develop a shear connection which provides a high stiffness and resistance, whilst being easily assembled on site. In this research project, experimental and

numerical investigations are performed using single-sided and standard push-out tests to assess the structural behaviour of shear connections of high resistances with various shear connectors for easy on-site assembly of prefabricated composite beams in bridge construction. The present study takes the following forms of investigation:

a) An experimental investigation of single-sided push-out tests

A total of 39 single-sided push-out tests were conducted on connections with six types of shear connectors to preliminary assess the structural behaviour of the shear connections and identify a suitable configuration of the shear connection with large shear resistance, high stiffness, and good ductility. Based on the comparative results, a new type of bolted shear connection with favourable structural performance was proposed, in which a steel block and two specially designed bolts were fixed onto the flange of the steel beam in the shop, and they were fully embedded into steel fibre reinforced concrete (SFRC) on site. It should be noted that the steel block was pre-welded onto the beam flange to increase the initial stiffness, while steel fibres were added into the infilled concrete to improve their tensile strengths.

b) An experimental investigation of large-scale standard push-out tests

Based on the results of the single-sided push-out tests, a total of twenty extensively instrumented standard push-out tests were carried out on the structural behaviour of the shear connections with various configurations. Shear connections with four different types of shear connectors were tested, and the load-slippage responses of these connections were extracted together with their shear resistances and modes of failure. A comparison of the load-slippage curves of these connections was conducted to quantify relative influence of connection configuration, steel block thickness, bolt diameter, concrete block size, and strength of the concrete block on the structural behaviour of these connections.

c) Numerical simulations

A non-linear numerical simulation was conducted on the test specimens using the Standard/static module of an advanced finite element software Abaqus. Detailed modelling techniques including the element types and sizes, boundary conditions and interactions, as well as the material properties of the concrete and the steel were fully described. After calibration against the test results, the distributions of the internal forces and moments along the height of the shear connectors, together with the concrete bearing forces are analysed, and the modelling techniques were applied to the parametric study for subsequent analyses. Moreover, a systematic parametric study was then performed to identify load transfer mechanisms.

d) Design development

Based on the experimental and the numerical investigations, effective design rules for shear resistances and load-slippage curves of the connections were formulated for applications in prefabricated composite beams. The proposed load-slippage curves of the shear connections were then numerically validated against the results of three practical composite beams tests with similar shear connections.

Key areas of interest in the present investigation include:

i. structural behaviour of various shear connections in terms of initial stiffness, shear resistance, slippage at failure and their typical modes of failure;
ii. influence of connection configuration, steel block thickness, bolt diameter, concrete block sizes, strengths of the concrete block and the precast concrete slab, as well as fibre content in the concrete block on the structural behaviour of the proposed shear connections;
iii. constitutive models of the concrete and the bolt steel considering various material damage;
iv. distributions of internal forces and moments together with the concrete bearing forces

along the height of the connectors;

v. design rules for shear resistances and load-slippage curves of the connections based on the experimental and the numerical results.

1.5 Overview of the thesis

Chapter 2: Literature Review

A comprehensive literature review is presented to evaluate experimental and numerical investigations into the structural behaviour of various types of shear connectors with cast in-situ and precast concrete slabs. Standard push-out tests on the structural behaviour of commonly used headed stud shear connectors, bolted shear connectors and their variations, as well as solid connectors, box connectors, perfobond rib shear connectors are introduced. Non-linear numerical analyses on these shear connectors are listed and various key parameters including material constitutive models, element types, element sizes, interactions, and boundary conditions are presented. Moreover, design methods for shear resistances and load-slippage curves of these shear connectors are summarised.

Chapter 3: Experimental Investigations using Single-sided Push-out Tests

A total of 39 single-sided push-out tests are conducted to investigate the deformation characteristics of shear connections with welded and bolted shear connectors. A detailed account of the experimental investigation in terms of the test programme, fabrication of test specimens, test setup and instrumentation, as well as loading procedures are presented. Together with the results of the single-sided push-out tests, material tests on the concrete blocks, the precast concrete slabs, the steel bolts, the steel plates and the steel reinforcements are reported. Typical

failure modes are identified, and the deformation characteristics in terms of shear resistances, initial stiffness, and slippage limits are analysed. The load-slippage curves of the connections with various connector types, fibre content, and bolt diameters are fully compared to identify a suitable shear connection. Furthermore, a design method is developed for these shear connections with various types of shear connectors.

Chapter 4: Experimental Investigations using Standard Push-out Tests

Based on the results of the single-sided push-out tests presented in Chapter 3, a suitable shear connection with favourable deformation characteristics is selected for further investigation with standard push-out tests. A total of twenty standard push-out tests are conducted to assess the effect of various parameters on the structural behaviour of the shear connections. A detailed account of the experimental investigation in terms of test programme, fabrication of test specimens, test setup and instrumentation, as well as loading procedures are presented. Together with the test results of the standard push-out tests, material tests on the concrete blocks, precast concrete slabs, steel bolts, welded steel sections and steel reinforcements are reported. Typical failure modes together with the measured load-slippage curves and load-separation curves are provided, and the deformation characteristics are illustrated on the representative load-slippage curves.

Chapter 5: Analysis of Test Results of Standard Push-out Tests

A comprehensive analysis is conducted to further investigate the deformation characteristics of the shear connections reported in Chapter 4. Key results of the standard push-out tests are analysed, and the influence of connection configuration, steel block thickness, concrete block

size, bolt diameter, and strength of concrete block on the structural behaviour of the shear connections have been assessed. It should be noted that for the shear connections with concrete failure, the strengths of the concrete blocks are linearly normalized to standard values of either 80 or 100 N/mm^2, and the corresponding shear resistances are used for comparison. The test results are also compared with those results reported in the literature for easy understanding of the structural behaviour of the shear connections. The measured shear resistances are compared with the design values, and a preliminary design approach is proposed through regression of the test results.

Chapter 6: Numerical Simulations of Standard Push-out Tests

Non-linear numerical simulations on the structural responses of four types of shear connections are conducted. Detailed modelling techniques such as the element types and sizes, boundary conditions and interactions, as well as the material properties of the concrete and the steel are fully described, and they are calibrated against the test results in terms of "stress and damage" distributions, load-slippage curves, and deformation characteristics. The internal force distributions along the height of the shear connectors, and the distributions of the concrete bearing forces are analysed for deep understanding of the structural behaviour of the shear connections.

Chapter 7: Parametric Study and Design Rules

A comprehensive parametric study is conducted to assess the influence of bolt diameter, steel block thickness, concrete block width, strengths of the concrete block and the precast concrete slab, fibre content in the concrete block, and longitudinal spacing of shear connections on the

structural behaviour of the proposed bolted shear connections. The internal force distributions along the bolt height and the distributions of the concrete bearing force in the parametric models are analysed and the load transfer mechanisms are identified. A complementary design approach is proposed for shear resistances and load-slippage curves of the bolted shear connections for practical design of the composite beams. Finite element models of practical composite beams with similar shear connections are established, and the simulation results are compared with the test data to validate the simplified load-slippage curves.

Chapter 8: Conclusions and Future Work

Key findings of the experimental investigations, numerical simulations, and design development of the proposed shear connections are summarised. The significance of the present study is identified. In order to promote the application of the proposed shear connections for simple on-site assembly of the composite beams, the future work on the present topic is presented.

CHAPTER 2

LITERATURE REVIEW

2.1 Introduction

This chapter presents a comprehensive literature review on the structural behaviour of various kinds of shear connectors in composite beams. A detailed account of the experimental investigations, numerical simulations, as well as the design rules are presented. The following parts are included:

a) Experimental investigation

   Experimental investigations into the structural behaviour of shear connections with various types of shear connectors, such as headed shear studs, bolted shear connectors, and block shear connectors, are presented. The shear connectors are encased either in normal concrete (NC) or in high performance concrete (HPC). The structural behaviour of these shear connections in cast-in-situ concrete slabs and precast concrete slabs are summarised.

b) Numerical simulation

   Non-linear numerical simulations on the structural behaviour of shear connections with various types of shear connectors are conducted using advanced finite element (FE) software Abaqus. Key parameters in constitutive models, element types, element sizes, interactions, and boundary conditions are summarised. The simulated and measured structural responses in terms of “stress and strain” distributions, load-slippage curves, and deformation characteristics of the shear connections are compared to validate the accuracy of the simulations. In addition, parametric studies are used to systematically investigate the influence of various parameters on the structural behaviour of the shear connections.

c) Design rule

The codified rules in BS EN 1994-1-1, Hong Kong Code of Practice for the Structural Use of Steel, AISC 360-22, and GB 50017-2017 for shear resistances of various types of shear connectors are summarised. Moreover, design rules for shear resistances of bolted shear connectors suggested in literature are also reviewed.

2.2 Experimental investigation

In the past thirty years, investigations into the structural behaviour of various types of shear connectors have been conducted, and typical connector configurations are shown in Fig. 2.1. Details of the experimental investigations are presented as follows:

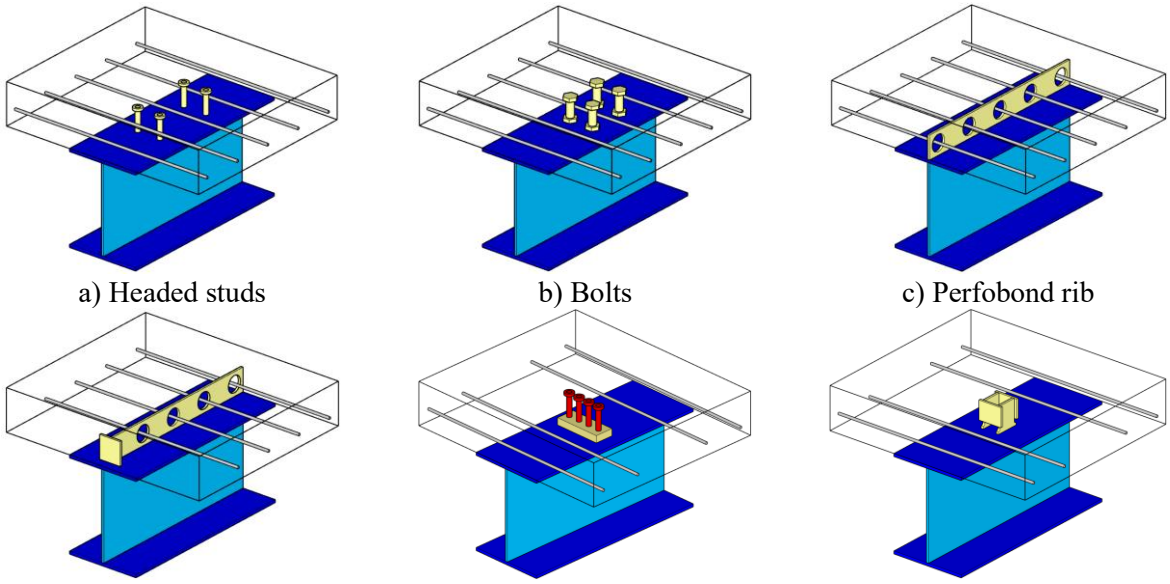

Fig. 2.1 Various types of shear connectors (Ding *et al.*, 2024)

2.2.1 Standard push-out tests on headed shear studs

a) Headed shear studs in normal concrete (NC)

A total of forty-eight standard push-out tests were conducted by Ollgaard (1971) to investigate the structural behaviour of headed shear studs in normal-weight and light-weight

concrete. The connector configuration is shown in Fig. 2.1 a). The stud diameters were 16 and 19 mm respectively. The tensile strength of the headed shear stud was 485 N/mm^2. The concrete compressive strength ranged from 18.4 to 35.0 N/mm^2. Shear fracture of headed studs and concrete failure were identified as two typical failure modes. Design formulae for shear resistances Q_m , and load-slippage curves of headed shear studs were proposed, as shown in Eq. (2.1).

$$Q_m = 0.5\, A_s \sqrt{f_c\, E_c} \tag{2.1a}$$

where,

f_c is the compressive strength of the concrete;

E_c is the elastic modulus of the concrete; and

A_s is the cross-sectional area of the stud shear connector.

$$Q = Q_m(1\text{-}e^{-18s})^{0.4} \tag{2.1b}$$

where,

Q is the applied load; and

s is the slippage.

Standard and modified push-out tests, as well as numerical simulations were carried out by Shen *et al*. (2017; 2020; 2023) to investigate the structural behaviour of headed shear studs with various connector arrangements under different loading conditions. The diameter and height of the headed stud were 19 and 100 mm respectively. The tensile strength of the headed stud was 500 N/mm^2. The concrete compressive strength was 35 N/mm^2. It was found that the headed studs in composite slabs with unfavourable troughs were more ductile than those with favourable troughs. Based on numerical analyses, the distributions of internal forces along the height of the shear studs, together with the concrete bearing forces acting onto the studs were plotted in Fig.

2.2, and hence, the load transfer mechanisms of these shear connectors were proposed, as shown in Fig. 2.2. An interaction curve for stud shear connections under combined shear and pull-out forces was also proposed.

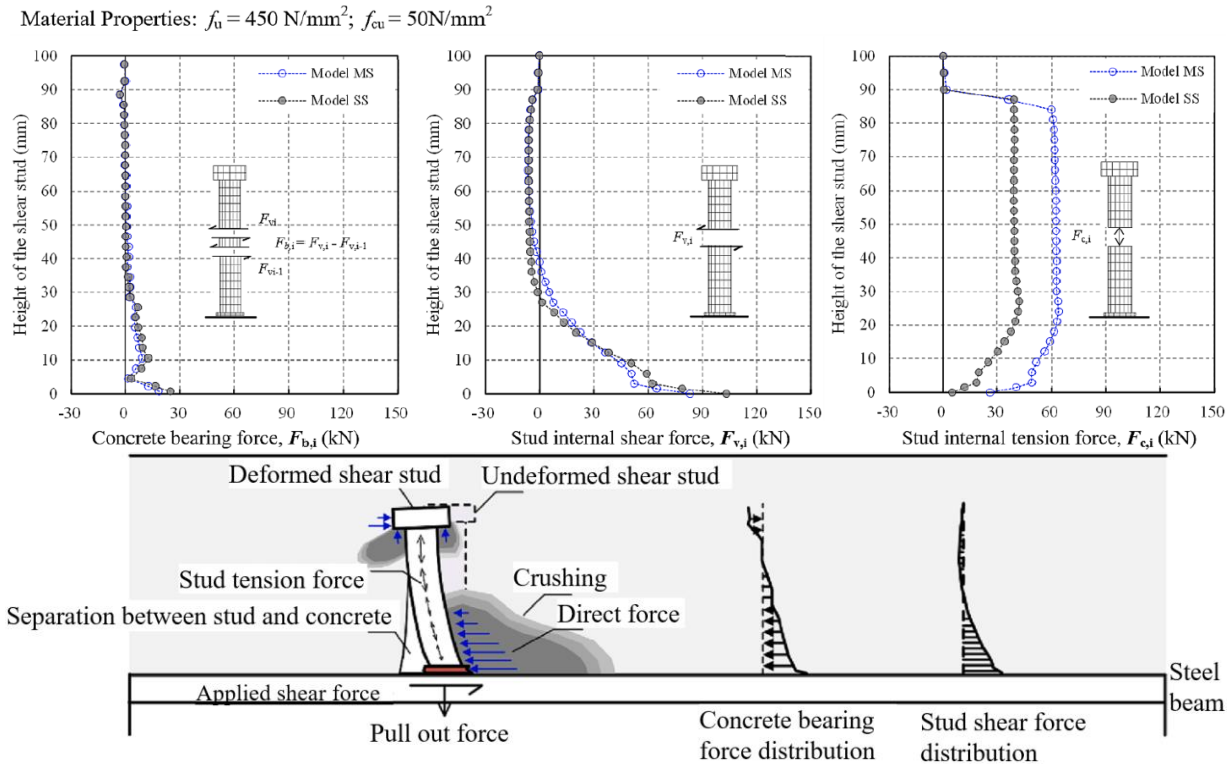

Fig. 2.2 Load-transfer mechanisms within stud shear connections (Shen *et al*., 2023)

b) Headed shear studs in high performance concrete (HPC)

A total of ten standard push-out tests were conducted by Hu *et al*. (2021) to investigate the shear resistance and the stiffness of the headed shear stud encased by high performance concrete (HPC). The diameters of headed shear studs were 16 and 19 mm respectively, and the height of the stud was 80 mm. The yield and tensile strengths of the 16 mm diameter stud were 354.5 and 454.5 N/mm^2 respectively, while those of the 19 mm diameter stud were 400.6 and 494.6 N/mm^2 respectively. The compressive strength of HPC was 54.4 N/mm^2. It was found that the stud diameter, the compressive strength, and elastic modulus of the concrete were main factors that

influenced the stiffness of the stud embedded in HPC according to the proposed formula derived by elastic foundation beam theory. A formula for shear resistances Q_m of headed studs, considering the interaction between stud and concrete was proposed, as shown in Eq. (2.2).

$$Q_m = 3.8\, A_s f_u \left(\frac{E_c}{E_s}\right)^{0.4} \left(\frac{f_c}{f_u}\right)^{0.35} + 0.25 f_c d^2 \qquad \text{for stud failure} \tag{2.2a}$$

$$Q_m = \varphi\, 0.5\, A_s \sqrt{f_c E_c} \qquad \text{for concrete failure} \tag{2.2b}$$

where,

f_u is the tensile strength of the stud steel;

E_s is the elastic modulus of the stud steel;

d is the diameter of the stud; and

φ is the resistance factor for headed shear studs which is taken as 0.85.

Xue *et al*. (2008) proposed a similar formula to predict the shear resistances of headed shear studs against stud failure, considering the effect of welding technique, as shown in Eq. (2.3a). A formula for load-slippage curves of headed studs was proposed, as shown in Eq. (2.3b).

$$Q_m = 3\,\lambda\, A_s f_u \left(\frac{E_c}{E_s}\right)^{0.4} \left(\frac{f_c}{f_u}\right)^{0.2} \tag{2.3a}$$

where,

$$\lambda = \begin{cases} 6 - H/1.05d & (H/d \le 5) \\ 1 & (5 < H/d < 7) \\ H/d - 6 & (H/d \ge 7) \end{cases}$$

$$\frac{Q}{Q_m} = \frac{s}{0.5 + 0.97s} \tag{2.3b}$$

c) Grouped headed shear studs in NC

A total of twenty-five standard push-out tests were conducted by Spremic *et al*. (2013) to investigate the structural behaviour of grouped headed studs with precast concrete slabs. The sizes of concrete blocks were 240×240 and 240×140 mm respectively. The diameter of the headed stud

was 16 mm. The strength grade of the concrete slab was C30/C37, and the compressive strength of the concrete block ranged from 32 to 40 N/mm^2. The key parameters included the shape and orientation of the stud group arrangement relative to the applied load, as well as the longitudinal distance between the studs. It was found that the longitudinal distance could be reduced smaller than the minimum required (5*d*). Grouped headed studs were considered to be more ductile than large diameter headed studs. Moreover, the structural behaviour of the headed shear stud and the perfobond rib shear connector was compared experimentally and numerically (Spremić *et al*., 2017). It was found that the headed stud was ductile while the perfobond rib shear connector could not be classified as ductile since its ultimate slippage was smaller than 6 mm. When steel reinforcements passed through the preformed holes, the shear resistance and the ultimate slippage of the perfobond rib shear connector were significantly improved.

d) Grouped headed shear studs in HPC

A total of sixteen standard push-out tests were carried out by Luo *et al*. (2016) to investigate the structural behaviour of grouped headed shear studs encased by HPC. The diameters of the studs were 13 and 22 mm respectively, and the yield and tensile strengths were 394 and 472 N/mm^2 respectively. The concrete compressive strength ranged from 104 to 132 N/mm^2 with fibre content ranging from 2 to 6%. Key parameters included the diameter and the number of the studs, the transverse spacing, the longitudinal spacing, and the fibre content in the concrete. It was found that when the transverse spacing was reduced from 6.9*d* to 2.3*d*, no reduction was found in the shear resistances of the studs. The ductility of the grouped headed studs was significantly enhanced when the fibre content in HPC was 6%.

The structural behaviour of grouped headed shear studs in high-strength steel - prefabricated

HPC composite beams was investigated by Tong *et al*. (2020). The compressive strength of HPC was 149.8 N/mm^2 with steel fibre content of 2.2%. The yield and tensile strengths of the high strength steel beams were 777 and 870 N/mm^2 respectively. Key parameters included stud diameters (13 and 19 mm), and layouts of studs (single stud and grouped studs). It was found that the shear resistance and stiffness of the headed studs were increased when they were embedded in HPC, while the ductility was decreased. However, the use of high strength steel beam did not have any influence on the shear behaviour of the studs. Empirical formulae for the load-slippage curves of the single stud and grouped studs were proposed, as shown in Eq. (2.4).

$$\frac{Q}{Q_{\mathrm{m}}}=\frac{S/d}{0.0092+0.93S/d} \qquad \text{for single stud} \tag{2.4a}$$

$$\frac{Q}{Q_{\mathrm{m}}}=(1-e^{-1.55s})^{0.64} \qquad \text{for grouped studs} \tag{2.4b}$$

A total of twenty-six standard push-out tests were carried out by Fang *et al*. (2020) to investigate the structural behaviour of grouped headed shear studs in precast concrete slabs. The compressive strength of the precast concrete slab was 72.1 N/mm^2. The steel fibre content in concrete blocks was 0, 1%, and 2% respectively. It was found that increasing the stud diameter, the strength of concrete block, and the steel fibre content led to an increase in the stiffness of the connector, while casting method of concrete slabs had slight influence on stiffness. With an increase in the fibre content, the shear resistance of the shear connector was slightly increased while the ductility was decreased. A regressive formula for shear resistances of headed shear studs with precast concrete slabs and steel fibre reinforced concrete (SFRC) blocks was proposed, as shown in Eq. (2.5).

$$Q_{\mathrm{m}} = 0.11\, A_{\mathrm{s}} f_{\mathrm{u}} \sqrt{f_{\mathrm{c}}} \tag{2.5}$$

e) Large diameter headed shear studs in NC

Standard push-out tests and beam tests were conducted by Lee *et al*. (2005) and Shim *et al*. (2004) to investigate the static and fatigue behaviour of large diameter headed shear studs. The diameters of the headed studs were 25, 27, and 30 mm respectively. The nominal compressive strength of the concrete slab was 40 N/mm^2. It was found that large diameter headed studs had sufficient deformation capacity for load redistribution. Formulae for initial shear stiffness K and ultimate slippage s_u of large diameter headed studs were proposed, as shown in Eq. (2.6). It was found in the beam tests that the static behaviour of composite beams with the same degree of shear connection was not influenced by the diameter or distribution of the headed studs.

$$K = \frac{Q_m}{d\,(0.16 - 0.0017 f_c)} \tag{2.6a}$$

$$s_u = (0.48 - 0.0042 f_c)\, d \tag{2.6b}$$

f) Large diameter headed shear studs in HPC

A total of fifteen standard push-out tests were conducted by Xu *et al*. (2021; 2022) to investigate the structural behaviour of large diameter headed shear studs with thin HPC slabs. The thickness of HPC slabs was as small as 75 mm. The diameters of studs were 22 and 30 mm respectively. The concrete compressive strength was 125 N/mm^2. Two typical failure modes were identified: i) stud fracture with local concrete crushing; and ii) stud fracture with HPC pry-out (Separation between HPC slab and flange of the steel beam). It was found that HPC pry-out was more obvious in tests with 30 mm diameter studs. The portion of the long stud length involved in bearing shear force was 18% to 25%, while that for the short stud was 40% to 50%.

Wang *et al*. (2018) proposed a novel steel-HPC composite system with 30 mm diameter

headed studs in conjunction with the concrete slab and the steel beam. A total of six standard push-out tests were conducted on single studs and a total of eighteen tests were conducted on grouped studs to investigate the structural behaviour of these headed studs with HPC and NC slabs. The yield and tensile strengths of the studs were 390.4 and 435.6 N/mm^2 respectively. The compressive strengths of UHPC-I and UHPC-II, reinforced with steel fibres, were 124.2 and 125.4 N/mm^2 respectively. The compressive strengths of NC and non-shrinking grouting material were 49.0 and 56.7 N/mm^2 respectively. It was shown that the ultimate slippage of the specimen with precast NC slab was 17% higher than that with cast-in-situ concrete slab. Moreover, the stiffness of the headed stud with precast NC slab was 40% lower than that with precast HPC slab, while the resistances of the stud with NC and HPC were comparable, as shown in Fig. 2.3.

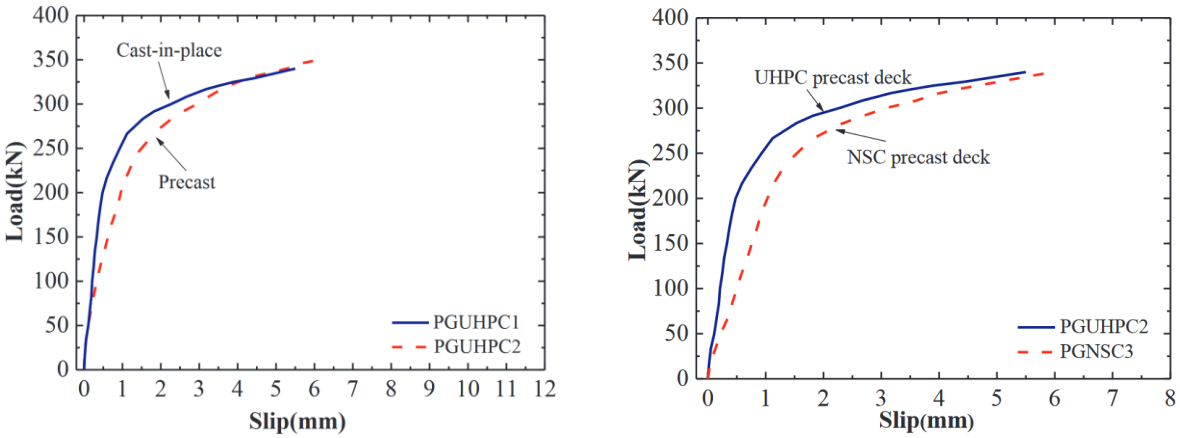

a) Effect of casting method b) Effect of precast slab strength

Fig. 2.3 Load-slippage curves of large diameter headed studs in HPC (Wang *et al.*, 2018)

2.2.2 Standard push-out tests on bolted shear connectors

a) Bolted shear connectors

In order to promote the application of bolted shear connectors to prefabricated composite beams and to obtain a deep insight into the structural behaviour of bolted shear connectors, standard push-out tests together with non-linear finite element (FE) simulations were conducted

by Pavlović *et al*. (2013). The connector configuration is shown in Fig. 2.1 b). Grade 8.8 bolts with a diameter of 16 mm were used as shear connectors in the tests. The compressive strength of the concrete slab was 40 N/mm^2. It was found that the shear resistance of a bolted shear connector achieved 95% of the shear resistance of a headed stud, while the initial stiffness of the bolted shear connector was 50% smaller, as shown in Fig. 2.4.

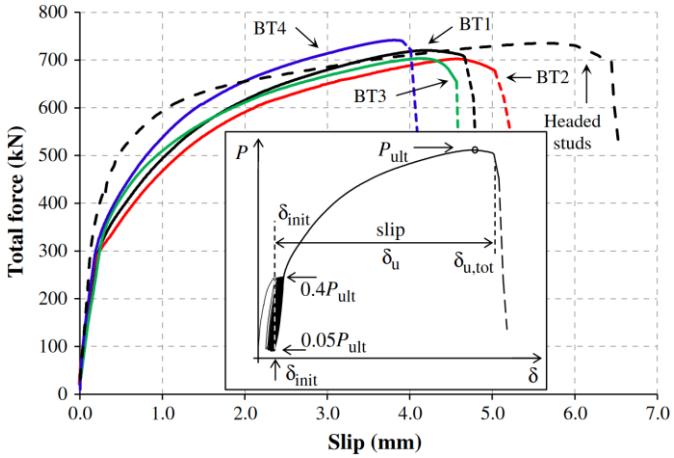

Fig. 2.4 Comparison of load-slippage curves of headed studs and bolts (Pavlović *et al*., 2013)

A total of 12 standard push-out tests were conducted by Du *et al*. (2020) to investigate the structural behaviour of bolted shear connectors in prefabricated steel-bar truss concrete slabs. A total of three full-scale composite beams with various degrees of shear connectors were tested to investigate the bending resistances of the composite beams. The diameter of the bolt was 16 mm, and the yield and tensile strengths of the bolt were 660 and 886 N/mm^2 respectively. The compressive strengths of the grouting material and the concrete slab were 40.3 and 30.7 N/mm^2 respectively. It was found that the shear resistance of the bolted shear connector with prefabricated steel-bars truss concrete slab was increased by 7.0 % over that of the connector with prefabricated concrete slab, due to the constraint provided by the steel-bar truss on the concrete slab. The shear resistance of the bolt with a prefabricated concrete slab was approximately equal to that of the

bolt with a cast-in-situ concrete slab, while the initial stiffness of the bolt with a prefabricated concrete slab was relatively small. Design formulae for shear resistances of bolted shear connectors against concrete failure and bolt fracture were shown in Eq. (2.7). Similar standard push-out tests were conducted by Lee *et al*. (2013) to investigate the structural behaviour of Grade 8.8 bolts in precast geopolymer concrete (GPC) slab. It was found that the reusability of the bolts under service load was demonstrated to be applicable.

$$Q_{\mathrm{m}} = 0.22\,(h_{\mathrm{b}} / d)^{0.4}\, A_{\mathrm{s}} \sqrt{f_{\mathrm{c}}\, E_{\mathrm{c}}} \tag{2.7a}$$

where,

h_{b} is the embedded length of bolted connectors into the concrete slab.

$$Q_{\mathrm{m}} = \alpha_{\mathrm{v}}\, A_{\mathrm{s}} f_{\mathrm{u}} \tag{2.7b}$$

where,

α_{v} = 0.6 for classes 4.5, 5.6 and 8.8 bolts; and

α_{v} = 0.5 for classes 4.8, 5.5, 6.8 and 10.9 bolts.

b) Locking nut shear connector (LNSC)

Standard push-out tests and FE simulations were conducted by He *et al*. (2022) to examine the structural behaviour of a LNSC. As shown in Fig. 2.5, this connector consisted of a grout-filled headed steel tube with internal partial thread fastened over a compatible partial thread bolt. The compressive strengths of the concrete slabs were 50.4 and 63.3 N/mm^2 respectively. The bolt diameter was 20 mm. It was found that the tensile force resisted by the steel tubes was about 15% of the shear force by extracting the internal forces from the FE models. The strength of the infilled grout in the steel tube had a significant influence on the initial stiffness, while it had marginal influence on the shear resistance. The shear resistance Q_{m} was predicted by Eq. (2.8).

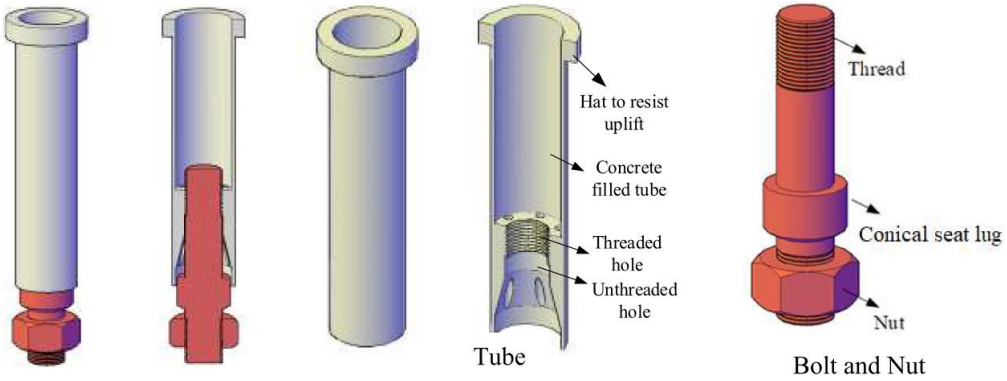

Fig. 2.5 Details of the LNSC (He *et al.*, 2022)

$$Q_m = \min\left(\eta_1 A_t \sqrt{E_c f_{ck}}\ , \eta_2 A_b f_u\right) \tag{2.8}$$

$$\eta_2 = \alpha_b \left(\frac{d_{ref}}{d}\right)^{\beta} \le 1 \quad \text{for } d \ge 16 \text{ mm}$$

where,

A_t is cross-sectional area of grout-infilled tube;

A_b is cross-sectional area of the bolt shank;

f_{ck} is characteristic compressive strength of the concrete;

η_1 is taken as 0.30 for concrete failure;

d_{ref} is a reference bolt diameter, and is taken as 20 mm;

d is the bolt diameter; and

α_b and β are coefficients that were fitted as 0.84 and 0.84, respectively.

Both the standard push-out tests and the beam tests were conducted by Luo *et al*. (2022) to investigate the structural behaviour of a steel-yielding demountable bolt connectors (SYDBCs) for applications in prefabricated steel-concrete composite beams. The detailed configuration of the shear connector is shown in Fig. 2.6. The bolt diameters were 14, 18 and 22 mm respectively, and the yield and tensile strengths were 674 and 849 N/mm^2 respectively. HPC with a compressive strength of 133.6 N/mm^2 and a tensile strength of 8 N/mm^2 was used in both the prefabricated concrete slabs and the concrete blocks. It was found that when compared with bolted shear

connectors in cast-in-situ concrete slabs, the stiffness of SYDBCs in precast concrete slabs was reduced by 20% whereas the shear resistance was unchanged. It was suggested that the size of the concrete block should be carefully designed to avoid premature concrete crushing.

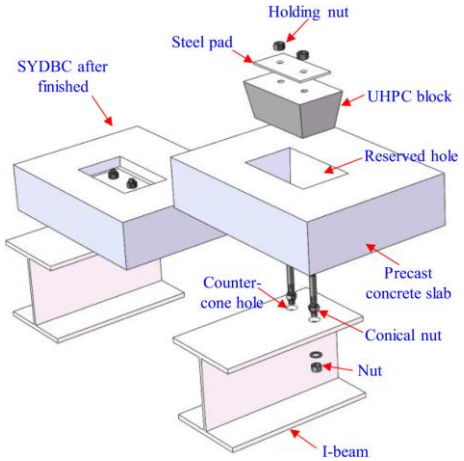

Fig. 2.6 Detailed configuration of SYDBCs (Luo *et al.*, 2022)

c) High-strength friction-grip bolted (HSFGB) shear connectors

A total of fifteen standard push-out tests were conducted by Zhao *et al*. (2020) to investigate the structural behaviour of HSFGB shear connectors. The bolt diameter was 22 mm, and the yield and tensile strengths of the bolt were 1,055 and 1,158 N/mm^2 respectively. The concrete compressive strength was 46.7 N/mm^2. It was found that with an increase in the pad size, the cracks on the concrete slab could be effectively reduced while the shear resistance of the shear connector was not influenced. However, the stiffness of the shear connector was decreased with an increase in the diameter of the bolt hole.

A total of 18 standard push-out tests were conducted by Fang *et al*. (2021) to investigate the structural behaviour of HSFGB shear connectors in prefabricated HPC and NC slabs. The bolt diameters were 16, 22, and 27 mm respectively. The compressive strengths of HPC and NC were 150.3 and 61.2 N/mm^2 respectively. It was found that a slab thickness of 75 mm was sufficient

for the precast HPC slab with HSFGB shear connectors. The group effect of the HSFGB shear connectors in the HPC slab could be neglected even when the transverse spacing was as low as 80 mm. The shear resistance was significantly increased with an increase in the bolt diameter and the bolt grade, while the slab concrete type and pretension force had only a minor influence on the shear resistance. The shear stiffness was increased with an increase in the bolt diameter and the bolt grade, while the concrete type had a minor influence. Design formulae for shear resistances and load-slippage curves of HSFGB shear connectors were proposed, as shown in Eq. (2.9).

$$Q_{\mathrm{m}} = 0.76\, A_{\mathrm{s}} f_{\mathrm{u}} \tag{2.9a}$$

$$Q / Q_{\mathrm{m}} = (1\text{-}e^{-0.47s})^{k} \tag{2.9b}$$

where,

k is the factor related to bolt grade. Based on the experimental result, it is suggested that 0.36 for grade 8.8 and 10.9 bolts and 0.5 for grade 12.9 bolts.

Similarly, a total of 22 standard push-out tests were conducted by Zhang *et al*. (2019; 2020) to investigate the structural behaviour of HSFGB shear connectors in steel-SFRC composite beams, as shown in Fig. 2.7 a). The bolt diameters were 22, 24 and 27 mm respectively. Grades 8.8 and 10.9 bolts with a diameter of 24 mm were used. The compressive strengths of SFRC and NC were 62.2 and 58.8 N/mm^2 respectively. It should be noted that high performance grouting material with a compressive strength of 100 N/mm^2 was filled into the bolt holes in most of the specimens to avoid sudden slippages in the load slippage curves, and the load-slippage curves are shown in Fig. 2.7 b). Theoretical formulae for shear resistances and load-slippage curves of HSFGB shear connectors were shown in Eq. (2.10).

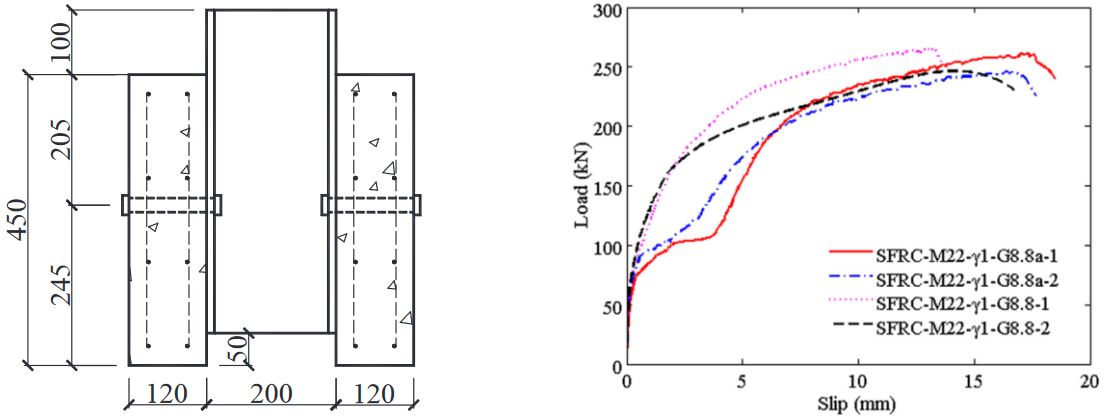

a) Elevation view of the test specimens

b) Comparison of connectors with or without fillers in bolt holes

Fig. 2.7 Tests on HSFGB shear connectors (Zhang *et al.*, 2019; 2020)

$$Q_{\mathrm{m}} = \min\left(0.76\, A_{\mathrm{s}} f_{\mathrm{u}},\ 0.5\, A_{\mathrm{s}} \sqrt{f_{\mathrm{c}}\, E_{\mathrm{c}}}\right) \tag{2.10a}$$

$$Q = Q_{\mathrm{m}} \left(1\text{-}e^{-0.2s}\right)^{0.4} \tag{2.10b}$$

2.2.3 Standard push-out tests on the other shear connectors

a) Perfobond rib shear connectors

A total of eighteen push-out tests were conducted by Zhao *et al*. (2018) to investigate the structural behaviour of perfobond rib shear connectors, as shown in Fig. 2.1c). The perforated steel plate was 500×380×25 mm in dimensions, and the nominal tensile strength was 345 N/mm^2. The diameters of passing reinforcements were 8, 10 and 12 mm respectively, and the nominal yield strength was 400 N/mm^2. The nominal concrete strengths were 40, 55 and 65 N/mm^2 respectively. The strain distributions of the perforated steel plate and the reinforcement were measured by optical fibres. It was found that the shear resistance of the perfobond rib shear connector was primarily derived from bonding and friction between the concrete and the steel. The perfobond rib shear connector with a larger diameter of passing reinforcement exhibited higher shear resistance and ductility.

Similar push-out tests were carried out by Ahn *et al*. (2010) to investigate the structural behaviour of perfobond rib shear connectors. It was found that the shear resistance of the perfobond rib shear connector was in proportion to the concrete strength due to the contributions of the concrete end-bearing resistance and the concrete dowel. The shear resistance of the twin type perfobond rib shear connector was about 80% that of the single perfobond rib shear connector due to a reduction in the shear resistance caused by the overlap of the concrete end-bearing zone, and the passing reinforcement in the perforated hole.

Two series of standard push-out tests were conducted by Vianna *et al*. (2008; 2009; 2013) to investigate the structural behaviour of perfobond rib shear connector and perfobond rib with an end plate (T-perfobond rib shear connector, as shown in Fig. 2.1d)) with Classes C25/30, and C50/60 concrete. The perfobond rib was made of 12.5 mm thick steel plate, with a nominal yield strength of 355 N/mm^2. The heights of the perfobond ribs were 76.2 and 150 mm for the concrete slabs with thicknesses of 120 and 200 mm, respectively. It was found that compared with the perfobond rib shear connector, both the shear resistance and the stiffness of the T-perfobond rib shear connector were increased, while the ductility was reduced significantly to less than 6 mm. The addition of passing reinforcements in perforated holes resulted in a significant increase in both the shear resistance and the ultimate slippage of the perfobond rib shear connectors.

b) Steel block shear connector (SBSC)

Standard push-out tests and cyclic tests were carried out by Wang *et al*. (2019) to investigate the structural behaviour of steel block shear connectors (SBSCs). The steel block was 140×60×60 mm in dimensions, with a 20 mm diameter bent rebars welded onto the steel block. The compressive strengths of the concrete slab and the grouting material were 34.0 and 53.5 N/mm^2

respectively. Local concrete crushing in the vicinity of the steel block appeared in all the tests. It was found that the shear resistance and the stiffness of SBSC were 48% and 27% higher than those of grouped headed studs in shear pockets with similar dimensions. A formula for the shear resistance of SBSC was developed, as shown in Eq. (2.11).

$$Q_{\mathrm{m}} = a\,A_{\mathrm{l}} f_{\mathrm{cb}} + b\,A_{\mathrm{r}} f_{\mathrm{y}} + c\,f_{\mathrm{t}}\,b\,h_{\mathrm{slab}} \tag{2.11}$$

$$\text{with} \quad f_{\mathrm{cb}} = f_{\mathrm{c}} \sqrt{\frac{A_{\mathrm{cp1}}}{A_{\mathrm{cl}}}} \leq 2.5\,f_{\mathrm{c}}$$

where:

f_{c} is the compressive strength of the concrete;

A_{cl} is the bearing area of the concrete in the vicinity of the connector;

A_{cp1} is the projected area following a slope of 1:5;

h_{slab} is the thickness of the concrete slab;

f_{t} is the tensile strength of the concrete ($=0.375 f_{\mathrm{c}}^{0.55}$);

a, b are coefficients related to resistances provided by the concrete and the steel einforcements, which are taken as 0.3; and

$c =$ 17.2 / (-29.7γ+3.53) with $\gamma = f_{\mathrm{t}}/f_{\mathrm{c}}$.

A total of thirteen standard push-out tests were conducted by Liu *et al*. (2023) to investigate the structural behaviour of headed stud-steel block connectors (HSBCs) (shown in Fig. 2.1e)) in prefabricated composite beams, in which a group of studs were welded onto the steel block to provide pull-out forces. The compressive strengths of the concrete slab, the C55 concrete block, and the HPC were 40.6, 50.9, and 76.1 N/mm^2 respectively. Q355 steel was used in both the steel beams and the steel blocks. It should be noted that the end of the concrete slab was strengthened with fibre reinforced polymer (FRP) to avoid local concrete crushing. It was found that the inclination rate from the basic area to the projected area was 1:5.

c) Bearing-shear connector (B-S connector)

Zou *et al*. (2021) proposed an innovative bearing-shear (B-S) connector with a compact structure to be used in prefabricated concrete beams to substitute grouped studs in high shear force region, as shown in Fig. 2.1 f). Standard push-out tests together with FE simulations were conducted to investigate the monotonic and cyclic behaviour of the proposed shear connector. The compressive strengths of the precast concrete slab and the infilled mortar were 36.7 and 43.6 N/mm^2 respectively. Q420 steel with yield and tensile strengths of 449.6 and 600.2 N/mm^2 was used for the shear plate of the connector. Q345 steel with yield and tensile strengths of 361.3 and 479.6N/mm^2 was used for the bearing plate of the connector. The concrete crushing and shear plate fracture were two typical failure modes in the tests. It was found that the shear resistance of a B-S connector exceeded 1,180 kN, which was close to that of nine studs with a diameter of 19 mm, while the required area of the reserved holes in prefabricated concrete slab was about 1/3 of that required for a stud group with the same shear resistance. A formula for the shear resistance of the B-S connector was proposed and the deviations between the predicted and the measured values were within 4%.

d) Channel connectors

A total of fifteen single-sided push-out tests were conducted by Baran *et al*. (2012) to investigate the structural behaviour of channel shear connectors. The channel height ranged from 65 to 140 mm, and the section lengths were 50, 75, and 100 mm, respectively. The yield and tensile strengths of the steel were 318 and 451 N/mm^2 respectively. The concrete compressive strengths ranged from 31.8 to 39.9 N/mm^2. It was found that for a constant channel length, increasing the channel height led to an increase in the shear resistance, while the increase in the

initial stiffness was insignificant.

2.2.4 Beam tests

a) Large diameter headed studs in precast concrete slab

Push-out tests and beam tests were conducted by Badie *et al*. (2010; 2011) to investigate the structural behaviour of large diameter headed studs in precast concrete slabs to try to extend the spacing of the shear pockets from 610 to 1,220 mm. The shear pockets were reinforced with various methods including steel tube and closed-tie confinement to protect the grout around the stud from crushing. It was found that the spacing between the shear pockets was able to be extended from 610 up to 1,220 mm when full composite action between precast concrete slabs and steel girders could be achieved. It was suggested that using large diameter studs with a diameter of 31.8 mm to reduce the number of studs and the size of shear pockets was effective.

b) HSFGB in precast concrete slabs

A total of four full-scale beam tests were carried out by Ataei *et al*. (2016) to investigate the structural behaviour of prefabricated composite beams with high strength friction-grip bolted (HSFGB) shear connectors and precast geopolymer concrete (GPC) slabs. The diameter of the Grade 8.8 bolt was 20 mm, and a pretension force of 145 kN was applied onto the bolt shanks. The compressive strength of the precast concrete slab was 44.9 N/mm^2, and the slab thickness was 150 mm. It was found that the beams with HSFGB shear connectors were much more ductile than those with bolts, while the bending resistances of the beams with HSFGB shear connectors were smaller. The composite beams with GPC slabs and HSFGB shear connectors were able to be deconstructed in serviceability limit state and the components were able to be reused.

2.2.5 Summary

This section reviews a number of experimental investigations into various kinds of shear connectors for applications in cast-in-situ and precast concrete slabs. To further summarise the structural behaviour of various shear connectors, the geometries and strengths together with the deformation characteristics of the connectors are summarised in Table 2.1. It should be noted that the shear resistance Q_m denotes the resistance per stud/bolt in stud /bolted shear connectors. s_u denotes the ultimate slippage, and K denotes the initial stiffness.

Table 2.1 Key deformation characteristics of various shear connectors

Connection type	Designation	Dimension (mm)	Concrete strength (N/mm^2)	Stud/steel strength (N/mm^2)	Q_m (kN)	s_u (mm)	K (kN/mm)
Headed studs (Hu *et al*., 2021)	D16N2H80-0.53	d=16	54.4	f_y =355	95.6	4.3	162
	D19N2H80-0.53	d=19	56.5	f_y =401	145.4	7.1	251
Grouped studs in SFRC (Wang *et al*., 2018)	PSNSC1	d=30	49	f_y =390	324.8	8.1	297
	PGNSC1		49	f_u =436	318.0	10.3	252
	PGNSC2		49 (56.7)		289.5	12.1	180
	PGNSC3		49 (124.2)		335.6	6.7	197
	PSUHPC1		124 (125)		375.2	5.1	641
	PGUHPC1		124 (125)		354.1	5.8	524
	PGUHPC2		124 (125)		338.3	5.5	565
	PGUHPC3		124 (125)		333.8	6.1	888
Single nut embedded bolts (Du *et al*., 2020)	DBC1	d=16	29.8 (30.9)	f_y =660	85.6	13.2	-
	DBC2		29.4 (40.3)	f_u =886	106.4	13.1	
	DBC3		30.7 (28.8)		80.0	10.2	
	DBC4		30.9		89.9	11.4	
LNSC (He *et al*., 2022)	LB-DSC1	d=20	50.4 (48)	f_y =818	263	10.9	141
	LB-DSC2		50.4	f_u =990	239	12.7	61
	LB-DSC3		63.3 (48)		295	12.6	157
	LB-DSC4		50.4 (48)		219	9.8	160
HSFGB connector (Zhang *et al*., 2020)	NC-M22-γ1-G8.8	d=22	58.8	f_y =640	241.8	12.9	127
	NC-M27-γ1-G8.8	d=27		f_u =800	305.5	21.8	155
	SFRC-M22-γ1-G8.8	d=22	62.2		248.2	14.4	137
	SFRC-M22-γ1-G8.8[a]	d=22			253.4	17.5	55
	SFRC-M27-γ1-G8.8	d=27			370.2	27.8	171
	SFRC-M24-γ1-G8.8	d=24			294.5	19.3	151
	SFRC-M24-γ1-G10.9	d=24		f_y =900	354.6	26.1	156
Perfobond connector (Vianna *et al*., 2009)	P_2F_120	h_{sc} =76.2	26.1	f_y =275	326.9	9.5	-
	P_2F_200	h_{sc} = 150	26.7		447.1	19.3	
	P_4F_200	h_{sc} = 150	26.9		433.8	22.1	
T-perfobond	TP_2F_120	h_{sc} =76.2	26.9	f_y =275	524.1	3.0	-

connector (Vianna *et al*., 2009)	TP_2F_200	h_{sc} = 150	26.2		682.8	5.5	
	TP_4F_120	h_{sc} = 150	27.1		691.2	4.3	
Headed stud-steel block connector (Liu *et al*., 2023)	T1-U-550-I	h_{sc} = 50	40.6 (76.1)	f_y =431	1,754.5	8.8	1,946
	T1-U-550-N	h_{sc} = 50	40.6 (76.1)	f_u =498	1,597.7	7.6	1,769
	T1-C-550-I	h_{sc} = 50	40.6 (50.9)		1,387.7	8.6	2,743
	T1-U-350-N	h_{sc} = 50	40.6 (76.1)		1,146.7	4.9	3,038
	T1-U-750-I	h_{sc} = 50	40.6 (76.1)		1,565.1	7.4	2,257
	T2-U-550-I	h_{sc} = 35	40.6 (76.1)		1,387.7	7.8	3,262
	T3-U-550-I	h_{sc} = 65	40.6 (76.1)		1,821.2	8.1	3,026
B-S connector (Zou *et al*., 2021)	SB-r20-h120	h_b =120	36.7 (43.6)	f_y =361.3	1,200.9	23.2	1,549
	SB-r20-h80	h_b =80		f_u =479.6	1,138.9	20.3	1,887
	SB-r20-h160	h_b =160			1,184.2	18.9	1,806
	SB-r0-h120	h_b =120			1,121.4	22.4	1,531
	SB-r20-h50d	h_b =50+20			1,207.9	21.1	2,099

Note:
For the concrete strength, the values in brackets denote the compressive strengths of the infilled concrete blocks pockets or the grouting materials.

Key findings of the experimental investigations are summarised as follows:

i) The shear resistances of headed shear studs are highly related to stud diameter, stud strength, concrete strength, and concrete elastic modulus. The shear resistance of a headed shear stud with a diameter of 19 mm and a height of 100 mm is about 100 kN (Shen *et al*., 2017). Consequently, a shear resistance of 1,000 kN should be provided by at least nine studs. Hence, grouped and large diameter headed studs encased by HPC were proposed to increase the shear resistance of the connectors. The shear resistance of a headed stud with a diameter of 30 mm, and embedded into HPC is about 350 kN, and the stiffness of the grouped headed shear studs with HPC is larger than those with NC, while the ductility of the former is smaller (Ding *et al*., 2024).

ii) Bolted shear connectors are able to be disassembled and they are widely used in prefabricated composite beams. The shear resistance of a bolted shear connector is comparable to a headed shear stud with similar dimensions and material strengths while the stiffness of the bolted shear connector is 50% smaller than the headed shear stud (Pavlović *et al*., 2013; Du *et al*.,

2020). Sudden slippage is found on the load-slippage curve of the bolted shear connector due to the clearance between the bolt shank and the hole, which results in a small initial stiffness in serviceability limit state.

Since the initial stiffness of a bolted shear connector is only about 100 kN/mm, LNSC and SYDBCs are proposed to solve the problem of small initial stiffness in bolted shear connectors. However, these methods make the construction process more complex, and the initial stiffness is increased to only about 200 kN/mm.

iii) The shear resistances of perfobond rib shear connectors are highly related to the thickness of the perforated steel plate, diameter of the perforated hole, diameter of the passing reinforcement, and concrete strength (Zhao *et al*., 2018; Ahn *et al*., 2010). The provision of passing reinforcements in perforated holes has a significant increase in both the resistance and the ultimate slippage. Compared with perfobond rib shear connector, the shear resistance and stiffness of T-perfobond rib shear connector are increased, while the ductility is decreased significantly to less than 6 mm (Vianna *et al*., 2009; 2013).

The shear resistance and stiffness of SBSC are 48% and 27% higher than grouped headed studs (Wang *et al*., 2019). However, although the stiffness of the welded steel block is remarkably large, the stress concentration at the root of steel block is severe, which results in severe local concrete crushing and reduced ductility. The use of HPC is demonstrated to be able to limit the concrete cracking and local crushing and increase the resistance of the shear connector (Liu *et al*., 2023).

Consequently, to propose a type of shear connector with large shear resistance, initial stiffness, and good ductility for easy on-site assembly of composite beams, it is favourable to combine

block shear connectors and bolted shear connectors. The welded steel block is able to increase the bearing resistance against the surrounding concrete, and the bolts are able to provide shear resistance, as well as pull-out resistance. Moreover, HPC with provision of fibres can be used to encase the shear connector to improve the tensile strength of the concrete in the vicinity of the steel block.

2.3 Numerical simulation

2.3.1 Numerical simulation on headed shear studs

a) Headed shear studs in profiled steel decking

A non-linear FE software Abaqus was employed by Lam *et al*. (2005) and Ellobody *et al*. (2006) to investigate the structural behaviour of headed shear studs in profiled steel decking. A quarter of the specimen was modelled to simulate the loading process due to double axes symmetry of the specimen, as shown in Fig. 2.8a). The yielding part of the concrete stress-strain curve was simulated using the Drucker Prager yield criterion model in the Abaqus material library. A tri-linear model was used to simulate the mechanical properties of the headed stud. However, no damage parameter was assigned to the concrete and the steel model, and hence, no descending part of the load-slippage curve is obtained in the simulated load-slippage curve, as shown in Fig. 2.8b).

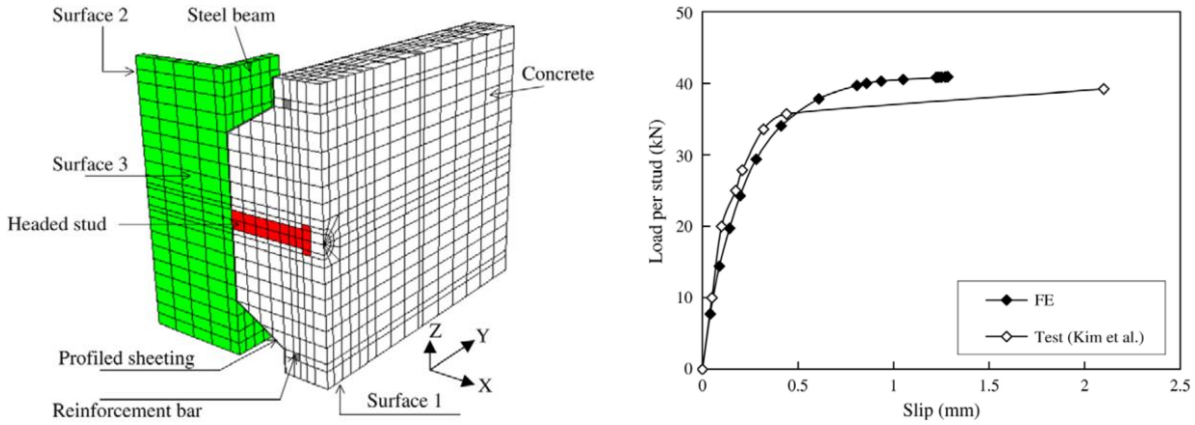

a) FE model

b) Comparison of the simulated and the measured load-slippage curves

Fig. 2.8 Modelling of headed studs by Ellobody *et al.* (2006)

b) Headed shear studs with SFRC

FE simulations were conducted by Nguyen *et al*. (2009) to investigate the structural behaviour of large diameter headed studs with diameters of 22, 25, 27, and 30 mm respectively. Eight-node reduced integration element (C3D8R) was used to model the steel beam, the headed stud and the concrete slab while truss element (T3D2) was used to model the steel reinforcement. The overall mesh size was 25 mm, and the smallest mesh size was about 3 mm. The stud was connected to the surrounding concrete using tie constraint, in which the nodes on the surfaces of the two components deformed together. Dynamic/ Explicit module in Abaqus was employed to simulate the loading process, and the loading rate was suggested to be 0.01 mm/s. Concrete damage plasticity (CDP) model was employed to simulate the mechanical property of the concrete. The material dilation angle (ψ) and eccentricity (ε) were taken as 20° and 0.1, respectively. The ratio of biaxial to uniaxial compressive strength (f_{b0} / f_{c0}) was taken as 1.16. The concrete constitutive model specified in BS EN 1992-1-1 (EC2, 2004) was used, in which the ultimate compressive strain and the ultimate tensile strain at zero stress were taken as 0.01 and 0.005, respectively. However, no damage parameter was incorporated in the concrete constitutive models.

A tri-linear stress-strain curve was used to simulate the mechanical properties of the headed stud. Both the damage initiation criterion and the evolution law for progressive damage of the steel material were employed to simulate the ductile fracture of the headed studs, and hence, the simulated load-slippage curve correlated well with the test results, as shown in Fig. 2.9.

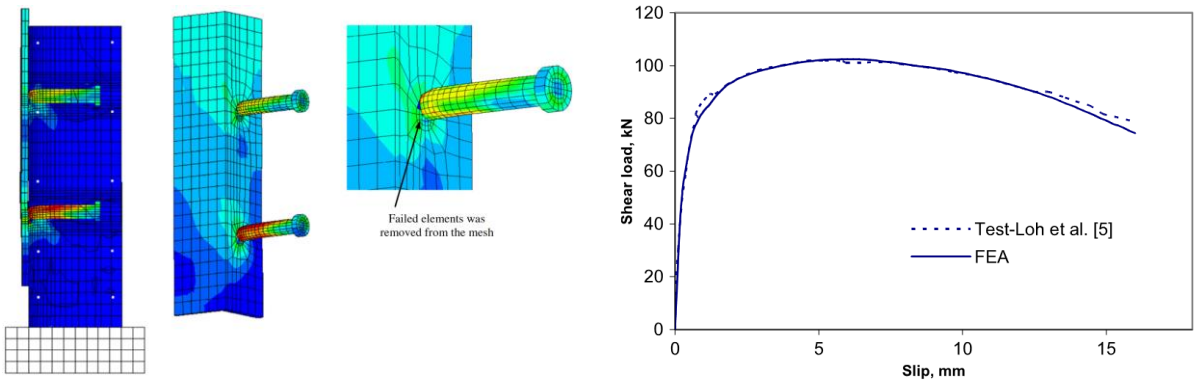

Fig. 2.9 Comparison of the measured and the simulated results (Nguyen *et al*., 2009)

c) Grouped headed shear studs in SFRCC

FE simulations were conducted by Luo *et al*. (2016) to further investigate the structural behaviour of grouped headed shear studs in steel fibre reinforced cementitious composite (SFRCC) using Abaqus 6.10.1. It should be noted that the weld collar was modelled using solid elements. The friction coefficient between the concrete slab and the beam flange was taken as 0.4. A tri-linear model was used to simulate the mechanical properties of the headed shear stud. It was assumed that the headed stud had fractured when the equivalent plastic strain (PEEQ) exceeded 0.2, and the SFRCC had crushed when the PEEQ exceeded 0.003. No damage parameter was incorporated in the constitutive models of the headed stud and the SFRCC. It was found that with an arrangement of small longitudinal spacing, the failure of SFRCC in the vicinity of the front stud lessened the confinement of the rear stud, and hence, the shear resistance of the rear stud was decreased. The plastic strain contour is shown in Fig. 2.10.

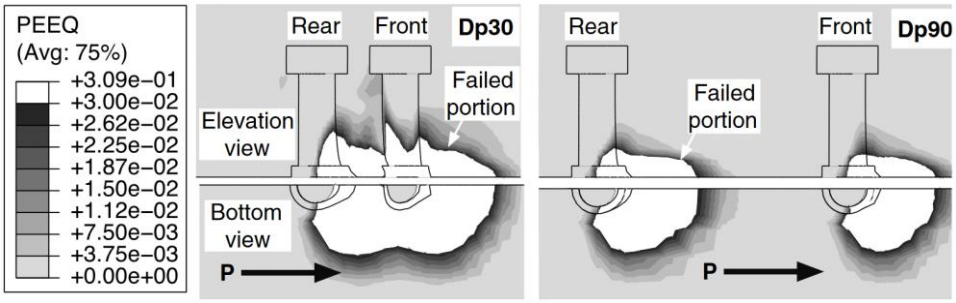

Fig. 2.10 Comparison of the plastic strain contour (Luo *et al.*, 2016)

Non-linear FE models were developed by Xu *et al*. (2022) to investigate the structural behaviour of large diameter short headed studs in thin UHPC slabs. The friction coefficient between the headed studs and the surrounding concrete was taken as 0.4. Both the compressive and the tensile damage parameters were incorporated into the models. The ratio of biaxial to uniaxial compressive strength (f_{b0}/f_{c0}) was taken as 1.16. The dilation angle (ψ) and flow potential eccentricity (ε) were taken as 30° and 0.1, respectively. A tri-linear model was employed to simulate the mechanical properties of the headed stud, and both the ductile damage and the damage evolution law were incorporated into the steel constitutive model. The equivalent fracture strain was assigned as 0.2. A uniformed load was applied on the top of the specimen with a loading rate of 0.01 mm/s to investigate its structural behaviour under quasi-static conditions. It was found that with an increase in stud diameter and concrete strength, the shear resistance was increased as parabolic and linear functions, respectively.

d) Grouped headed shear studs in precast concrete slab

Non-linear FE models were developed by Wang *et al*. (2021) to investigate the structural behaviour of grouped headed shear studs in precast concrete slab. The studs were fully encased by HPC blocks of the precast concrete slab. The mechanical properties of concrete were simulated

using the concrete constitutive models codified in Eurocode 4 (EC4, 2004). Both the concrete compressive and the tensile damage parameters were incorporated into the constitutive models. A tri-linear model was employed to simulate the mechanical properties of the headed studs. The strain ε_{us} corresponding to the ultimate stress σ_{us} of the stud steel was taken as 0.6%. The overall element size was taken as 25 mm, with a refined mesh of 3 mm applied in the regions where the headed studs were prone to failure. The friction coefficient between the headed studs and the surrounding concrete was taken as 0.25 and the friction coefficient between the concrete slab and the shear pocket was taken as 0.6. The simulated results were found to correlate well with the test results, demonstrating the validity of the numerical model.

2.3.2 Numerical simulation on bolted shear connectors

a) Bolted shear connectors in precast concrete slab

Non-linear FE simulations were conducted by Pavlović *et al*. (2013; 2016) to investigate the structural behaviour of bolted shear connectors and headed shear studs in precast concrete slabs. The threads on the bolt shanks were carefully modelled using tetra-hedron finite elements (C3D4). Specified pretension forces were applied onto the bolt shanks before loading. The friction coefficient between the bolt nuts and the threads as well as between the steel and the concrete was taken as 0.14. Both the concrete compressive and the tensile damage parameters were incorporated into the concrete constitutive models. The nominal ultimate compressive strain of the concrete was taken as 0.0035, and the cracking strain was taken as 0.001. Ductile fracture parameters with damage initiation and evolution criterions were incorporated into the constitutive model of the bolt steel. The equivalent plastic strain at the onset of damage was taken as 0.095 for bolts and 0.2 for headed studs. The equivalent plastic displacement at failure was taken as 0.2 mm

for bolts and 0.1 mm for headed studs. Comparison of the measured and the simulated stress-strain curves of the bolts and the headed studs is shown in Fig. 2.11 a). It was found that the simulation results correlated well with the test results, as shown in Fig. 2.11b), demonstrating the effectiveness of the numerical models. The non-linear behaviour of the bolted shear connectors resulted from both reduced bearing stress ahead of the embedded nut, and thread-hole penetration.

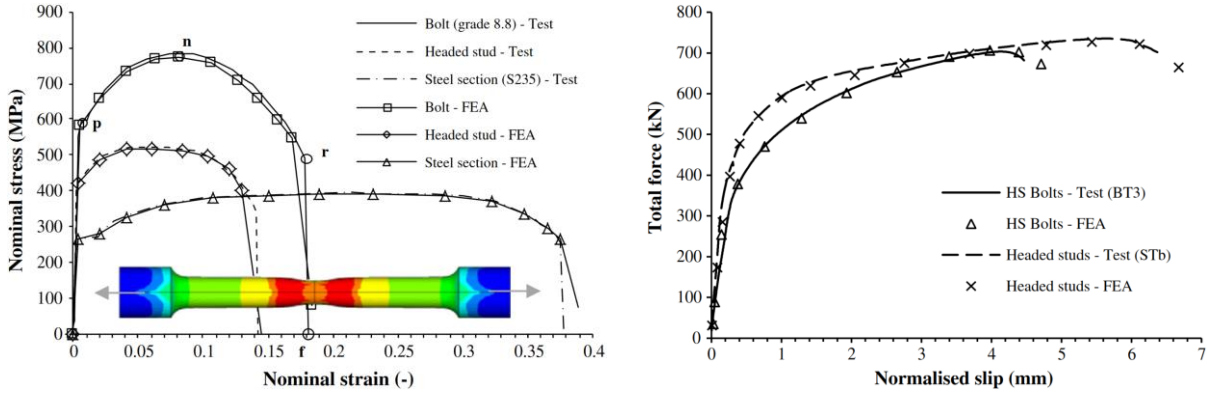

a) Comparison of the measured and the simulated stress-strain curves

b) Comparison of the measured and the simulated load-slippage curves

Fig. 2.11 Numerical simulations on headed studs and bolts (Pavlović *et al*., 2013)

b) HSFGB shear connectors in precast concrete slab

The structural behaviour of HSFGB shear connectors was investigated by Ataei *et al*. (2021) experimentally and numerically. The compressive peak strain of the concrete was taken as 0.002. The tensile strength of the concrete was considered to increase linearly up to 10% of the compressive strength, and then dropped to 0.0 at a strain of about 10 times of its failure strain. The friction coefficient between the steel beam and precast concrete slab was taken as 0.45, and the friction coefficient between the other components was taken as 0.25. It was found that the modelling technique was able to simulate the structural behaviour of HSFGB shear connectors in terms of failure modes and load-slippage curves, as shown in Fig. 2.12.

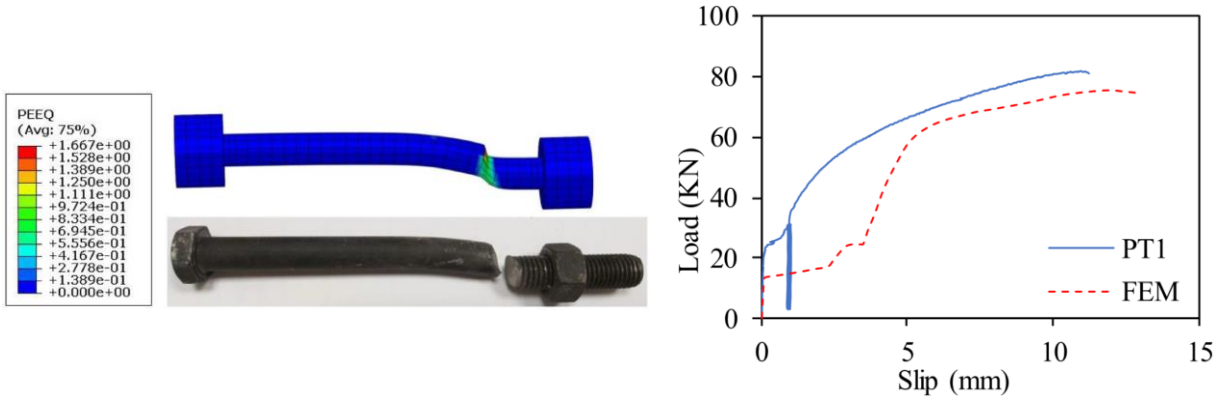

a) Plastic strain contour of bolts

b) Comparison of the measured and the simulated load-slippage curves

Fig. 2.12 Numerical simulations on HSFGB (Ataei *et al*., 2021)

Non-linear numerical simulations were conducted by Liu *et al*. (2015; 2016; 2017) to investigate the structural behaviour of HSFGB shear connectors. Grade 8.8 bolts with diameters of 16 and 20 mm were used as shear connectors. The compressive strength of geopolymer concrete (GPC) was 42 N/mm^2. Twenty-node quadratic brick element (C3D20R) was employed to model the bolted shear connectors due to their ability to capture stress concentrations. The overall mesh size was 20 mm, while the smallest mesh size was 3 mm. A tri-linear stress-strain model was employed to simulate the mechanical properties of the high-strength bolt with a fracture strain of 0.15. The friction coefficient between the steel and the concrete components was taken as 0.45, and the friction coefficient between the other components was 0.25. The simulated results correlated well with the test results in both the standard push-out tests and the beam tests, as shown in Fig. 2.13, demonstrating the effectiveness of the numerical models.

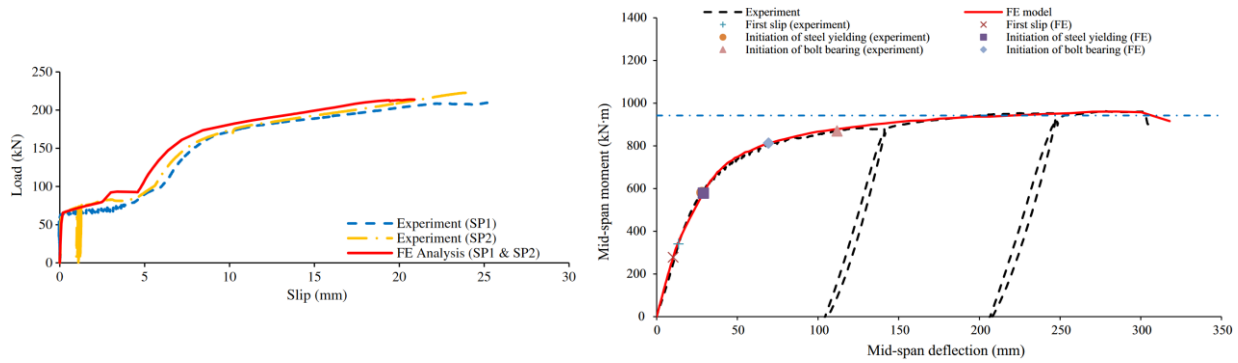

a) Comparison of load-slippage curves in standard push-out tests (Liu *et al.*, 2015)

b) Comparison of load-slippage curves in beam tests (Liu *et al*., 2017)

Fig. 2.13 Comparison of the simulated and the test results of HSFGB shear connectors

c) Tapered-nut stud bolt

In order to solve the problem of small initial stiffness in ordinary bolted shear connectors, a novel bolted shear connector with a tapered embedded nut and a Y-shaped stud bolt was proposed by Jung *et al*. (2022). Both the standard push-out tests and the numerical simulations were conducted to investigate the structural behaviour of the proposed bolted shear connectors. The diameter of the bolt shank was 22 mm with a steel grade of S275. The concrete compressive strength was 30 N/mm^2. In the FE models, the ultimate compressive strain was taken as 0.01 while the ultimate tensile strain was taken as 0.005. Both the compressive and the tensile damage parameters were incorporated to simulate the crushing and the cracking of the concrete. A tri-linear model was used to simulate the mechanical properties of the bolt. The friction coefficient between i) H-beam and nut; and ii) bolt and nut thread, was taken as 0.3, and the friction coefficient between the other components was taken as 0.14. The modelling results correlated well with the test results, demonstrating the effectiveness of the numerical models.

2.3.4 Summary

This section reviews the numerical simulations on headed shear studs and bolted shear connectors

in cast-in-situ and precast concrete slabs. Element types, element sizes, interactions, boundary conditions, and material constitutive models of the concrete and the shear connectors are described in detail. Key findings of the FE simulations are summarised as follows:

i) Dynamic/Explicit module in Abaqus are commonly used to simulate the quasi-static structural behaviour of the shear connectors to avoid the convergence problems. A uniformly displacement is applied onto the top of the specimen to act as a displacement control with a rate of 0.01 mm/s (Nguyen *et al*., 2009; Xu *et al*., 2022) or 0.5 mm/s (Shen *et al*., 2017; 2023). The loading rate should be carefully calibrated to guarantee that the kinetic energy does not exceed 10% of the internal energy. Due to double axes symmetry, a quarter of the specimen in the standard push-out test is modelled to investigate the structural behaviour of the shear connectors.

ii) Eight-node reduced integration elements (C3D8R) are commonly used to simulate the steel and the concrete components while truss elements (T3D2) are used to simulate the steel reinforcements in concrete slabs. The overall element size is taken as 25 mm, and a finer element size of about 3 mm is used in the regions where the components are prone to failure.

iii) Surface-to-surface contact with hard contact in the normal direction and coulomb friction in the tangential direction is employed on the surfaces of the structural components. The friction coefficients between the concrete and the steel, as well as between the steel and the steel components range from 0.14 to 0.45, while the friction coefficient between the precast concrete slab and the shear pocket is 0.6 (Wang *et al*., 2021). The friction coefficients between various components are summarised in Table 2.2. It should be noted that in bolted shear connectors, bolt threads have a great influence on the plastic ranges of the load-slippage curves, and hence, the contact conditions between the bolt threads and the bolt holes should

also be created.

Table 2.2 Friction coefficients between various components

Connector type	Contact surfaces	Friction coefficient
Headed studs (Luo *et al*., 2016; Xu *et al*., 2022)	Concrete slab and beam flange	0.40
Grouped headed studs (Wang *et al*., 2021)	Stud and surrounding concrete;	0.25
	Concrete slab and shear pocket	0.60
Bolts (Pavlović *et al*., 2016)	Bolt nuts and threads;	0.14
	Steel and concrete components	
HSFGB (Ataei *et al*., 2021; Liu *et al*., 2015)	Steel beam and precast concrete slab;	0.45
	Other components	0.25

iv) Concrete damage plasticity (CDP) model is employed to simulate the mechanical properties of concrete. The constitutive models of concrete codified in BS EN 1992-1-1 (EC2, 2004), GB20010-2010 (GB50010, 2010), and FIB Model Code 2010 (FIB, 2012) are able to be adopted, and both the compressive and the tensile damage parameters should be incorporated into the concrete material model to simulate concrete crushing and cracking.

v) A tri-linear model is employed to simulate the mechanical properties of the steel shear connectors, and both the damage initiation and the damage evolution parameters are incorporated into the constitutive model to simulate the ductile fracture of the shear connectors. The fracture strain and the displacement at failure are key parameters that influence the failure of the shear connectors, which are summarised in Table 2.3.

Table 2.3 The fracture strain and the displacement at failure for the steel connectors

Connector type	Fracture strain	Displacement at failure
Headed shear studs (Xu *et al*., 2022)	0.2	-
Bolts (Pavlović *et al*., 2016)	0.095	0.2
HSFGB (Liu *et al*., 2015)	0.15	-

2.4 Design rule

2.4.1 Codified rules for headed shear studs

a) Eurocode

In BS EN 1994-1-1 (EC4, 2004) and Hong Kong Code of Practice for the Structural Use of Steel (COP, 2011), formulae for shear resistance of a headed shear stud are shown as follows:

$$Q_m = \frac{0.8 f_u \pi d^2/4}{\gamma_v} \tag{2.12a}$$

or:

$$Q_m = \frac{0.29 \alpha d^2 \sqrt{f_c E_c}}{\gamma_v} \tag{2.12b}$$

whichever is smaller, with:

$\alpha = 0.2(\frac{h_{sc}}{d}+1)$ for $3 \le h_{sc}/d \le 4$

$\alpha = 1$ for $h_{sc}/d > 4$

where,

d is the diameter of the shank of the stud, $16\text{mm} \le d \le 25\text{mm}$;

f_u is the specified ultimate tensile strength of the material of the studs but not greater than 500 N/mm^2;

f_c is the compressive strength of the concrete at the age considered, of density not less than 1750 kg/m^3;

γ_v is the partial factor. The recommended value is 1.25;

h_{sc} is the overall nominal height of the stud.

The design formulae codified in Hong Kong Code of Practice for the Structural Use of Steel (COP, 2011) are similar to the formulae codified in BS EN 1994-1-1 (EC4, 2004) while the design value of E_c is different.

In BS EN 1994-1-1 (EC4, 2004), the elastic modulus for concrete is defined according to BS EN 1992-1-1 (EC2, 2004), which is shown as follows:

$$E_c=22(\frac{f_{cm}}{10})^{0.3} \quad (2.13)$$

where,

E_c is the modulus of elasticity, which is defined by the secant value between $\sigma_c=0$ and $0.4\,f_{cm}$; and

f_{cm} is the mean compressive strength at 28 days.

In Hong Kong Code of Practice for the Structural Use of Concrete (COP, 2013), the design values of f_{cu} and E_c are limited to a maximum concrete grade of C60. The concrete elastic modulus is determined by:

$$E_c=3.46\sqrt{f_{cu}}+3.21 \quad (2.14)$$

where,

E_c is the short-term static modulus of elasticity; and

f_c is the concrete compressive strength in N/mm^2.

b) American specification

In AISC360-22 (AISC, 2022), the design shear resistance of a headed shear stud embedded in a solid concrete slab or in a composite slab with decking is determined by:

$$Q_m = 0.5A_s\sqrt{f_cE_c} \le 0.75A_s f_u \quad (2.15)$$

where,

A_s is cross-sectional area of headed shear studs;

f_c is compressive strength of concrete;

E_c is modulus of elasticity of concrete. $E_c=4{,}739\sqrt{f_c}$ for normal weight concrete; and

f_u is specified minimum tensile strength of a headed shear stud.

c) Chinese Standard for Design of Steel Structures

In GB50017-2017 (GB50017, 2017), the design formula for shear resistance of a headed shear stud in normal weight concrete or light weight concrete is determined by:

$$Q_m = 0.43\, A_s \sqrt{E_c f_c} \leq 0.7\, A_s f_u \tag{2.16}$$

where,

E_c is the elastic modulus of concrete; $E_c = 10^5/(2.2+\frac{34.7}{f_c})$

f_c is characteristic compressive strength of concrete;

A_s is the cross-sectional area of headed shear studs; and

f_u is the ultimate strength of a steel stud.

2.4.2 Codified rules for channel shear connectors

a) American specifications

In AISC 360-22 (AISC, 2022), the nominal shear strength of a hot-rolled channel anchor embedded in a solid concrete slab is determined by:

$$Q_m = 0.3(t_f+0.5t_w)\, l_a \sqrt{f_c\, E_c} \tag{2.17}$$

where,

l_a is length of the channel section;

t_f is thickness of the channel flange; and

t_w is thickness of the channel web.

b) Chinese Standard for Design of Steel Structures

In GB50017-2017 (GB50017, 2017), the design shear resistance of a channel shear connector is determined as follows:

$$Q_m = 0.26\,(t + 0.5\, t_w)\, l_a \sqrt{E_c f_c} \tag{2.18}$$

where,

t_f is the average thickness of channel flange;

t_w is the thickness of the channel web; and

l_a is the length of the channel section.

2.4.3 Design rules for block connectors

In ENV1994-1-1 (EC4, 1992), the connectors may be designed as block connectors if the front is so stiff that it can reasonably be assumed that at failure the pressure on the concrete in front of the connector is uniformly distributed, and the design shear resistance of a block connector is determined by:

$$Q_m = \alpha_1 A_{c1} f_{ck} \tag{2.19}$$

where

A_{c1} is the bearing area of the concrete in the vicinity of the steel block, as shown in Fig. 2.14;

A_{cp1} is the projected area of the concrete in the front surface of the connector enlarged at a slope of 1:5 to the rear surface of the adjacent connector. Only the parts of A_{cp1} falling within the concrete section may be taken into account;

α_1 is equal to $\sqrt{A_{cp1}/A_{c1}}$ but not larger than 2.5 for normal density concrete or 2.0 for lightweight aggregate concrete; and

f_{ck} is the characteristic concrete cylinder strength in compression.

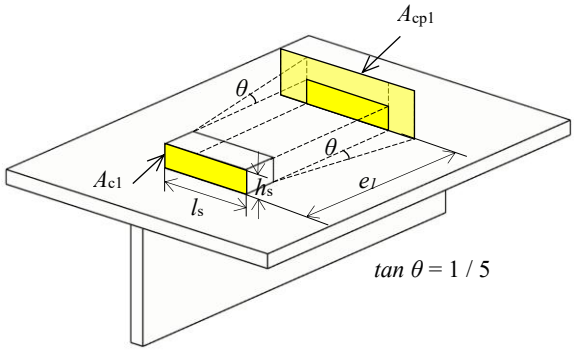

Fig. 2.14 Schematic diagram of a block connector (EC4, 1992)

2.4.4 Design rules suggested in literature

Based on the literature review presented in Section 2.2, design rules for shear resistances and load-slippage models of various types of connectors are summarised in Table 2.4.

Table 2.4 Design rules for shear resistances and load-slippage models of shear connectors

Connector types	Shear resistances	Load-slippage models
Headed studs in NC (Ernst, 2006)	$Q_m = 0.5\, A_s \sqrt{f_c E_c}$	$Q = Q_m(1\text{-}e^{-18s})^{0.4}$
Headed studs in HSC (Xue *et al*., 2008)	$Q_m = 3\lambda A_s f_u (\frac{E_c}{E_s})^{0.4} (\frac{f_c}{f_u})^{0.2}$	$\frac{Q}{Q_m} = \frac{s}{0.5+0.97s}$
Grouped headed studs in HPC (Wang *et al*., 2021)	-	$\frac{Q}{Q_m} = (1\text{-}e^{-1.55s})^{0.64}$
Single nut embedded bolts (Du *et al*., 2020)	$Q_m = 0.22(h_b / d)^{0.4} A_s \sqrt{f_c E_c}$ $Q_m = \alpha_v A_s f_u$	-
LNSC (He *et al*. 2022)	$Q_m = \min(\eta_1 A_t \sqrt{E_c f_{ck}}, \eta_2 A_b f_u)$	-
HSFGB (Zhang *et al*., 2020)	$Q_m = \min(0.76\, A_s f_u, 0.5\, A_s \sqrt{f_c\, E_c})$	$Q = Q_m(1\text{-}e^{-0.2\,s})^{0.4}$
SBSCs (Wang *et al*., 2019)	$Q_m = a\, A_l f_{cb} + b\, A_r f_y + c\, f_t\, b\, h_{slab}$	-

2.4.5 Summary

This section reviews the design rules for shear resistances and load-slippage models of headed shear studs, bolted shear connectors, channel shear connectors, perfobond shear connectors, and block shear connectors. In general, the geometries of the shear connectors (cross-sectional area, width and height of steel connectors) and material strengths (yield and tensile strengths of the steel connector as well as the compressive strengths of the concrete) are key parameters that influence the structural behaviour of the shear connectors. Semi-empirical approach is employed to predict the shear resistances of these shear connectors.

i) In headed shear studs, concrete failure and stud failure are identified as two typical failure modes. The minimum of the shear resistances against these two failure modes are determined as the predicted shear resistances. In addition, several studies proposed design formulae against stud failure considering the effect of weld collars.

ii) Since bolted shear connectors and headed shear studs exhibit similar failure modes, their

design formulae share analogous form but differ in the coefficient in each term.

2.5 Conclusions

A comprehensive literature review on experimental investigations, numerical simulations, and design rules of various types of shear connectors is conducted. Typical failure modes and deformation characteristics in terms of initial stiffness, shear resistance, and ultimate slippage are presented. Non-linear FE models were developed to investigate the "stress and strain" distributions and deformation characteristics of the shear connectors. The modelling techniques are listed in detail, and they are calibrated against the test results to validate their efficiency. The key findings have a great inspiring effect on the investigation into new types of shear connectors. Based on the literature review, the research gaps are identified as follows:

i) Although various methods have been used to increase the initial stiffness of a bolted shear connector, and the initial stiffness is able to be increased to about 200 kN/mm, which is only 10% of the initial stiffness of a block shear connector. However, limited research has focused on the structural behaviour of block shear connectors.

ii) One typical failure mode of a block shear connector is local concrete crushing in the vicinity of the steel block, and hence, it is necessary to use HPC to encase the block shear connector to improve the tensile strength of the concrete in the vicinity of the steel block.

iii) The shear resistances of bolted shear connectors in cast-in-situ concrete slab and precast concrete slab are almost the same, while the initial stiffness of those in precast concrete slab is smaller (Pavlović *et al*., 2013). Moreover, these bolted shear connectors are easy to be assembled and demounted on site. Hence, it is applicable to use bolted shear connectors together with precast concrete slabs for easy on-site assembly of prefabricated composite

beams. As the preformed holes in the precast concrete slab are usually filled with HPC, the size of the infilled concrete block may have a certain influence on the structural behaviour of the shear connections. However, there is limited research focused on the influence of the size of the concrete block on the structural behaviour of the shear connection, and further research is needed in this area.

iv) Although the threads of the bolt shank have a significant influence on the initial stiffness of the bolted shear connectors, limited research created the threads in the FE models. Moreover, to solve convergence problems in Abaqus, Dynamic/Explicit analysis method is commonly used to simulate the quasi-static behaviour of the shear connectors, and it is necessary to simulate the structural behaviour using the Standard/Static module in Abaqus. In addition, compressive and tensile damage parameters of the concrete are necessary to be incorporated into the FE models to simulate the concrete cracking and crushing. Ductile damage parameters of the steel connectors are necessary to be incorporated into the models to simulate the failure of the shear connectors.

v) There is no systematic design method available for bolted shear connections with the provision of steel blocks in prefabricated composite beams.

CHAPTER 3

EXPERIMENTAL INVESTIGATIONS USING SINGLE-SIDED PUSH-OUT TESTS

3.1 Introduction

This chapter presents an experimental investigation into the structural behaviour of shear connections with various types of shear connectors. The shear connectors are encased by concrete blocks of 180×180×180 mm in dimensions to act as twin shear connections, and these shear connections were subject to single-sided push-out tests to investigate the influence of connector configuration, fibre content, and bolt diameter on the deformation characteristics of the shear connections. A total of 39 single-sided push-out tests were conducted to quantify the deformation characteristics of the shear connections with three types of bolted shear connectors, i.e. Types A, B, and C, and three types of welded shear connectors, i.e. Types SC, BC and PC. A detailed account of the experimental investigation in terms of test programme, fabrication of test specimens, test setup and instrumentation, as well as loading procedures are presented. Together with the results of the single-sided push-out tests, results of the material tests on concrete blocks, steel bolts, steel plates and steel reinforcements are also reported.

In general, when presenting the test results of these single-sided push-out tests, the deformations at failure of all shear connections are firstly presented, followed by measured load-slippage curves and key deformation characteristics. Then, the load-slippage curves of the connections with various connector types, fibre content, and bolt diameters are thoroughly compared. Afterwards, a design method is developed for the proposed shear connections with various types of shear connectors.

Based on the investigation, the shear connections with favourable structural behaviour are selected for subsequent standard push-out tests to further investigate the structural behaviour of these shear connections for applications in prefabricated composite beams in highway bridges.

3.2 Experimental assessments

3.2.1 Test programme

The test programme of the single-sided push-out tests is summarised in Table 3.1. A total of 39 shear connections with six types of shear connectors are investigated as follows:

- Type A denotes a pair of specially designed bolts (each having a partially threaded shank) with a steel block, i.e. Configuration RBN, with a nominal bolt diameter of 30 mm.
- Type B denotes a pair of specially designed bolts (each having a partially threaded shank) with a steel block, i.e. Configuration RBN, *but* with a nominal bolt diameter of 24 mm.
- Type C denotes a pair of Grade 8.8 bolts, i.e. Configuration R, with a nominal bolt diameter of 30 mm. It should be noted that no steel block is provided.
- Type SC denotes a solid connector with two welded steel reinforcements. This is a basic form of the proposed welded shear connector, which is simple to fabricate and stiff under shear forces. However, as there is a sudden change in its lateral stiffness at the top of the shear connector, extensive local concrete cracking may take place.
- Type BC denotes a box connector which consists of four welded steel plates. It is proposed to reduce the problem of a sudden change in the lateral stiffness near the top of the shear connector to reduce potential concrete cracking.
- Type PC denotes a U-shaped profiled connector. It is proposed to simplify fabrication and to reduce the extent of welding as a cold-bent steel plate is adopted.

Table 3.1 Test programme of single-sided push-out tests

Connector type	Bolt diameter / plate thickness (mm)	Designation	Size of concrete blocks (mm)	Materials of concrete blocks	Dimensions of connectors (mm)
RBN	30	A-C1-p-a/b/c	180×180×180	C100+1.5%	120×60×30
		A-C1-q-a/b/c		C100+0.8%	
		A-C1-r-a/b/c		C100+0.4%	
		A-C1-s-a/b/c		C100+0.0%	
		A-C0-p-a/b/c	180×180×180	C100+1.5%	
		A-C0-q-a/b/c		C100+0.8%	
		A-C0-r-a/b/c		C100+0.4%	
		A-C0-s-a/b/c		C100+0.0%	
RBN	24	B-C1-p-a/b	180×180×180	C100+1.5%	120×60×30
R	30	C-C1-p-a/b	180×180×180	C100+1.5%	-
SC	-	SC-h3-C1	180×180×180	C100+1.5%	H = 65
		SC-h2-C1			H = 50
		SC-h1-C1			H = 35
BC-a 4	12	BC-a -C1	180×180×180	C100+1.5%	H = 80
BC-b 3		BC-b -C1			
BC-c T		BC-c -C1			
BC-d L		BC-d -C1			
PC-r	12	PC-r - C1	180×180×180	C100+1.5%	H = 80
PC		PC-C1-a/b		C100+1.5%	
		PC-C1-s		C100+0.0%	

Fig. 3.1 shows details of different types of shear connectors in the proposed connections. It is worth noting that for Connector RBN, the steel block is pre-welded onto the base plate in fabrication shop. It should be further noted that:

a) In Series A, there are four groups of shear connections with Type A connector and Concrete C1, namely Tests A-C1-p, A-C1-q, A-C1-r, and A-C1-s, with fibre content in concrete blocks of 1.5%, 0.8%, 0.4%, and 0.0%, respectively. Moreover, there are four groups of shear connections with Type A connector and Concrete C0, namely Tests A-C0-p, A-C0-q, A-C0-r, and A-C0-s, with fibre content in concrete blocks of 1.5%, 0.8%, 0.4%, and 0.0%, respectively.

b) In Series SC, there are three shear connector variations, namely Tests SC-h1, SC-h2 and SC-h3, with heights of the solid steel blocks, h, of 35, 50, and 65 mm respectively.

c) In Series BC, there are four shear connector variations, namely, Tests BC-a, BC-b, BC-c and BC-d, with different welding arrangements as follows:

- In Test BC-a, all *four* steel plates of the fabricated box connector are welded onto the base plate.
- However, in Tests BC-b and BC-c, only *three* and *two* steel plates of the fabricated box

connector are welded onto the base plate, respectively.

- In Test BC-d, only those *two* steel plates of the fabricated box connector *running parallel to* the direction of the applied load are welded onto the base plate.

d) In Series PC, two shear connectors with the same sizes and shapes are considered, but with different orientations, as follows:

- In Test PC, the profiled connector is arranged in such a way that the U-shaped profile runs against the direction of the applied load.
- In Test PC-r, the profiled connector is arranged to be opposite to that in Test PC.

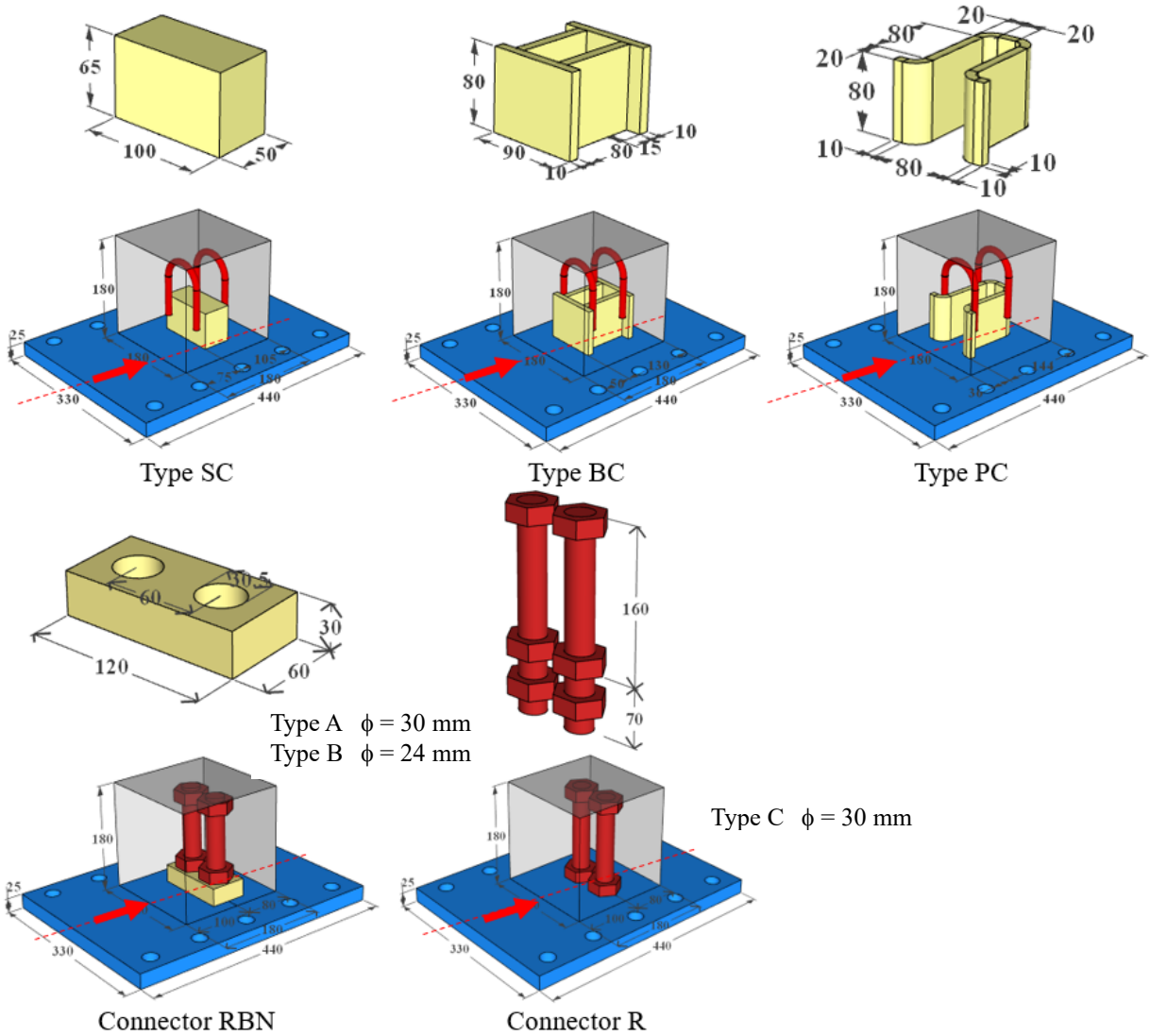

Fig. 3.1 Arrangements of the proposed shear connectors

It should be noted that there are three different types of steel plates used in the shear connectors. Shear connectors of Types A, B, and C are manufactured with S355 steel plates and G8.8 steel bolts. Shear connectors of Types SC and BC are manufactured with S235 steel plates while connectors of Type PC are manufactured with S275 steel plates. Moreover, two different types of concrete designated as Types C1 and C0 are used as follows:

- Type C1 denotes high strength concrete with a compressive cube strength of 100 N/mm^2. The raw materials are shown in Fig. 3.2. The concrete mix proportion is shown in Table 3.2, and the water cement ratio of Concrete C1 is 0.21. The steel fibre content in Concrete C1 is: a) 1.5% in Test A-C1-p; b) 0.8% in Test A-C1-q; c) 0.4% in Test A-C1-r; and d) 0.0% in Test A-C1-s.
- Type C0 denotes normal strength concrete with a compressive cube strength of 50 N/mm^2. The concrete mix proportion is shown in Table 3.2, and the water cement ratio of Concrete C0 is 0.50. The steel fibre content in Concrete C0 is: a) 1.5% in Test A-C0-p; b) 0.8% in Test A-C0-q; c) 0.4% in Test A-C0-r; and d) 0.0% in Test A-C0-s.

It should be noted that steel fibres are introduced to distribute stresses and strains effectively within the concrete blocks to reduce concrete crushing and cracking. Samples of these fibres are shown in Fig. 3.2. The following two types of steel fibres are used together: a) straight steel fibres with a length l_f of 13 mm and a diameter d_f of 0.2 mm; and b) hooked steel fibres with a length l_f of 22 mm and a diameter d_f of 0.2 mm.

The dimensions of the concrete blocks in all the shear connections are 180×180×180 mm while detailed dimensions of the test specimens are shown in Fig. 3.3.

Fig. 3.2 Concrete and raw materials

Table 3.2 Concrete mix proportion (kg / m^3)

Concrete	Fibre content (%)	Cement	Silica fume	Fly ash	Water	Super-plasticizer	Steel fibre	River sand	Coarse aggregate (10 mm)	Coarse aggregate (20 mm)
C1-p	1.5	558.5	128.9	171.9	180.4	25.8	117.8	859.3	408.0	-
C1-q	0.8	563.2	130.0	173.3	182.0	26.0	62.8	866.5	408.0	-
C1-r	0.4	565.9	130.6	174.1	182.8	26.1	31.4	870.6	408.0	-
C1-s	0.0	568.6	131.2	174.9	183.7	26.2	0.0	874.7	408.0	-
C0-p	1.5	391.6	-	-	195.8	3.69	117.8	669.6	364.2	728.3
C0-q	0.8	394.3	-	-	197.2	3.69	62.8	674.3	366.7	733.5
C0-r	0.4	395.9	-	-	198.0	3.69	31.4	677.0	368.2	736.4
C0-s	0.0	400.0	-	-	200.0	3.69	0.0	684.0	372.0	744.0

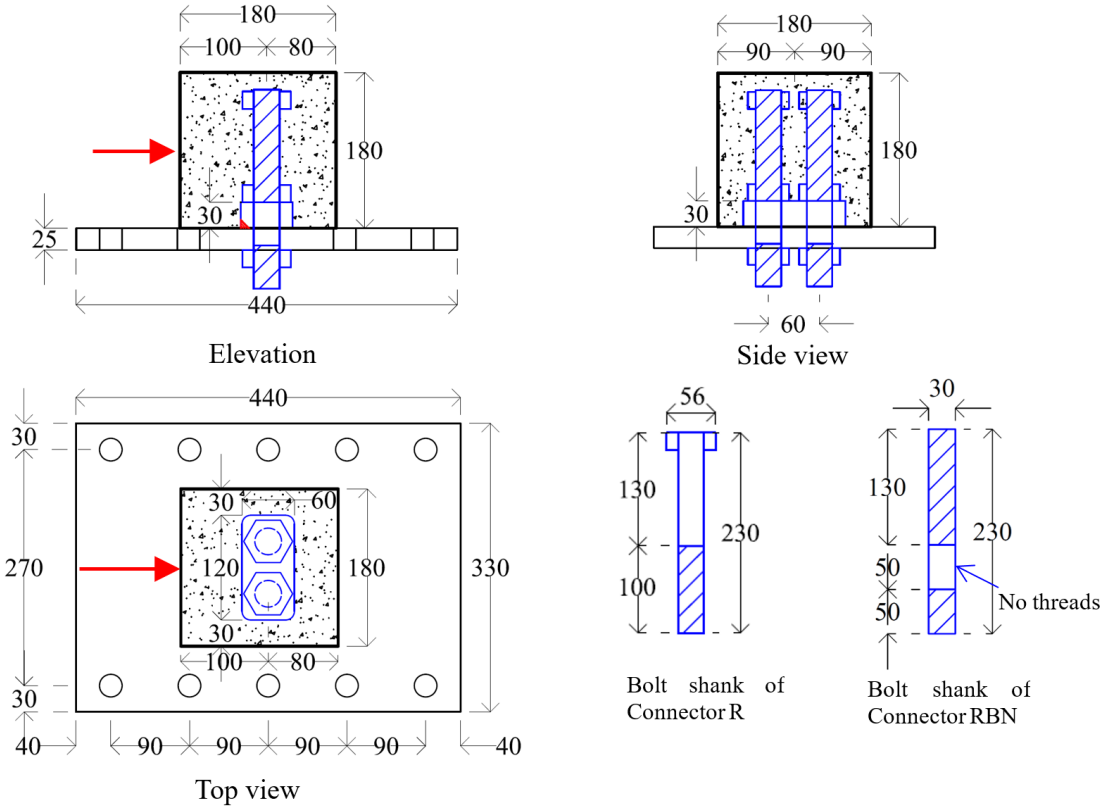

Fig. 3.3 Detailed dimensions of the test specimens

3.2.2 Specimen preparation

The fabrication procedure of the test specimens are shown in Fig. 3.4, and it is described as follows:

i) Application of pretension forces in bolts

- For bolts with a diameter of 30 mm, a torque of 1,200 N•m was applied through a torque wrench to produce a pre-tension force of 280 kN onto the bolt shank, i.e. 60% of its tensile resistance.

- For bolts with a diameter of 24 mm, a torque of 600 N•m was applied through a torque wrench to produce a pretension force of 156 kN onto the bolt shank.

For each test specimen, a pair of bolts were installed onto the base plates according to the specified torque mentioned above.

ii) Installation of steel formwork and placement of infilled concrete

Two pieces of C-shaped steel plates were installed onto the base plates with four M24 steel bolts to act as formwork. Steel fibre reinforced concrete (SFRC) was cast onto the steel formwork, and it was cured for at least 3 days before removing the formwork.

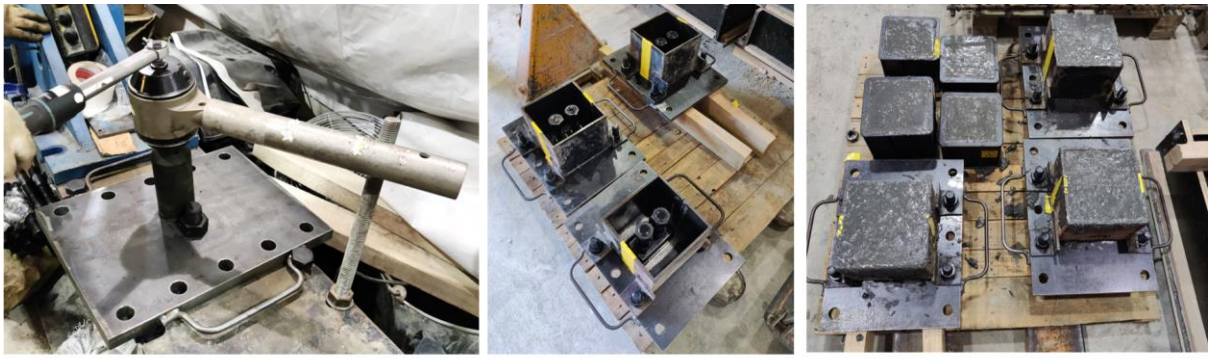

Application of pre-tension force Installation of formwork Cast of concrete blocks

Fig. 3.4 Fabrication procedures of test specimens

In order to obtain mechanical properties of various constituent components, three coupons were extracted from the bolts, the steel plates as well as from the steel reinforcements for standard tensile tests to attain their yield and tensile strengths, and elastic modulus. The dimensions of the coupons for steel bolts and plates were designed according to ISO 6892-1:2019 (ISO6892, 2019), as shown in Fig. 3.5. Moreover, for each batch of concrete, a total of five concrete cubes of 150 mm in size, and three cylinders of 150 mm in diameter and 300 mm in height, were prepared for compression tests. A total of three cylinders of 100 mm in diameter and 200 mm in height were also prepared for splitting tests. These concrete cubes were tested 28 days after casting as well as on the day of the push-out tests to obtain the compressive strengths of the concrete. The material tests for concrete are shown in Fig. 3.6.

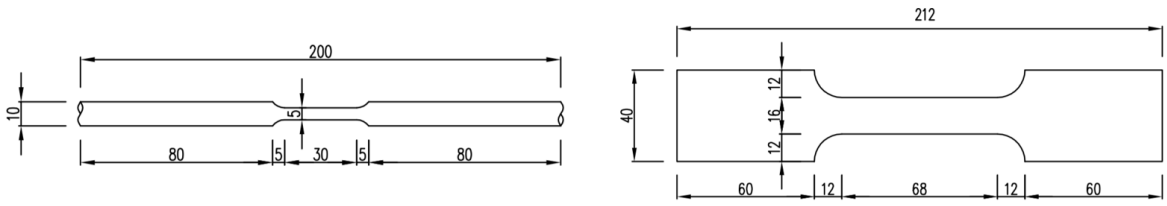

a) Coupon for steel bolts b) Coupon for steel plates

Fig. 3.5 Dimensions of steel coupons

a) Concrete cube test

b) Concrete splitting test

c) Concrete cylinder test

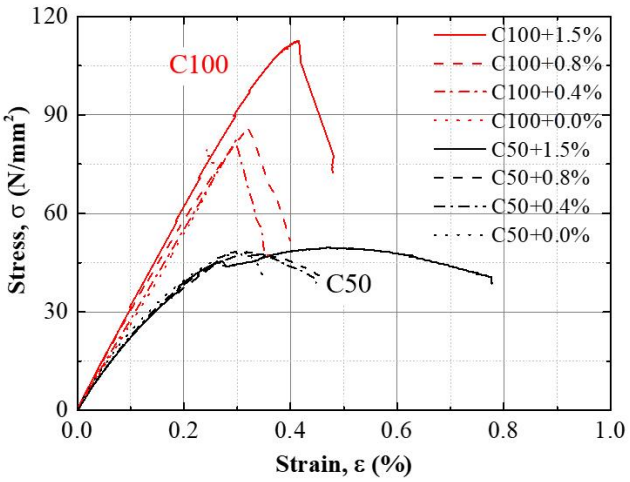

d) Stress-strain curves for concrete cylinders

Fig. 3.6 Material tests for concrete

3.2.3 Test setup and loading procedures

Typical test setup and instrumentation of the single-sided push-out tests are illustrated in Fig. 3.7. In each test, the base plate was firmly bolted onto the testing system through ten bolts, and a hydraulic jack with a capacity of 1,500 kN was employed to apply a horizontal load onto the

concrete block. Five LVDTs were provided to measure the displacements of concrete blocks and steel plates to obtain the relative slippages between the concrete block and the base plate. All measurements of the applied forces and the displacements of the test specimens were acquired at a close time interval with a data logger, and all the measured data were stored in a computer for subsequent data analysis.

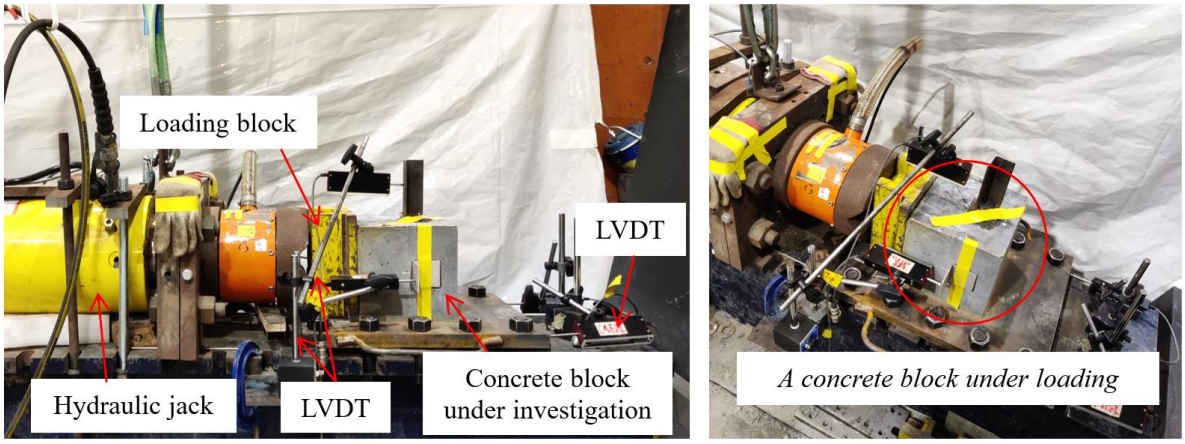

Fig. 3.7 Test setup and instrumentation

The following loading procedure was adopted for each test:

- In order to ensure adequate response in the initial deformation range, a small lateral force of 2 to 3 % of the expected failure load was applied onto the test specimen. Then, the applied force was increased up to 40% of the expected failure load at a rate of 25 to 50 kN per minute. After that, the applied force was gradually decreased to 2 to 3 % of the expected failure load. This pre-loading process was repeated 25 times in not less than 30 to 40 minutes.
- After completion of the loading and unloading process, the applied force was increased at a rate of 25 to 50 kN per minute until there was a significant unloading, i.e. about 80 to 85 % of the maximum applied force, or there was a sudden failure in the test specimen.

The maximum applied force was then regarded as the measured shear resistance of the test specimen, and photos of the test specimen were taken at this point as representative of failure.

3.3 Test results

Key results of the single-sided push-out tests on shear connections with various shear connectors, as well as the material tests on both the steel and the concrete, are presented in this section.

3.3.1 Material tests

A servo hydraulic testing system with a loading capacity of 500 kN was employed to obtain the mechanical properties of the bolts, the steel plates and the steel reinforcements. The mechanical properties, including the Young's modulus E, the yield strength f_y, and the tensile strength f_u, are shown in Table 3.3. According to ISO 6892-1: 2019 (ISO6892, 2019),

- for the steel plate of each of the shear connectors, the yield strength is defined as the *lower* yield value in the yield plateau of the stress-strain curve, i.e. the *minimum* stress during yielding without any rapid initial transient effect; and
- for the steel reinforcement, the yield strength is defined as the stress at either i) the *lower* first yield value along the yield plateau, or ii) a proof strain of 0.2% of the stress-strain curve.

For both cases, the tensile strengths of the steel are the maximum stresses of the stress-strain curves while the elastic modulus of the steel is defined as the slope of the line between the points where the stresses are 10% f_y and 40% f_y.

Table 3.3 Mechanical properties of the steel

Material	E_s (kN/mm^2)	f_y (N/mm^2)	f_u (N/mm^2)
M24 bolt: d = 5 mm	223	615	886
M30 bolt: d = 5 mm	213	553	835
S235 steel: t = 10 mm	218	278	430
S275 steel: t = 10 mm	212	305	450
S355 steel: t = 10 mm	222	375	519
Steel reinforcement ϕ = 12 mm	213	485	634

The mechanical properties of the concrete with various fibre content are shown in Table 3.4 and Fig. 3.6. It is shown that for Concrete C100, the average ratio of concrete cylinder to cube

strength is 0.92, while in Concrete C50, the average ratio of concrete cylinder to cube strength is merely 0.81. It should be noted that the average ratio of the measured to the design elastic modulus of concrete given in the Code of practice for the structural use of concrete (COP, 2013) is 0.80.

For those Concrete C100 with or without steel fibres, the compressive strength of the concrete with 1.5% steel fibres is found to have increased with a factor of 1.33, and their tensile strength is increased with a factor of 2.24. For those Concrete C50 with or without steel fibres, the compressive strength of the concrete with 1.5% steel fibres is slightly increased with merely a factor of 1.07, and the tensile strength is increased with a factor of 1.34. Hence, addition of steel fibres to C100 concrete is demonstrated to be highly effective in increasing both the compressive and the tensile strengths of the concrete. Addition of steel fibres to the C50 concrete is shown to be effective in increasing only its tensile strengths.

Table 3.4 Mechanical properties of the concrete with various fibre content

Test	$f_{cu,28}$ (N/mm^2)	$f_{cu,test}$ (N/mm^2)	$f_{cy,test}$ (N/mm^2)	$f_{cy,test}$ / $f_{cu,test}$	f_{ct} (N/mm^2)	E_c (N/mm^2)	$E_{c,HK}$ (N/mm^2)	E_c / $E_{c,HK}$
A-C1-p	106.0	111.2	111.1	**1.00**	11.2	32.4	39.7	**0.82**
A-C1-q	96.7	105.0	87.2	**0.83**	7.9	31.0	38.7	**0.80**
A-C1-r	85.4	92.3	85.6	**0.93**	6.4	29.8	36.5	**0.82**
A-C1-s	78.7	83.5	90.3	**1.08**	5.0	28.2	34.8	**0.81**
A-C0-p	61.8	63.3	49.7	**0.79**	5.5	22.5	30.7	**0.73**
A-C0-q	54.7	56.1	45.9	**0.82**	4.3	23.1	29.1	**0.79**
A-C0-r	57.4	59.7	48.0	**0.80**	4.3	25.0	29.9	**0.83**
A-C0-s	57.7	59.4	48.6	**0.82**	4.1	24.6	29.9	**0.82**

Notes:

$f_{cu,28}$ denotes the measured cube strengths of concrete blocks at 28 days;
$f_{cu,test}$ denotes the measured cube strengths of concrete blocks on the testing days;
$f_{cy,test}$ denotes the measured cylinder strengths of concrete blocks on the testing days;
f_{ct} denotes the measured tensile strengths of concrete blocks at 28 days;
E_c denotes the measured elastic modulus of concrete blocks; and
$E_{c,HK}$ denotes the elastic modulus of concrete blocks according to the Hong Kong Concrete Code.

It should be noted that compression tests on the concrete cubes of 150 × 150 × 150 mm after 28 days of casting were carried out, and the measured compressive cube strengths $f_{cu,150}$ are presented in Table 3.4. In addition, compression tests on similar concrete cubes were carried out at the days of single-sided push-out tests, and they are also provided in Table 3.5 for comparison.

Typical failure modes and key results of the single-sided push-out tests are summarised in Table 3.5. The following two typical failure modes were identified in the tests:

a) Concrete failure: Mode CF

Mode CF is critical in connections with Types A, B, and SC connectors. Owing to an abrupt change in stiffness near the top of the shear connectors inside the concrete blocks, the concrete suffers from severe cracking and crushing.

b) Shear fracture of steel connectors: Mode SFS

This failure mode is critical in all connections with Types C, BC and PC connectors, in which all bolts in Connector R, and steel plates in the box and the profiled connectors are completely fractured in shear.

In Table 3.5, Q_m is the measured shear resistance, s_m is the measured slippage corresponding to Q_m, s_u is the measured slippage at failure, K is the initial stiffness of the load-slippage curve, and $Q_{0.5}$ is the applied load corresponding to a slippage of 0.5 mm. It should be noted that the slippage is defined as the difference between the displacement of the concrete block and that of the base plate. The initial stiffness is defined as the slope of the line between the points where the applied loads are 0 and 0.5 Q_m .

In order to further investigate the structural behaviour of each specimen, the failure pattern and load-slippage curves are presented below.

Table 3.5 Key results of single-sided push-out tests

Test	$f_{cu,150}$ (N/mm^2)	Q_m (kN)	s_m (mm)	s_u (mm)	Failure mode	K (kN/mm)	$Q_{0.5}/Q_m$ (%)
A-C1-p-a	111.2	939.5	10.9	21.5	CF	365	16
A-C1-p-b	111.2	865.3	13.7	21.2	CF	330	12
A-C1-p-c	111.2	946.0	11.0	29.6	CF	255	-
A-C1-q-a	105.0	841.4	7.7	18.9	CF	289	-
A-C1-q-b	*105.0*	*739.7*	*7.5*	*27.9*	*CF*	*267*	*18*
A-C1-q-c	105.0	822.3	9.3	23.8	CF	376	-
A-C1-r-a	92.3	742.7	6.3	15.2	CF	368	-
A-C1-r-b	92.3	732.6	6.1	16.0	CF	318	17

A-C1-r-c	92.3	720.6	5.2	11.2	CF	225	14
A-C1-s-a	83.5	479.0	3.8	13.9	CF	323	-
A-C1-s-b	83.5	483.2	3.5	9.8	CF	281	29
A-C1-s-c	83.5	485.6	5.1	16.7	CF	206	-
A-C0-p-a	63.3	369.6	3.1	7.0	CF	384	37
A-C0-p-b	63.3	346.2	3.0	8.1	CF	379	21
A-C0-p-c	63.3	381.5	5.0	9.5	CF	371	-
A-C0-q-a	56.1	468.8	3.8	18.0	CF	376	24
A-C0-q-b	56.1	499.3	4.3	15.7	CF	463	18
A-C0-q-c	*56.1*	*587.8*	*7.0*	*17.0*	*CF*	*339*	*20*
A-C0-r-a	59.7	482.6	5.4	12.5	CF	342	10
A-C0-r-b	*59.7*	*518.5*	*4.1*	*12.4*	*CF*	*317*	*25*
A-C0-r-c	59.7	456.9	3.9	11.1	CF	300	17
A-C0-s-a	59.4	423.4	3.1	10.7	CF	251	13
A-C0-s-b	*59.4*	*480.2*	*4.4*	*7.8*	*CF*	*351*	*30*
A-C0-s-c	59.4	431.2	3.2	6.1	CF	284	37
B-C1-p-a	118.4	716.4	4.5	11.1	CF	307	16
B-C1-p-b	118.4	708.0	5.2	6.9	CF	233	9
C-C1-p-a	108.2	700.8	16.2	20.2	SFS	155	25
C-C1-p-b	108.2	695.4	9.3	20.0	SFS	155	22
SC-C1-h3	99.9	1,173.3	9.6	14.8	CF	596	25
SC-C1-h2	99.9	976.5	3.1	7.2	CF	521	26
SC-C1-h1	99.9	702.1	1.7	4.1	CF	329	30
BC-C1-a	89.8	1,069.8	10.9	12.9	CF	587	28
BC-C1-b	89.8	969.4	10.5	11.9	SFS	535	28
BC-C1-c	89.8	803.1	9.6	10.6	SFS	409	26
BC-C1-d	87.5	635.1	8.7	15.6	SFS	395	32
PC-r-C1	109.2	1,010.0	5.0	10.5	SFS	593	29
PC-C1-a	109.2	911.4	4.2	15.3	SFS	520	29
PC-C1-b	109.2	934.1	4.7	8.5	SFS	459	25
PC-C1-s	80.1	788.2	4.4	10.4	CF	428	27

3.3.2 Results of Tests A-C1

In those shear connections with Type A connector and C100 concrete, four groups of specimens were tested to investigate the effects of fibre content, i.e. 1.5%, 0.8%, 0.4%, and 0.0%, onto the structural behaviour of the shear connections. In each group, there are three nominally identical specimens. It should be noted that:

- Concrete failure (Mode CF) with extensive concrete cracking and crushing was found in these tests, as shown in Fig. 3.8.

- For those specimens with provision of steel fibres, only extensive concrete cracks were found on the concrete blocks. For those specimens without steel fibres, severe concrete crushing was found in the concrete blocks, and the concrete blocks could be removed easily after testing.
- For those specimens with a fibre content of 0.8%, a bolt shank was found to have fractured in one of the specimens at the end of the test.

Concrete C100 with 1.5% steel fibres

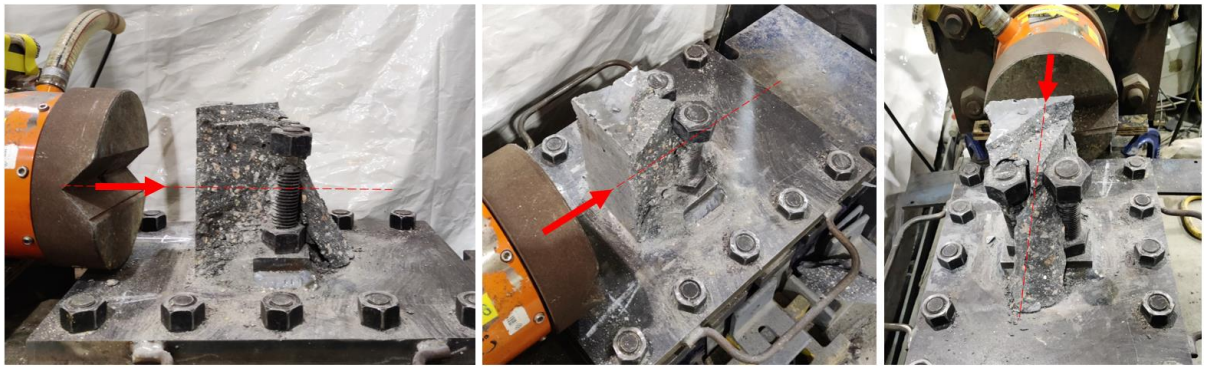

Concrete C100 with 0.0% steel fibres

Fig. 3.8 Concrete failure in Type A connections with concrete C100 and various fibre content

a) Results of Tests A-C1-p

Fig. 3.9 presents the load-slippage curves of Tests A-C1-p-a, -b, and -c. The average shear resistance of these tests is 916.9 kN, and the corresponding average slippage is 11.9 mm. Moreover, the average slippage limit is 24.1 mm, and the average initial stiffness is 317 kN/mm.

b) Results of Tests A-C1-q

Fig. 3.10 presents the load-slippage curves of Tests A-C1-q-a, -b, and -c. It should be noted

that as the deviation of the shear resistances between Test A-C1-q-b and the other two specimens is larger than 10%, the representative shear resistance, initial slippage and slippage limit of Test A-C1-q are determined by averaging the corresponding values of only Tests A-C1-q-a and A-C1-q-c. Hence, the average shear resistance of these tests is 831.9 kN, and the corresponding slippage is 8.5 mm. Moreover, the average slippage limit is 21.4 mm, and the average initial stiffness is 333 kN/mm.

c) Results of Tests A-C1-r

Fig. 3.11 presents the load-slippage curves of Tests A-C1-r-a, -b, and -c. The average shear resistance of these tests is 732.0 kN, and the corresponding slippage is 5.9 mm. Moreover, the average slippage limit is 14.1 mm, and the average initial stiffness is 304 kN/mm.

d) Results of Tests A-C1-s

Fig. 3.12 presents the load-slippage curves of Tests A-C1-s-a, -b, and -c. The average shear resistance of these tests is 482.6 kN, and the corresponding slippage is 4.1 mm. Moreover, the average slippage limit is 13.5 mm, and the average initial stiffness is 270 kN/mm.

In general, the shear resistances of the shear connections with Type A connector and C100 concrete are smaller than 1,000 kN despite the slippage limits of these connections are larger than 6.0 mm. However, the initial stiffnesses are smaller than 1,500 kN/mm.

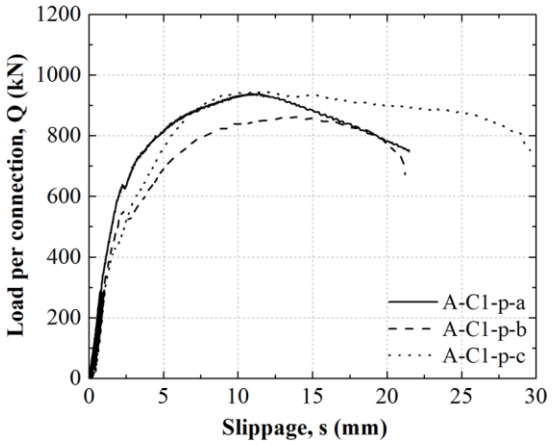

Test	$f_{cu,150}$ (N/mm²)	Q_m (kN)	s_m (mm)	s_u (mm)	K (kN/mm)
A-C1-p-a	111.2	939.5	10.9	21.5	365
A-C1-p-b	111.2	865.3	13.7	21.2	330
A-C1-p-c	111.2	946.0	11.0	29.6	255
Average	111.2	916.9	11.9	24.1	317

Fig. 3.9 Key results of Tests A-C1-p

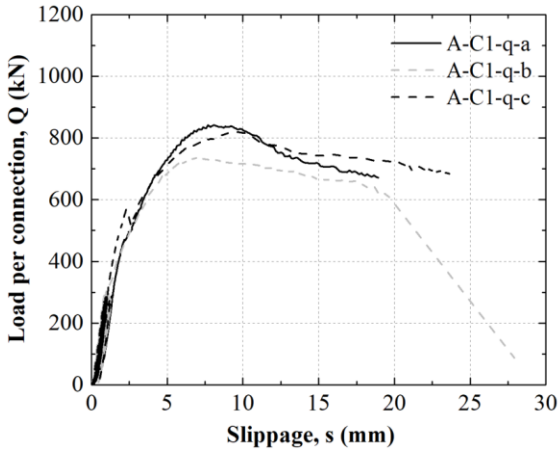

Test	$f_{cu,150}$ (N/mm^2)	Q_m (kN)	s_m (mm)	s_u (mm)	K (kN/mm)
A-C1-q-a	105.0	841.4	7.7	18.9	289
A-C1-q-b	105.0	739.7	7.5	27.9	267
A-C1-q-c	105.0	822.3	9.3	23.8	376
Average	105.0	831.9	8.5	21.4	333

Fig. 3.10 Key results of Tests A-C1-q

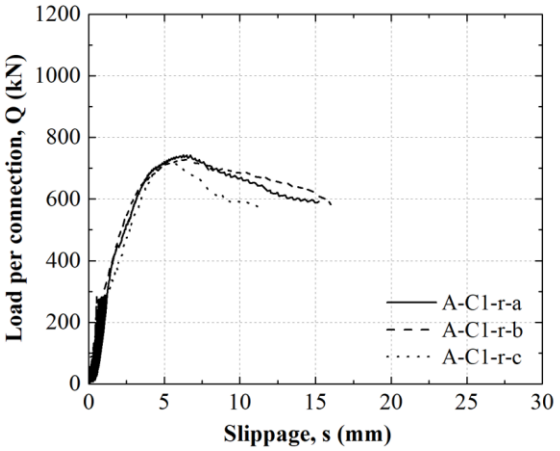

Test	$f_{cu,150}$ (N/mm^2)	Q_m (kN)	s_m (mm)	s_u (mm)	K (kN/mm)
A-C1-r-a	92.3	742.7	6.3	15.2	368
A-C1-r-b	92.3	732.6	6.1	16.0	318
A-C1-r-c	92.3	720.6	5.2	11.2	225
Average	92.3	732.0	5.9	14.1	304

Fig. 3.11 Key results of Tests A-C1-r

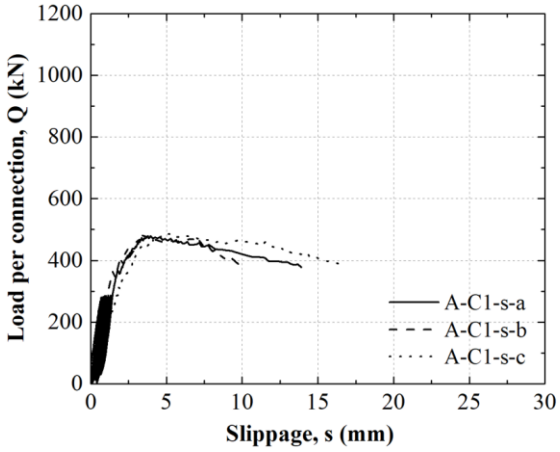

Test	$f_{cu,150}$ (N/mm^2)	Q_m (kN)	s_m (mm)	s_u (mm)	K (kN/mm)
A-C1-s-a	83.5	479.0	3.8	13.9	323
A-C1-s-b	83.5	483.2	3.5	9.8	281
A-C1-s-c	83.5	485.6	5.1	16.7	206
Average	83.5	482.6	4.1	13.5	270

Fig. 3.12 Key results of Tests A-C1-s

3.3.3 Results of Tests A-C0

In those shear connections with Type A connector and C50 concrete, four groups of specimens were tested to investigate the effect of fibre content, i.e. 1.5%, 0.8%, 0.4%, and 0.0%, onto the structural behaviour of the shear connections. In each group, there are three nominally identical specimens. It should be noted that:

- Concrete failure (Mode CF) with extensive concrete cracking and crushing was found in these tests, as shown in Fig. 3.13.
- For those specimens with provision of steel fibres, only extensive concrete cracks were found on the concrete blocks. For those specimens without steel fibres, severe concrete crushing was found in the concrete blocks, and the concrete blocks could be removed easily after testing.
- In all specimens, no shear fracture was observed in any of the bolts at the end of these tests.

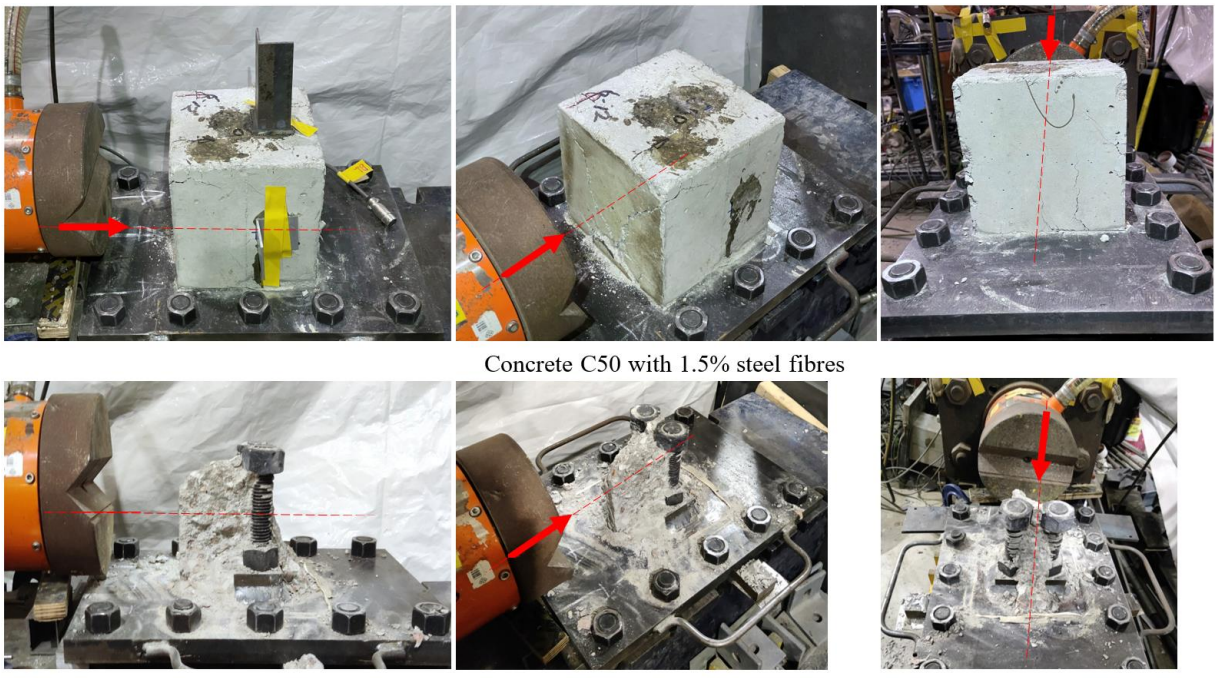

Concrete C50 with 1.5% steel fibres

Concrete C50 with 0.0% steel fibres

Fig. 3.13 Concrete failure in Type A connections with concrete C50 and various fibre content

a) Results of Tests A-C0-p

Fig. 3.14 presents the load-slippage curves of Tests A-C0-p-a, -b, and -c. The average shear

resistance of these tests is 365.8 kN, and the corresponding slippage is 3.7 mm. Moreover, the average slippage limit is 8.2 mm, and the average initial stiffness is 378 kN/mm.

b) Results of Tests A-C0-q

Fig. 3.15 presents the load-slippage curves of Tests A-C0-q-a, -b, and -c. It should be noted that as the deviation of the shear resistances between Test A-C0-q-c and the other two specimens is larger than 10%, the representative shear resistance, initial slippage and slippage limit of Test A-C0-q are determined by averaging the corresponding values of only Tests A-C0-q-a and A-C0-q-b. Hence, the average shear resistance of these tests is 484.1 kN, and the corresponding slippage is 4.1 mm. Moreover, the average slippage limit is 16.9 mm, and the average initial stiffness is 420 kN/mm.

c) Results of Tests A-C0-r

Fig. 3.16 presents the load-slippage curves of Tests A-C0-r-a, -b, and -c. It should be noted that as the deviation of the shear resistances between Test A-C0-r-b and the other two specimens is larger than 10%, the representative shear resistance, initial slippage and slippage limit of Test A-C0-r are determined by averaging the corresponding values of only Tests A-C0-r-a and A-C0-r-c. Hence, the average shear resistance of these tests is 469.8 kN, and the corresponding slippage is 4.7 mm. Moreover, the average slippage limit is 11.8 mm, and the average initial stiffness is 321 kN/mm.

d) Results of Tests A-C0-s

Fig. 3.17 presents the load-slippage curves of Tests A-C0-s-a, -b, and -c. It should be noted that as the deviation of the shear resistances between Test A-C0-s-b and the other two specimens is larger than 10%, the representative shear resistance, initial slippage and slippage limit of Test A-C0-s are determined by averaging the corresponding values of only Tests A-C0-s-a and A-C0-

s-c. Hence, the average shear resistance of these tests is 427.3 kN, and the corresponding slippage is 3.2 mm. Moreover, the average slippage limit is 8.4 mm, and the average initial stiffness is 268 kN/mm.

In general, the shear resistances of the shear connections with Type A connector and C50 concrete are smaller than 1,000 kN despite the slippage limits of these connections are larger than 6.0 mm. However, the initial stiffnesses are smaller than 1,500 kN/mm.

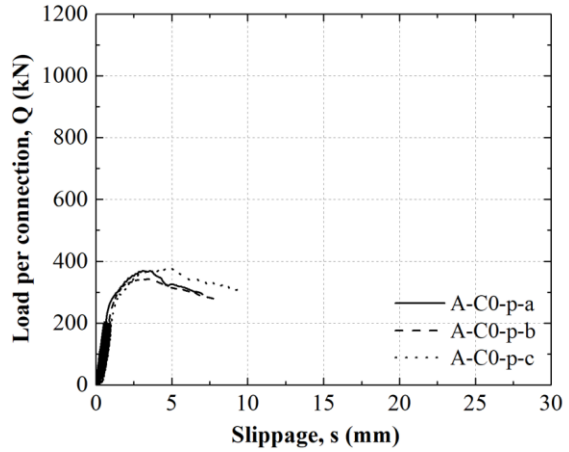

Test	$f_{cu,150}$ (N/mm²)	Q_m (kN)	s_m (mm)	s_u (mm)	K (kN/mm)
A-C0-p-a	63.3	369.6	3.1	7.0	384
A-C0-p-b	63.3	346.2	3.0	8.1	379
A-C0-p-c	63.3	381.5	5.0	9.5	371
Average	63.3	365.8	3.7	8.2	378

Fig. 3.14 Key results of Tests A-C0-p

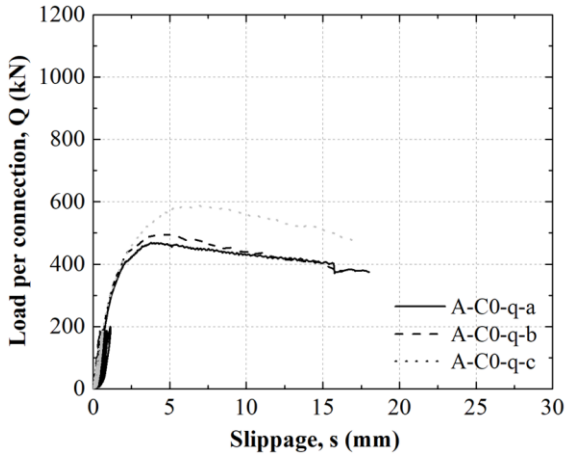

Test	$f_{cu,150}$ (N/mm²)	Q_m (kN)	s_m (mm)	s_u (mm)	K (kN/mm)
A-C0-q-a	56.1	468.8	3.8	18.0	376
A-C0-q-b	56.1	499.3	4.3	15.7	463
A-C0-q-c	56.1	587.8	7.0	17.0	339
Average	56.1	484.1	4.1	16.9	420

Fig. 3.15 Key results of Tests A-C0-q

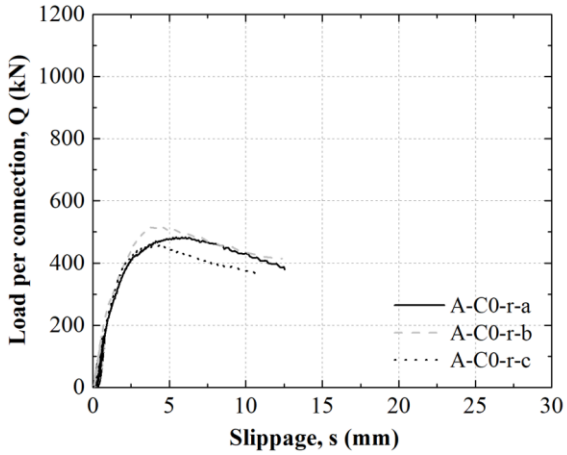

Test	$f_{cu,150}$ (N/mm²)	Q_m (kN)	s_m (mm)	s_u (mm)	K (kN/mm)
A-C0-r-a	59.7	482.6	5.4	12.5	342
A-C0-r-b	59.7	518.5	4.1	12.4	317
A-C0-r-c	59.7	456.9	3.9	11.1	300
Average	59.7	469.8	4.7	11.8	321

Fig. 3.16 Key results of Tests A-C0-r

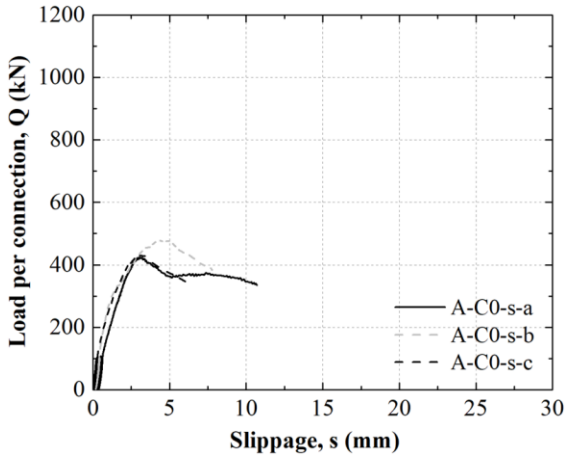

Test	$f_{cu,150}$ (N/mm²)	Q_m (kN)	s_m (mm)	s_u (mm)	K (kN/mm)
A-C0-s-a	59.4	423.4	3.1	10.7	251
A-C0-s-b	59.4	480.2	4.4	7.8	351
A-C0-s-c	59.4	431.2	3.2	6.1	284
Average	59.4	427.3	3.2	8.4	268

Fig. 3.17 Key results of Tests A-C0-s

3.3.4 Results of Tests B-C1-p

In those shear connections with Type B connector and C100 concrete, only one group of specimens with two nominally identical specimens were tested. Concrete failure (Mode CF) with extensive concrete cracking and crushing was found in these tests, as shown in Fig. 3.18. After testing, it was found that the two bolts were completely fractured and the concrete in the vicinity of the steel bock was crushed.

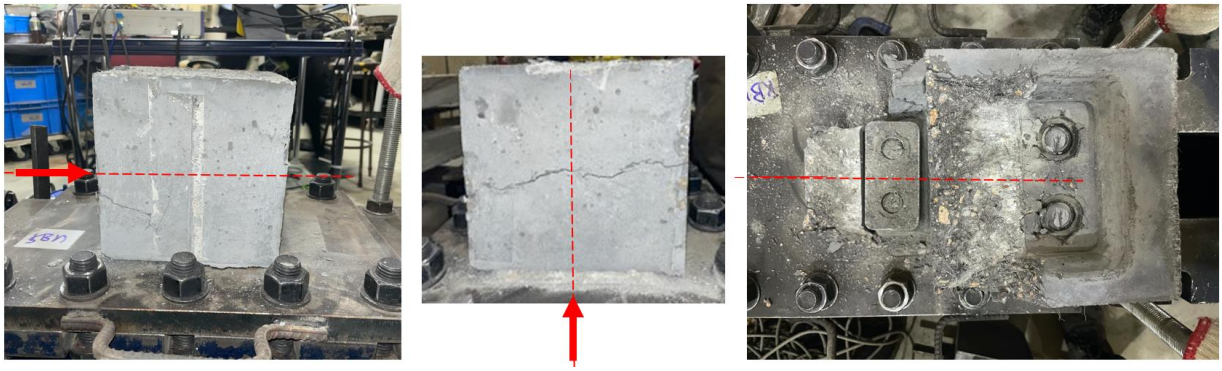

Fig. 3.18 Concrete failure in connections with 24 mm diameter bolts

Fig. 3.19 presents the load-slippage curves of Tests B-C1-p-a, and -b. The average shear resistance of these tests is 712.2 kN, and the corresponding slippage is 4.9 mm. Moreover, the average slippage limit is 9.0 mm, and the average initial stiffness is 270 kN/mm.

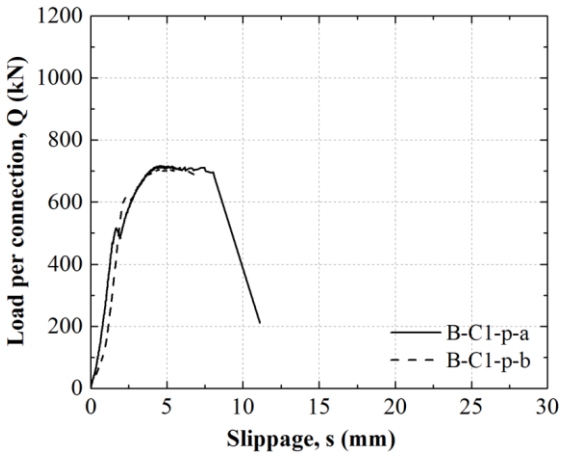

Test	$f_{cu,150}$ (N/mm^2)	Q_m (kN)	s_m (mm)	s_u (mm)	K (kN/mm)
B-C1-p-a	118.4	716.4	4.5	11.1	307
B-C1-p-b	118.4	708.0	5.2	6.9	233
Average	118.4	712.2	4.9	9.0	270

Fig. 3.19 Key results of Tests B-C1-p

3.3.5 Results of Tests C-C1-p

In those shear connections with Type C connector and C100 concrete, only one group of specimens with two nominally identical specimens were tested. Shear fracture of steel connector (Mode SFS) was found in these tests, as shown in Fig. 3.20. After testing, it was found that the two bolts were completely fractured in shear, and little concrete crushing was found in the vicinity of the embedded nuts.

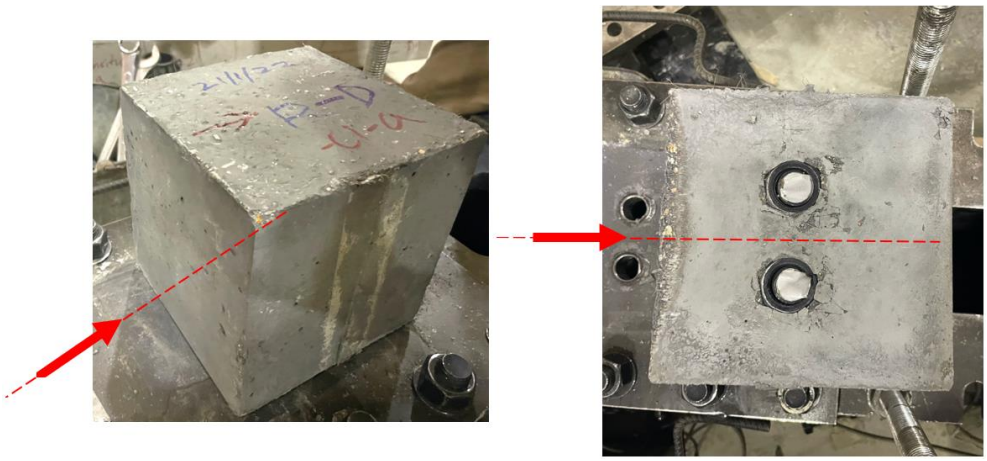

Fig. 3.20 Shear fracture of steel bolts in connection with Connector R

Fig. 3.21 presents the load-slippage curves of Tests C-C1-p-a, and -b. The average shear resistance of these tests is 698.1 kN, and the corresponding slippage is 12.8 mm. Moreover, the average slippage limit is 20.1 mm, and the average initial stiffness is 155 kN/mm.

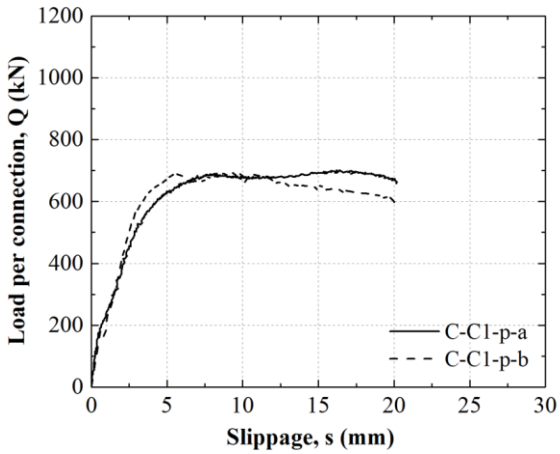

Test	$f_{cu,150}$ (N/mm^2)	Q_m (kN)	s_m (mm)	s_u (mm)	K (kN/mm)
C-C1-p-a	108.2	700.8	16.2	20.2	155
C-C1-p-b	108.2	695.4	9.3	20.0	155
Average	108.2	698.1	12.8	20.1	155

Fig. 3.21 Results of Tests C-C1

3.3.6 Results of Tests SC, BC, and PC

In those shear connections with Types SC, BC, and PC connectors, a total of 11 specimens were tested to investigate the effect of the hight of the steel block, the weld length, and the orientation of the profiles on the structural behaviour of these shear connections. As shown in Fig. 3.22, two typical failure modes were identified: a) Concrete failure, i.e. Mode CF; and b) Shear fracture of steel connectors, i.e. Mode SFS. It should be noted that Mode CF was critical in all connections

with Type SC connectors. Owing to an abrupt change in stiffness near the top of the shear connectors inside the concrete blocks, the concrete suffered from severe cracking and crushing while the bent reinforcements completely fractured in shear. Mode SFS was critical in all test specimens of Types BC and PC, in which the steel plates of the box and the profiled connectors fractured in shear. In many cases, the steel connectors remained fully embedded inside the concrete blocks after failure while severe damage in the concrete was apparent. It should be noted that no weld failure was observed in the test specimens after a close visual examination.

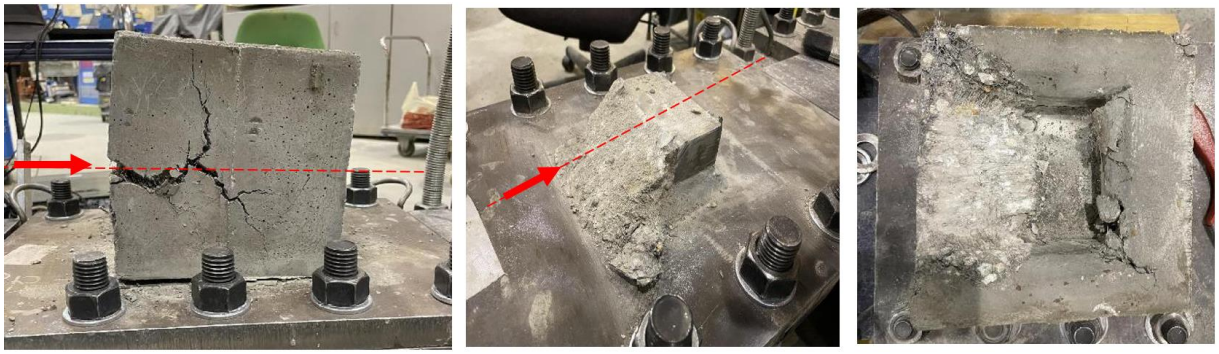

a) Concrete failure – Mode CF

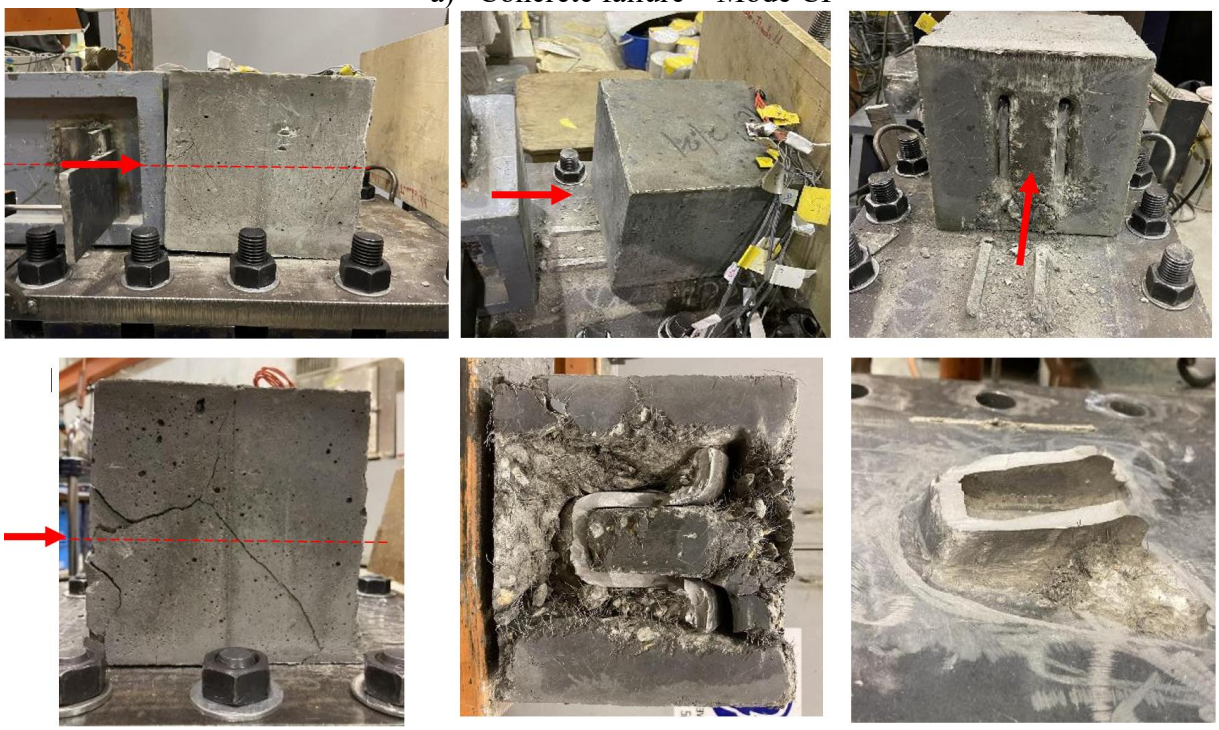

b) Shear fracture of steel plates – Mode SFS

Fig. 3.22 Typical failure modes in connections with Connectors SC, BC and PC

The deformation characteristics of Types SC, BC, and PC connections are presented as follows:

a) Type SC – Solid connectors

i. Concrete fracture, i.e. Mode CF, in these three test specimens was apparent with complete shear fracture in the bent reinforcements. Extensive cracking was also evident at the surface of the concrete blocks during testing.

ii. As shown in Fig. 3.23, the shear resistances Q_m of Tests SC-h1, SC-h2 and SC-h3 are 702.1, 976.5 and 1,173.3 kN, respectively, and the corresponding slippage limits s_u are 4.1, 7.2 and 14.8 mm, respectively.

iii. Based on the above, increasing the height of the solid blocks is shown to be effective in providing an enlarged bearing area to receive compressive forces from the surrounding concrete. The bent reinforcements are also shown to be effective in providing sufficiently large pull-out resistances to prevent separation between the solid blocks and the concrete blocks up to failure. It is shown that *Type SC-h3 with a height at 65 mm can be considered as an effective shear connector.*

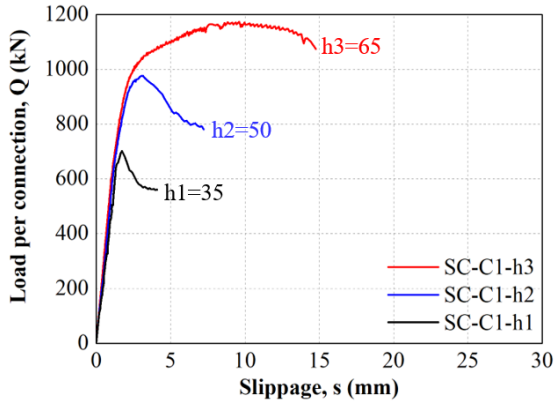

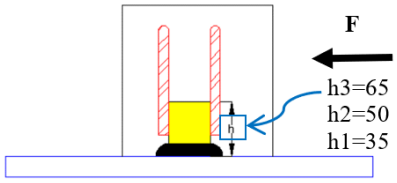

Test	$f_{cu,150}$ (N/mm^2)	Q_m (kN)	s_m (mm)	s_u (mm)	K (kN/mm)
SC-C1-h3	104.9	1,173.3	9.6	14.8	596
SC-C1-h2	104.9	976.5	3.1	7.2	521
SC-C1-h1	104.9	702.1	1.7	4.1	329

Fig. 3.23 Results of Tests SC

b) Type BC – Box connectors

i. Shear fracture of the welded steel plates of the shear connectors, i.e. Mode SFS, was critical in all the test specimens while significant concrete crushing was observed at the compression surfaces of the concrete blocks in Tests BC-a, BC-b and BC-c. It should be noted that in Test BC-d, only little concrete crushing was observed.

ii. As shown in Fig. 3.24, the shear resistances Q_m of Tests BC-a, BC-b, BC-c and BC-d are 1,069.8, 969.4, 803.1, and 635.1 kN, respectively, and the corresponding slippage limits s_u are 12.9, 11.9, 10.6 and 15.6 mm, respectively.

iii. Hence, increasing the weld lengths between the box sections and the base plates is effective in mobilizing increased shear resistances and slippage limits. It is shown that *Test BC-a with 4-sided welded steel plates can be considered as an effective shear connector.*

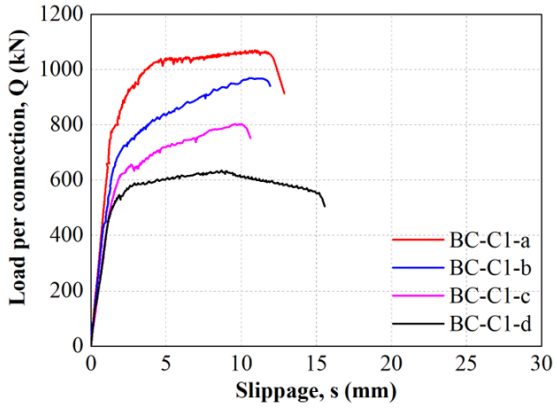

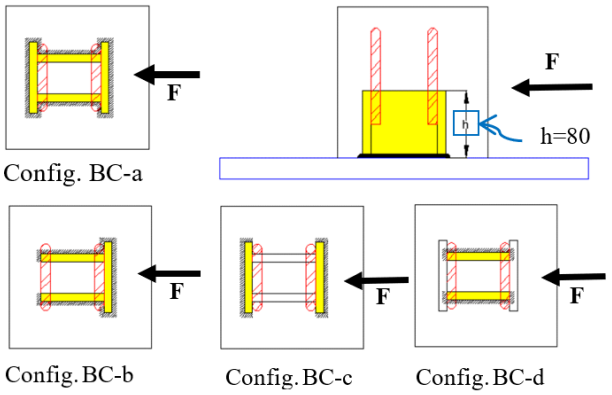

Test	$f_{cu,150}$ (N/mm²)	Q_m (kN)	s_m (mm)	s_u (mm)	K (kN/mm)
BC-C1-a	94.3	1,069.8	10.9	12.9	587
BC-C1-b	94.3	969.4	10.5	11.9	535
BC-C1-c	94.3	803.1	9.6	10.6	409
BC-C1-d	91.9	635.1	8.7	15.6	395

Fig. 3.24 Results of Tests BC

c) Type PC – Profiled connectors

i. Shear fracture of the profiled steel plates of the shear connectors, i.e. Mode SFS, was critical in all the test specimens with a fibre content of 1.5% in concrete blocks, while significant concrete crushing was observed at the compression sides of all the concrete blocks.

ii. As shown in Fig. 3.25, the shear resistances Q_m of Tests PC and PC-r are 911.4 and 1,010.0 kN, respectively, and the corresponding slippage limits s_u are 15.3 and 10.5 mm, respectively.

iii. It is hence shown that the orientation of the U-shaped profiles does affect the behaviour of the shear connections, and *the U-shaped profile running along the direction of the applied load is considered to be an effective shear connector with a relatively large shear resistance*.

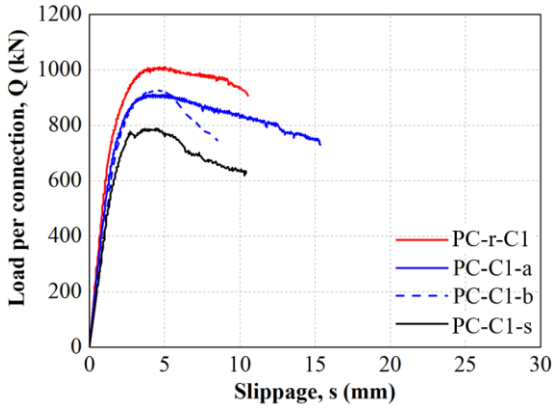

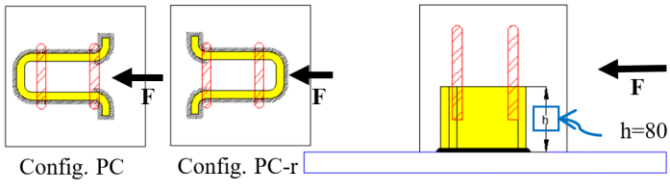

Test	$f_{cu,150}$ (N/mm^2)	Q_m (kN)	s_m (mm)	s_u (mm)	K (kN/mm)
PC-r-C1	114.7	1,010.0	5.0	10.5	593
PC-C1-a	114.7	911.4	4.2	15.3	520
PC-C1-b	114.7	934.1	4.7	8.5	459
PC-C1-s	84.1	788.2	4.4	10.4	428

Fig. 3.25 Results of Tests PC

As a whole, Connectors SC-h3, BC-a and PC-r are shown to be highly effective in transferring shear forces. Their load-slippage curves are plotted onto the same graph in Fig. 3.26 for direct comparison. It is shown that these shear connections have large pull-out resistances so that their shear resistances are fully mobilized with large deformation capacities in the tests well before fracture of the U-shaped steel reinforcements. It should also be noted that among these three connectors, Connector SC is able to provide the largest shear resistance together with a high level of ductility, though crushing and cracking on the surfaces of the concrete blocks is also apparent.

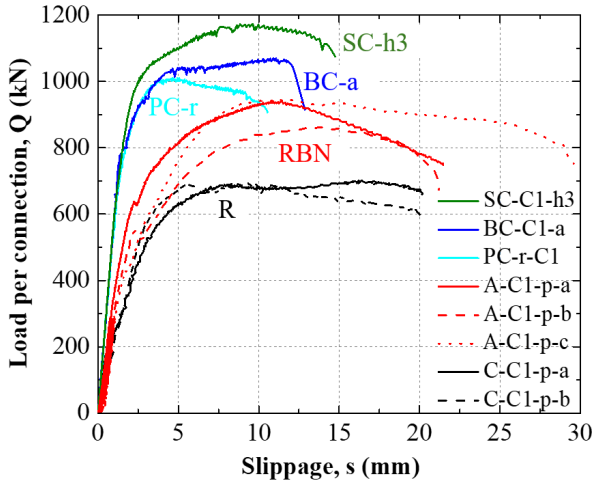

Test	$f_{cu,150}$ (N/mm^2)	Q_m (kN)	s_m (mm)	s_u (mm)	K (kN/mm)
SC-C1-h3	104.9	1,173.3	9.6	14.8	596
BC-C1-a	94.3	1,069.8	10.9	12.9	587
PC-r-C1	114.7	1,010.0	5.0	10.5	593
A-C1-p	111.2	916.9	11.9	24.1	317
C-C1-p	108.2	698.1	12.8	20.1	155

Fig. 3.26 Effect of connector type

3.4 Comparison of deformation characteristics

As shown in Table 3.6, the effects of connector type, fibre content, and bolt diameter on the deformation characteristics of the shear connections are discussed and compared below.

Table 3.6 Comparison of test results

Comparison	
Connector type	Types SC-C1-h3, BC-C1-a, and PC-r-C1
	Types A-C1-p and C-C1-p
Fibre content	Types A-C1-p, A-C1-q, A-C1-r and A-C1-s
	Types A-C0-p, A-C0-q, A-C0-r and A-C0-s
Bolt diameter	Types A-C1-p and B-C1-p

3.4.1 Effect of Connector type

The load-slippage curves of those tests with Concrete C100 and various connector types, i.e. Tests SC-C1-h3, BC-C1-a, and PC-r -C1 as well as Tests A-C1-p and C-C1-p, are compared in Fig. 3.26. Mode CF is found to appear in Tests SC-C1-h3, BC-C1-a, and A-C1-p while Mode SFS is found to appear in Tests PC-r -C1 and C-C1-p. It is found that:

i) The average shear resistances Q_m of Tests SC-C1-h3, BC-C1-a, PC-r -C1 are 1,173.3, 1,069.8, and 1,010.0 kN respectively while those of Tests A-C1-p and C-C1-p are 916.9, and 698.1 kN respectively. The corresponding slippage limits s_u of Tests SC-C1-h3, BC-C1-a, PC-r -C1

are 14.8, 12.9, and 10.5 mm respectively while those of Tests A-C1-p and C-C1-p are 24.1, and 20.1 mm respectively. The initial stiffnesses are 596, 587, 593, 317, and 155 kN/mm respectively.

It is worth noting that compared with Test C-C1-p, i.e. the shear connection with the basic configuration of a bolted connector, the shear resistances of Tests SC-C1-h3, BC-C1-a, PC -r-C1, and A-C1-p are increased by 1.68, 1.53, 1.45, and 1.31 respectively while the initial stiffnesses are increased by 3.85, 3.79, 3.83, and 2.05 respectively. The slippage limits of Tests SC-C1-h3, BC-C1-a, and PC-r -C1 are decreased by 5.3, 7.2, and 9.6 mm respectively, while the slippage limit of Test A-C1-p is increased by 4.0 mm.

ii) Hence, although the shear resistances and the initial stiffnesses of Tests SC-C1-h3, BC-C1-a, and PC-r -C1 are significantly larger than those of Test C-C1-p, their slippage limits are found to be smaller. Compared with Test C-C1-p, i.e. a shear connection with Connector R, the provision of the welded steel block in Test A-C1-p, i.e. a shear connection with Connector RBN, is shown to be efficient to increase the shear resistance, the initial stiffness, and the ductility. It is reckoned that local bearing stresses in the proximity of the steel block are effectively distributed within the concrete blocks due to the presence of steel fibres. It is also demonstrated that the connections with Type A connector and a 30 mm thick steel block is highly effective in both the shear resistance and the ductility.

3.4.2 Effect of fibre content

a) Tests on concrete blocks with C100 concrete

The load-slippage curves of those tests with C100 concrete and various fibre content, i.e. Tests A-C1-p, A-C1-q, A-C1-r, and A-C1-s, are compared as shown in Fig. 3.27. Mode CF is found to appear in all these tests. It is found that:

i) The average shear resistances Q_m of Tests A-C1-p, A-C1-q, A-C1-r, and A-C1-s are 916.9, 831.9, 732.0, and 482.6 kN respectively, and the corresponding ultimate slippages s_u are 24.1, 21.4, 14.1, and 13.5 mm respectively. The initial stiffnesses are 317, 333, 304, and 270

kN/mm respectively.

It is worth noting that when compared with Test A-C1-s, the shear resistances of Tests A-C1-p, A-C1-q, A-C1-r are increased by 1.90, 1.72, and 1.52 respectively, and the initial stiffnesses are increased by 1.17, 1.23, and 1.13 respectively. The corresponding slippage limits are increased by 10.6, 7.9, and 0.6 mm respectively.

ii. Hence, the addition of steel fibres to C100 concrete is shown to be efficient to increase the shear resistances, the initial stiffnesses and the slippage limits of the connections with Type A connector. It is obvious that the steel fibres are able to improve both tensile strength and ductility of the high strength concrete, and they contribute significantly to crack control by bridging microcracks and preventing their propagation. It is demonstrated that when the fibre content is 1.5%, the structural behaviour of the shear connection with Type A connector and C100 concrete is highly effective.

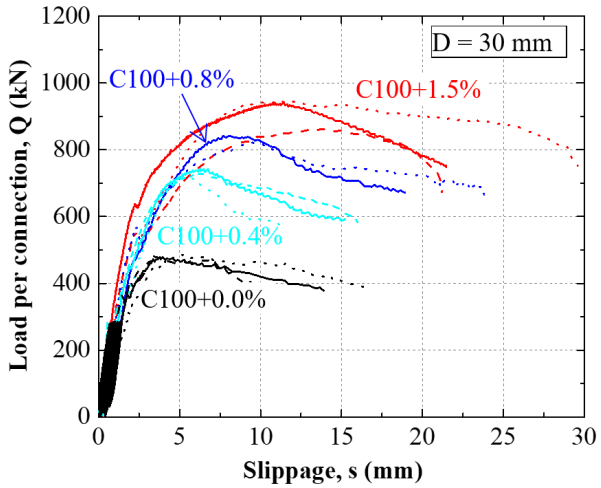

Test	$f_{cu,150}$ (N/mm^2)	Q_m (kN)	s_m (mm)	s_u (mm)	K (kN/mm)
A-C1-p	111.2	916.9	11.9	24.1	317
A-C1-q	105.0	831.9	8.5	21.4	333
A-C1-r	92.3	732.0	5.9	14.1	304
A-C1-s	83.5	482.6	4.1	13.5	270

Fig. 3.27 Effect of fibre content in shear connections with C100 concrete blocks

b) Tests on concrete blocks with C50 concrete

The load-slippage curves of those tests with C50 concrete and various fibre content, i.e. Tests A-C0-p, A-C0-q, A-C0-r, and A-C0-s, are compared as shown in Fig. 3.28. Mode CF is found to appear in all of these tests. It is found that:

i) The average shear resistances Q_m of Tests A-C0-p, A-C0-q, A-C0-r, and A-C0-s are 365.8, 484.1, 469.8, and 427.3 kN respectively, and the corresponding ultimate slippages s_u are 8.2, 16.9, 11.8, and 8.4 mm respectively. The initial stiffnesses are 378, 420, 321, and 268 kN/mm respectively. It is worth noting that when compared with Test A-C0-s, the shear resistances of

Tests A-C0-q, A-C0-r are increased by 1.13 and 1.10 respectively, and the initial stiffnesses are increased by 1.57 and 1.20 respectively. The corresponding slippage limits are increased by 8.5 and 3.4 mm respectively. However, despite a higher fibre content of 1.5% is provided in the concrete block of Test A-C0-p, its shear resistance is found to be smaller than that of Test A-C0-s, in which no fibres are provided in the concrete block.

ii) Hence, the shear resistances, the initial stiffnesses, and the slippage limits of the proposed connections with Concrete C50 are found to have slightly increased with an increase in the fibre content. It should be noted that the steel fibres are able to limit cracks on the concrete blocks and prevent sudden concrete crushing. When the fibre content is 0.8%, the structural behaviour of the shear connection with Type A connector and C50 concrete is highly effective. However, an addition of 1.5% steel fibres is found to have unfavourable influence on the structural behaviour of shear connections. The reason is that when the fibre content reaches 0.8%, the strength of the cement paste attains its maximum value, and any further increase in the fibre content may have adverse influence on the concrete strength.

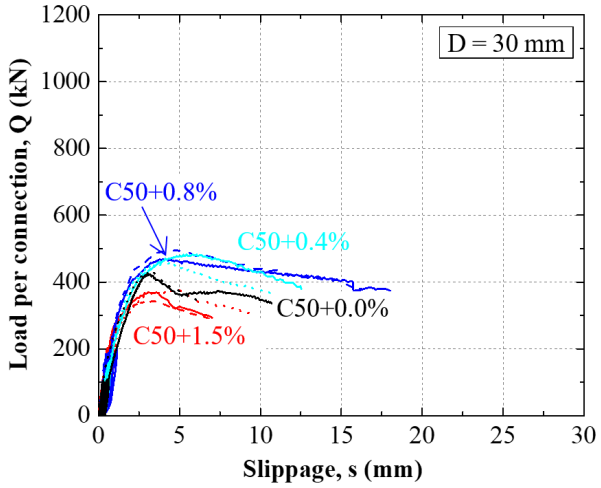

Test	$f_{cu,150}$ (N/mm^2)	Q_m (kN)	s_m (mm)	s_u (mm)	K (kN/mm)
A-C0-p	63.3	365.8	3.7	8.2	378
A-C0-q	56.1	484.1	4.1	16.9	420
A-C0-r	59.7	469.8	4.7	11.8	321
A-C0-s	59.4	427.3	3.2	8.4	268

Fig. 3.28 Effect of fibre content in shear connections with C50 concrete blocks

3.4.3 Effect of bolt diameter

The load-slippage curves of those tests with C100 concrete and Types A and B connectors, i.e. Tests A-C1-p and B-C1-p, are compared as shown in Fig. 3.29. Mode CF is found to appear in all of these tests. It is found that:

i) The average shear resistances Q_m of Tests A-C1-p and B-C1-p are 916.9 and 712.2 kN

respectively, and the corresponding ultimate slippages s_u are 24.1 and 9.0 mm respectively. The initial stiffnesses are 317 and 270 kN/mm respectively. It is worth noting that when compared with Test B-C1-p, the shear resistance of Test A-C1-p is increased by 1.29, and the initial stiffness is increased by 1.17. The corresponding slippage limit is increased by 15.1 mm.

ii) Hence, with an increase in the bolt diameter of the shear connectors, the shear resistance, the initial stiffness and the slippage limit of the shear connections are increased. This is because the bolts with large diameters can readily withstand large shear and pull-out forces.

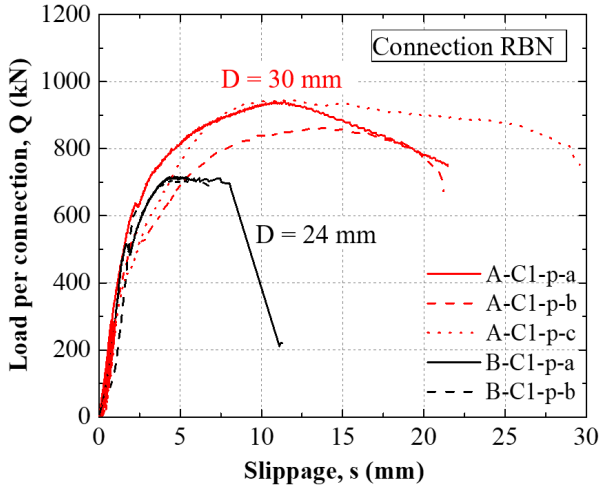

Test	$f_{cu,150}$ (N/mm²)	Q_m (kN)	s_m (mm)	s_u (mm)	K (kN/mm)
A-C1-p	111.2	916.9	11.9	24.1	317
B-C1-p	118.4	712.2	4.9	9.0	270

Fig. 3.29 Effect of bolt diameter

3.5 Design method

In order to develop a design approach for the proposed shear connections with various types of shear connectors, the shear resistances obtained from the tests are compared with those determined according to codified design rules (EC4, 1992; EC3, 2005).

3.5.1 Shear connections with large diameter high strength bolts

For Types A and B connections, the shear resistances of the shear connections are determined according to the design rule reported in literature (Ding *et al.*, 2024), which is presented in Chapter

5. In general, the design shear resistance of the shear connection of Types A and B is given by:

$$Q_{Rd} = \gamma_{cs} Q_{cbs} + \gamma_{cb} \min \{Q_{cbb} , Q_{sfb}\} \quad (3.1)$$

where

Q_{cbs} is the concrete bearing resistance against the steel block;

Q_{cbb} is the concrete bearing resistance against the two bolts;

Q_{sfb} is the steel shear resistance against shear fracture of bolts.

γ_{cs} is a reduction factor considering the influence of fibre content on the concrete bearing resistance against the steel block, which is taken as 1.00 after calibration against test data; and

γ_{cb} is a reduction factor considering the influence of fibre content on mobilization of the shear resistances of bolts; and it is found to be decreased with a decrease in the fibre content of concrete block after calibration against test data.

Refer to Reference (Ding *et al*., 2024) and Section 5.8 of Chapter 5 for details of the proposed design rule. The values of γ_{cb} in Types A and B shear connections with various fibre content are shown in Table 3.7.

Table 3.7 Values of γ_{cb} in shear connections with various concrete grades and fibre content

	Fibre content	C1 f_c = 100 N/mm^2	C0 f_c = 50 N/mm^2
p	1.5%	0.80	0.85
q	0.8%	0.75	0.80
r	0.4%	0.70	0.75
s	0.0%	0.35	0.65

In order to determine structural adequacy and efficiency of these design rules, a model factor η is established, and it is defined as follows:

$$\eta = Q_{Rt} / Q_{Rd} \quad (3.2)$$

In general, the value of η is expected to range from 1.0 to 1.3 so that the design rule is conservative, and yet effective. The values of η for these shear connections are also summarised in Table 3.8, and it is shown that:

- For Type A connections with Concrete C1, the values of η range from 1.02 to 1.14, and the average value of η is 1.06. Hence, the proposed design rule is demonstrated to be highly effective for these shear connections.
- For Type A connections with Concrete C0, the values of η range from 1.00 to 1.33, and the average value of η is 1.10. Hence, the proposed design rule is also demonstrated to be highly effective for these shear connections. It should be noted that for Test A-C0-p with a fibre content of 1.5%, the measured shear resistance is smaller than the design value, and it is probably due to the presence of too much steel fibres, i.e. 1.5%, in C50 concrete blocks.
- For Type B connections with Concrete C1, the values of η are found to be 1.13 and 1.15, and the average value of η is 1.14. Hence, the proposed design rule is demonstrated to be effective for these shear connections.
- For Type C connections with Concrete C1, the values of η are found to be 1.03 and 1.04, and the average value of η is 1.03. Hence, the proposed design rule is demonstrated to be highly effective for these shear connections.

Table 3.8 Comparison on measured and design shear resistances of Types A to C connections

Test	Q_{Rt} (kN)	Failure mode	Concrete failure								Fracture of shear connectors				Q_{Rd} (kN)	η
			$f_{cu,150}$ (N/mm^2)	f_{ck} (N/mm^2)	A_{c1} (mm^2)	A_{cp1} (mm^2)	Q_{cbs} (kN)	A_{c2} (mm^2)	A_{cp2} (mm^2)	Q_{cbb} (kN)	A_b (mm^2)	f_{ub} (N/mm^2)	Q_{sfb} (kN)	γ_{cb}		
A-C1-p-a	939.5	CF	111.2	81.0	3,600	6,512	**392.0**	3,016	7,020	723.8	490.9	795.3	**546.5**	0.80	**829.2**	**1.13**
A-C1-p-b	865.3	CF	111.2	81.0	3,600	6,512	**392.0**	3,016	7,020	723.8	490.9	795.3	**546.5**	0.80	**829.2**	**1.04**
A-C1-p-c	946.0	CF	111.2	81.0	3,600	6,512	**392.0**	3,016	7,020	723.8	490.9	795.3	**546.5**	0.80	**829.2**	**1.14**
A-C1-q-a	841.4	CF	105.0	76.0	3,600	6,512	**368.0**	3,016	7,020	679.4	490.9	795.3	**546.5***	0.75	**777.9**	**1.08**
A-C1-q-b	*739.7*	*CF*	*105.0*	*76.0*	*3,600*	*6,512*	***368.0***	*3,016*	*7,020*	*679.4*	*490.9*	*795.3*	***546.5****	*0.75*	***777.9***	***0.95***
A-C1-q-c	822.3	CF	105.0	76.0	3,600	6,512	**368.0**	3,016	7,020	679.4	490.9	795.3	**546.5***	0.75	**777.9**	**1.06**
A-C1-r-a	742.7	CF	92.3	65.8	3,600	6,512	**318.8**	3,016	7,020	588.6	490.9	795.3	**546.5***	0.70	**701.4**	**1.06**
A-C1-r-b	732.6	CF	92.3	65.8	3,600	6,512	**318.8**	3,016	7,020	588.6	490.9	795.3	**546.5***	0.70	**701.4**	**1.04**
A-C1-r-c	720.6	CF	92.3	65.8	3,600	6,512	**318.8**	3,016	7,020	588.6	490.9	795.3	**546.5***	0.70	**701.4**	**1.03**
A-C1-s-a	479.0	CF	83.5	58.8	3,600	6,512	**284.7**	3,016	7,020	**525.7***	490.9	795.3	546.5	0.35	**468.7**	**1.02**
A-C1-s-b	483.2	CF	83.5	58.8	3,600	6,512	**284.7**	3,016	7,020	**525.7***	490.9	795.3	546.5	0.35	**468.7**	**1.03**
A-C1-s-c	485.6	CF	83.5	58.8	3,600	6,512	**284.7**	3,016	7,020	**525.7***	490.9	795.3	546.5	0.35	**468.7**	**1.04**
A-C0-p-a	369.6	CF	63.3	42.6	3,600	6,512	**206.5**	3,016	7,020	**381.2***	490.9	795.3	546.5	0.85	**530.5**	**0.70**
A-C0-p-b	346.2	CF	63.3	42.6	3,600	6,512	**206.5**	3,016	7,020	**381.2***	490.9	795.3	546.5	0.85	**530.5**	**0.65**
A-C0-p-c	381.5	CF	63.3	42.6	3,600	6,512	**206.5**	3,016	7,020	**381.2***	490.9	795.3	546.5	0.85	**530.5**	**0.72**
A-C0-q-a	468.8	CF	56.1	36.9	3,600	6,512	**178.6**	3,016	7,020	**329.7***	490.9	795.3	546.5	0.80	**442.3**	**1.06**
A-C0-q-b	499.3	CF	56.1	36.9	3,600	6,512	**178.6**	3,016	7,020	**329.7***	490.9	795.3	546.5	0.80	**442.3**	**1.13**
A-C0-q-c	*587.8*	*CF*	*56.1*	*36.9*	*3,600*	*6,512*	***178.6***	*3,016*	*7,020*	***329.7****	*490.9*	*795.3*	*546.5*	*0.80*	***442.3***	***1.33***
A-C0-r-a	482.6	CF	59.7	39.8	3,600	6,512	**192.5**	3,016	7,020	**355.5***	490.9	795.3	546.5	0.75	**459.1**	**1.05**
A-C0-r-b	*518.5*	*CF*	*59.7*	*39.8*	*3,600*	*6,512*	***192.5***	*3,016*	*7,020*	***355.5****	*490.9*	*795.3*	*546.5*	*0.75*	***459.1***	***1.13***
A-C0-r-c	456.9	CF	59.7	39.8	3,600	6,512	**192.5**	3,016	7,020	**355.5***	490.9	795.3	546.5	0.75	**459.1**	**1.00**
A-C0-s-a	423.4	CF	59.4	39.5	3,600	6,512	**191.3**	3,016	7,020	**353.3***	490.9	795.3	546.5	0.65	**421.0**	**1.01**
A-C0-s-b	*480.2*	*CF*	*59.4*	*39.5*	*3,600*	*6,512*	***191.3***	*3,016*	*7,020*	***353.3****	*490.9*	*795.3*	*546.5*	*0.65*	***421.0***	***1.14***

A-C0-s-c	431.2	CF	59.4	39.5	3,600	6,512	**191.3**	3,016	7,020	**353.3***	490.9	795.3	546.5	0.65	**421.0**	**1.02**
B-C1-p-a	716.4	CF	118.4	86.7	3,600	6,512	**312.2**	2,320	6,240	402.4	314.2	886.5	**389.9***	0.80	**624.1**	**1.15**
B-C1-p-b	708.0	CF	118.4	86.7	3,600	6,512	**312.2**	2,320	6,240	402.4	314.2	886.5	**389.9***	0.80	**624.1**	**1.13**
C-C1-p-a	700.8	SFS	108.2	78.6	-	-	**-**	4,016	9,396	1,001.9	559.9	862.0	**675.7**	-	**675.7**	**1.04**
C-C1-p-b	695.4	SFS	108.2	78.6	-	-	**-**	4,016	9,396	1,001.9	559.9	862.0	**675.7**	-	**675.7**	**1.03**

Notes:

$f_{cu,150}$ is the average compressive strength of 150×150×150 mm concrete cubes;

Q_{Rd} is the design shear resistance of the shear connection, i.e. the minimum of the shear resistances of the shear connector, the concrete under direct bearing, and the weldment;

Q_{Rt} is the measured shear resistance of the shear connection, Q_m; and

The model factor $\eta = Q_{Rt} / Q_{Rd}$.

* denotes those connectors which resistances of bolts influenced by the fibre content of concrete block because of reduced ductility.

3.5.2 Shear connections with welded shear connectors

The shear resistances of Types SC, BC, and PC connections should be designed against the following failure modes:

- cracking and crushing failure of the encasing concrete block;
- shear fracture of the shear connector; and
- shear failure of the weldment between the shear connector and the base plate.

In general, the design shear resistance of the shear connection, Q_{Rd} , is given by:

$$Q_{Rd} = \min (Q_{cbs} , Q_{sfs} , Q_w) \tag{3.3}$$

in which the design rules for various resistances are presented as follows:

a) The bearing resistance of the concrete, Q_{cbs} , is given by (EC4, 1992):

$$Q_{cbs} = A_{c1} f_{ck} \left(\frac{A_{cp1}}{A_{c1}}\right)^{0.5} \tag{3.4}$$

where Q_{cbs} is the bearing resistance of concrete under direct bearing;

f_{ck} is the characteristic cylinder compressive strength of concrete;

A_{c1} is the bearing area of the concrete in the vicinity of the shear connector; and

A_{cp1} is the projected area of the concrete along the loading direction.

b) The shear resistance of the shear connector, Q_{sfs} , is given by:

$$Q_{sfs} = 0.8 \times 2A_s f_{usc} \tag{3.5}$$

where A_s is the cross-sectional area of a shear connector; and

f_{usc} is the tensile strength of the shear connector.

c) The shear resistance of the weldment Q_w attaching the shear connector onto the base plate is given by:

$$Q_w = p_w \; a_w \; (1.25\, L_T + L_L) \tag{3.6}$$

where p_w is the yield strength of the weld;

a_w is the throat size of the weld;

L_T is the transverse welding length; and

L_L is the longitudinal welding length.

Refer to Reference (Ding *et al*., 2024) and Section 5.8 of Chapter 5 for details of the proposed design rule. The design shear resistances of shear connections of various welded shear connectors covered in the present investigation are summarised in Table 3.9. It should be noted that:

- For Tests SC, the values of Q_{cbs} are shown to be smaller than those of Q_w , and hence, concrete failure is predicted to be critical, which agrees with the test results. The shear resistances of the solid connectors are expected to be very large, and hence, these are not critical.
- For Tests BC and PC, most of the values of Q_{sfs} are shown to be smaller than those of Q_{cbs} and Q_w, and hence, shear fracture of the shear connectors is predicted to be critical. This also agrees well with the test results.
- In all tests, the values of Q_w are shown to be larger than those of Q_{cbs} and Q_{sfs}, and hence, weld fracture is predicted *not* to be critical. This is also in agreement with the test results.

In order to determine structural adequacy and efficiency of these design rules, a model factor η is established, and it is defined as follows:

$$\eta = Q_{Rt} / Q_{Rd} \tag{3.7}$$

In general, the value of η is expected to range from 1.0 to 1.3 so that the design rule is conservative, and yet effective. The values of η for these shear connections are also summarised in Table 3.9, and it is shown that:

- For Tests SC-h3 and SC-h2 with Concrete C1, the values of η are found to be 1.12 and 1.07 respectively, and hence, the proposed design rule is demonstrated to be effective for these shear connections which fail predominantly in concrete crushing and cracking.

- For Tests BC-a, BC-b, BC-c and BC-d with Concrete C1, the values of η are found to range from 1.10 to 1.30, and hence, the proposed design rule is also demonstrated to be effective for these shear connections.
- For Tests PC-r-C1 and PC-C1 with Concrete C1, the values of η are found to range from 1.11 to 1.23, and hence, the proposed design rule is also demonstrated to be effective.
- For the test with profiled connector and Concrete C1-s, i.e. Test PC-C1-s, the value of η is found to be merely 0.98, and hence, the proposed design rule is demonstrated to be applicable to these shear connections only after improvement is made to ensure structural adequacy of the proposed rule.

Table 3.9 Comparison on measured and design shear resistances of Types SC, BC, and PC connections

Test	Q_{Rt} (kN)	Failure mode	Concrete failure				Fracture of shear connectors			Fracture of weld	Q_{Rd} (kN)	η
			$f_{cu,150}$ (N/mm^2)	f_{ck} (N/mm^2)	A_{c1} (mm^2)	Q_{cbs} (kN)	A_s (mm^2)	f_{usc} (N/mm^2)	Q_{sfs} (kN)	Q_w (kN)		
SC-C1-h3	1,173.3	CF	99.9	71.9	6,500	**1,043.8**	-	-	-	1,054.5	**1,043.8**	**1.12**
SC-C1-h2	976.5	CF	99.9	71.9	5,000	**915.5**	-	-	-	1,054.5	**915.5**	**1.07**
SC-C1-h1	702.1	CF	99.9	71.9	3,500	**766.0**	-	-	-	1,054.5	**766.0**	**0.92**
BC-C1-a	1,069.8	SFS	89.8	63.8	7,200	**975.1**	3,400	430.4	1,170.7	1,506.4	**975.1**	**1.10**
BC-C1-b	969.4	SFS	89.8	63.8	7,200	975.1	2,500	430.4	**860.8**	1,069.5	**860.8**	**1.13**
BC-C1-c	803.1	SFS	89.8	63.8	7,200	975.1	1,800	430.4	**619.8**	798.4	**619.8**	**1.30**
BC-C1-d	635.1	SFS	87.5	62.0	5,850	853.6	1,600	430.4	**550.9**	632.7	**550.9**	**1.15**
PC-r-C1	1,010.0	SFS	109.2	79.4	6,400	1,142.9	2,271	450.2	**818.0**	1,082.1	**818.0**	**1.23**
PC-C1-a	911.4	SFS	109.2	79.4	6,400	1,142.9	2,271	450.2	**818.0**	1,082.1	**818.0**	**1.11**
PC-C1-b	934.1	SFS	109.2	79.4	6,400	1,142.9	2,271	450.2	**818.0**	1,082.1	**818.0**	**1.14**
PC-C1-s	788.2	CF	80.1	56.1	6,400	**807.1**	2,271	450.2	818.0	1,082.1	**807.1**	**0.98**

Notes:
$f_{cu,150}$ is the average compressive strength of 150×150×150 mm concrete cubes;
Q_{Rd} is the design shear resistance of the shear connection, i.e. the minimum of the shear resistances of the shear connector, the concrete under direct bearing, and the weldment;
Q_{Rt} is the measured shear resistance of the shear connection, Q_m; and
The model factor $\eta = Q_{Rt} / Q_{Rd}$.

3.6 Conclusions

An investigation into the structural behaviour of the connections with six types of shear connectors and steel fibre reinforced concrete blocks was presented. The connector configurations were proposed to provide a favourable combination of high resistance and ductile responses, and ease of on-site assembly. The inelastic behaviour of 39 shear connections was examined experimentally,

and the effects of connector type, fibre content in concrete block, and bolt diameter were directly examined. Both the results and the observations of connections were used to evaluate applicability of existing codified formulae, and necessary modifications were highlighted where required. Key findings of the investigation are summarised as follows:

a) The structural behaviour of the connections with six different types of shear connectors with different forms and fabrication processes were examined under single-sided push-out tests. After comparing the deformation characteristics of these shear connections, four shear connections, i.e. Tests SC-C1-h3, BC-C1-a, PC-r-C1, and A-C1-p, were identified as effective based on their favourable combinations of shear resistance, initial stiffness, and ductility, coupled with their "simple on-site assembly" in large scale composite beams. The tests clearly indicated two distinct failure modes for the connections, namely i) Mode CF - failure of concrete blocks with severe crushing and cracking, and ii) Mode SFS - shear yielding of the steel connectors. As the shear connections with concrete blocks were loaded directly in the absence of concrete slabs, many of these concrete blocks were found to have significant tilting, especially towards the end of the tests.

b) Addition of steel fibres to C100 concrete blocks is shown to be efficient to increase the shear resistance, initial stiffness and slippage limit of the connections with Type A connector. It is obvious that the steel fibres are able to improve both the tensile strength and the ductility of the high strength concrete, and they contribute to crack control by bridging micro-cracks and preventing their propagation. When the steel fibre content is 1.5%, the structural behaviour of the shear connection with Type A connector and C100 concrete is demonstrated to be highly effective.

c) Codified design provisions, which account for concrete failure, and shear fracture of

connectors and weld failure, were shown to be largely effective in determining the shear resistances of the proposed shear connections with different shear connectors and concrete mixes, except for some specific cases in which modifications to the prediction expressions would be required.

Overall, this investigation proposes four different forms of large-resistance shear connectors that offer ductile behaviour as well as significant constructional benefits in terms of simple on-site assembly of large-scale composite beams consisting of precast concrete and steel sections. The inelastic performance of these shear connectors was examined and verified through experimental assessments, and suitability of the design approaches for predicting their shear resistances was evaluated and discussed.

Owing to an absence of precast concrete slabs in these tests, any potential failure in the vicinity of the per-formed pockets of the precast concrete slabs was untested, and hence, these proposed shear connectors should *only* be used after it is satisfied that any failure in the vicinity of these pre-formed pockets of the precast concrete slabs has been properly prevented.

Due to the favourable behaviour of Type A shear connector with C100 concrete block in terms of shear resistance, initial stiffness, and ductility, a series of standard push-out tests have been carried out to investigate the structural behaviour of this shear connection, and examine any possible failure in the vicinity of the pre-formed pockets of the precast concrete slabs. Details of the test programme, test results and key findings of these standard push-out tests are reported in Chapter 4.

CHAPTER 4

EXPERIMENTAL INVESTIGATIONS USING STANDARD PUSH-OUT TESTS

4.1 Introduction

This chapter presents experimental investigations into the structural behaviour of the proposed effective bolted shear connections with steel fibre reinforced concrete (SFRC), as presented in Chapter 3. A total of twenty large-scale standard push-out tests were conducted on the shear connections with three types of bolted shear connectors, i.e. Types A to C, and one type of modified T-perfobond rib shear connector, i.e. Type D, to examine and quantify the deformation characteristics of these shear connections. Key parameters include connector configuration, steel block thickness, concrete block size, bolt diameter, and concrete block strength. A detailed account of the experimental investigation in terms of test programme, fabrication of test specimens, test setup and instrumentation, as well as loading procedures are presented. Together with the results of the standard push-out tests, results of the material tests on the concrete blocks, precast concrete slabs, steel bolts, welded steel sections and steel reinforcements are reported.

In this chapter, when presenting the results of the standard push-out tests, typical failure modes in each type of shear connection is firstly presented, followed by the representative load-slippage curves, which are provided by averaging the relative slippages of the four shear connections to illustrate the detailed deformation characteristics of each specimen. Then, measured load-slippage curves and load-separation curves are presented.

This chapter provides a detailed amount of the measured data obtained from the standard push-out

tests on the proposed shear connections. A comprehensive analysis of the test results is presented in Chapter 5.

4.2 Test programme

The test programme of the standard push-out tests is summarised in Table 4.1. All the specimens are grouped into four types with the designations as follows:

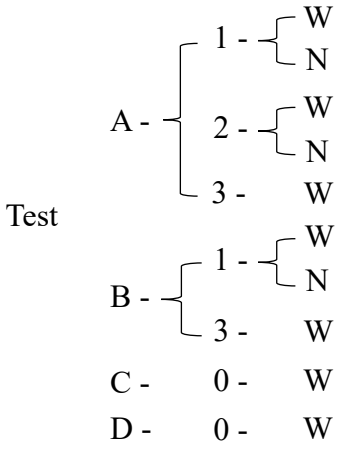

a) The first label specifies the connector types as follows:

A denotes a pair of specially designed bolts (each having a partially threaded shank) with a steel block, i.e., Configuration RBN, with a nominal bolt diameter of 30 mm.

B denotes a pair of specially designed bolts (each having a partially threaded shank) with a steel block, i.e., Configuration RBN, but with a nominal bolt diameter of 24 mm.

C denotes a pair of Grade 8.8 bolts, i.e., Configuration R, with a nominal bolt diameter of 30 mm. It should be noted that no steel block is provided in this case.

D denotes a modified T-perfobond rib shear connector with a 30 mm diameter perforation on the web, i.e. Configuration MTP, with a 16 mm diameter steel reinforcement passing through the perforation. It should be noted that the thickness and the height of the T-perfobond ribs are 12 and 120 mm respectively.

As shown in Figs. 4.1 and 4.2, compared with Connector R (ordinary bolts), the "specially designed bolt" has a partially threaded shank, in which no threads are provided in the shank

within the region to bear directly onto the steel block and the flange of the steel beam. These "specially designed bolts" are readily machined in practice. It is worth noting that for Configuration RBN, the steel block is pre-welded onto the flange of the steel beam in the shop.

b) The second label specifies the thickness of the steel block as follows:

1 denotes a 30 mm thick steel block, and hence, the dimensions of the steel block are 200(L) × 80(W) × 30 mm (H);

2 denotes a 50 mm thick steel block, and hence, the dimensions of the steel block are 200(L) × 80(W) × 50 mm (H);

3 denotes the nominal strength of the concrete block is 80 N/mm^2; and

0 denotes the absence of a steel block.

It should be noted that the second label appears as either 1 or 2 when Configuration RBN is used.

c) The third label specifies the size of the concrete block as follows:

W denotes a concrete block of 270 (L) × 240 (W) × 200 mm (H); and

N denotes a concrete block of 270 (L) × 140 (W) × 200 mm (H).

The overall arrangements of the test specimens are shown in Fig. 4.3, and it should be noted that:

- Three pieces of 30 mm thick S355 steel plates are welded together to form a welded H-section with a section depth of 260 mm and a section width of 350 mm.
- The welded H-section is sandwiched between two reinforced concrete slabs to form a standard push-out test specimen. The overall height of the specimen is 1,200 mm, in which the height of the steel section together with a 20 mm thick steel plate is 1,100 mm while the height of the reinforced concrete slabs is 1,110 mm. Hence, this setup allows a slippage between the H-section and the two concrete slabs up to 56 mm.
- Both the reinforced concrete slabs are 200 mm thick, and are made of Grade C50 normal concrete (NC) without any fibres. Steel reinforcements Y16 are provided in the concrete slabs at a spacing of about 100 mm to limit the length of any concrete cracks.
- Steel fibre reinforced concrete (SFRC) was employed to fill the preformed holes in the reinforced concrete slabs after assembling with the welded H-sections. The nominal compressive strengths of this concrete are 100 and 80 N/mm^2, and the proportional mix of the

SFRC is shown in Table 4.2. The following two types of steel fibres are used together:

- straight steel fibres (SSF) with a diameter of 0.2 mm and a length of 13 mm, and
- hooked steel fibres (HSF) with a diameter of 0.2 mm and a length of 15 mm.

In total, a total of 20 large-scale specimens were tested as indicated in Table 4.1, including two nominally identical specimens of each of the ten variations described above.

Table 4.1 Test programme of standard push-out tests

Connection configuration	Bolt diameter / Plate thickness (mm)	Designation	Size of concrete blocks (mm)	Concrete block	Size of steel block (mm)
RBN	30	A-1-W-a/b	270×240×200	C100	200×80×30
		A-1-N-a/b	*270×140×200*		
		A-2-W-a/b	270×240×200		200×80×50
		A-2-N-a/b	*270×140×200*		
		A-3-W-a/b	270×240×200	C80	200×80×30
RBN	24	B-1-W-a/b	270×240×200	C100	200×80×30
		B-1-N-a/b	*270×140×200*		
		B-3-W-a/b	270×240×200	C80	
R	30	C-0-W-a/b	270×240×200	C100	-
MTP	12	D-0-W-a/b	270×240×200		-

Table 4.2 Proportional mix of SFRC with a fibre content of 1.5% (kg / m^3)

Concrete grade	Cement	Silica fume	Fly ash	Water	SP	S/H steel fiber	River sand	Coarse aggregate (10 mm)
C80	531.7	122.7	163.6	211.9	24.5	58.9	818.0	408.0
C100	558.5	128.9	171.9	180.4	25.8	58.9	859.3	408.0

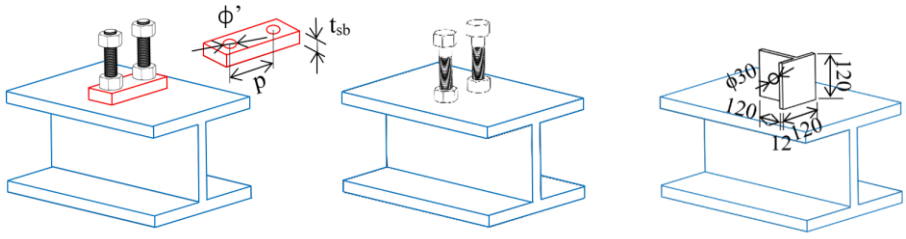

Connector RBN | Connector R | Connector MTP

Connection type	Bolt diameter ϕ (mm)	Steel block (mm)	p (mm)
RBN	30	200×80×30	120
	24		
	30	200×80×50	
R	30	-	

Fig. 4.1 Arrangements of the proposed shear connectors

Type A Type C Type D

Fig. 4.2 General views on various types of shear connectors (before concreting)

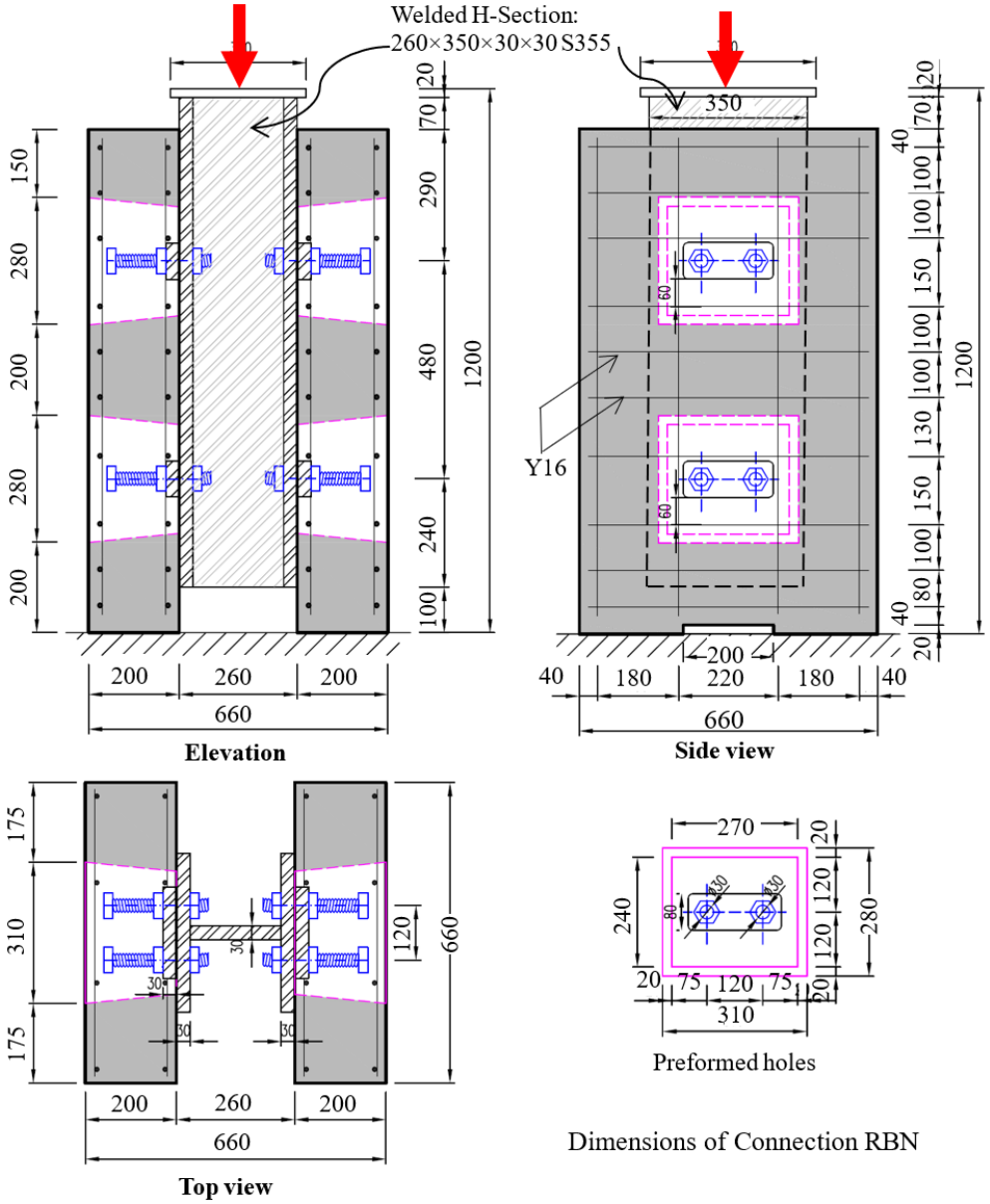

Fig. 4.3 Detailed dimensions of test specimens

4.3 Preparation of test specimens

The fabrication procedures of the test specimens are shown in Fig. 4.4 and described as follows:

i) Fabrication of reinforced concrete slabs

Steel reinforcement cages were prepared for casting of the concrete slabs, and two foam boards were placed onto the positions of the preformed holes. After securing the steel reinforcement cages onto the wooden formwork, Grade C50 concrete was placed onto the wooden formwork. After 3 days of curing, both the wooden formwork and the foam boards were removed.

ii) Application of pretension forces in bolts

- For bolts with a diameter of 30 mm, a torque of 1200 N•m was applied through a torque wrench to produce a pretension force of 280 kN onto the bolt shank.
- For bolts with a diameter of 24 mm, a torque of 600 N•m was applied through a torque wrench to produce a pretension force of 156 kN onto the bolt shank.

For each test specimen with steel bolts, a total of 8 bolts were installed onto both the flanges of the welded H-section according to the specified torque mentioned above.

iii) Assembly of test specimens and placements of infilled concrete

- Firstly, the concrete slab was placed along one side of the flange of the welded H-section, and the distance from the top surface of the concrete slab and the top steel plate of the H-section was strictly controlled as 90 mm. SFRC was then placed onto the preformed holes to encase the shear connectors.
- After two days of curing, the welded H-section was then flipped over, and SFRC was placed onto the preformed holes of the other slab to form a complete test specimen. It is worth noting that the bottom ends of both concrete slabs were carefully aligned within the same plane with the help of a specially designed device in order to avoid any significant tilting of the test specimen during the push-out test.

a) Reinforcement cages b) Slabs after concreting c) Slabs with preformed holes

d) Apply pretension force e) Specimen assembly f) Infilled concrete casting

Fig. 4.4 Fabrication procedures of test specimens

In order to obtain the mechanical properties of the various constituent components, three coupons were extracted from the bolts, the steel plates of the T-perfobond rib, as well as from the steel plates of the welded H-sections to measure their yield and tensile strengths and elastic modulus. The dimensions of the coupons for steel bolts and plates were designed according to ISO 6892-1:2019 (ISO 6892, 2019), as shown in Fig. 4.5. Additionally, for each batch of concrete, a total of four concrete cubes of 150 mm in size, and two cylinders of 150 mm in diameter and 300 mm in height, were prepared for compression tests. These were tested 28 days after casting as well as on the day of the push-out tests to obtain the compressive strengths of the concrete.

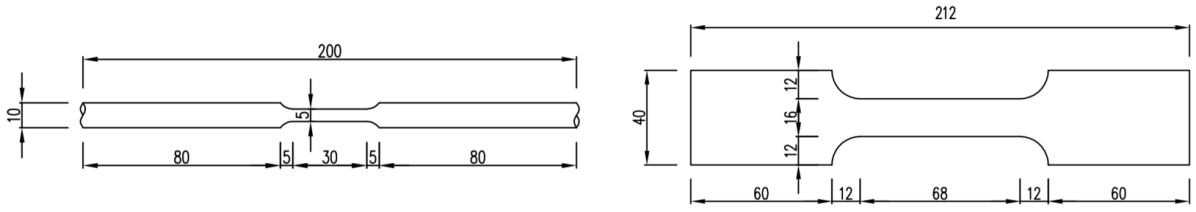

a) Steel bolts b) Steel plates

Fig. 4.5 Dimensions of steel coupons

4.4 Test setup and loading procedures

4.4.1 Test setup and instrumentation

Typical test setup and instrumentation arrangement of the standard push-out tests are illustrated in Fig. 4.6. A hydraulic testing machine with a capacity of 25,000 kN was employed to apply a vertical force onto the top steel plate of the test specimen. For each push-out test, after careful levelling and alignment, the bottom ends of the two concrete slabs in each specimen were then filled with gypsum to ensure a proper load transfer from the concrete slabs onto the reaction frame of the testing machine. Four LVDTs were placed to measure the relative slippage between the concrete slabs and the welded H-section. Two LVDTs were also provided between the bottom surface of the top plate of the welded H-section and the base plate of the testing machine to measure the absolute shortening of the test specimen. In addition, two LVDTs were provided on the left and right concrete slabs to monitor any lateral displacement of the slabs.

All measurements of the applied forces and the axial shortenings of the test specimens together with the slippages of the proposed shear connections were acquired at a close time interval with a data logger, and all the measured data was stored in a computer for subsequent data analysis.

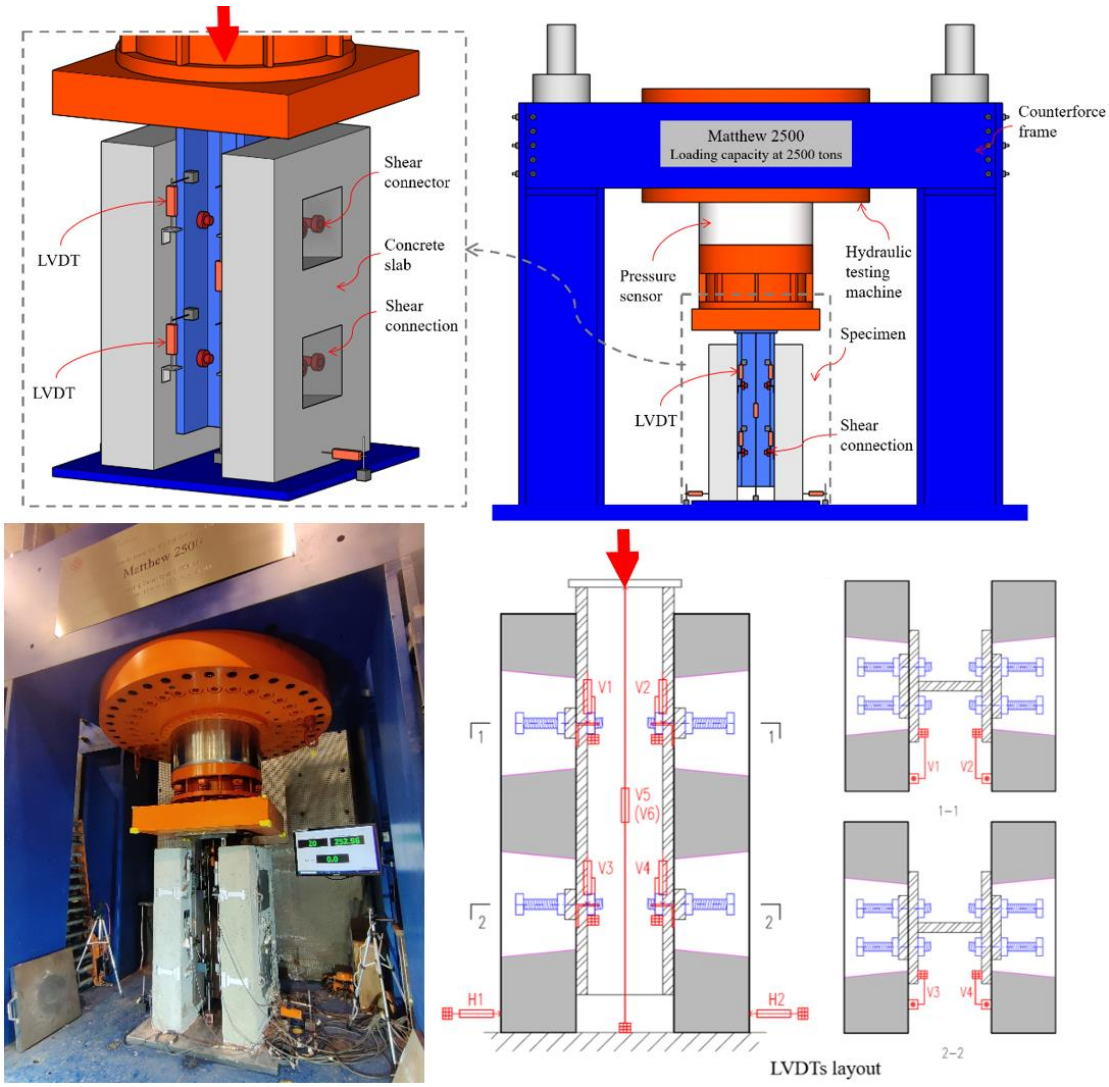

Fig. 4.6 Test setup and instrumentation

4.4.2 Loading procedures

The loading procedures of the push-out tests are illustrated in Fig. 4.7, and described as follows:

i) Preloading

- Firstly, the specimen was preloaded under load control, with the applied load increasing at a rate of 100 kN/min up to 5% of the predicted peak load of the test specimen.
- Secondly, the applied load was increased to 40% of the predicted failure load and then reduced to 5% failure load. This loading and unloading procedures were repeated 25 times over a range of 5 to 40% of the predicted peak load.

ii) Monotonic loading

- The test specimen was then loaded in displacement control, with the applied displacement

increasing at a rate of 0.2 mm/min up to failure.

- After the peak load was reached, the applied displacement was increased at a rate of up to 0.5 mm/min. The test was terminated when the applied load dropped to 80% of its peak value or there was a sudden failure, e.g. bolt fracture or concrete crushing.

After complete unloading, the test specimens were carefully inspected to identify any local failure in the shear connections, as well as surface cracking and crushing in the concrete slabs. The peak applied loads measured in the tests were recorded as the shear resistances of the test specimens.

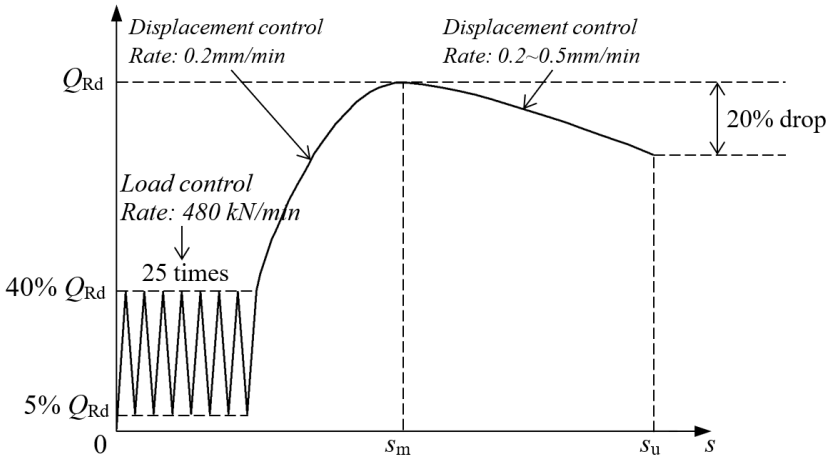

Fig. 4.7 Schematic presentation of loading procedures

4.5 Material tests

4.5.1 Steel material test

The mechanical properties of the bolt steel were tested using a servo hydraulic testing system with a loading capacity of 500 kN, as shown in Fig. 4.8a). The elastic modulus E, yield strength f_y and tensile strength f_u are presented in Table 4.3. The average yield strengths of M30 and M24 bolts are 632.1 and 629.4 N/mm^2 respectively, and their tensile strengths are 912.2 and 928.6 N/mm^2 respectively. The elastic modulus of the steel bolt is about 210 kN/mm^2. As shown in Fig. 4.8b), the stress-strain curves of M30 and M24 bolts are plotted onto the same graph for direct comparison. In addition, the measured yield and tensile strengths of the steel plates of the welded H-section are 362.7 and 477.7 N/mm^2 respectively. The measured yield and tensile strengths of the steel plates

of the T-perfobond rib are 334.4 and 504.0 N/mm^2 respectively. As shown in Fig. 4.8d), the stress-strain curves of H-section and T-perfobond rib are plotted onto the same graph for direct comparison.

a) Tensile tests for bolts

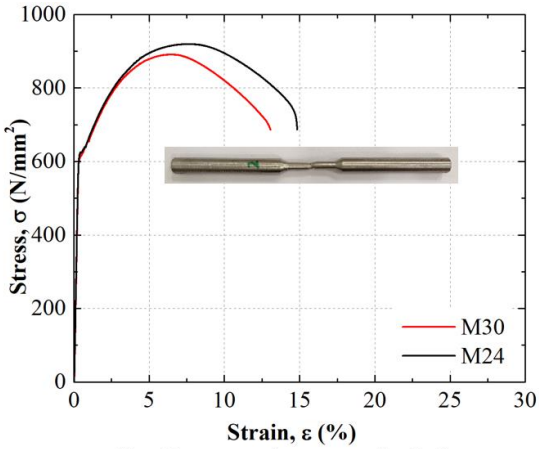

b) Stress-strain curves for bolts

c) Tensile tests for steel plates

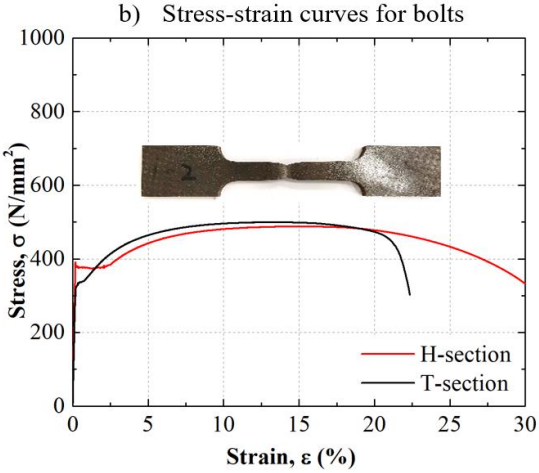

d) Stress-strain curves for steel plates

Fig. 4.8 Material tests for steel

Table 4.3 Mechanical properties of the steel

Materials	Specimen No.	t or d (mm)	f_y (N/mm^2)	f_u (N/mm^2)	E_s (kN/mm^2)
M30 bolt	1	5	615.6	891.5	218.9
	2	5	666.1	955.6	215.1
	3	5	614.6	889.5	218.6
	Average	**5**	**632.1**	**912.2**	**217.5**
M24 bolt	1	5	617.3	921.2	217.9
	2	5	645.9	944.6	220.8
	3	5	624.9	919.9	221.0
	Average	**5**	**629.4**	**928.6**	**219.9**
H-section	1	10	345.5	461.1	204.4
	2	10	366.8	483.7	206.3
	3	10	375.9	488.2	196.5
	Average	**10**	**362.7**	**477.7**	**202.4**
T-perfobond rib	1	10	331.8	504.3	176.9

	2	10	334.4	499.8	182.9
	3	10	337.1	508.0	170.9
	Average	**10**	**334.4**	**504.0**	**176.9**
Steel reinforcement	1	16	419.8	592.8	217.2
	2	16	423.2	594.3	201.1
	3	16	419.2	592.7	201.1
	Average	**16**	**420.7**	**593.3**	**206.5**

4.5.2 Concrete material test

The mechanical properties of NC and SFRC were tested using compressive machines with loading capacities of 2,000 and 4,600 kN respectively, as shown in Fig. 4.9a). The measured cube and cylinder strengths of NC in precast concrete slabs and SFRC in concrete blocks are shown in Table 4.4 a). The cube strength of NC is over 50 N/mm^2, and that of SFRC is about 100 N/mm^2. The ratios of the measured cylinder to cube strengths of NC ranged from 0.75 to 0.96, and the average value is 0.88. The ratios of the measured cylinder to cube strengths of SFRC ranged from 0.86 to 1.00, and the average value is 0.97. Additionally, as shown in Table 4.4b), the measured elastic modulus of SFRC is smaller than the values specified in EC2 (EC2, 2004), Hong Kong code of practice (COP, 2013) and GB50010 (GB50010, 2010). As shown in Fig. 4.9b), the compressive stress-strain curves of both SFRC and NC are plotted onto the same graph for direct comparison. It is evident that both the compressive stress and strain of SFRC are larger than those of NC, indicating its good mechanical properties under compression, as expected.

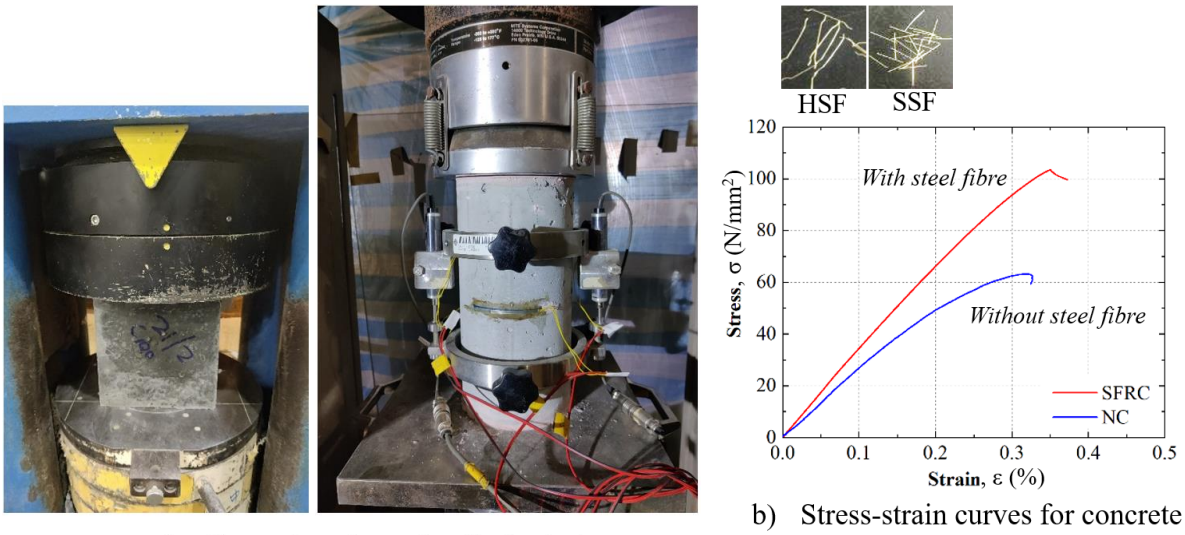

a) Concrete cube and cylinder tests

b) Stress-strain curves for concrete cylinders

Fig. 4.9 Material tests for concrete

Table 4.4 Measured data of the mechanical properties of concrete

a) Concrete strengths

Specimen No.	$f_{cup,28}$ (N/mm^2)	$f_{cup,test}$ (N/mm^2)	$f_{cyp,test}$ (N/mm^2)	$f_{cyp,test}$ / $f_{cup,test}$	$f_{cu,28}$ (N/mm^2)	$f_{cu,test}$ (N/mm^2)	$f_{cy,test}$ (N/mm^2)	$f_{cy,test}$ / $f_{cu,test}$
A-1-W-a	67.4	71.2	61.3	**0.86**	103.5	108.8	106.4	**0.98**
A-1-W-b	67.4	71.2	61.3	**0.86**	101.2	107.3	105.2	**0.98**
A-1-N-a	64.3	64.5	57.7	**0.89**	103.5	104.5	104.2	**1.00**
A-1-N-b	64.3	64.0	57.7	**0.90**	91.9	101.8	100.1	**0.98**
A-2-W-a	67.4	71.8	61.3	**0.85**	104.2	107.7	107.2	**1.00**
A-2-W-b	67.4	71.8	61.3	**0.85**	99.9	104.9	105.6	**1.01**
A-2-N-a	57.9	63.5	57.7	**0.91**	98.8	109.1	105.0	**0.96**
A-2-N-b	57.9	63.1	57.7	**0.91**	96.1	101.3	101.4	**1.00**
A-3-W-a	71.7	68.1	61.3	**0.90**	88.8	99.2	95.1	**0.96**
A-3-W-b	71.7	68.1	61.3	**0.90**	89.1	89.9	91.0	**1.01**
B-1-W-a	44.3	51.9	48.6	**0.94**	100.6	105.8	98.5	**0.93**
B-1-W-b	44.3	64.7	48.6	**0.75**	93.5	97.7	91.6	**0.94**
B-1-N-a	57.9	59.6	51.9	**0.87**	110.0	110.8	108.8	**0.98**
B-1-N-b	57.9	61.6	51.9	**0.84**	102.2	103.5	103.8	**1.00**
B-3-W-a	44.3	54.4	48.6	**0.89**	88.4	88.8	90.6	**1.02**
B-3-W-b	44.3	50.4	48.6	**0.96**	92.1	94.7	94.0	**0.99**
C-0-W-a	64.3	61.9	57.7	**0.93**	102.5	98.4	97.6	**0.99**
C-0-W-b	64.3	65.9	57.7	**0.88**	90.5	93.6	89.5	**0.96**
D-0-W-a	57.9	60.2	51.9	**0.86**	103.5	106.9	91.6	**0.86**
D-0-W-b	57.9	61.0	51.9	**0.85**	104.7	113.9	109.6	**0.96**

Notes:

$f_{cup,28}$ denotes the measured cube strengths of precast concrete slabs at 28 days;
$f_{cup,test}$ denotes the measured cube strengths of precast concrete slabs at testing days;
$f_{cyp,test}$ denotes the measured cylinder strengths of precast concrete slabs at testing days;
$f_{cu,28}$ denotes the measured cube strengths of concrete blocks at 28 days;
$f_{cu,test}$ denotes the measured cube strengths of concrete blocks at testing days; and
$f_{cy,test}$ denotes the measured cylinder strengths of concrete blocks at testing days.

b) Elastic modulus of concrete

Specimen No.	E_{cp} (kN/mm^2)	E_{ci} (kN/mm^2)	$E_{c,HK}$ (kN/mm^2)	E_c / $E_{ci,HK}$	$E_{c,EC2}$ (kN/mm^2)	E_c / $E_{ci,EC2}$	$E_{c,GB}$ (kN/mm^2)	E_c / $E_{c,GB}$

A-1-W-a	28.7	37.8	39.8	**0.95**	45.2	0.84	39.8	0.95
A-1-W-b	28.7	37.3	39.1	**0.95**	44.5	0.84	39.7	0.94
A-1-N-a	27.5	33.9	38.7	**0.87**	44.9	0.75	39.5	0.86
A-1-N-b	27.5	33.5	38.5	**0.87**	44.7	0.75	39.5	0.85
A-2-W-a	28.7	37.2	39.6	**0.94**	45.1	0.82	39.8	0.94
A-2-W-b	28.7	36.8	39.5	**0.93**	44.7	0.82	39.8	0.93
A-2-N-a	27.5	32.4	39.4	**0.82**	44.5	0.73	39.7	0.82
A-2-N-b	27.5	32.4	38.0	**0.85**	44.0	0.74	39.3	0.82
A-3-W-a	28.7	31.7	37.7	**0.84**	43.2	0.73	39.2	0.81
A-3-W-b	28.7	32.1	37.1	**0.87**	42.7	0.75	39.0	0.82
B-1-W-a	28.3	29.1	35.8	**0.81**	42.6	0.68	38.6	0.75
B-1-W-b	28.3	30.5	36.9	**0.83**	43.0	0.71	39.0	0.78
B-1-N-a	28.6	37.5	40.3	**0.93**	45.0	0.83	40.0	0.94
B-1-N-b	28.6	37.6	42.1	**0.89**	45.8	0.82	40.4	0.93
B-3-W-a	28.3	33.0	39.4	**0.84**	43.4	0.76	39.7	0.83
B-3-W-b	28.3	33.8	39.3	**0.86**	43.9	0.77	39.7	0.85
C-0-W-a	27.5	34.3	37.5	**0.91**	43.6	0.79	39.2	0.88
C-0-W-b	27.5	31.9	36.7	**0.87**	42.5	0.75	38.9	0.82
D-0-W-a	28.6	31.5	39.0	**0.81**	42.6	0.74	39.6	0.80
D-0-W-b	28.6	35.6	40.1	**0.89**	45.0	0.79	39.9	0.89

Notes:
E_{cp} denotes the measured elastic modulus of precast concrete slabs;
E_{ci} denotes the measured elastic modulus of concrete blocks;
$E_{c,HK}$ denotes the elastic modulus of concrete blocks according to Hong Kong code of practice;
$E_{c,EC2}$ denotes the elastic modulus of concrete blocks according to Eurocode 2; and
$E_{c,GB}$ denotes the elastic modulus of concrete blocks according to Chinese code GB50010-2010.

4.6 Results of the tests with Type A connections

In the tests with Type A connections, five groups of specimens were tested to investigate the effect of steel block thickness, size of concrete block, and strength of concrete block on the structural behaviour of the shear connections.

The connection is considered as a twin connection due to the provision of a steel connector fully embedded into an infilled concrete block. Concrete failure, i.e. Mode CF, primarily appeared in both the concrete blocks and the precast concrete slabs of these tests, as shown in Fig. 4.10. When the applied load was decreased to about 15-20% of the peak load, concrete crushing took place at the ends of the precast concrete slabs. After testing, severe longitudinal and diagonal cracks were found on the surfaces of the reinforced concrete slabs. After separating the concrete slab from the steel beam, diagonal concrete cracks were found in the concrete blocks, and local concrete crushing was found in the reinforced concrete slabs. It should be noted that in those tests with Type

A connections and 30 mm thick steel blocks, individual bolts were fractured at the end of the tests, while in those tests with Type A connections and 50 mm thick steel blocks, no bolts were fractured when the applied load was decreased to 80% of the peak load.

Key results of the tests with Type A connections are summarised in Table 4.5. It should be noted that the slippages are determined by averaging the values of the four vertical LVDTs, and the corresponding load-slippage curves are considered representative. Detailed deformation characteristics of these connections are presented as follows:·

Table 4.5 Key results of tests with Type A connections

Test	$f_{cu,150}$ (N/mm^2)		Q_a (kN)	Q_m (kN)	s_m (mm)	$Q_{6.0}$ (kN)	s_u (mm)	K (kN/mm)	$Q_{0.5}/Q_m$ (%)	Failure mode	Ductility index η	Adequacy
	SFRC	NC										
A-1-W-a	108.8	71.2	6,376	1,594.0	2.5	1,439.3	9.3	2,469	67	CF	0.90	Y
A-1-W-b	107.3	71.2	6,255	1,563.8	1.5	1,449.0	7.4	2,526	71	CF	0.93	Y
A-1-N-a	104.5	64.5	5,180	1,295.0	1.0	1,221.0	9.2	2,649	80	CF	0.94	Y
A-1-N-b	101.8	64.0	5,319	1,329.8	1.6	1,316.5	10.9	2,576	78	CF	0.99	Y
A-2-W-a	107.7	71.8	7,999	1,999.8	1.7	1,588.3	5.7	1,937	48	CF	0.79	---
A-2-W-b	104.9	71.8	7,959	1,989.8	1.6	1,529.8	5.3	2,314	57	CF	0.77	---
A-2-N-a	109.1	63.5	7,318	1,829.5	1.7	1,379.3	4.9	2,666	65	CF	0.75	---
A-2-N-b	101.3	63.1	6,251	1,562.8	1.2	1,149.5	4.9	2,386	70	CF	0.74	---
A-3-W-a	99.2	68.1	6,028	1,507.0	2.0	1,405.8	11.8	2,216	67	CF	0.93	Y
A-3-W-b	89.9	68.1	5,575	1,393.8	1.9	1,313.0	8.8	1,686	60	CF	0.94	Y

Notes:

Q_a denotes the maximum applied load.
Q_m denotes the maximum applied load per connection.
s_m denotes the average slippage at the maximum applied load.
s_u denotes the average slippage at 80% Q_m in descending segment of load-slippage curves.
K denotes the average initial stiffness of the shear connection between 0 and 0.5Q_m.
$Q_{0.5}$ denotes the applied load at a slippage of 0.5 mm.
$Q_{6.0}$ denotes the applied load at a slippage of 6.0 mm.
η denotes the ductility index, and it is defined by $Q_{6.0} / Q_m$.
Adequacy: i) $Q_m \geq 1{,}000$ kN; ii) $K \geq 1{,}500$ kN/mm, and iii) $s_u \geq 6.0$ mm.

a) Type A connection with 30 mm thick steel blocks

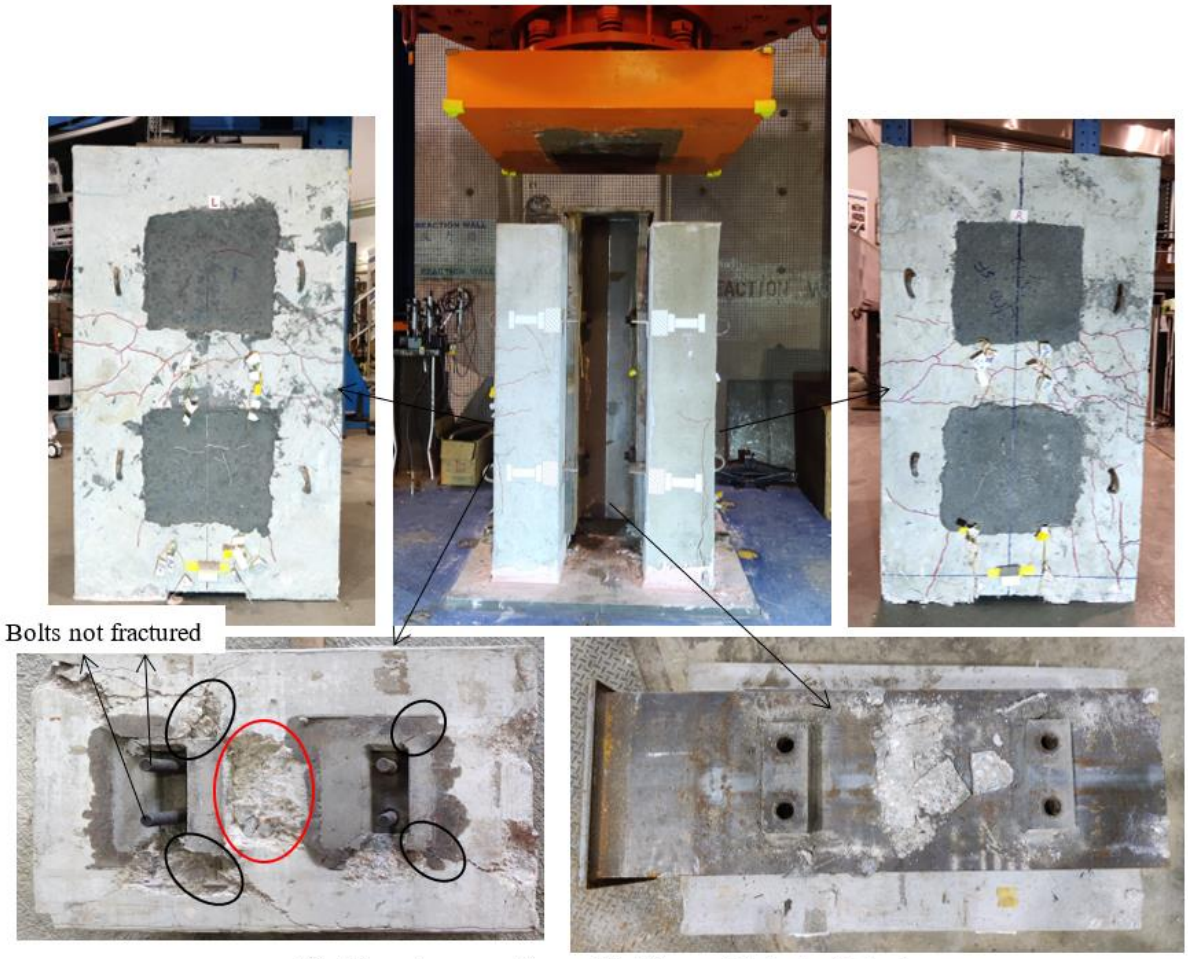

b) Type A connection with 50 mm thick steel blocks

Fig. 4.10 Mode CF in tests with Type A connections

4.6.1 Results of Test A-1-W

The representative load-slippage curves of the two nominally identical tests are shown in Fig. 4.11. Table 4.6 presents the figure Nos. of the measured curves for Tests A-1-W-a and -b. The deformation characteristics of these tests are marked on the representative load-slippage curves, and described as follows:

- Mode CF primarily appeared in the two tests, when the applied load was decreased to about 80% of the peak load, a bolt was fractured, and the middle parts of the bottom of the concrete slabs were crushed.
- The average shear resistance Q_m of Tests A-1-W is 1,578.9 kN and the corresponding slippage s_m is 2.0 mm. The ultimate slippage s_u is 8.4 mm. The average initial stiffness K is 2,498 kN/mm.
- The average lateral separations at peak loads in Tests A-1-W-a and A-1-W-b are 0.73 and 0.50 mm respectively, which are smaller than 10% of the ultimate slippage. Hence, the influence of the lateral separations of the two concrete slabs is considered to be negligible.

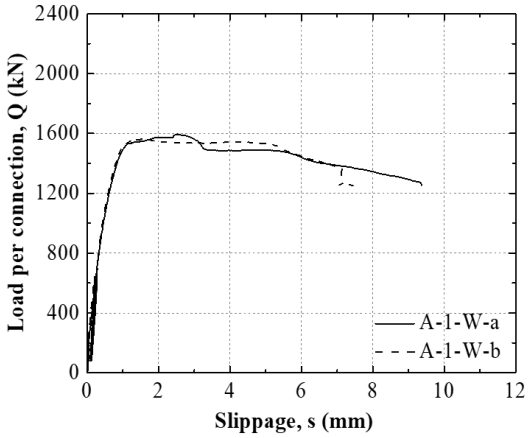

Tests	$f_{cu,150}$ (N/mm^2)	Q_m (kN)	s_m (mm)	s_u (mm)	K (kN/mm)	Failure mode
A-1-W-a	108.8	1,594.0	2.5	9.3	2,469	CF
A-1-W-b	107.3	1,563.8	1.5	7.4	2,526	CF
Average	108.1	1,578.9	2.0	8.4	2,498	CF

Fig. 4.11 Results of Tests A-1-W

Table 4.6 Measured curves for Tests A-1-W-a and -b

Figure No. for Tests		Measure curves
A-1-W-a	A-1-W-b	
4.12 a)	4.13 a)	a) Load-slippage curves measured at the upper row of shear connections
4.12 b)	4.13 b)	b) Load-slippage curves measured at the lower row of shear connections
4.12 c)	4.13 c)	c) Average of the load-slippage curves measured at the two rows
4.12 d)	4.13 d)	d) Representative load-slippage curves
4.12 e)	4.13 e)	e) Load-separation curves

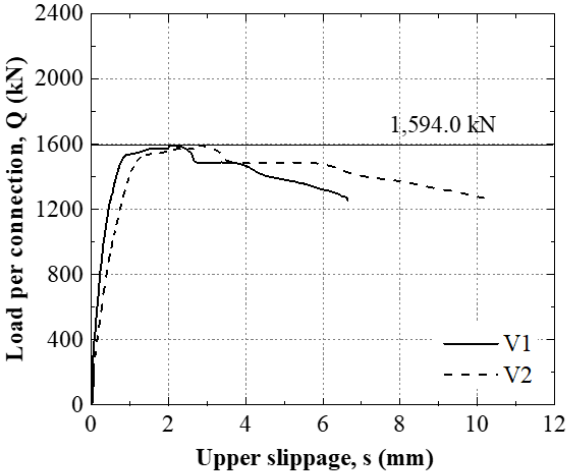

a) Load-slippage curves measured at the upper row of shear connections

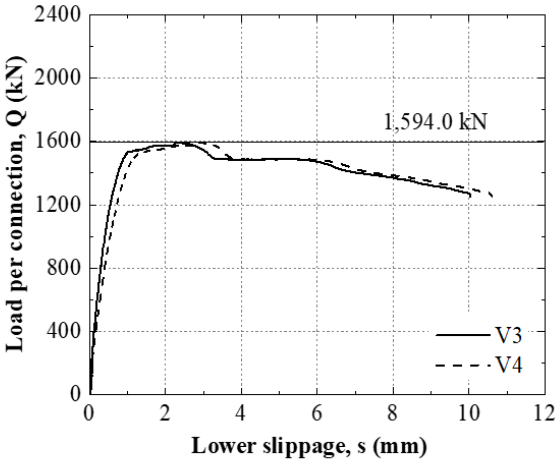

b) Load-slippage curves measured at the lower row of shear connections

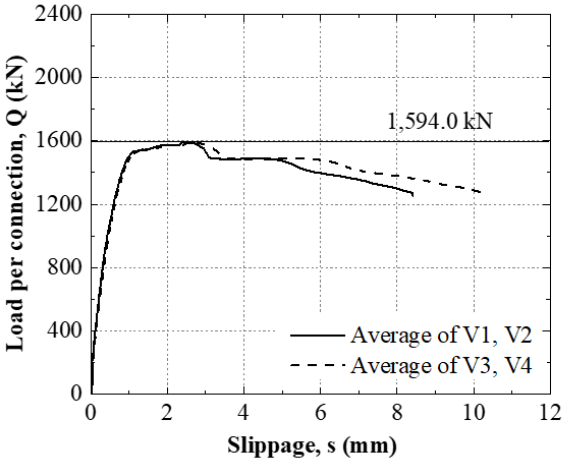

c) Average of the load-slippage curves measured at the two rows

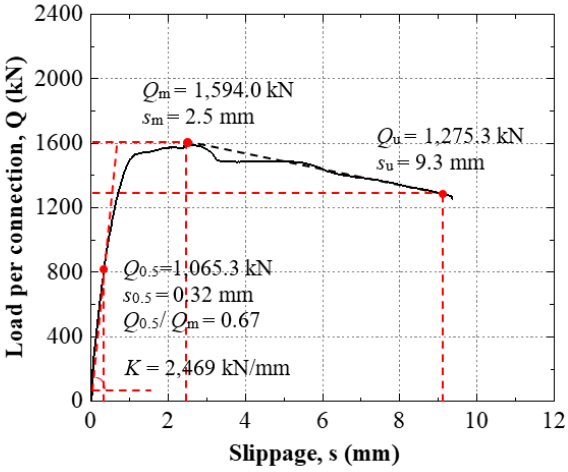

d) Representative load-slippage curves

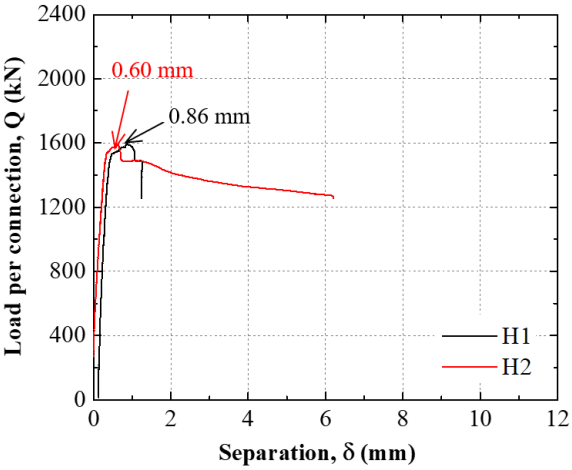

e) Load-separation curves of Test A-1-W-a

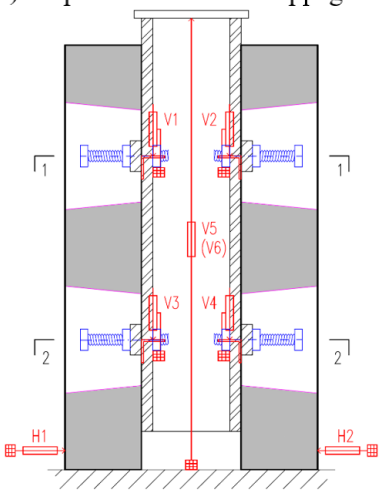

Fig. 4.12 Measured curves of Test A-1-W-a

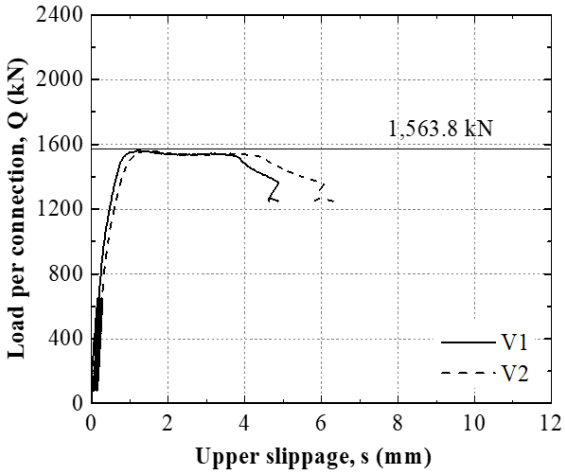

a) Load-slippage curves measured at the upper row of shear connections

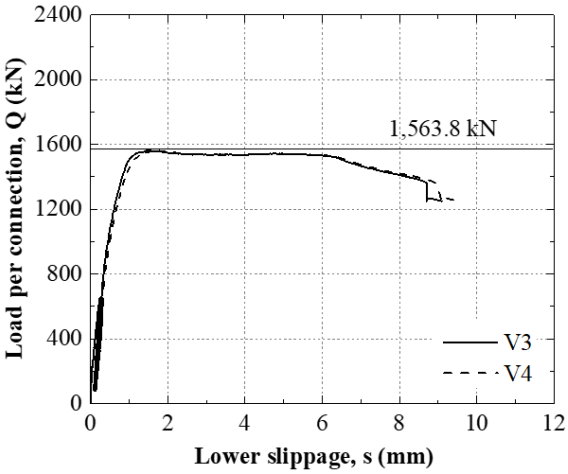

b) Load-slippage curves measured at the lower row of shear connections

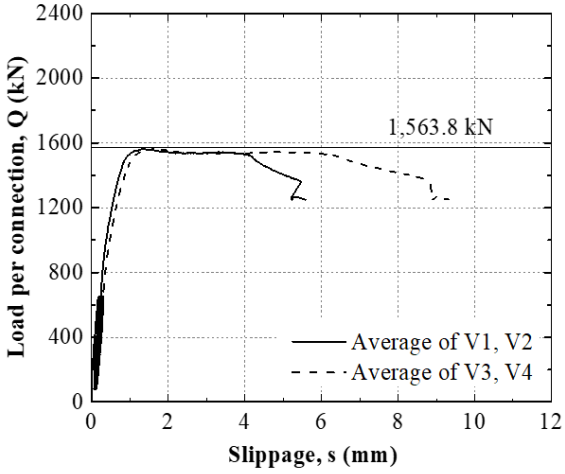

c) Average of the load-slippage curves measured at the two rows

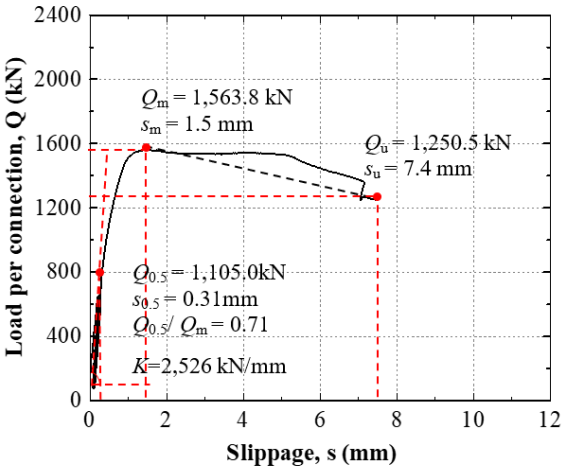

d) Representative load-slippage curves

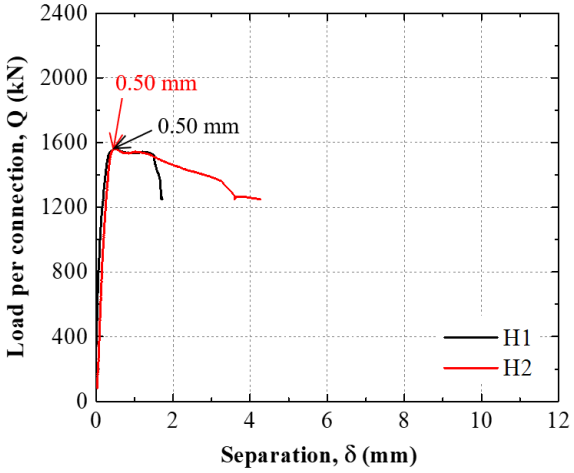

e) Load-separation curves of Test A-1-W-b

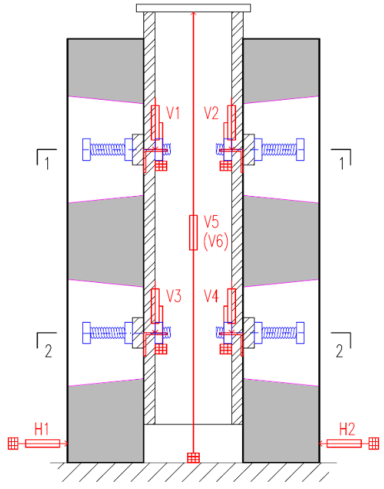

Fig. 4.13 Measured curves of Test A-1-W-b

4.6.2 Results of Test A-1-N

The representative load-slippage curves of the two nominally identical tests are shown in Fig. 4.14. Table 4.7 presents the figure Nos. of the measured curves for Tests A-1-N-a and -b. The deformation characteristics of these tests are marked on the representative load-slippage curves, and described as follows:

- Mode CF primarily appeared in the two tests, when the applied load was decreased to about 80% of the peak load, two bolts were fractured, and the middle parts of the bottom of the concrete slabs were crushed.
- The average shear resistance Q_m of Tests A-1-N is 1,312.4 kN and the corresponding slippage s_m is 1.3 mm. The ultimate slippage s_u is 10.1 mm. The average initial stiffness K is 2,613 kN/mm.
- The average lateral separations at peak loads in Tests A-1-N-a and A-1-N-b are 0.57 and 1.03 mm respectively, which are smaller than or close to 10% of the ultimate slippage. Hence, the influence of the lateral separations of the two concrete slabs is considered to be negligible.

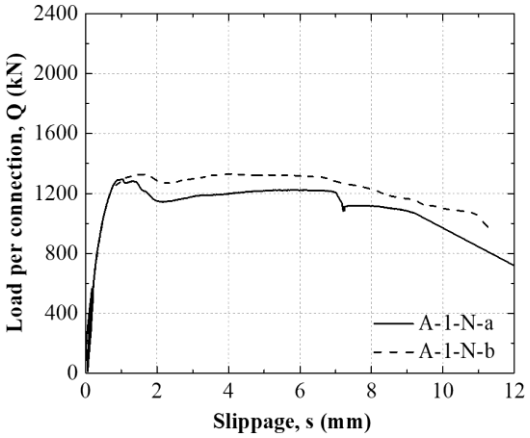

Tests	$f_{cu,150}$ (N/mm²)	Q_m (kN)	s_m (mm)	s_u (mm)	K (kN/mm)	Failure mode
A-1-N-a	104.5	1,295.0	1.0	9.2	2,649	CF
A-1-N-b	101.8	1,329.8	1.6	10.9	2,576	CF
Average	103.2	1,312.4	1.3	10.1	2,613	CF

Fig. 4.14 Results of Tests A-1-N

Table 4.7 Measured curves for Tests A-1-N-a and -b

Figure No. for Tests		Measure curves
A-1-N-a	A-1-N-b	
4.15 a)	4.16 a)	a) Load-slippage curves measured at the upper row of shear connections
4.15 b)	4.16 b)	b) Load-slippage curves measured at the lower row of shear connections
4.15 c)	4.16 c)	c) Average of the load-slippage curves measured at the two rows
4.15 d)	4.16 d)	d) Representative load-slippage curves
4.15 e)	4.16 e)	e) Load-separation curves

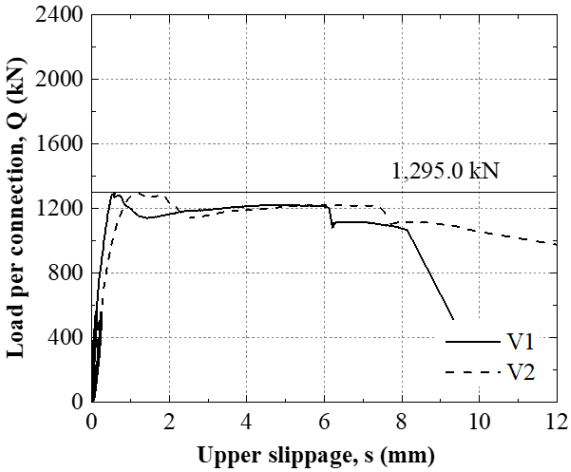

a) Load-slippage curves measured at the upper row of shear connections

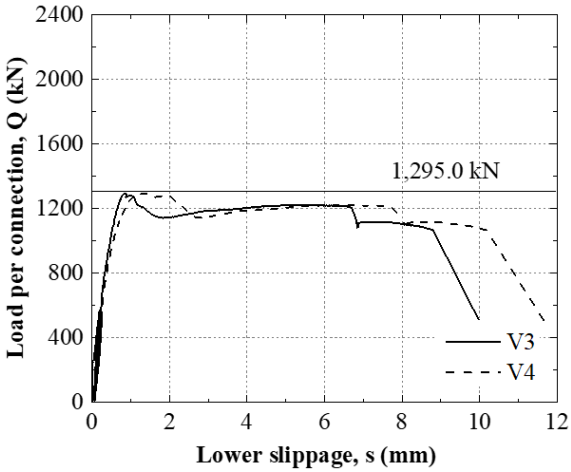

b) Load-slippage curves measured at the lower row of shear connections

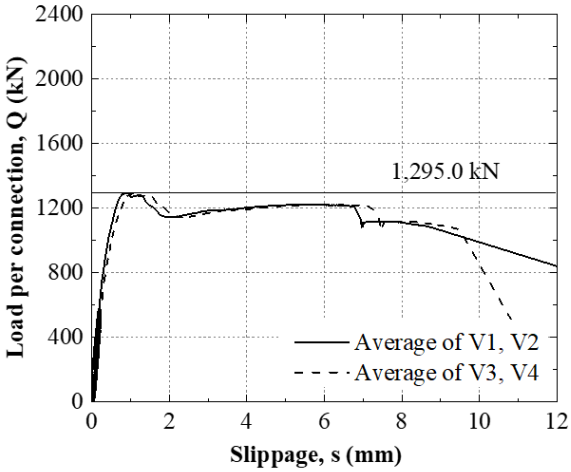

c) Average of the load-slippage curves measured at the two rows

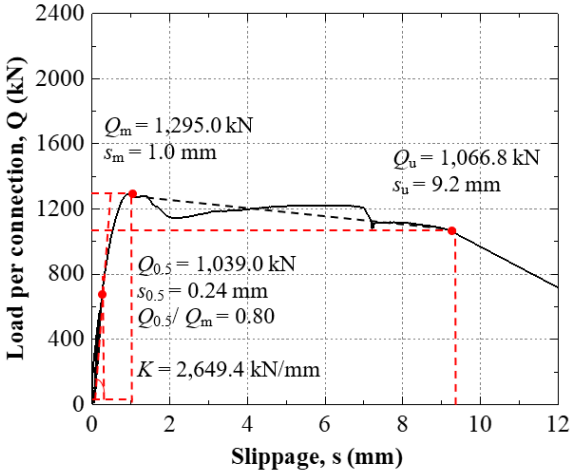

d) Representative load-slippage curves

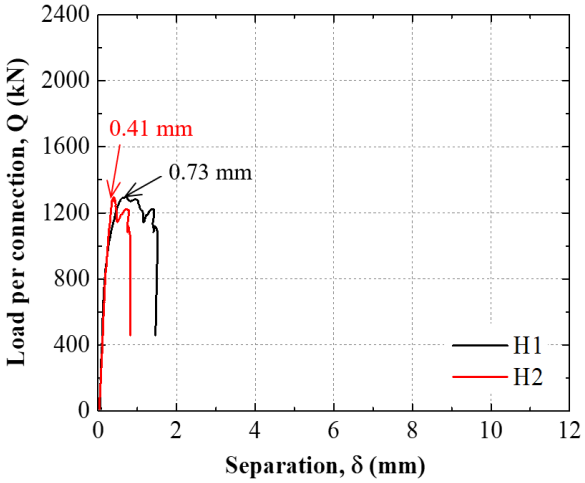

e) Load-separation curves of Test A-1-N-a

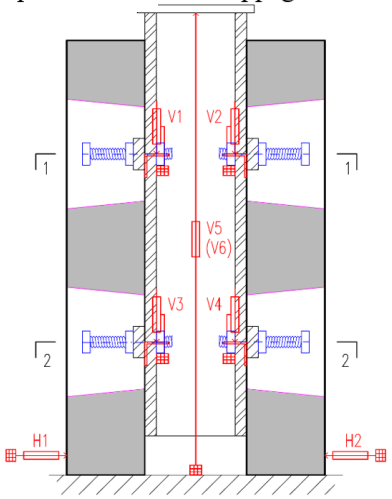

Fig. 4.15 Measured curves of Test A-1-N-a

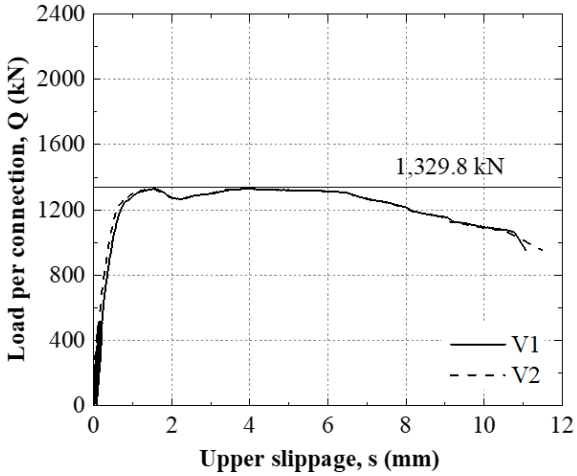

a) Load-slippage curves measured at the upper row of shear connections

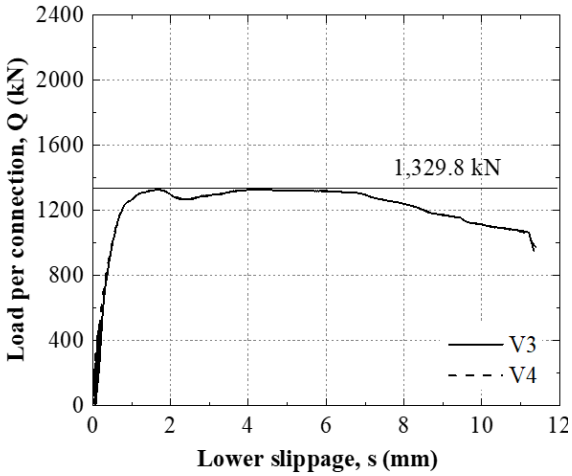

b) Load-slippage curves measured at the lower row of shear connections

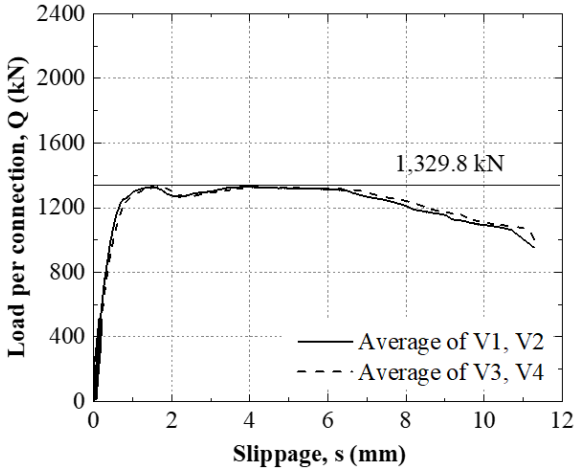

c) Average of the load-slippage curves measured at the two rows

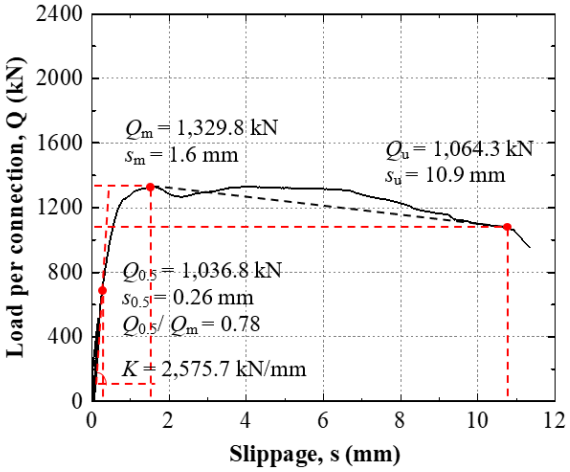

d) Representative load-slippage curves

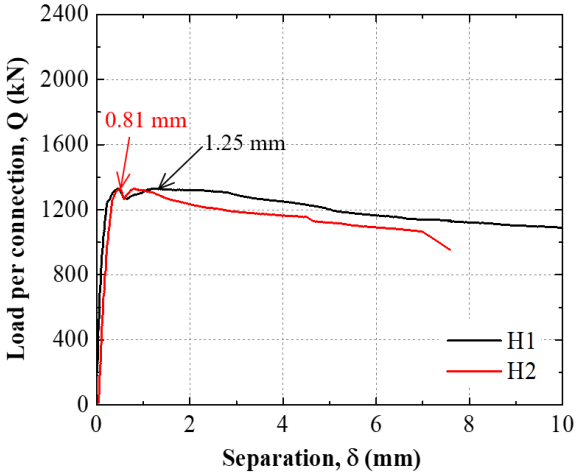

e) Load-separation curves of Test A-1-N-b

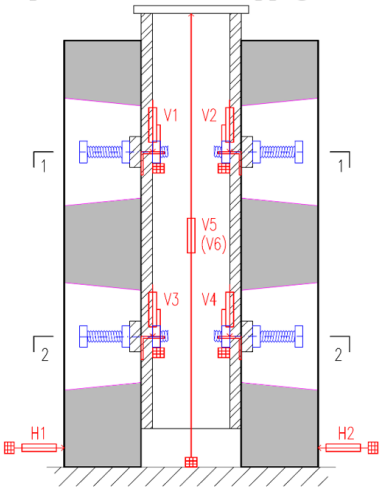

Fig. 4.16 Measured curves of Test A-1-N-b

4.6.3 Results of Test A-2-W

The representative load-slippage curves of the two nominally identical tests are shown in Fig. 4.17. Table 4.8 presents the figure Nos. of the measured curves for Tests A-2-W-a and -b. The deformation characteristics of these tests are marked on the representative load-slippage curves, and described as follows:

- Mode CF primarily appeared in the two tests, when the applied load was decreased to about 90% of the peak load, the middle parts of the bottom of the concrete slabs were crushed, while no bolts were fractured after testing.
- The average shear resistance Q_m of Tests A-2-W is 1,994.8 kN and the corresponding slippage s_m is 1.7 mm. The ultimate slippage s_u is 5.5 mm. The average initial stiffness K is 2,126 kN/mm. It should be noted that the ultimate slippage is smaller than 6.0 mm, indicating the poor ductility of these shear connections.
- The average lateral separations at peak loads in Tests A-2-W-a and A-2-W-b are 0.94 and 1.01 mm respectively, which are about 18% of the ultimate slippage.

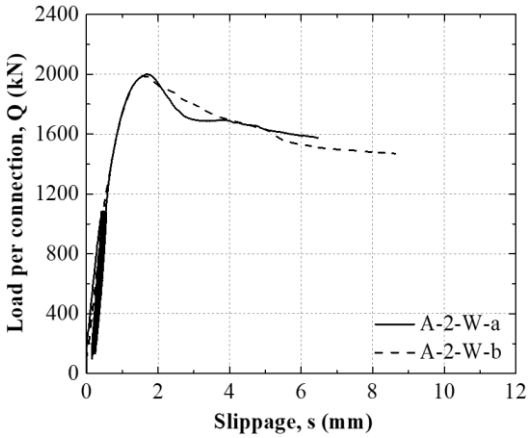

Tests	$f_{cu,150}$ (N/mm²)	Q_m (kN)	s_m (mm)	s_u (mm)	K (kN/mm)	Failure mode
A-2-W-a	107.7	1,999.8	1.7	5.7	1,937	CF
A-2-W-b	104.9	1,989.8	1.6	5.3	2,314	CF
Average	106.3	1,994.8	1.7	5.5	2,126	CF

Fig. 4.17 Results of Tests A-2-W

Table 4.8 Measured curves for Tests A-2-W-a and -b.

Figure No. for Tests		Measure curves
A-2-W-a	A-2-W-b	
4.18 a)	4.19 a)	a) Load-slippage curves measured at the upper row of shear connections
4.18 b)	4.19 b)	b) Load-slippage curves measured at the lower row of shear connections
4.18 c)	4.19 c)	c) Average of the load-slippage curves measured at the two rows
4.18 d)	4.19 d)	d) Representative load-slippage curves
4.18 e)	4.19 e)	e) Load-separation curves

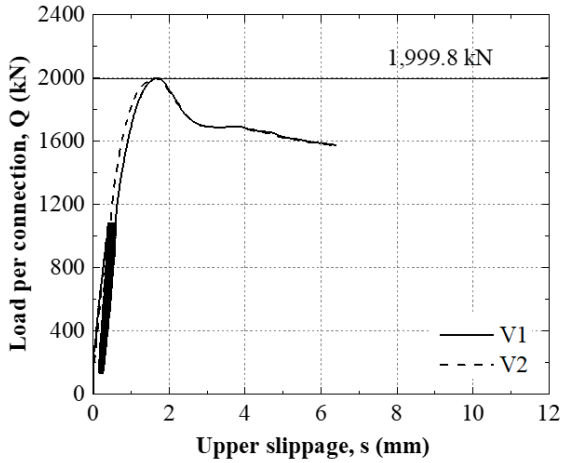

a) Load-slippage curves measured at the upper row of shear connections

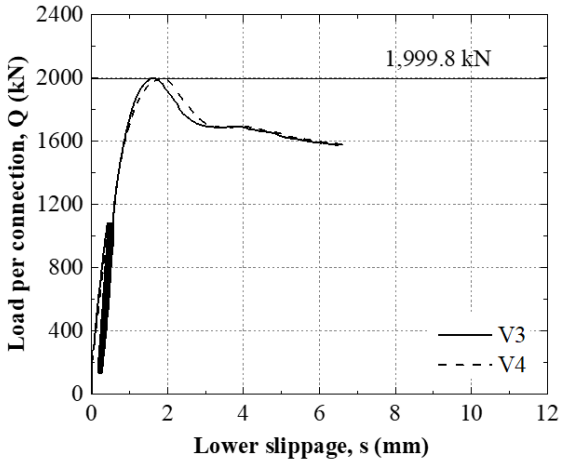

b) Load-slippage curves measured at the lower row of shear connections

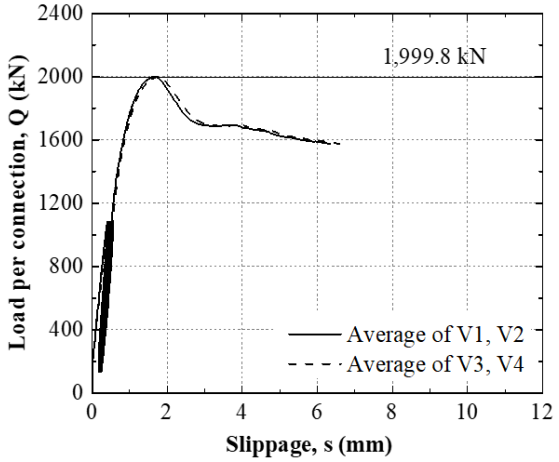

c) Average of the load-slippage curves measured at the two rows

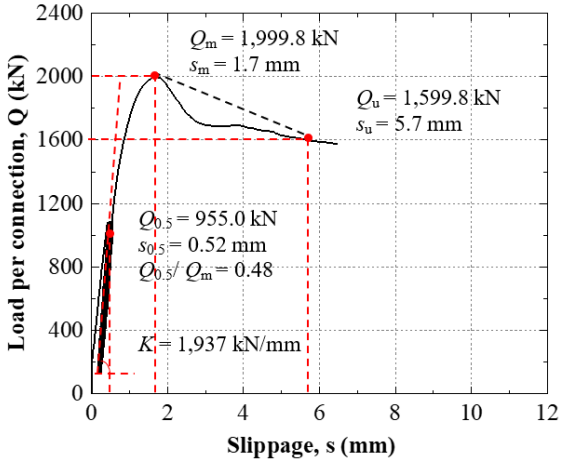

d) Representative load-slippage curves

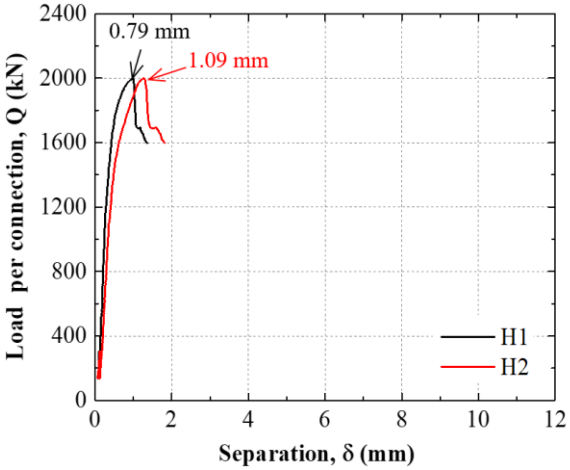

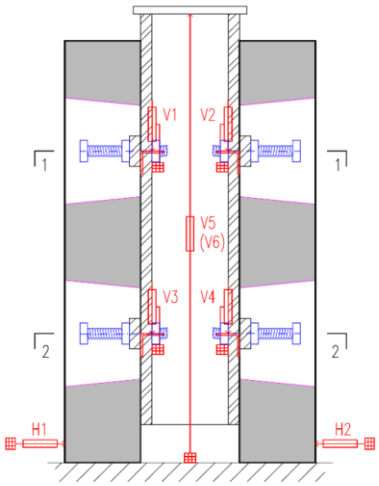

e) Load-separation curves of Test A-2-W-a

Fig. 4.18 Measured curves of Test A-2-W-a

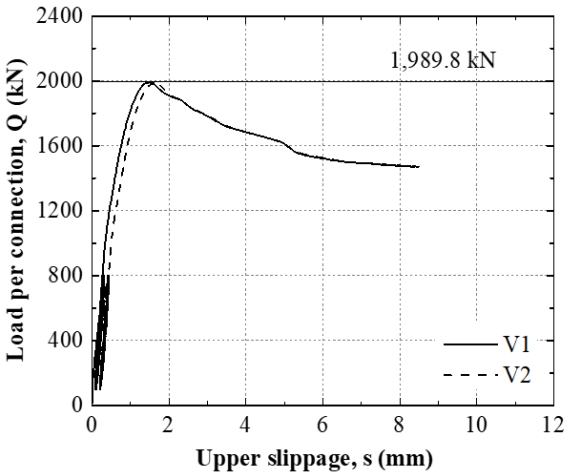

a) Load-slippage curves measured at the upper row of shear connections

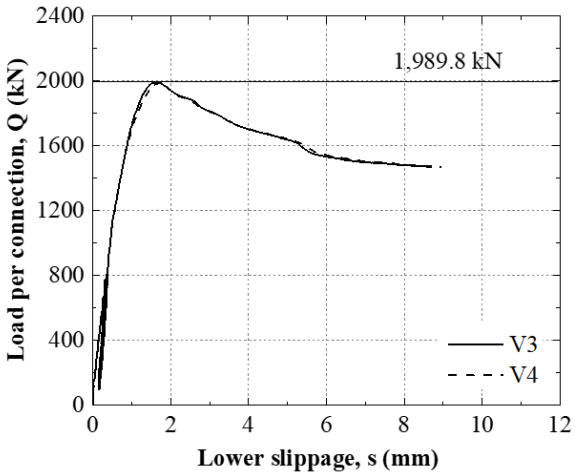

b) Load-slippage curves measured at the lower row of shear connections

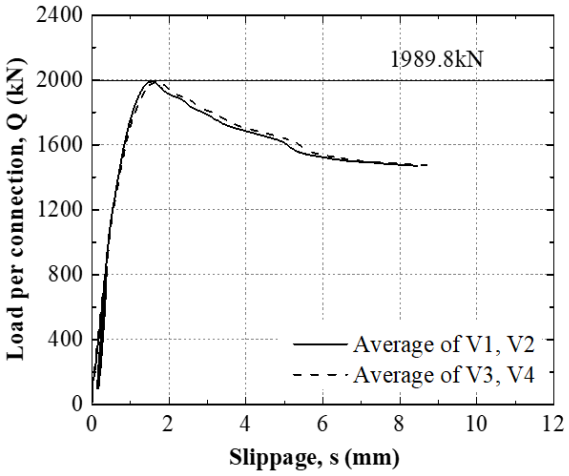

c) Average of the load-slippage curves measured at the two rows

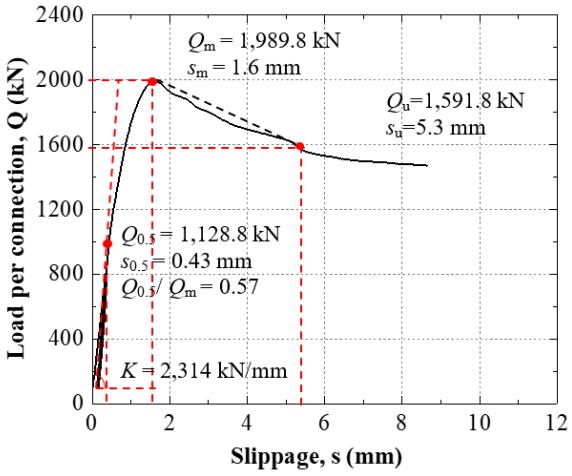

d) Representative load-slippage curves

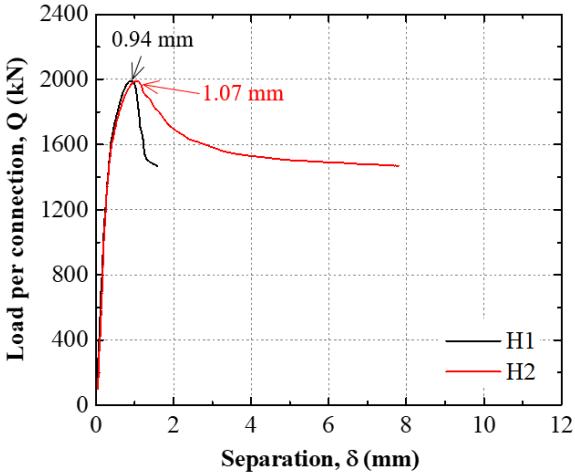

e) Load-separation curves of Test A-2-W-b

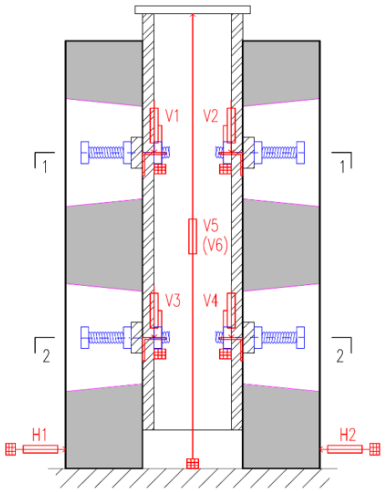

Fig. 4.19 Measured curves of Test A-2-W-b

4.6.4 Results of Tests A-2-N

The representative load-slippage curves of the two nominally identical tests are shown in Fig. 4.20. Table 4.9 presents the figure Nos. of the measured curves for Tests A-2-N-a and -b. The deformation characteristics of these tests are marked on the representative load-slippage curves, and described as follows:

- Mode CF primarily appeared in the two tests, when the applied load was decreased to about 75% of the peak load, a bolt was fractured, and the middle parts of the bottom of the concrete slabs were crushed.
- The average shear resistance Q_m of Tests A-2-N is 1,696.2 kN and the corresponding slippage s_m is 1.5 mm. The ultimate slippage s_u is 4.9 mm. The average initial stiffness K is 2,526 kN/mm. It should be noted that the two nominally identical specimens exhibit comparable initial stiffness and ultimate slippage, while the shear resistance of Test A-2-N-a is 17% larger than that of Test A-2-N-b. The reasons are: i) the concrete block strength in Test A-2-N-a is 8% larger than that in Test A-2-N-b; and ii) the levelling methods of Tests A-2-N-a and -b are different. Test A-2-N-a is levelled by gypsum, while Test A-2-N-b is levelled by cement mortar, and hence, the shear resistances of the two specimens are different.
- The average lateral separations at peak loads in Tests A-2-N-a and A-2-N-b are 0.87 and 0.81 mm respectively, which are about 17% of the ultimate slippage.

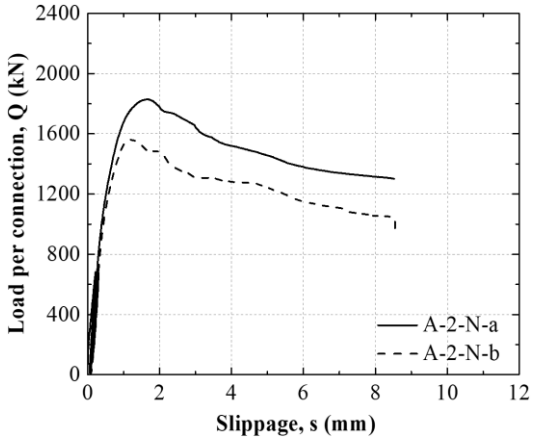

Tests	$f_{cu,150}$ (N/mm^2)	Q_m (kN)	s_m (mm)	s_u (mm)	K (kN/mm)	Failure mode
A-2-N-a	109.1	1,829.5	1.7	4.9	2,666	CF
A-2-N-b	101.3	1,562.8	1.2	4.9	2,386	CF
Average	105.2	1,696.2	1.5	4.9	2,526	CF

Fig. 4.20 Results of Tests A-2-N

Table 4.9 Measured curves for Tests A-2-N-a and -b

Figure No. for Tests		Measure curves
A-2-N-a	A-2-N-b	
4.21 a)	4.22 a)	a) Load-slippage curves measured at the upper row of shear connections
4.21 b)	4.22 b)	b) Load-slippage curves measured at the lower row of shear connections
4.21 c)	4.22 c)	c) Average of the load-slippage curves measured at the two rows
4.21 d)	4.22 d)	d) Representative load-slippage curves
4.21 e)	4.22 e)	e) Load-separation curves

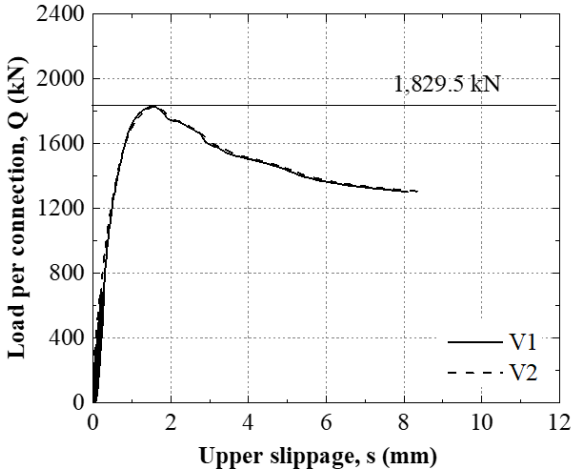

a) Load-slippage curves measured at the upper row of shear connections

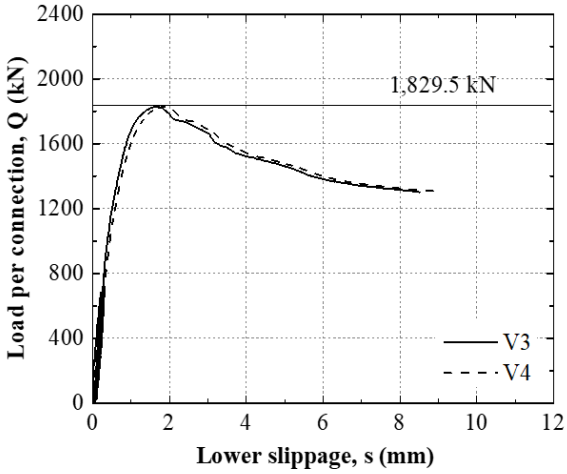

b) Load-slippage curves measured at the lower row of shear connections

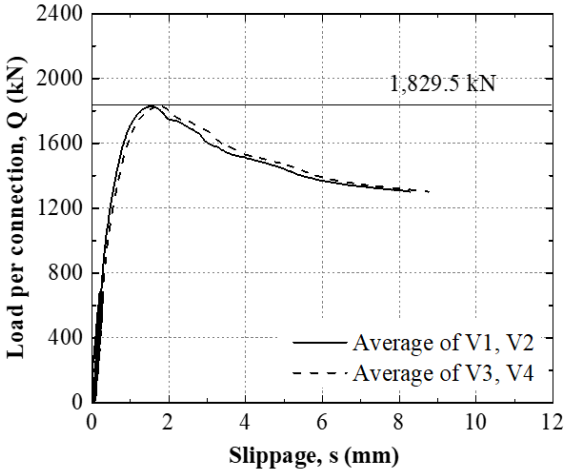

c) Average of the load-slippage curves measured at the two rows

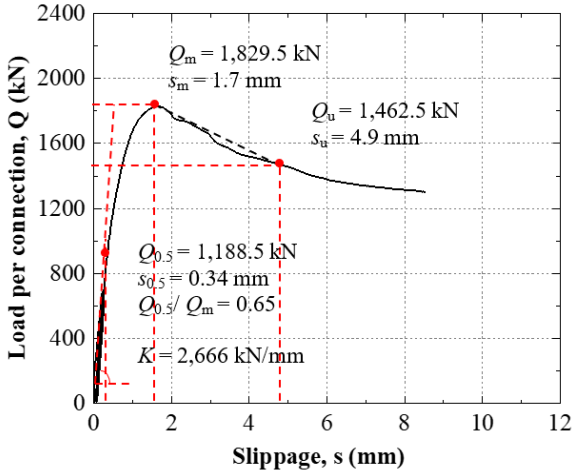

d) Representative load-slippage curves

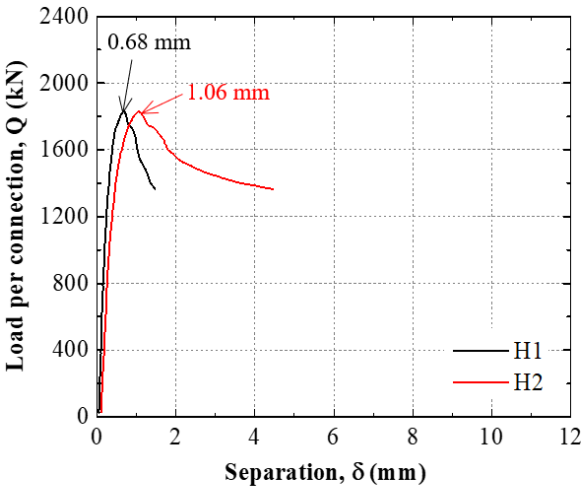

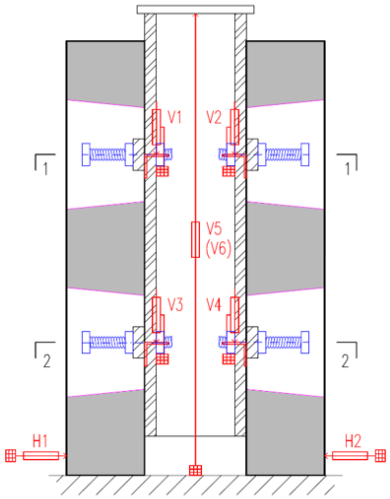

e) Load-separation curves of Test A-2-N-a

Fig. 4.21 Measured curves of Test A-2-N-a

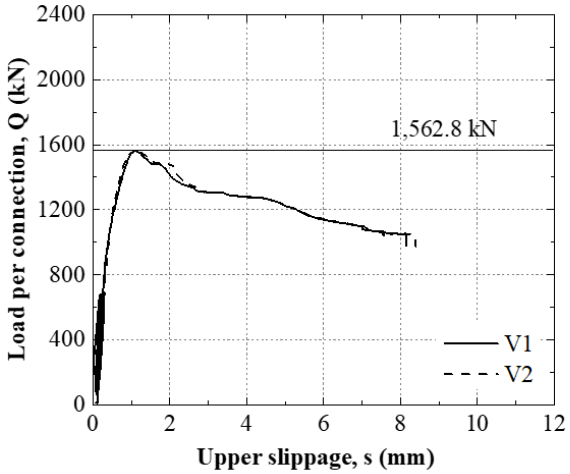

a) Load-slippage curves measured at the upper row of shear connections

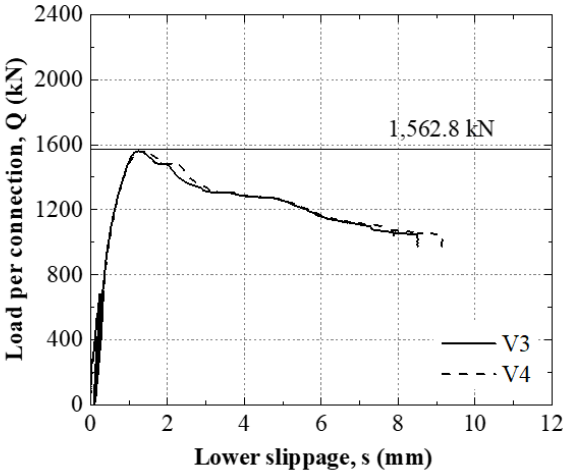

b) Load-slippage curves measured at the lower row of shear connections

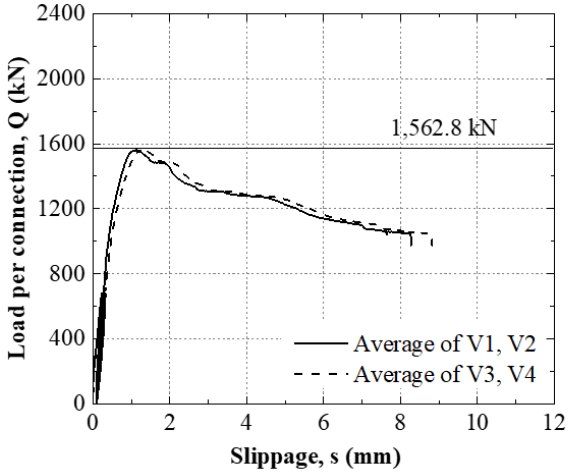

c) Average of the load-slippage curves measured at the two rows

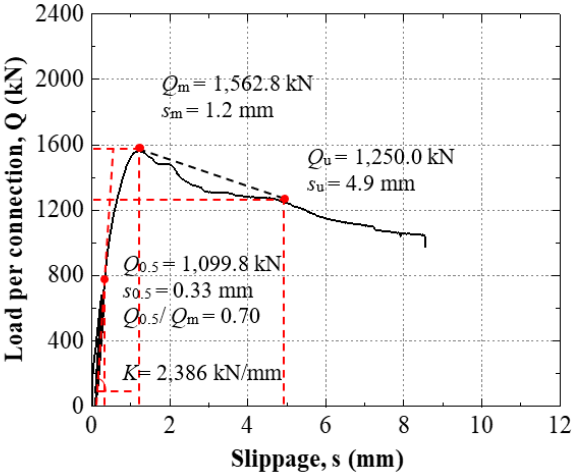

d) Representative load-slippage curves

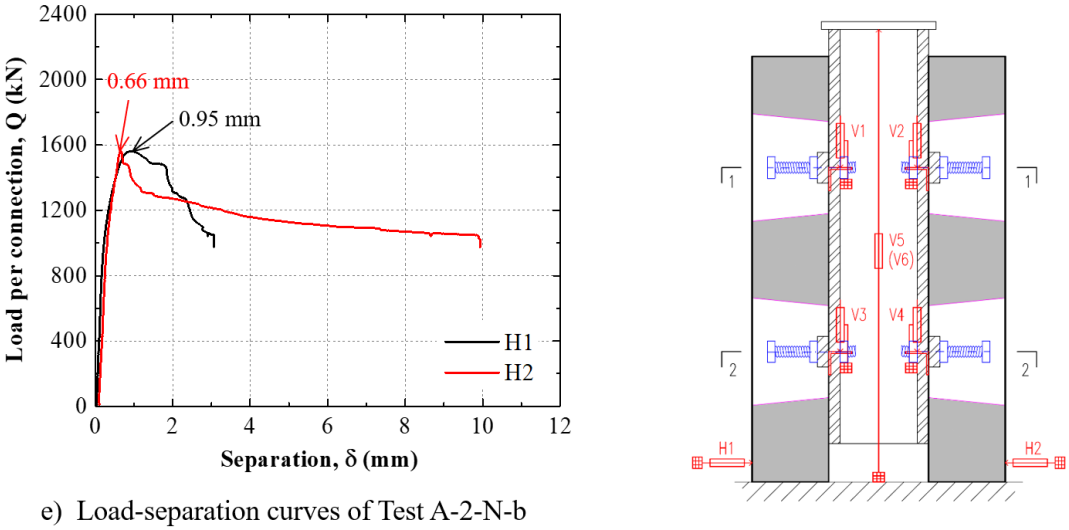

e) Load-separation curves of Test A-2-N-b

Fig. 4.22 Load-slippage curves of Test A-2-N-b

4.6.5 Results of Test A-3-W

The representative load-slippage curves of the two nominally identical tests are shown in Fig. 4.23. Table 4.10 presents the figure Nos. of the measured curves for Tests A-3-W-a and -b. The deformation characteristics of these tests are marked on the representative load-slippage curves, and described as follows:

- Mode CF primarily appeared in the two tests, when the applied load was decreased to about 80% of the peak load, a bolt was fractured, and the middle parts of the bottom of the concrete slabs were crushed.
- The average shear resistance Q_m of Tests A-3-W is 1,450.4 kN and the corresponding slippage s_m is 2.0 mm. The ultimate slippage s_u is 10.3 mm. The average initial stiffness K is 1,951 kN/mm.
- The average lateral separations at peak loads in Tests A-3-W-a and A-3-W-b are 0.62 and 0.56 mm respectively, which are smaller than 10% of the ultimate slippage. Hence, the influence of the lateral separations of the two concrete slabs is considered to be negligible.

Table 4.10 Measured curves for Tests A-3-W-a and -b

Figure No. for Tests		Measure curves
A-3-W-a	A-3-W-b	
4.24 a)	4.25 a)	a) Load-slippage curves measured at the upper row of shear connections
4.24 b)	4.25 b)	b) Load-slippage curves measured at the lower row of shear connections
4.24 c)	4.25 c)	c) Average of the load-slippage curves measured at the two rows
4.24 d)	4.25 d)	d) Representative load-slippage curves
4.24 e)	4.25 e)	e) Load-separation curves

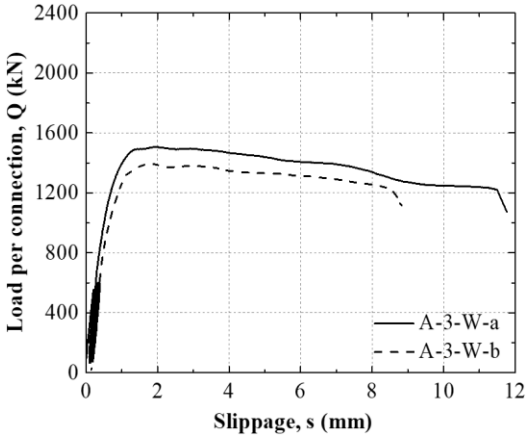

Tests	$f_{cu,150}$ (N/mm²)	Q_m (kN)	s_m (mm)	s_u (mm)	K (kN/mm)	Failure mode
A-3-W-a	99.2	1,507.0	2.0	11.8	2,216	CF
A-3-W-b	95.9	1,393.8	1.9	8.8	1,686	CF
Average	97.6	1,450.4	2.0	10.3	1,951	CF

Fig. 4.23 Results of Tests A-3-W

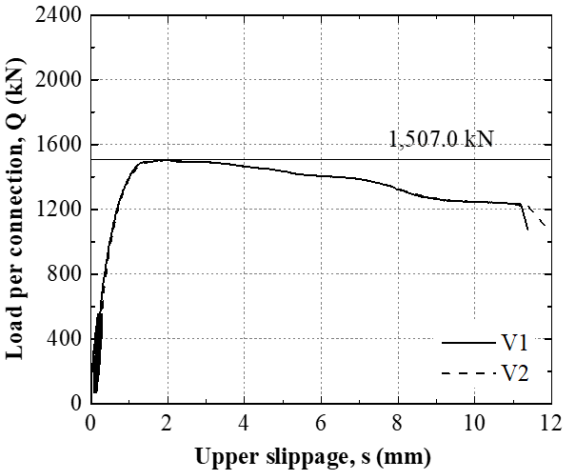

a) Load-slippage curves measured at the upper row of shear connections

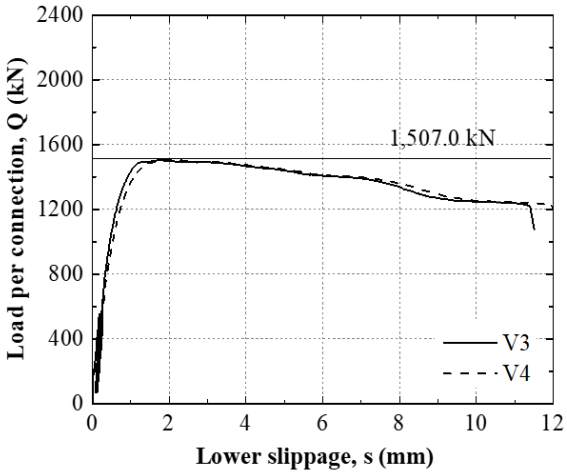

b) Load-slippage curves measured at the lower row of shear connections

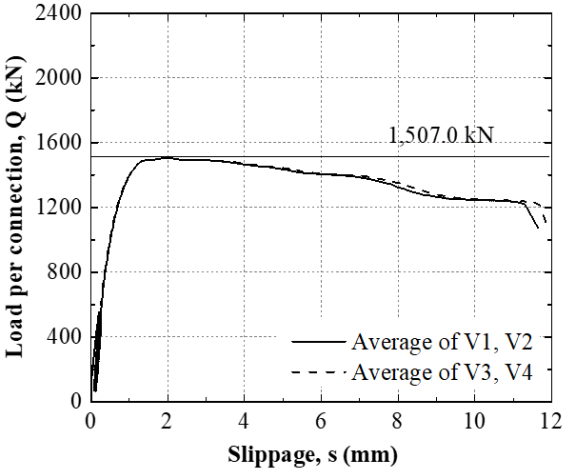

c) Average of the load-slippage curves measured at the two rows

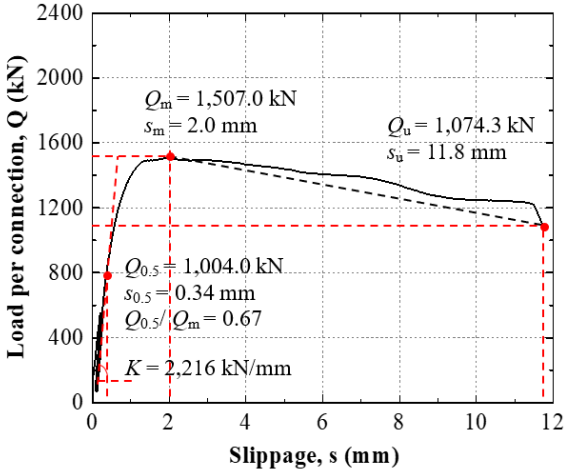

d) Representative load-slippage curves

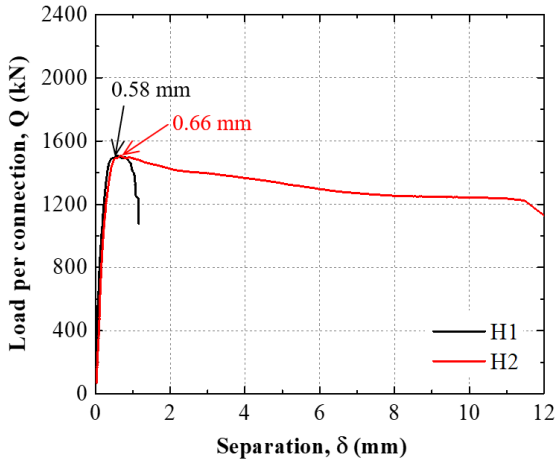

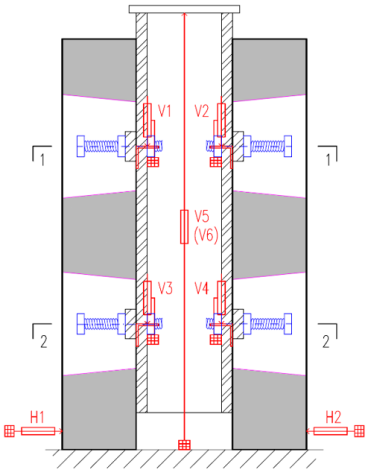

e) Load-separation curves of Test A-3-W-a

Fig. 4.24 Measured curves of Test A-3-W-a

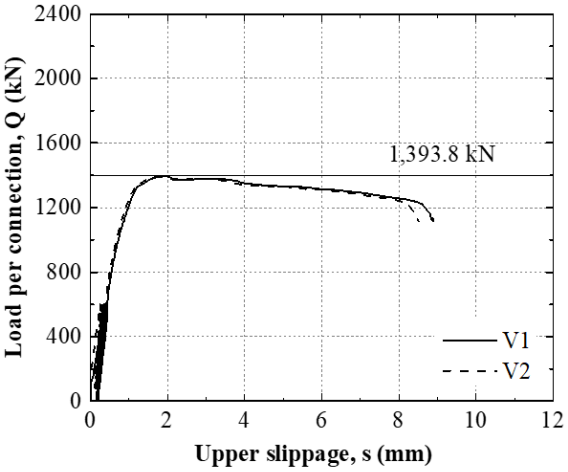

a) Load-slippage curves measured at the upper row of shear connections

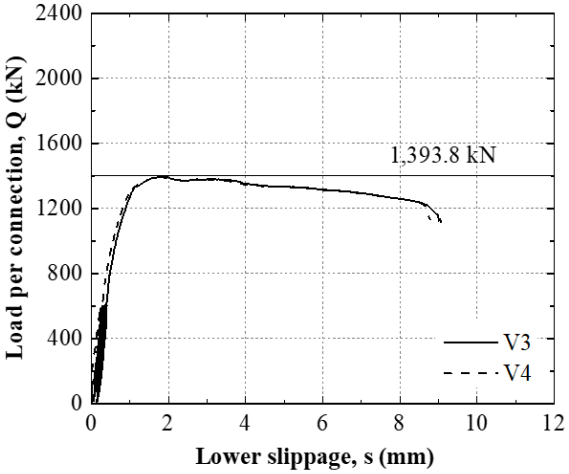

b) Load-slippage curves measured at the lower row of shear connections

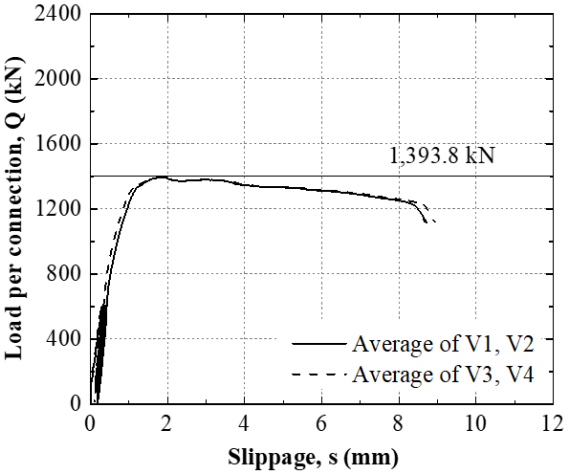

c) Average of the load-slippage curves measured at the two rows

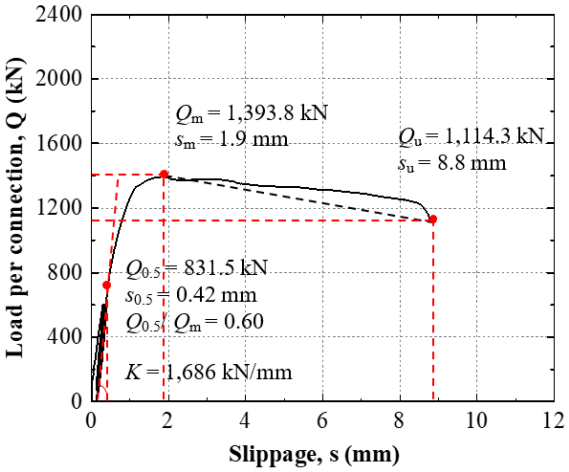

d) Representative load-slippage curves

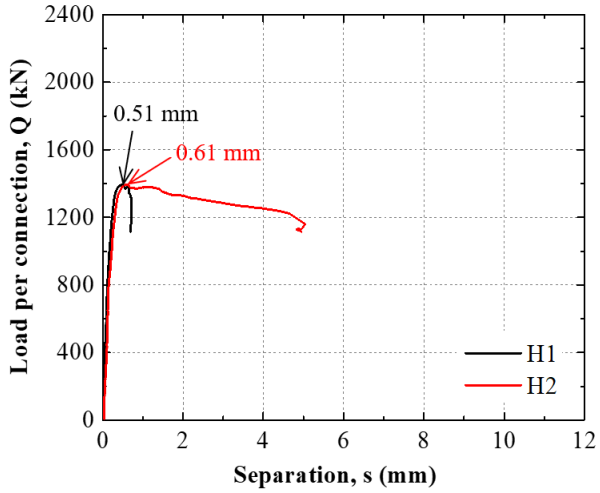

e) Load-separation curves of Test A-3-W-b

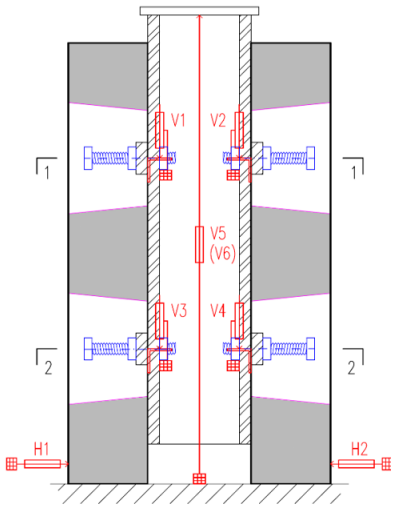

Fig. 4.25 Measured curves of Test A-3-W-b

In general, due to the provision of a steel connector fully embedded into an infilled concrete block, Type A connection is regarded as a twin connection, and concrete failure appears in both the concrete blocks and the concrete slabs. In addition, shear fracture of individual bolts appears in connections with 30 mm thick steel blocks, while no fracture of bolts appears in connections with 50 mm thick steel blocks when the applied load is decreased to 80% of the peak load.

The shear resistance of Type A shear connections is larger than 1,000 kN, and the initial stiffness is larger than 1,500 kN/mm. The ultimate slippage of Tests A-1-W, A-1-N, and A-3-W is larger than 6.0 mm, while that of Tests A-2-W and A-2-N is smaller than 6.0 mm. Hence, Type A connections with 30 mm thick steel blocks are demonstrated to meet all the structural requirements for composite beams in highway bridges.

4.7 Results of the tests with Type B connections

In the tests with Type B connections, three groups of specimens were tested to investigate the effect of size and strength of concrete blocks on the structural behaviour of the shear connections.

The connection is considered as a twin connection due to the provision of a steel connector fully embedded into an infilled concrete block. Concrete failure, i.e. Mode CF, primarily appeared

in both the concrete blocks and the precast concrete slabs of these tests, as shown in Fig. 4.26. For most of the tests, no apparent crack was observed before the applied loads reached 80% of the peak loads, and only a small sound of concrete cracking was heard when the load approached the peak load. In some cases, when the applied load was decreased to about 5-10% of the peak load, concrete crushing took place at the ends of the precast concrete slabs. After testing, severe longitudinal and diagonal cracks were found on the surfaces of the reinforced concrete slabs. Bolt fractures appeared in all the specimens at the end of the tests. After separating the concrete slab from the steel beam, concrete crushing was found in both the concrete blocks and the precast concrete slabs.

Key results of the tests with Type B connections are summarised in Table 4.11. It should be noted that the slippages are determined by averaging the values of the four vertical LVDTs, and the corresponding load-slippage curves are considered representative. Detailed deformation characteristics of these connections are presented as follows:·

Fig. 4.26 Mode CF in tests with Type B connections

Table 4.11 Key results of tests with Type B connections

Test	$f_{cu,150}$ (N/mm^2)		Q_a (kN)	Q_m (kN)	s_m (mm)	$Q_{6.0}$ (kN)	s_u (mm)	K (kN/mm)	$Q_{0.5}/Q_m$ (%)	Failure mode	Ductility index η	Adequacy
	SFRC	NC										
B-1-W-a	105.8	51.9	5,758	1,439.5	1.5	1,002.5	4.2	2,303	68	CF	0.70	---
B-1-W-b	97.7	64.7	5,130	1,282.5	1.0	1,097.8	6.7	2,728	82	CF	0.86	Y
B-1-N-a	110.8	59.6	5,037	1,259.3	1.2	1,079.5	7.2	2,885	80	CF	0.86	Y
B-1-N-b	103.5	61.6	4,748	1,187.0	1.1	828.5	5.5	2,856	81	CF	0.70	---
B-3-W-a	88.8	54.4	5016	1,254.0	3.9	1,109.8	7.4	2,147	71	CF	0.89	Y
B-3-W-b	94.7	50.4	5494	1,373.5	1.4	1,300.5	8.4	2,667	75	CF	0.95	Y

4.7.1 Results of Test B-1-W

The representative load-slippage curves of the two nominally identical tests are shown in Fig. 4.27. Table 4.12 presents the figure Nos. of the measured curves for Tests B-1-W-a and -b. The deformation characteristics of these tests are marked on the representative load-slippage curves, and described as follows:

- Mode CF primarily appeared in the two tests, when the applied load was decreased to about 80% of the peak load, individual bolts were fractured, and the middle parts of the bottom of the concrete slabs were crushed.
- The average shear resistance Q_m of Tests B-1-W is 1,361.0 kN and the corresponding slippage s_m is 1.3 mm. The ultimate slippage s_u is 5.5 mm. The average initial stiffness K is 2,516 kN/mm. It should be noted that the shear resistance of Test B-1-W-a is 12% larger than that of Test B-1-W-b. The reasons are: i) the concrete block strength in Test B-1-W-a is 8% larger than that in Test B-1-W-b; and ii) premature failure of the bolts appears in Test B-1-W-b.
- The average lateral separations at peak loads in Tests B-1-W-a and B-1-W-b are 0.81 and 0.56 mm respectively, which are 15% and 10% of the ultimate slippage.

Table 4.12 Measured curves for Tests B-1-W-a and -b.

Figure No. for Tests		Measure curves
B-1-W-a	B-1-W-b	
4.28 a)	4.29 a)	a) Load-slippage curves measured at the upper row of shear connections
4.28 b)	4.29 b)	b) Load-slippage curves measured at the lower row of shear connections
4.28 c)	4.29 c)	c) Average of the load-slippage curves measured at the two rows
4.28 d)	4.29 d)	d) Representative load-slippage curves
4.28 e)	4.29 e)	e) Load-separation curves

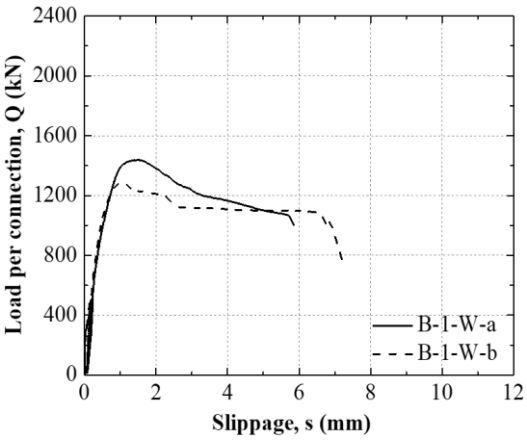

Tests	$f_{cu,150}$ (N/mm^2)	Q_m (kN)	s_m (mm)	s_u (mm)	K (kN/mm)	Failure mode
B-1-W-a	105.8	1,439.5	1.5	4.2	2,303	CF
B-1-W-b	97.7	1,282.5	1.0	6.7	2,728	CF
Average	101.8	1,361.0	1.3	5.5	2,516	CF

Fig. 4.27 Results of Tests B-1-W

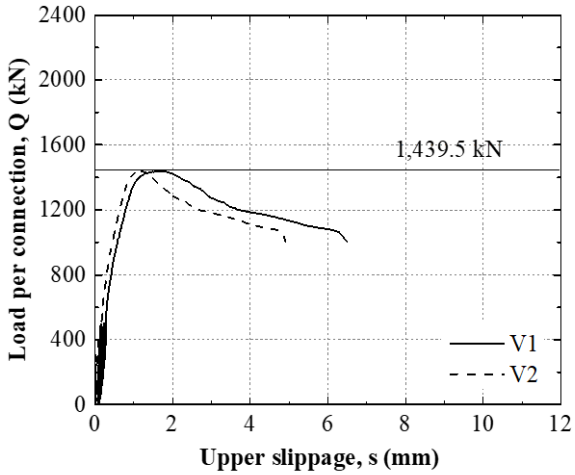

a) Load-slippage curves measured at the upper row of shear connections

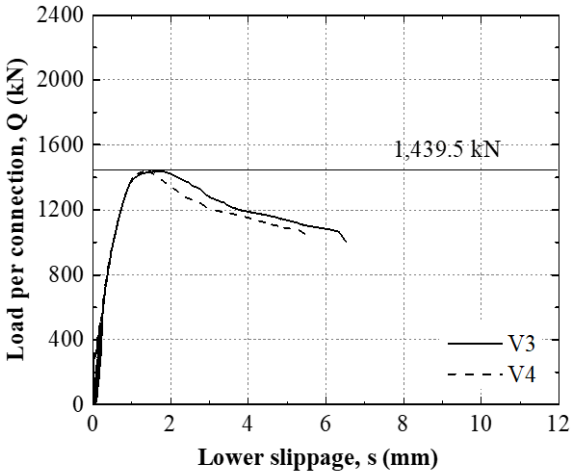

b) Load-slippage curves measured at the lower row of shear connections

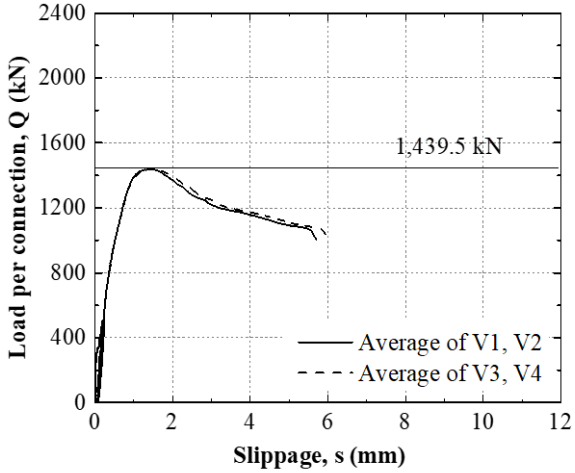

c) Average of the load-slippage curves measured at the two rows

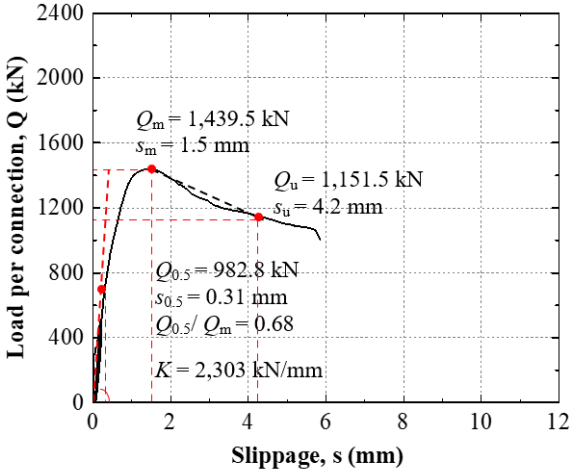

d) Representative load-slippage curves

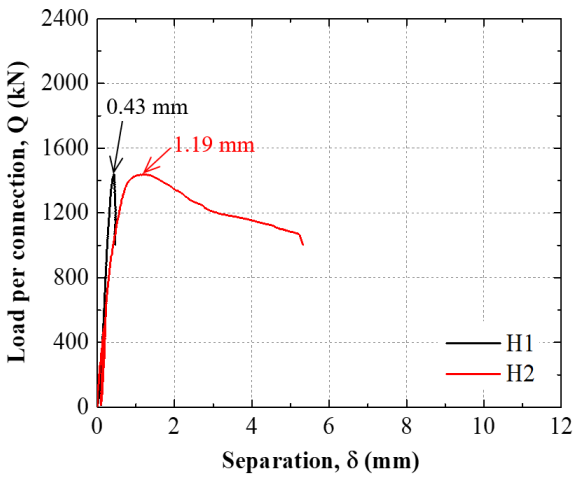

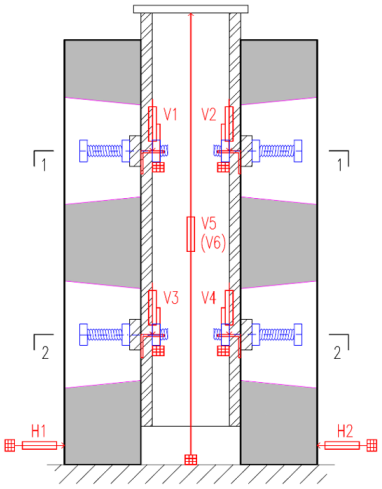

e) Load-separation curves of Test B-1-W-a

Fig. 4.28 Measured curves of Test B-1-W-a

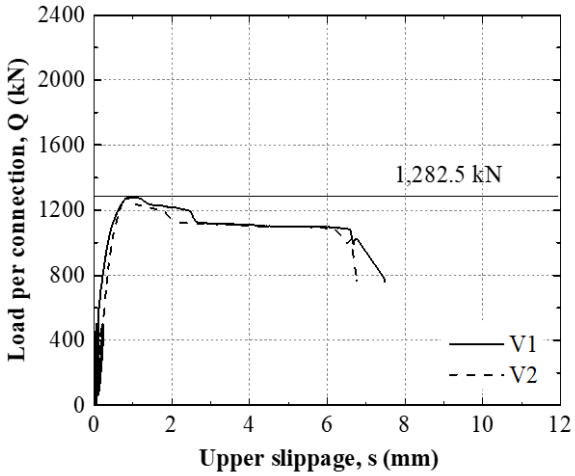

a) Load-slippage curves measured at the upper row of shear connections

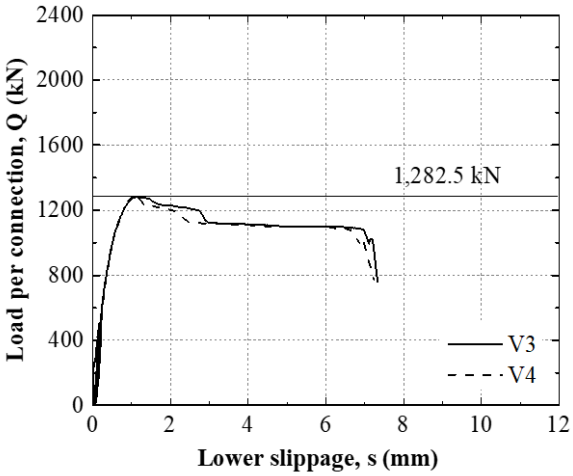

b) Load-slippage curves measured at the lower row of shear connections

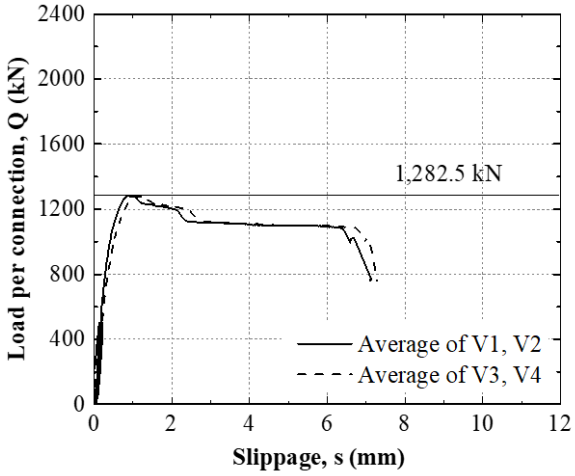

c) Average of the load-slippage curves measured at the two rows

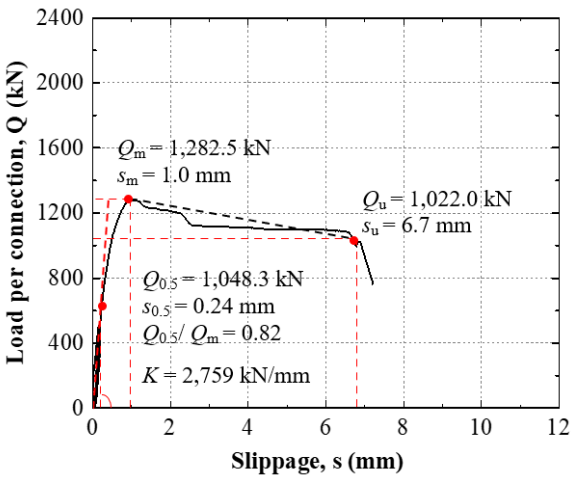

d) Representative load-slippage curves

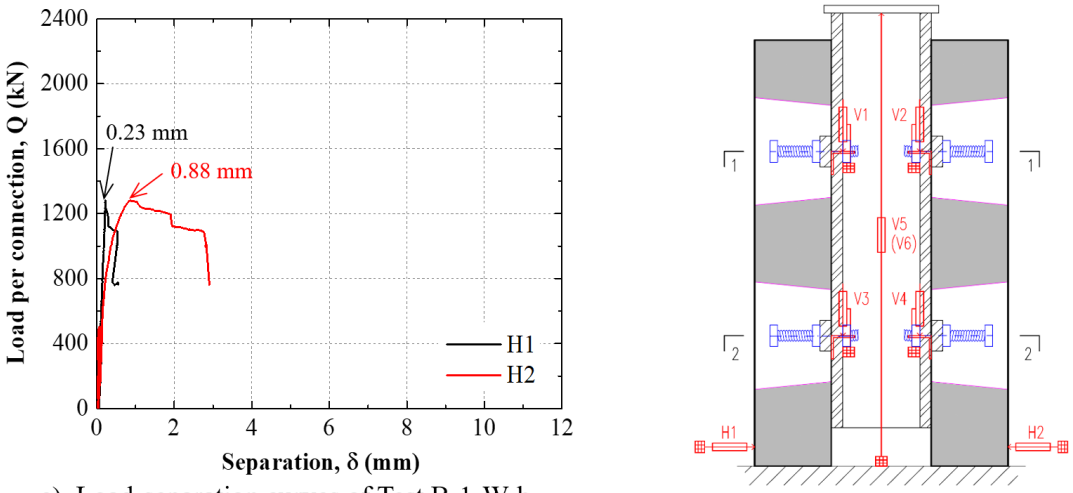

e) Load-separation curves of Test B-1-W-b

Fig. 4.29 Measured curves of Test B-1-W-b

4.7.2 Results of Test B-1-N

The representative load-slippage curves of the two nominally identical tests are shown in Fig. 4.30. Table 4.13 presents the figure Nos. of the measured curves for Tests B-1-N-a and -b. The deformation characteristics of these tests are marked on the representative load-slippage curves, and described as follows:

- Mode CF primarily appeared in the two tests, when the applied load was decreased to about 85% - 93% of the peak load, individual bolts were fractured, and the middle parts of the bottom of the concrete slabs were crushed.
- The average shear resistance Q_m of Tests B-1-N is 1,223.2 kN and the corresponding slippage s_m is 1.2 mm. The ultimate slippage s_u is 6.4 mm. The average initial stiffness K is 2,871 kN/mm. It should be noted that the ultimate slippage of Test B-1-N-b is smaller than 6.0 mm due to the premature failure of the bolts.
- The average lateral separations at peak loads in Tests B-1-N-a and B-1-N-b are 0.60 and 0.63 mm respectively, which are smaller than 10% of the ultimate slippage. Hence, the influence of the lateral separations of the two concrete slabs is considered to be negligible.

Table 4.13 Measured curves for Tests B-1-N-a and -b.

Figure No. for Tests		Measure curves
B-1-N-a	B-1-N-b	
4.31 a)	4.32 a)	a) Load-slippage curves measured at the upper row of shear connections
4.31 b)	4.32 b)	b) Load-slippage curves measured at the lower row of shear connections
4.31 c)	4.32 c)	c) Average of the load-slippage curves measured at the two rows

4.31 d)	4.32 d)	d) Representative load-slippage curves
4.31 e)	4.32 e)	e) Load-separation curves

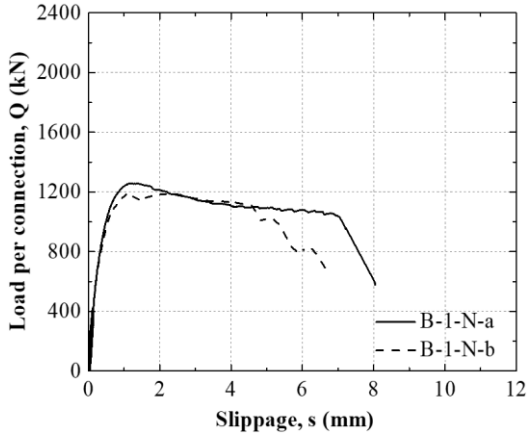

Tests	$f_{cu,150}$ (N/mm^2)	Q_m (kN)	s_m (mm)	s_u (mm)	K (kN/mm)	Failure mode
B-1-N-a	110.8	1,259.3	1.2	7.2	2,885	CF
B-1-N-b	103.5	1,187.0	1.1	5.5	2,856	CF
Average	107.2	1,223.2	1.2	6.4	2,871	CF

Fig. 4.30 Results of Tests B-1-N

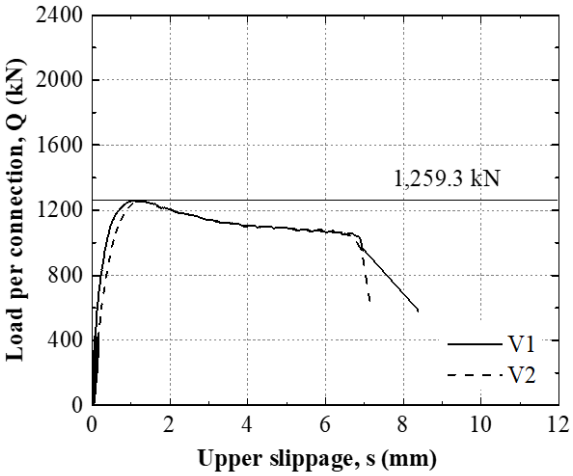

a) Load-slippage curves measured at the upper row of shear connections

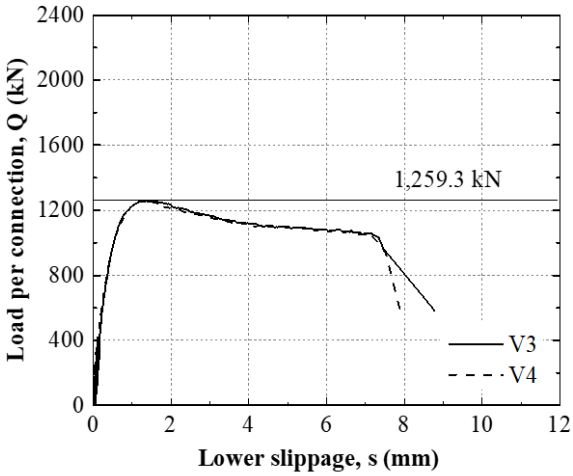

b) Load-slippage curves measured at the lower row of shear connections

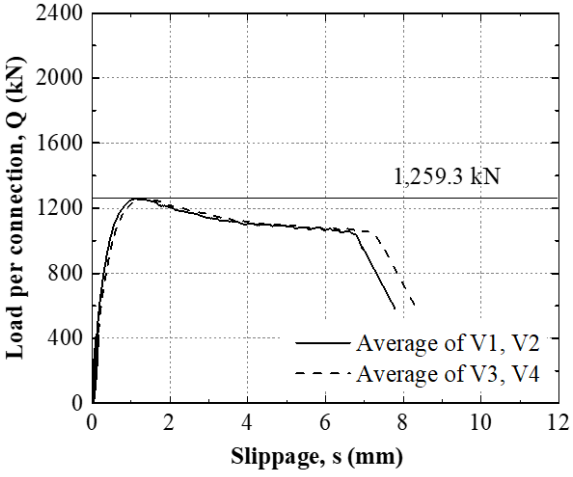

c) Average of the load-slippage curves measured at the two rows

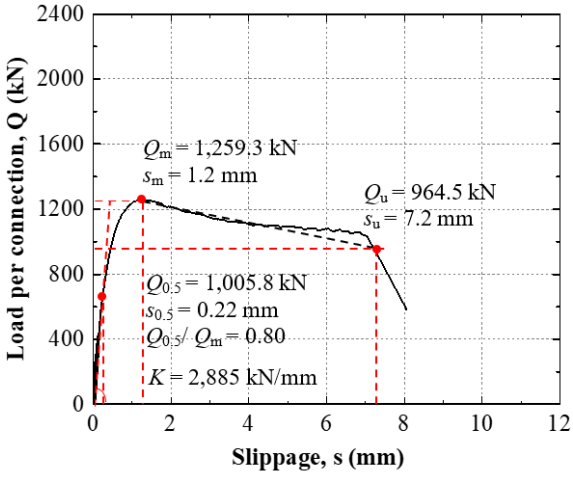

d) Representative load-slippage curves

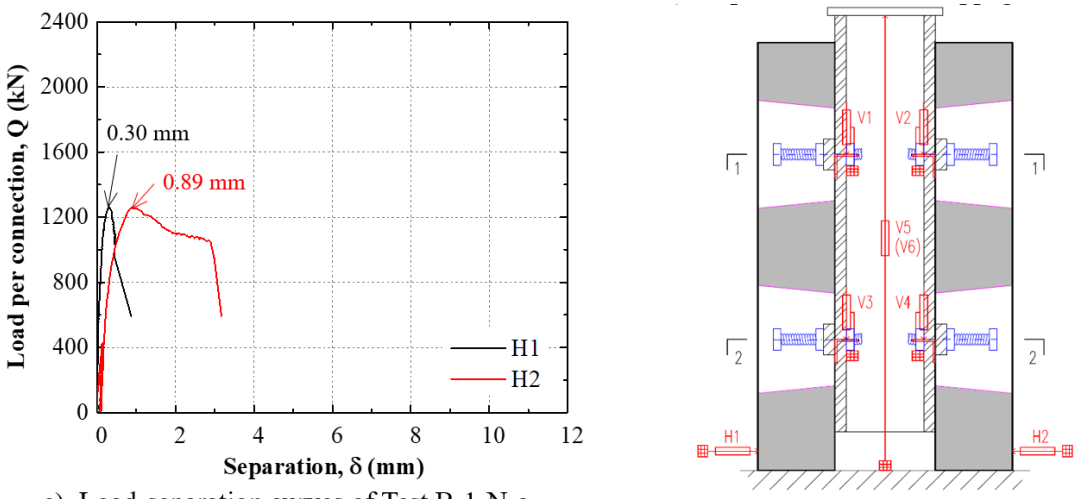

e) Load-separation curves of Test B-1-N-a

Fig. 4.31 Measured curves of Test B-1-N-a

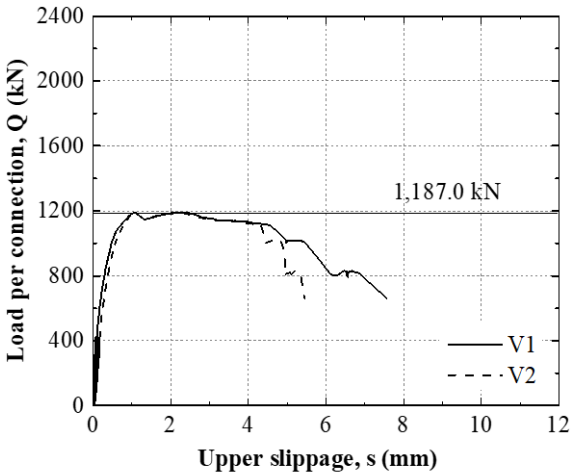

a) Load-slippage curves measured at the upper row of shear connections

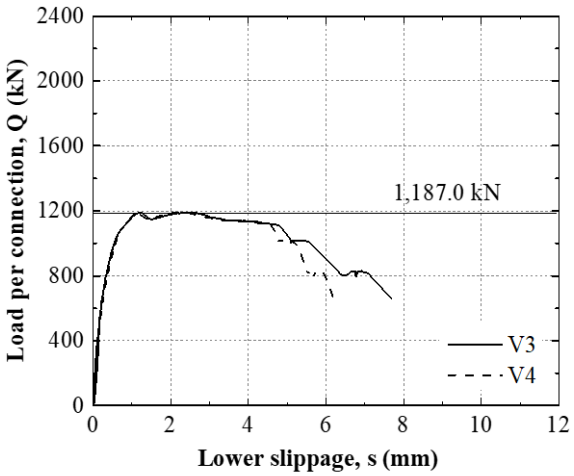

b) Load-slippage curves measured at the lower row of shear connections

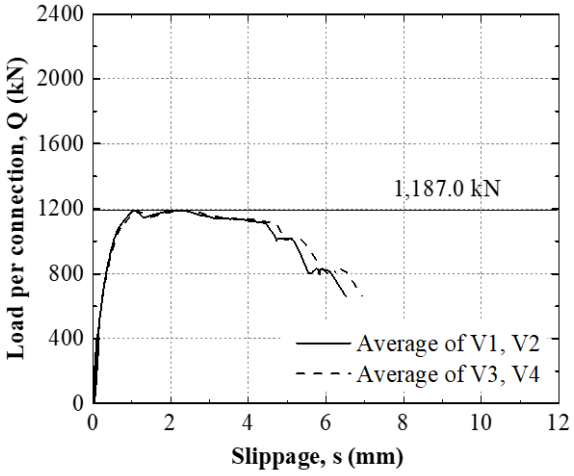

c) Average of the load-slippage curves measured at the two rows

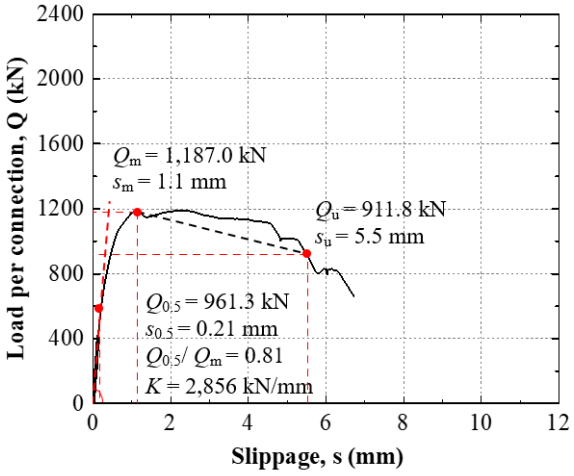

d) Representative load-slippage curves

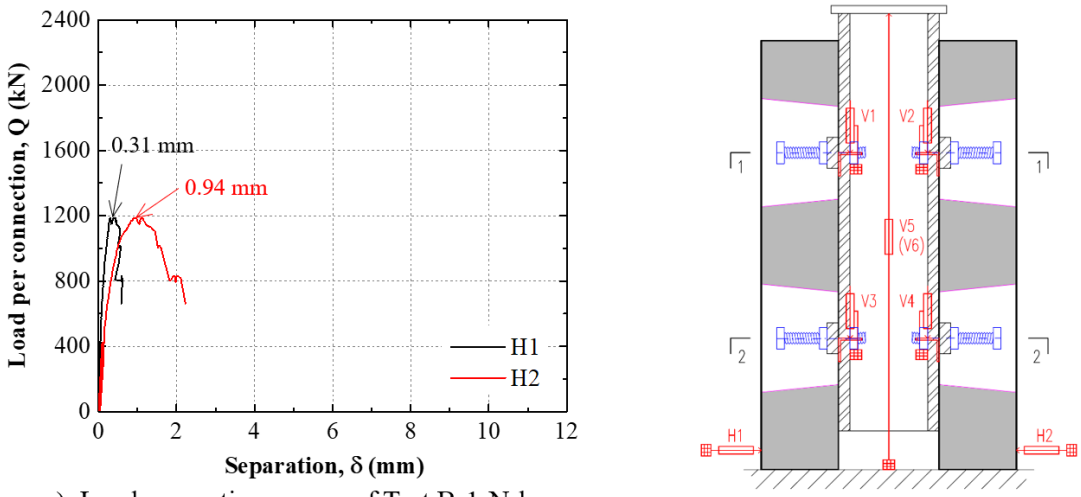

e) Load-separation curves of Test B-1-N-b

Fig. 4.32 Measured curves of Test B-1-N-b

4.7.2 Results of Test B-3-W

The representative load-slippage curves of the two nominally identical tests are shown in Fig. 4.33. Table 4.14 presents the figure Nos. of the measured curves for Tests B-3-W-a and -b. The deformation characteristics of these tests are marked on the representative load-slippage curves, and described as follows:

- Mode CF primarily appeared in the two tests, when the applied load was decreased to about 90% of the peak load, a bolt was fractured and the middle parts of the bottom of the concrete slabs were crushed.
- The average shear resistance Q_m of Tests B-3-W is 1,313.8 kN and the corresponding slippage s_m is 2.7 mm. The ultimate slippage s_u is 7.9 mm. The average initial stiffness K is 2,407 kN/mm.
- The average lateral separations at peak loads in Tests B-3-W-a and B-3-W-b are 1.46 and 0.5 mm respectively. It should be noted that the lateral separation of the left concrete slab of Test B-3-W-a is 31% of the ultimate slippage, and hence the two concrete slabs were unevenly loaded. As a result, the shear resistance of Test B-3-W-a is 9% smaller than that of Test B-3-W-b.

Table 4.14 Measured curves for Tests B-3-W-a and -b.

Figure No. for Tests		Measure curves
B-3-W-a	B-3-W-b	
4.34 a)	4.35 a)	a) Load-slippage curves measured at the upper row of shear connections

4.34 b)	4.35 b)	b) Load-slippage curves measured at the lower row of shear connections
4.34 c)	4.35 c)	c) Average of the load-slippage curves measured at the two rows
4.34 d)	4.35 d)	d) Representative load-slippage curves
4.34 e)	4.35 e)	e) Load-separation curves

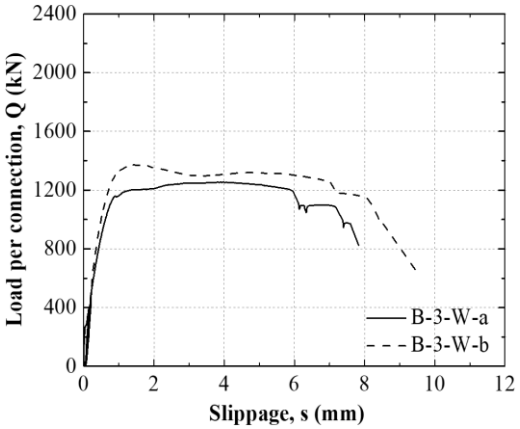

Tests	$f_{cu,150}$ (N/mm²)	Q_m (kN)	s_m (mm)	s_u (mm)	K (kN/mm)	Failure mode
B-3-W-a	88.8	1,254.0	3.9	7.4	2,147	CF
B-3-W-b	94.7	1,373.5	1.4	8.4	2,667	CF
Average	91.8	1,313.8	2.7	7.9	2,407	CF

Fig. 4.33 Results of Tests B-3-W

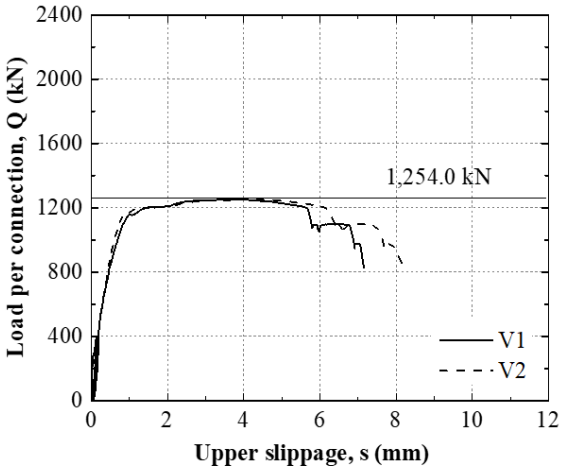

a) Load-slippage curves measured at the upper row of shear connections

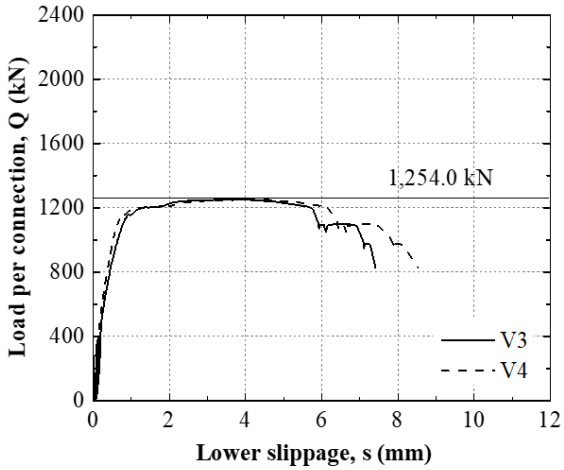

b) Load-slippage curves measured at the lower row of shear connections

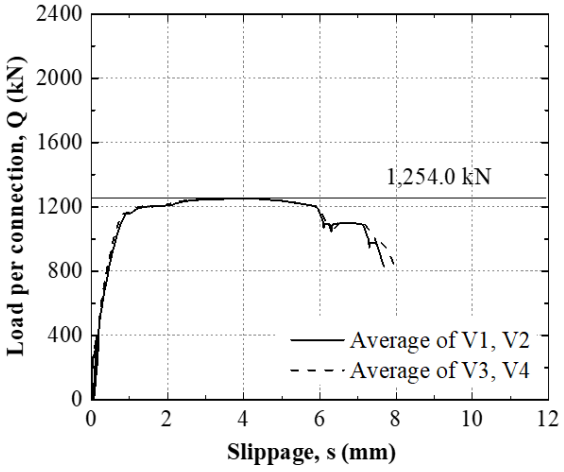

c) Average of the load-slippage curves measured at the two rows

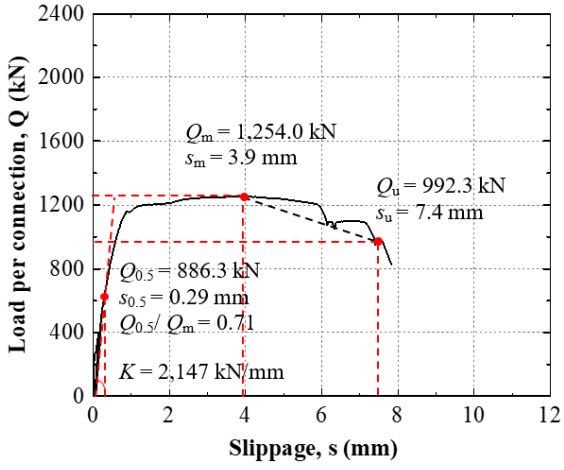

d) Representative load-slippage curves

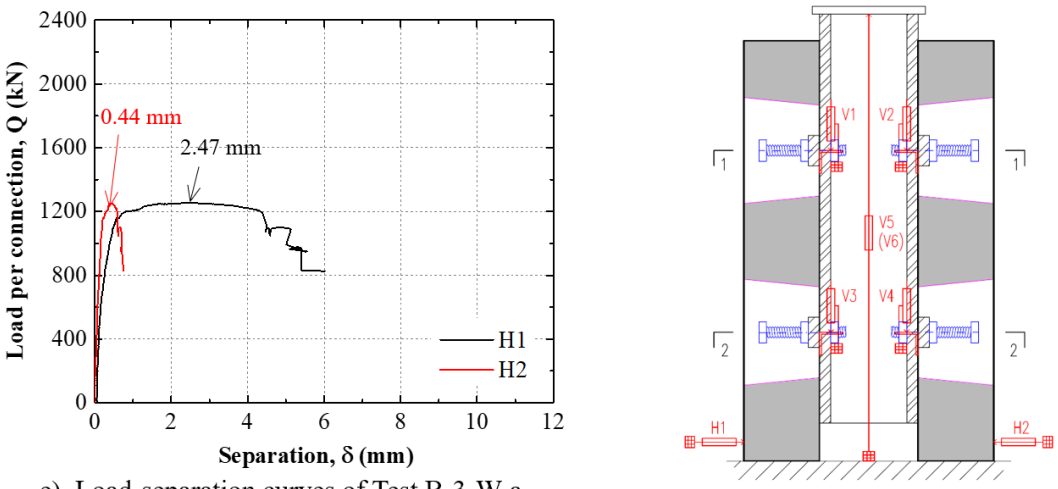

e) Load-separation curves of Test B-3-W-a

Fig. 4.34 Measured curves of Test B-3-W-a

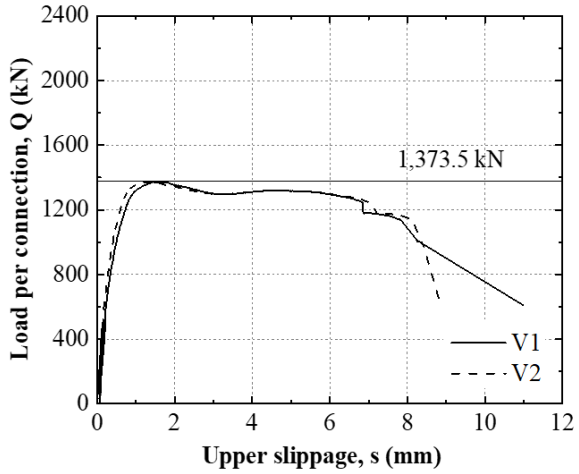

a) Load-slippage curves measured at the upper row of shear connections

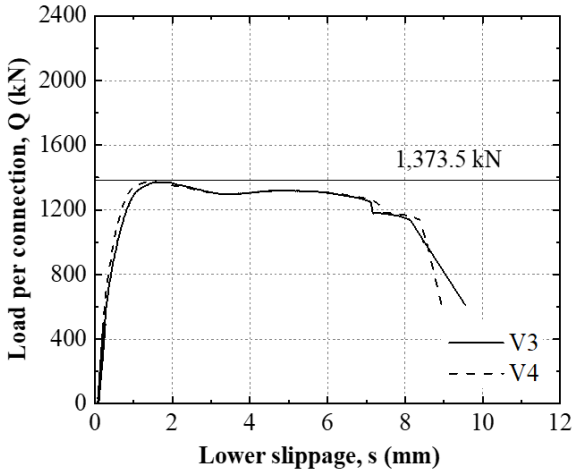

b) Load-slippage curves measured at the lower row of shear connections

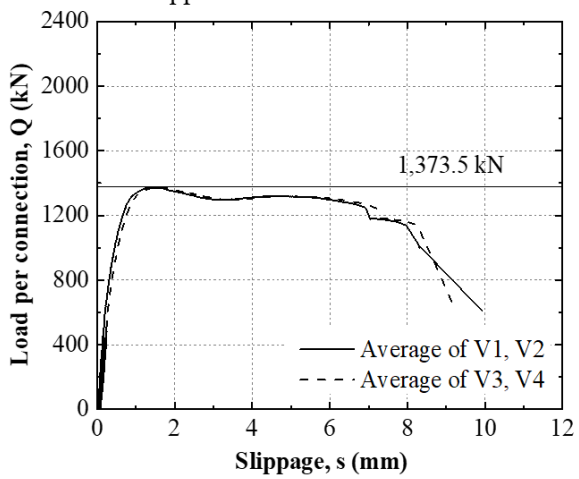

c) Average of the load-slippage curves measured at the two rows

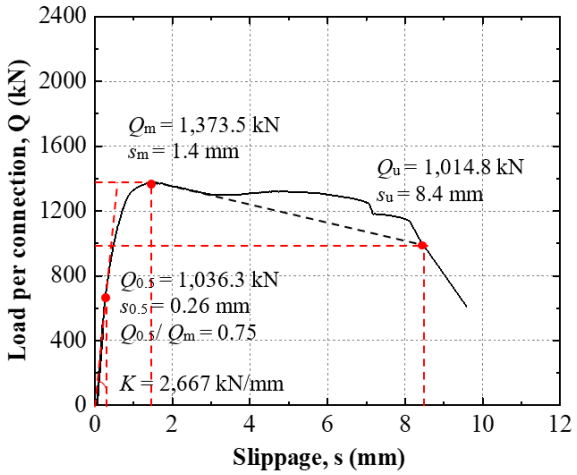

d) Representative load-slippage curves

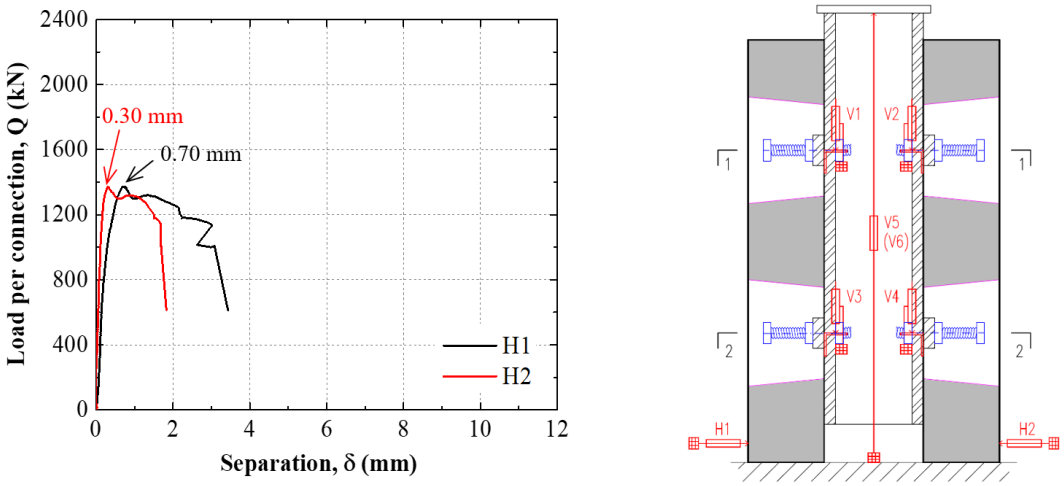

e) Load-separation curves of Test B-3-W-b

Fig. 4.35 Measured curves of Test B-3-W-b

In general, due to the provision of a steel connector fully embedded into an infilled concrete block, Type B connection is regarded as a twin connection, and concrete failure appears in both the concrete blocks and the concrete slabs. In addition, shear fracture of bolts appears in all the Type B connections with 24 mm diameter bolts.

The shear resistance of Type B shear connections is larger than 1,000 kN, and the initial stiffness is larger than 1,500 kN/mm. The ultimate slippage of most of the tests with Type B connections is larger than 6.0 mm, while that of the other tests is smaller than 6.0 mm due to the abrupt fracture of the bolts.

4.8 Results of the tests with Type C connections

In the tests with Type C connections, one group of specimens were tested. It should be noted that each group has two nominally identical specimens.

The connection is considered as a twin connection due to the provision of a pair of steel bolts fully embedded into an infilled concrete block. Shear fracture of bolts, i.e. Mode SFB, primarily appeared in these tests, as shown in Fig. 4.36. However, no apparent concrete cracks were observed on the surface of the reinforced concrete slabs during and after testing.

Key results of the tests with Type C connections are summarised in Table 4.15. It should be noted that the slippages are determined by averaging the values of the four vertical LVDTs, and the corresponding load-slippage curves are considered representative. Detailed deformation characteristics of these connections are presented as follows:

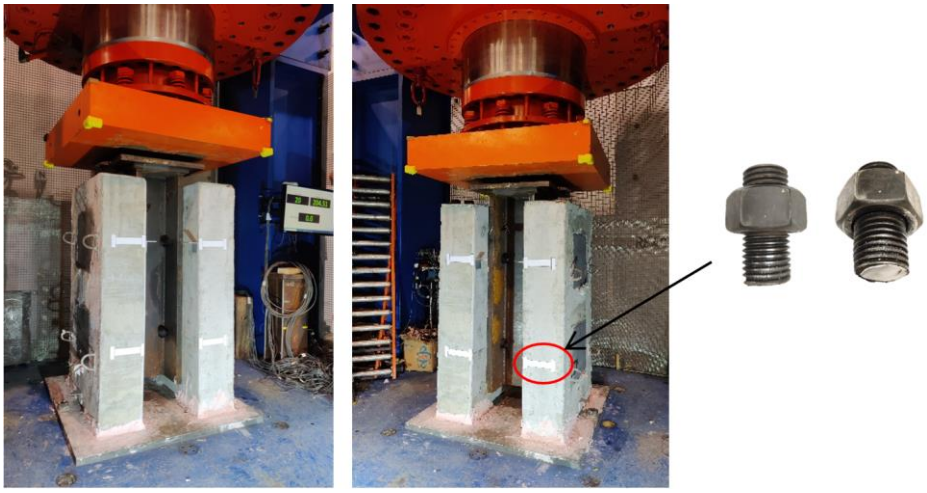

Fig. 4.36 Mode SFB in tests with Type C connections

Table 4.15 Key results of tests with Type C connections

Test	$f_{cu,150}$ (N/mm^2)		Q_a (kN)	Q_m (kN)	s_m (mm)	$Q_{6.0}$ (kN)	s_u (mm)	K (kN/mm)	$Q_{0.5}/Q_m$ (%)	Failure mode	Ductility index η	Adequacy
	SFRC	NC										
C-0-W-a	98.4	61.9	2,835	708.8	5.8	707.0	7.3	169	30	SFB	1.00	---
C-0-W-b	93.6	65.9	2,903	725.8	5.7	722.8	7.1	147	23	SFB	1.00	---

4.8.1 Results of Test C-0-W

The representative load-slippage curves of the two nominally identical tests are shown in Fig. 4.37. The measured curves are shown in Figs. 4.38 and 4.39. The deformation characteristics of these tests are marked on the representative load-slippage curves, and described as follows:

- The average shear resistance Q_m of Tests C-0-W is 717.3 kN and the corresponding slippage s_m is 5.8 mm. The ultimate slippage s_u is 7.2 mm. The average initial stiffness K is 158 kN/mm.
- The average lateral separations at peak loads in Tests C-0-W-a and C-0-W-b are 0.29 and 0.19 mm respectively, which are smaller than 10% of the ultimate slippage. Hence, the influence of the lateral separations of the two concrete slabs is considered to be negligible.

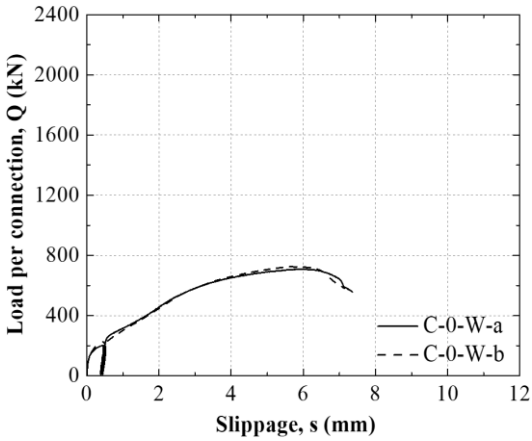

Tests	$f_{cu,150}$ (N/mm²)	Q_m (kN)	s_m (mm)	s_u (mm)	K (kN/mm)	Failure mode
C-0-W-a	98.4	708.8	5.8	7.3	169	SFB
C-0-W-b	93.6	725.8	5.7	7.1	147	SFB
Average	96.0	717.3	5.8	7.2	158	SFB

Fig. 4.37 Results of Tests C-0-W

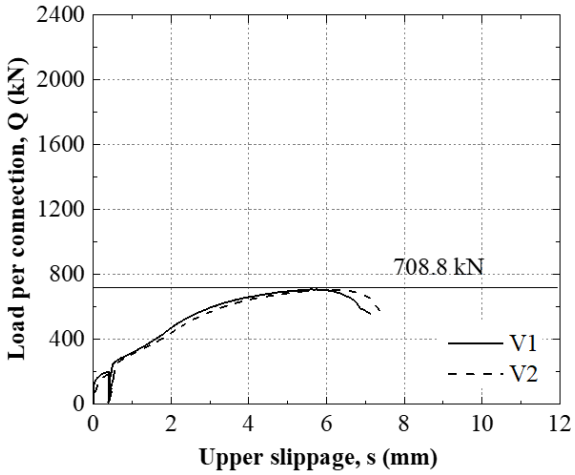

a) Load-slippage curves measured at the upper row of shear connections

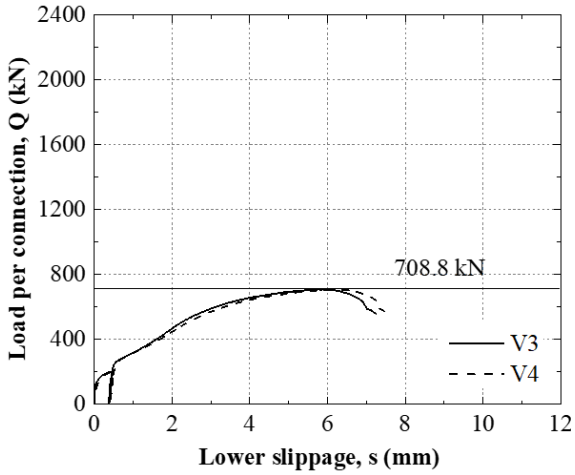

b) Load-slippage curves measured at the lower row of shear connections

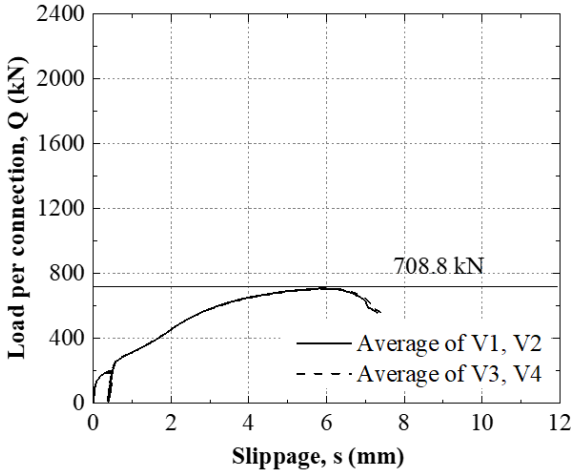

c) Average of the load-slippage curves measured at the two rows

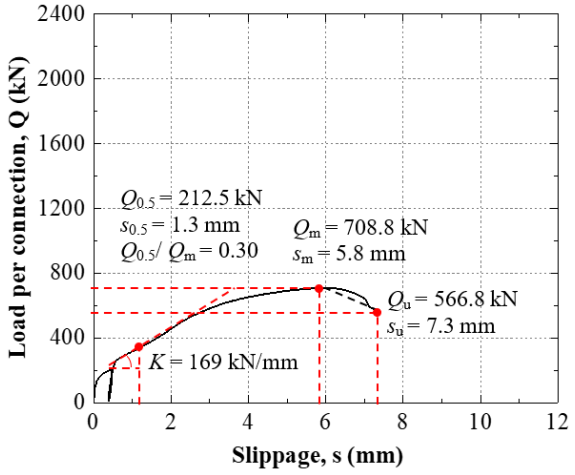

d) Representative load-slippage curves

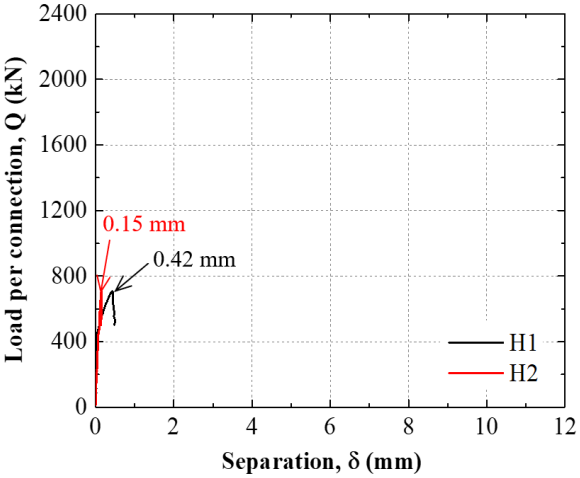

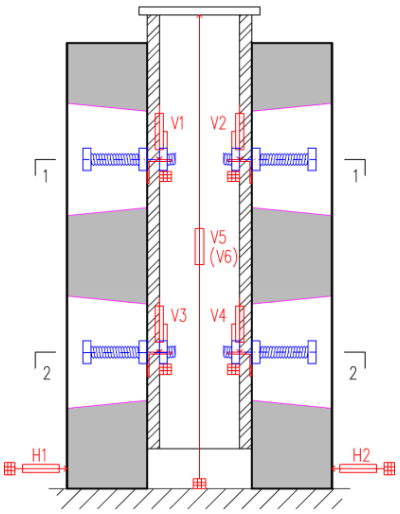

e) Load-separation curves of Test C-0-W-a

Fig. 4.38 Measured curves of Test C-0-W-a

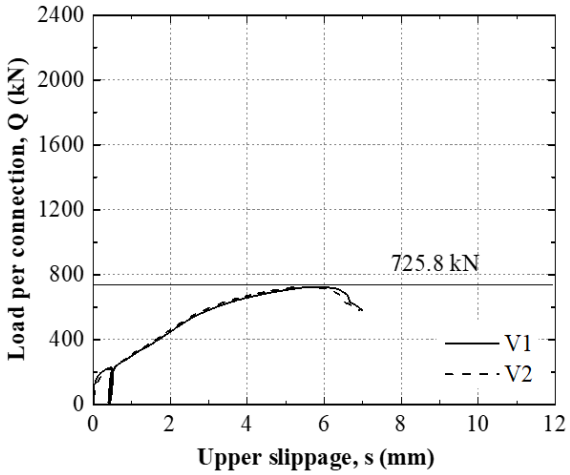

a) Load-slippage curves measured at the upper row of shear connections

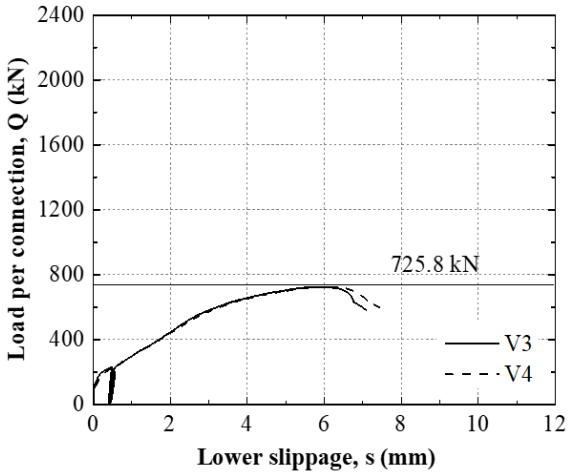

b) Load-slippage curves measured at the lower row of shear connections

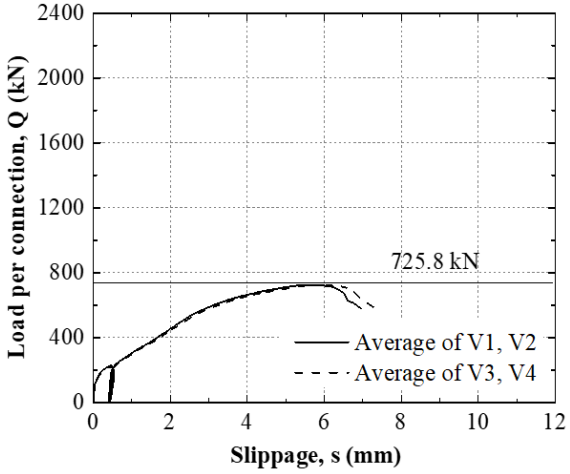

c) Average of the load-slippage curves measured at the two rows

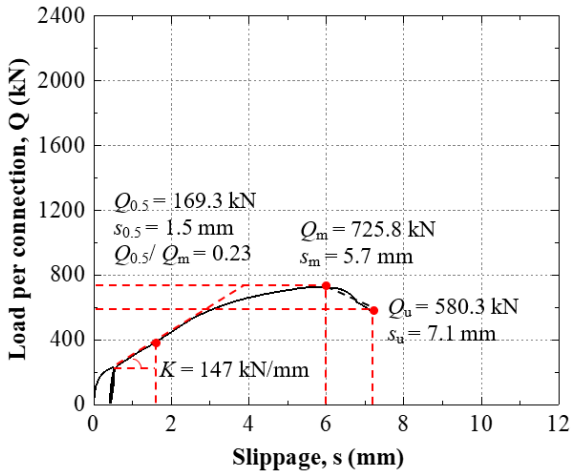

d) Representative load-slippage curves

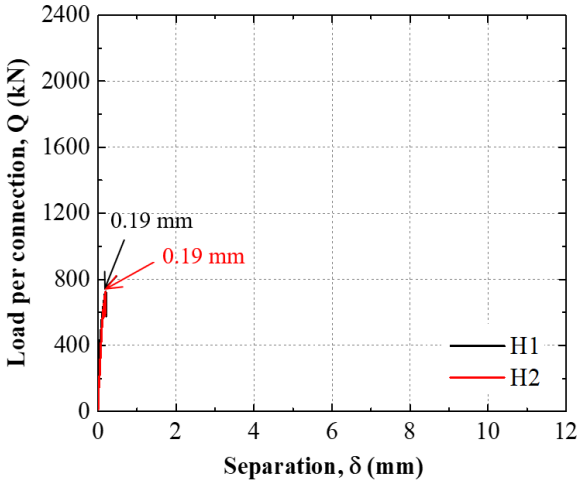

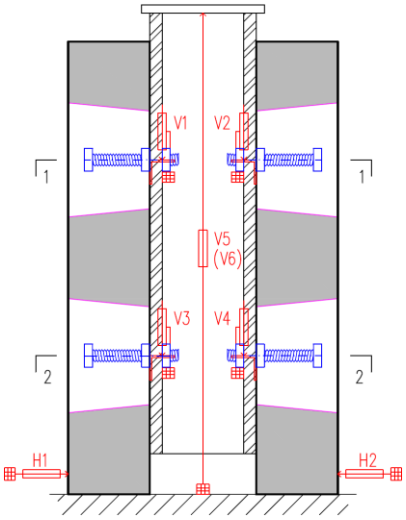

e) Load-separation curves of Test C-0-W-b

Fig. 4.39 Measured curves of Test C-0-W-b

In general, shear fracture of bolts primarily appears in tests with Type C shear connections without any visible concrete cracking and crushing in the reinforced concrete slabs.

The shear resistance of Type C shear connections is smaller than 1,000 kN, and the initial stiffness is smaller than 1,500 kN/mm. The ultimate slippage of Test C-0-W is larger than 6.0 mm. Hence, Type C shear connections do not meet the structural requirements for composite beams in highway bridges.

4.9 Results of the tests with Type D connections

In the tests with Type D connections, one group of specimens were tested. It should be noted that each group has two nominally identical specimens.

The connection is considered as a twin connection due to the provision of a steel connector fully embedded into an infilled concrete block. Concrete failure, i.e. Mode CF, primarily appeared in both the concrete blocks and the precast concrete slabs of these tests, as shown in Fig. 4.40. When the applied load was decreased to about 90% of the peak load, a noise of concrete crushing was heard, and the middle parts of the bottom of the concrete slabs were crushed, while no fracture of the steel plates was found after testing.

Key results of the tests with Type D connections are summarised in Table 4.16. It should be noted that the slippages are determined by averaging the values of the four vertical LVDTs, and the corresponding load-slippage curves are considered representative. Detailed deformation characteristics of these connections are presented as follows:

Fig. 4.40 Mode CF in tests with Type D connections

Table 4.16 Key results of tests with Type D connections

Test	$f_{cu,150}$ (N/mm^2)		Q_a (kN)	Q_m (kN)	s_m (mm)	$Q_{6.0}$ (kN)	s_u (mm)	K (kN/mm)	$Q_{0.5}/Q_m$ (%)	Failure mode	Ductility index η	Adequacy
	SFRC	NC										
D-0-W-a	106.9	60.2	5067	1,266.8	3.9	1195.8	7.6	1,598	60	CF	0.94	Y
D-0-W-b	113.9	61.0	5576	1,394.0	5.2	1335.8	7.9	1,544	54	CF	0.96	Y

4.9.1 Results of Test D-0-W

The representative load-slippage curves of the two nominally identical tests are shown in Fig. 4.41. The measured curves are shown in Figs. 4.42 and 4.43. The deformation characteristics of these tests are marked on the representative load-slippage curves, and described as follows:

- The average shear resistance Q_m of Tests D-0-W is 1,330.4 kN and the corresponding slippage s_m is 4.6 mm. The ultimate slippage s_u is 7.8 mm. The average initial stiffness K is 1,571 kN/mm.
- The average lateral separations at peak loads in Tests D-0-W-a and D-0-W-b are 1.32 and 1.02

mm respectively, which are 17% and 13% of the ultimate slippage respectively. Hence, the lateral separations have a certain influence on the shear resistance of the connections.

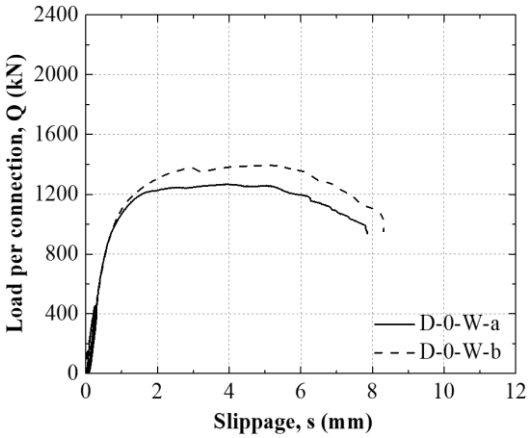

Tests	$f_{cu,150}$ (N/mm^2)	Q_m (kN)	s_m (mm)	s_u (mm)	K (kN/mm)	Failure mode
D-0-W-a	106.9	1,266.8	3.9	7.6	1,598	CF
D-0-W-b	113.9	1,394.0	5.2	7.9	1,544	CF
Average	110.4	1,330.4	4.6	7.8	1,571	CF

Fig. 4.41 Results of Tests D-0-W

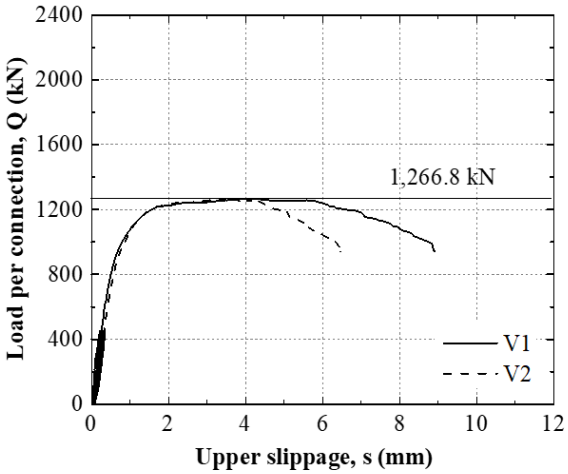

a) Load-slippage curves measured at the upper row of shear connections

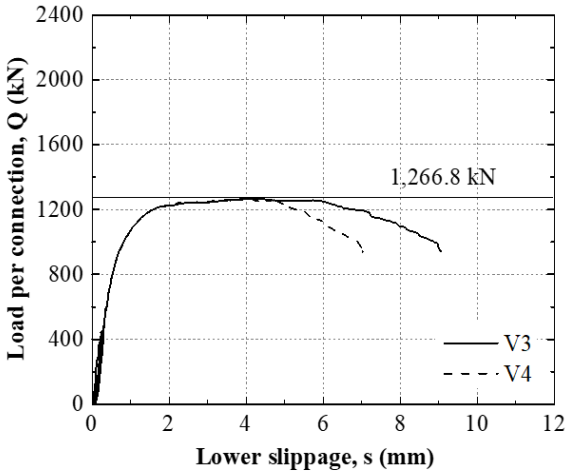

b) Load-slippage curves measured at the lower row of shear connections

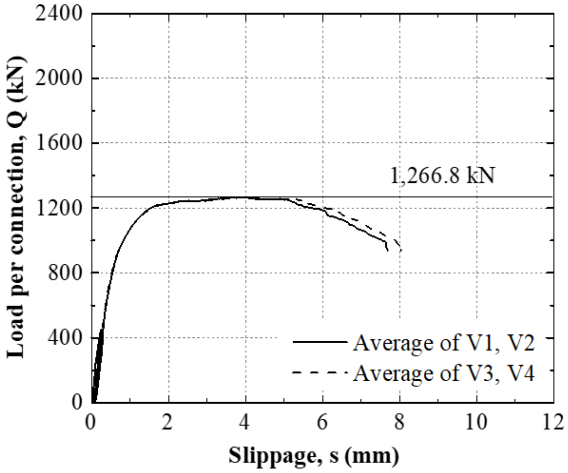

c) Average of the load-slippage curves measured at the two rows

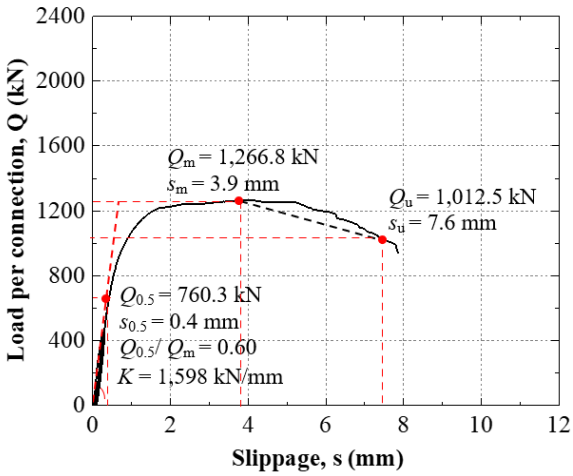

d) Representative load-slippage curves

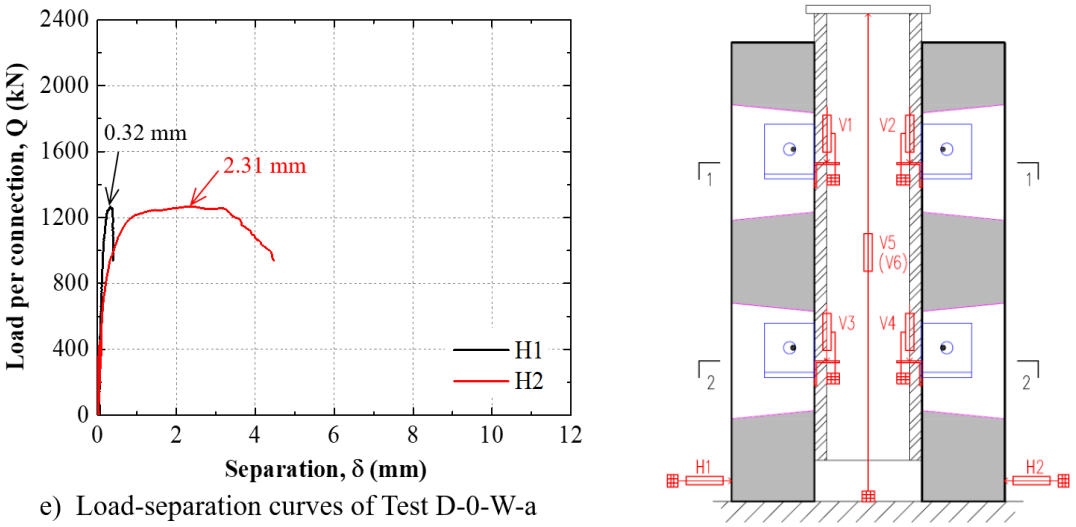

e) Load-separation curves of Test D-0-W-a

Fig. 4.42 Measured curves of Test D-0-W-a

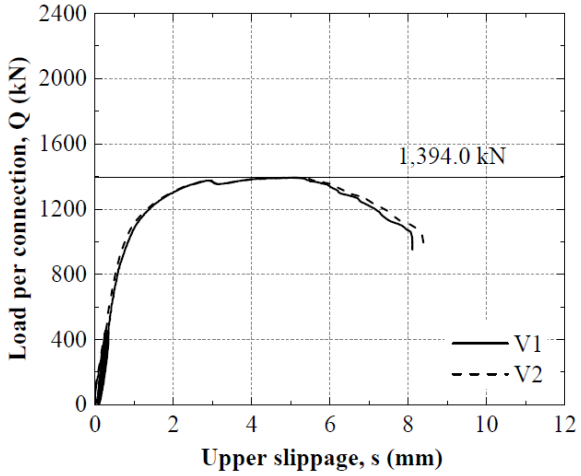

a) Load-slippage curves measured at the upper row of shear connections

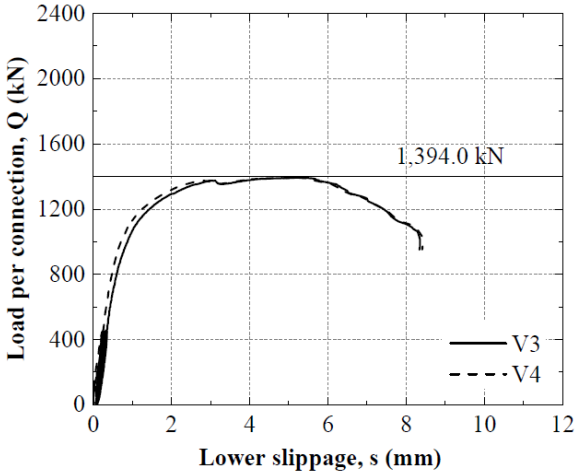

b) Load-slippage curves measured at the lower row of shear connections

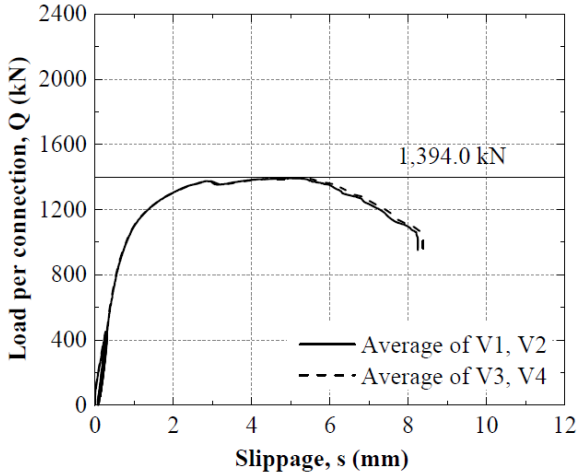

c) Average of the load-slippage curves measured at the two rows

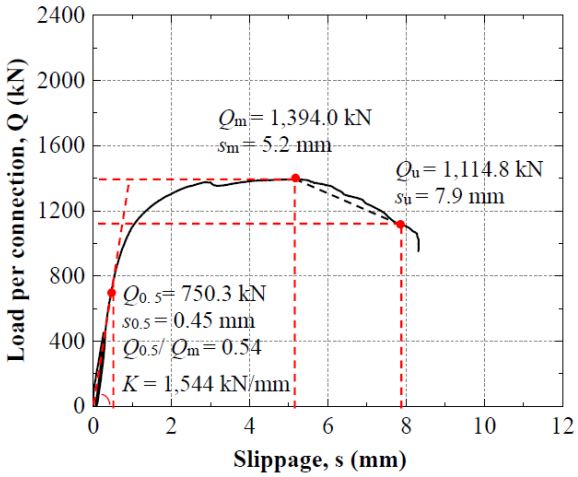

d) Representative load-slippage curves

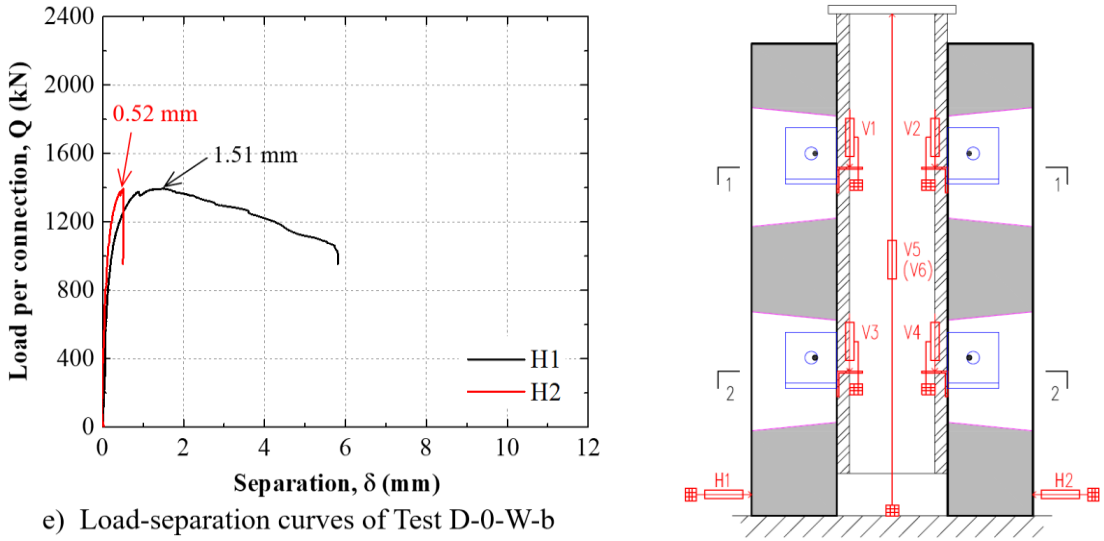

e) Load-separation curves of Test D-0-W-b

Fig. 4.43 Measured curves of Test D-0-W-b

In general, due to the provision of a steel connector fully embedded into an infilled concrete block, Type D connection is regarded as a twin connection, and concrete failure appears in both the concrete blocks and the concrete slabs. No fracture of the steel plates is found during and at the end of the tests.

The shear resistance of Type D shear connections is larger than 1,000 kN, the initial stiffness is larger than 1,500 kN/mm, and the ultimate slippage is larger than 6.0 mm. Hence, Type D connection is demonstrated to meet all the structural requirements for composite beams in highway bridges.

4.10 Conclusions

Based on the results of the single-sided push-out tests presented in Chapter 3, a total of 20 large-scale and extensively instrumented push-out tests were conducted to investigate the structural behaviour of the effective bolted shear connections with Connectors RBN and R. In addition, the structural behaviour of the connections with Connector MTP was tested for comparison. The results

provided detailed information on the deformation characteristics of these connections, in terms of their load-slippage curves, shear resistances and modes of failure. Key findings are summarised as follows:

a) According to the measured compressive strengths of NC and SFRC, the compressive stress and strain of SFRC are larger than those of NC, indicating its good mechanical properties under compression, as expected. The average ratio of the measured cylinder to cube strength in the precast concrete slab is 0.88, and the ratio of the measured cylinder to cube strength in the concrete block is 0.97. The elastic modulus of SFRC is smaller than the value specified in Hong Kong code of practice.

b) The shear connection is considered as a twin connection due to the provision of a steel connector fully embedded into an infilled concrete block. Two typical failure modes were identified in these standard push-out tests. Concrete failure, i.e. Mode CF, primarily appeared in both the concrete blocks and the precast concrete slabs of the tests with Connections RBN and MTP. Severe longitudinal and diagonal cracks were found on the surfaces of the reinforced concrete slabs, and concrete crushing took place at the ends of the precast concrete slabs. It should be noted that in those tests with Type A connections and 30 mm thick steel blocks, individual bolts were fractured at the end of the tests, while in those tests with Type A connections and 50 mm thick steel blocks, no bolts were fractured when the applied load was decreased to 80% of the peak load. Moreover, shear fracture of bolts, i.e. Mode SFB, primarily appeared in the tests with Connection R.

c) Type A shear connection with Connector RBN and a 30 mm thick steel block is found to be highly effective in terms of resistance, stiffness, and ductility. This connection is demonstrated to meet all the requirements for prefabricated composite beams in highway bridges. However, Type A connection with Connector RBN and a 50 mm thick steel block is found to have a

limited ductility.

d) Type B shear connection with Connector RBN and a pair of 24 mm diameter bolts is found to have adequate shear resistance and initial stiffness, while the ultimate slippages of some test specimens are smaller than 6.0 mm due to the abrupt fracture of the bolts.

e) Type C connection with Connection R is found to have an adequate ductility, but small shear resistance and initial stiffness.

f) Type D shear connection with Connector MTP is demonstrated to meet all the structural requirements for composite beams in highway bridges. However, this shear connection is difficult to be used for simple on-site assembly of prefabricated composite beams due to the presence of the steel reinforcement in the perforation of the perfobond rib.

CHAPTER 5

ANALYSIS OF THE RESULTS OF STANDARD PUSH-OUT TESTS

5.1 Introduction

This chapter presents a comprehensive analysis on the deformation characteristics of the shear connections reported in Chapter 4. According to the design method presented in Chapter 3, the shear resistance against concrete failure is proportional to the compressive strength of concrete. Hence, to enable comparative analysis, the strengths of the concrete blocks are linearly normalized to standard values of either 80 or 100 N/mm^2, and the corresponding shear resistances are used for comparison.

For practical application, simplified load-slippage curves are proposed through a regression analysis on the test data, and they are used to illustrate the influence of various parameters on the structure behaviour of these shear connections. A comprehensive comparison is conducted to examine the effect of connection configuration, steel block thickness, concrete block size, bolt diameter, and strength of concrete block on the structural behaviour of the shear connections. Moreover, the results of the single-sided push-out tests and the standard push-out tests on the connections with Connector RBN are compared to evaluate the difference of the results obtained through the two testing methods.

The deformation characteristics of the proposed shear connections are compared with those of the existing shear connectors, i.e. large-diameter headed studs (Luo *et al*., 2016), bolted shear connectors (Zhang *et al*., 2020), block shear connectors (Wang *et al*., 2019) and T-perfobond shear

connectors (Vianna *et al*., 2009), to illustrate the structural benefits of the proposed shear connections.

In accordance with design provisions specified in relevant codes and literature, the design resistances of the proposed connections are compared with the measured data, and a suitable design rule is proposed for predicting the shear resistances of the connections with Connectors RBN and R based on the test data.

5.2 Normalized shear resistances

In standard push-out tests, variations in the strengths of the concrete blocks and the concrete slabs are inevitable due to curing conditions. Since the shear resistances of the connections are significantly influenced by the strength of the concrete blocks, the measured strengths of the concrete blocks are linearly normalized to standard values of either 80 or 100 N/mm^2, and the normalized shear resistance Q_n is defined by:

$$Q_n = \eta_n Q_m \tag{5.1}$$

where,

Q_m is the measured shear resistance;

Q_n is the normalized shear resistance; and

η_n is a reduction factor, which is defined as : i) $\eta_n = 100 / f_{cu}$, when the nominal strength of concrete block is 100 N/mm^2; and ii) $\eta_n = 80 / f_{cu}$, when the nominal strength of concrete block is 80 N/mm^2.

All the normalized shear resistances together with reduction factors are summarised in Table 5.1, and the smaller resistances of the two nominally identical tests are then used in the simplified load-slippage curves, as presented in Section 5.3. It should be noted that the shear resistance of Test C-0-W has no need to be normalized as the typical failure mode is shear fracture of bolts (Mode SFB),

and the strength of the concrete block is considered to have minor influence on the shear resistance.

Table 5.1 Normalized results of the standard push out tests

Connection type	Designation	$f_{cu,150}$ (N/mm^2)	Q_m (kN)	η_n	$\boldsymbol{Q_n = \eta_n Q_m}$ **(kN)**	s_m (mm)	s_u (mm)	Failure mode
RBN	A-1-W-a	108.8	1,594.0	0.92	**1,465.1**	2.5	9.3	CF
	A-1-W-b	107.3	1,563.8	0.93	**1,457.4**	1.5	7.4	CF
	A-1-N-a	104.5	1,295.0	0.96	**1,239.2**	1.0	9.2	CF
	A-1-N-b	101.8	1,329.8	0.98	**1,306.3**	1.6	10.9	CF
	A-2-W-a	107.7	1,999.8	0.93	**1,856.8**	1.7	5.7	CF
	A-2-W-b	104.9	1,989.8	0.95	**1,896.9**	1.6	5.3	CF
	A-2-N-a	109.1	1,829.5	0.92	**1,676.9**	1.7	4.9	CF
	A-2-N-b	101.3	1,562.8	0.99	**1,542.7**	1.2	4.9	CF
	A-3-W-a	99.2	1,507.0	0.81	**1,215.3**	2.0	11.8	CF
	A-3-W-b	89.9	1,393.8	0.89	**1,240.3**	1.9	8.8	CF
RBN	B-1-W-a	105.8	1,439.5	0.95	**1,360.6**	1.5	4.2	CF
	B-1-W-b	97.7	1,282.5	1.02	**1,312.7**	1.0	6.7	CF
	B-1-N-a	110.8	1,259.3	0.90	**1,136.6**	1.2	7.2	CF
	B-1-N-b	103.5	1,187.0	0.97	**1,146.9**	1.1	5.5	CF
	B-3-W-a	88.8	1,254.0	0.90	**1,129.7**	3.9	7.4	CF
	B-3-W-b	94.7	1,373.5	0.84	**1,160.3**	1.4	8.4	CF
R	C-0-W-a	98.4	708.8	1.00	**708.8**	5.8	7.3	SFB
	C-0-W-b	93.6	725.8	1.00	**725.8**	5.7	7.1	SFB
MTP	D-0-W-a	106.9	1,266.8	0.94	**1,185.0**	3.9	7.6	CF
	D-0-W-b	113.9	1,394.0	0.88	**1,223.9**	5.2	7.9	CF

5.3 Simplified load-slippage curves

In order to describe the load-slippage curves of these shear connections using a more practical representation, two formulae are provided to depict the ascending and the descending parts of the curves. The first formula is based on a typical exponential simplification (Zhang *et al*., 2020) while the second formula follows a linear relationship, as follows:

i) The first formula describes the *ascending* exponential relationship between the shear resistance and the slippage of the shear connection, and is given by:

$$\frac{Q}{Q_n} = (1\text{-}e^{-\alpha s})^{\beta} \quad \leq \quad \Theta \tag{5.2a}$$

where:

s is the slippage;

Q is the shear force at slippage s;

Q_n is the normalized shear resistance of the shear connection;

α and β are coefficients depending on the connection type; and

Θ is the limiting value of the proposed relationship, and its value is often obtained through a regression analysis on test data.

ii) The second formula describes the *descending* linear relationship between the shear resistance and the slippage of the shear connection, and is given by:

$$Q = Q_n + k\,Q_n\,(s - s_m) \tag{5.2b}$$

where:

k is the slope of the descending part of the load-slippage curve.

Based on a detailed regression against the test data, the values of α, β and k are found to be (Ding *et al*., 2024):

a) Type A shear connections
   - $\alpha = 2.5$, $\beta = 1.0$ and $k = -0.03$ when a 30 mm thick steel block is used; and
   - $\alpha = 2.5$, $\beta = 2.0$ and $k = -0.05$ when a 50 mm thick steel block is used

b) Type B shear connections
   - $\alpha = 2.5$, $\beta = 1.0$ and $k = -0.05$

c) Type C shear connections
   - $\alpha = 0.6$, $\beta = 1.0$ and $k = -0.14$

d) Type D shear connections
   - $\alpha = 2.0$, $\beta = 1.0$ and $k = -0.05$

After a rigorous regression analysis of all test data covered in this paper, the value of Ψ is found to be 0.97. The resulting simplified load-slippage curves are plotted using red lines on the same graphs of the measured curves of the corresponding shear connections, as shown in Fig. 5.1. It is shown that the simplified representation matches reasonably well the measured curves in both the ascending and the descending parts. In addition, the simplified load-slippage curves for those shear connections investigated by Liu *et al*. (2023) have been plotted in Fig. 5.2, and various parameters of Eq. (5.2) are selected according to the case of Type A connection. It is also shown that these

simplified load-slippage curves correlate well with the test results. Consequently, the simplified load-slippage curves are considered to be effective for those connections which are within applicability of the proposed design method listed below.

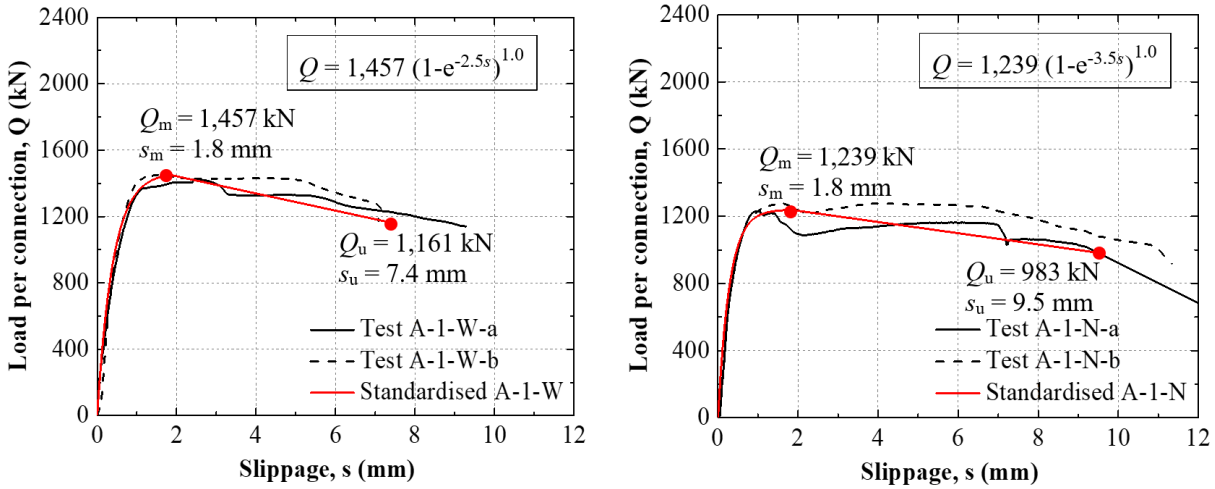

a) Test A-1-W b) Test A-1-N

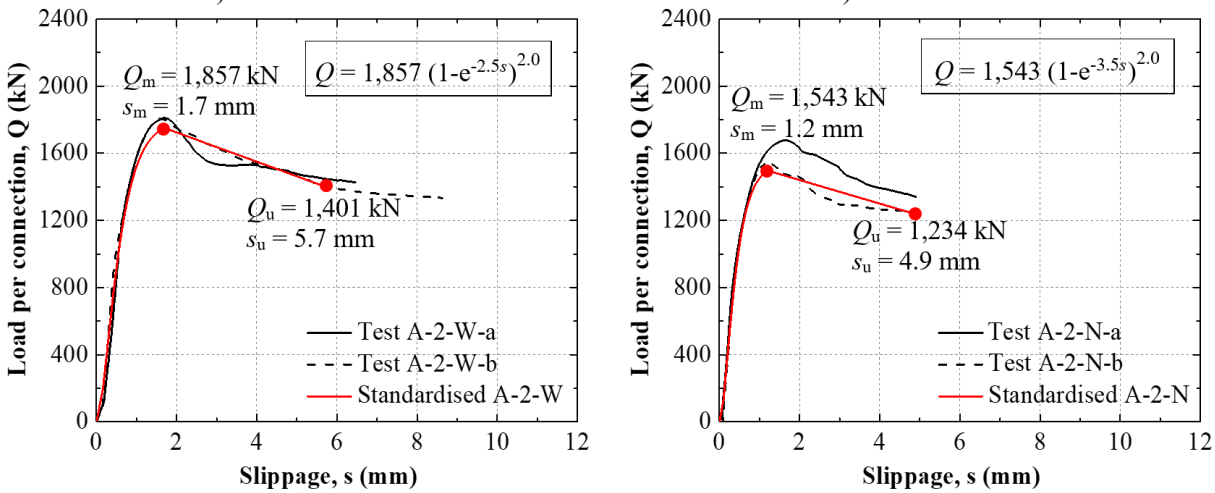

c) Test A-2-W d) Test A-2-N

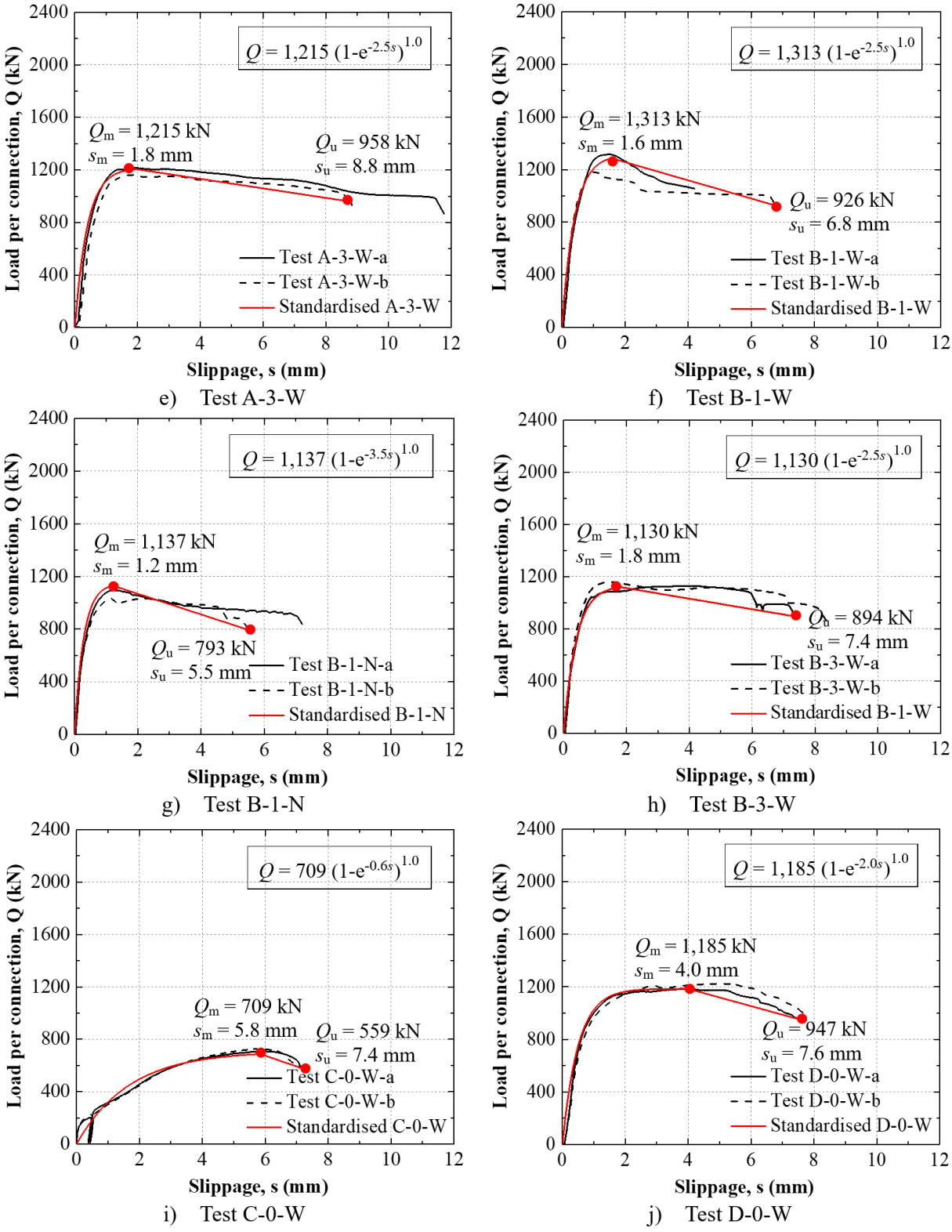

Fig. 5.1 Normalized load-slippage curves

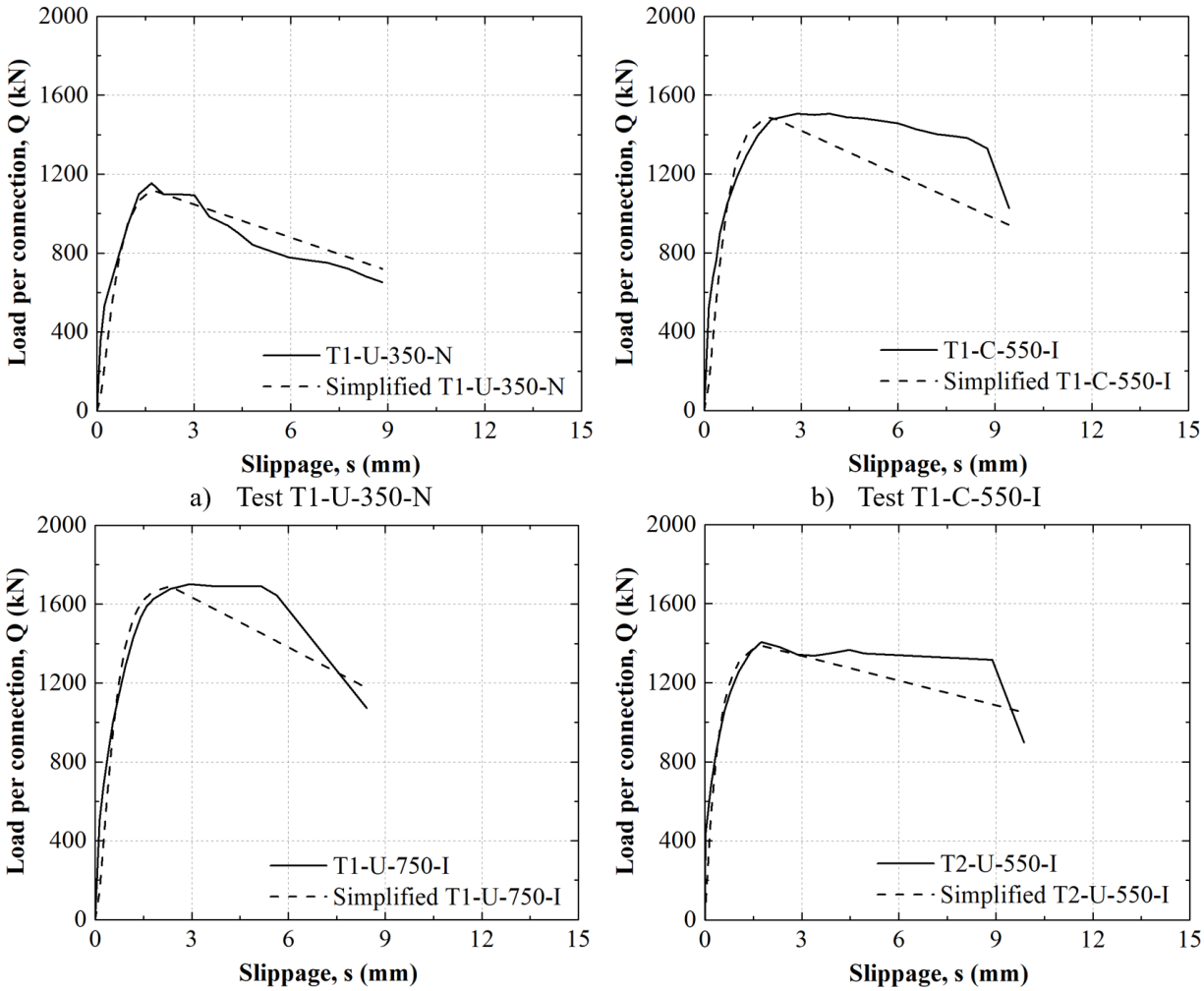

a) Test T1-U-350-N b) Test T1-C-550-I

c) Test T1-U-750-I d) Test T2-U-550-I

Fig. 5.2 Validation of the simplified load slippage curves (Liu *et al*., 2023)

Key parameters of the simplified load-slippage curves are summarised in Table 5.2. It should be noted that the simplified load-slippage curves of the tests with Types A, B, C, and D connections are categorized as four types:

i) In tests with Type A connections, the shear resistances are larger than 1,000 kN. The slippage at peak load ranges from 1.2 to 1.8 mm. The slippage corresponding to half of the peak load ranges from 0.20 to 0.49 mm, indicating excellent initial stiffnesses. The ultimate slippage in the connections with 30 mm thick steel blocks is larger than 6.0 mm, while that in the connections with 50 mm thick steel blocks are smaller than 6.0 mm. Hence, Type A connections with 30 mm thick steel blocks are demonstrated to meet all the requirements for prefabricated composite beams in highway bridges.

ii) In tests with Type B connections, the shear resistances are larger than 1,000 kN. The slippage

at peak load ranges from 1.2 to 1.8 mm. The slippage corresponding to half of the peak load ranges from 0.20 to 0.28 mm, indicating excellent initial stiffness. The ultimate slippage is larger than 6.0 mm in most of the tests except for Test B-1-N. Hence, the Type B connections with wide concrete blocks are demonstrated to meet all the requirements for prefabricated composite beams in highway bridges.

iii) In tests with Type C connections, the shear resistance is 709 kN. The slippage at peak load is found to be 5.8 mm, and the slippage corresponding to half of the peak load is found to be 1.16, indicating a small initial stiffness. The ultimate slippage is larger than 6.0 mm, while the applied load drops rapidly after reaching the peak load due to the abrupt fracture of bolts.

iv) In Tests with Type D connections, the shear resistance is 1,185 kN. The slippage at peak load is found to be 4.0 mm, and the slippage corresponding to half of the peak load is found to be 0.35 mm, indicating a good initial stiffness. The ultimate slippage is larger than 6.0 mm, and the applied load drops slowly after reaching the peak load. Hence, Type D connection is demonstrated to meet all the requirements for prefabricated composite beams in highway bridges.

Table 5.2 Simplified load-slippage curves of the shear connections

Test	Load-slippage curves $Q = Q_n (1\text{-}e^{-\alpha s})^{\beta}$	Q_n (kN)	α	β	s_m (mm)	s_u (mm)	$s_{0.5}$ (mm)	Failure mode
A-1-W	$Q = 1{,}457\ (1\text{-}e^{-2.5s})^{1.0}$	1,457	2.5	1.0	1.8	7.4	0.28	CF
A-1-N	$Q = 1{,}239\ (1\text{-}e^{-3.5s})^{1.0}$	1,239	3.5	1.0	1.8	9.5	0.20	CF
A-2-W	$Q = 1{,}857\ (1\text{-}e^{-2.5s})^{2.0}$	1,857	2.5	2.0	1.7	5.7	0.49	CF
A-2-N	$Q = 1{,}543\ (1\text{-}e^{-3.5s})^{2.0}$	1,543	3.5	2.0	1.2	4.9	0.36	CF
A-3-W	$Q = 1{,}215\ (1\text{-}e^{-2.5s})^{1.0}$	1,215	2.5	1.0	1.8	8.8	0.28	CF
B-1-W	$Q = 1{,}313\ (1\text{-}e^{-2.5s})^{1.0}$	1,313	2.5	1.0	1.6	6.8	0.28	CF
B-1-N	$Q = 1{,}137\ (1\text{-}e^{-3.5s})^{1.0}$	1,137	3.5	1.0	1.2	5.5	0.20	CF
B-3-W	$Q = 1{,}130\ (1\text{-}e^{-2.5s})^{1.0}$	1,130	2.5	1.0	1.8	7.4	0.28	CF
C-0-W	$Q = 709\ (1\text{-}e^{-0.6s})^{1.0}$	709	0.6	1.0	5.8	7.4	1.16	SFB
D-0-W	$Q = 1{,}185\ (1\text{-}e^{-2.0s})^{1.0}$	1,185	2.0	1.0	4.0	7.6	0.35	CF

5.4 Comparative deformation characteristics

All the load-slippage curves are plotted in Figs. 5.3 to 5.7, and they comprise three segments. Initially, the shear connection withstands highly localized bearing forces from the surrounding concrete in the first segment. As the deformation increases, local cracks develop within the concrete

block while yielding at the bolt root is initiated in the second segment. This results in a decrease in the stiffness of the shear connection until the peak value of the applied force, i.e. the shear resistance Q_m, is attained. In the third segment, individual bolts are sheared off, and local concrete crushing within the concrete slab takes place, leading to overall failure of the test specimen. Comparison of the test results are summarised in Table 5.3, and the effects of connection configuration, steel block thickness, concrete block size, bolt diameter, and strength of the concrete block on the structural behaviour of these shear connections are discussed below. It should be noted that the normalized shear resistances and simplified load-slippage curves are used for comparison to assess the influencing trend of various parameters on the structural behaviour of shear connections.

Table 5.3 Comparison of the test results

Comparison	
Connection configuration	Tests A-1-W, C-0-W, and D-0-W
Thickness of steel block	Tests A-1-W and A-2-W
	Tests A-1-N and A-2-N
Size of concrete block	Tests A-1-W and A-1-N
	Tests A-2-W and A-2-N
	Tests B-1-W and B-1-N
Bolt diameter	Tests A-1-W and B-1-W
	Tests A-1-N and B-1-N
Strength concrete block	Tests A-1-W and A-3-W
	Tests B-1-W and B-3-W

5.4.1 Effect of connection configuration

The load-slippage curves of those tests with different connection configurations, i.e. Tests A-1-W, C-0-W, and D-0-W, are shown in Fig. 5.3. The following two failure modes are identified: i) Concrete failure, i.e. Mode CF, in Tests A-1-W and D-0-W; and ii) Shear fracture of bolts, i.e. Mode SFB, in Test C-0-W. It is found that:

i. The shear resistances of Tests A-1-W and C-0-W are 1,457 and 709 kN respectively, and the corresponding ultimate slippages are 7.4 and 7.4 mm respectively. The initial stiffnesses are 2,614 and 301 kN/mm respectively. It is worth noting that compared with Test C-0-W, the shear resistance of Test A-1-W is increased with a factor of 2.06, and the initial stiffness is increased with a factor of 8.68. The ultimate slippages of the two connections are almost the same. The shear resistance of Test D-0-W is 1,185 kN, and the corresponding ultimate slippage is 7.6 mm. The initial stiffness is 1,693 kN/mm. It is worth noting that compared with Test A-1-W, the shear resistance of Test D-0-W is decreased with a factor of 0.81, the ultimate slippages are almost the same, and the initial stiffness is decreased with a factor of 0.65.

ii. Hence, the provision of the welded steel blocks is shown to be efficient to increase both the shear resistances and the initial stiffnesses of the proposed connections. It is reckoned that local bearing stresses in the proximity of the steel blocks are effectively distributed within the concrete blocks due to the presence of steel fibres. It is also demonstrated that Type A connection with a 30 mm thick steel block and a large concrete block is highly effective.

iii. The load-slippage curve of a shear connection with a pair of 30 mm diameter headed shear studs (Luo *et al*., 2016) is plotted onto the same graph for direct comparison with that of Test C-0-W. It should be noted that both the dimensions and the material grades of both the bolted and the stud shear connections are similar. It is apparent that the load-slippage curves of both shear connections are fairly similar at large deformations though that of the bolted shear connection exhibits a smaller initial stiffness, when compared with that of the stud shear connection.

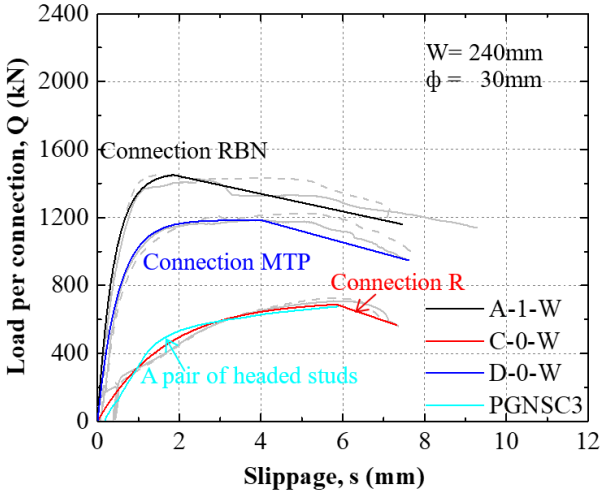

Test	Load-slippage curves $Q = Q_n (1-e^{-\alpha s})^{\beta}$	Q_n (kN)	s_u (mm)	K (kN/mm)
A-1-W	$Q = 1{,}457\ (1-e^{-2.5s})^{1.0}$	1,457	7.4	2,614
C-0-W	$Q = 709\ (1-e^{-0.6s})^{1.0}$	709	7.4	301
D-0-W	$Q = 1{,}185\ (1-e^{-2.0s})^{1.0}$	1,185	7.6	1,693
PGNSC3	-	675	5.9	327

Fig. 5.3 Effect of connection configuration

5.4.2 Effect of steel block thickness

The load-slippage curves of the tests with Type A shear connections with different steel block thicknesses are compared, and the main observations are listed below.

a) Type A connectors with large concrete blocks

   i. All these tests failed in concrete fracture, i.e. Mode CF. As shown in Fig. 5.4a), the load-slippage curve of Test A-1-W exhibits a ductile behaviour at large deformation while that of Test A-2-W indicates some reduction in resistance at large deformation. The shear resistances of Tests A-1-W and A-2-W are 1,457 and 1,857 kN, respectively, and the corresponding ultimate slippages are 7.4 and 5.7 mm, respectively. The initial stiffnesses are 2,614 and 2,146 kN/mm, respectively. Compared with Test A-1-W, the shear resistance of Test A-2-W is increased with a factor of 1.27, the ultimate slippage is decreased by 1.7 mm while the initial stiffness is decreased with a factor of 0.82.

   ii. By increasing the thickness of the steel blocks, the bearing areas against the surrounding concrete are enlarged, and hence, the shear resistances of the connections are significantly increased. However, their ultimate slippages are decreased to lower than 6.0 mm together with a significant reduction in their resistances.

b) Type A connectors with small concrete blocks

   i. All these tests failed in concrete fracture, i.e. Mode CF. As shown in Fig. 5.4b), the load-slippage curve of Test A-1-N indicates a ductile behaviour at large deformation while that of Test A-2-N exhibit some reduction in resistance at large deformation. The shear resistances of Tests A-1-N and A-2-N are 1,239 and 1,543 kN, respectively, while their corresponding ultimate slippages are 9.5 and 4.9 mm, respectively, and their initial stiffnesses are 2,831 and 2,143 kN/mm, respectively. Compared with Test A-1-N, the shear resistance of Test A-2-N is increased with a factor of 1.25, the ultimate slippage is decreased by 4.6 mm, and the initial stiffness is decreased with a factor of 0.76.

   ii. Similar to the findings in Point a) above, by increasing the thickness of the steel blocks, the bearing areas against the surrounding concrete are enlarged, and hence, the shear resistances of the connections are significantly increased. However, their ultimate slippages are decreased accordingly to less than 6.0 mm, i.e. inferior to the requirements stipulated in EN 1994-1-1, together with a significant reduction in their stiffnesses.

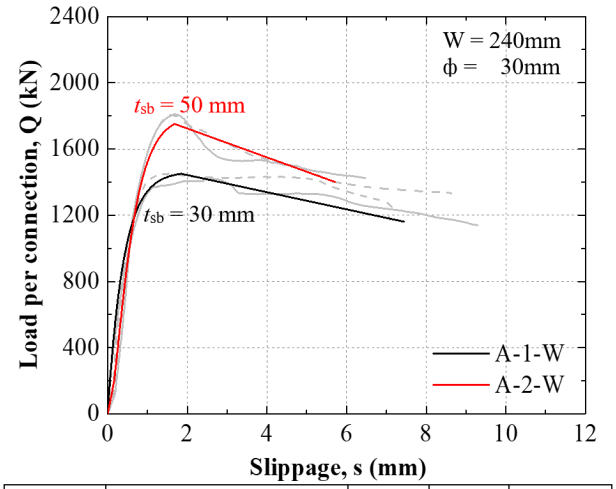

Test	Load-slippage curves $Q = Q_n (1\text{-}e^{-\alpha s})^{\beta}$	Q_m (kN)	s_u (mm)	K (kN/mm)
A-1-W	$Q = 1{,}457\ (1\text{-}e^{-2.5s})^{1.0}$	1,457	7.4	2,614
A-2-W	$Q = 1{,}857\ (1\text{-}e^{-2.5s})^{2.0}$	1,857	5.7	2,146

a) Type A connectors with large concrete blocks

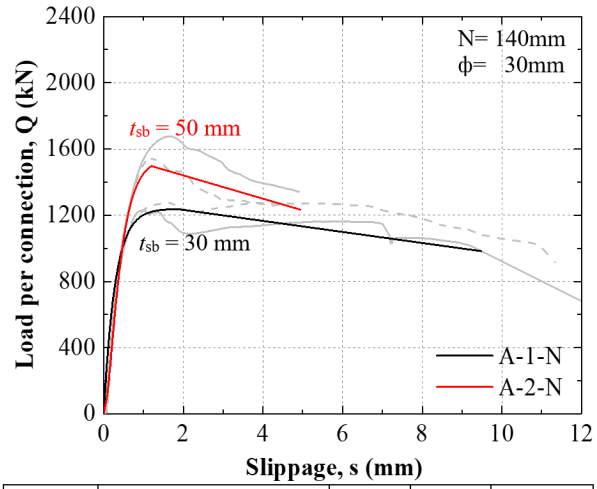

Test	Load-slippage curves $Q = Q_n (1\text{-}e^{-\alpha s})^{\beta}$	Q_m (kN)	s_u (mm)	K (kN/mm)
A-1-N	$Q = 1{,}239\ (1\text{-}e^{-3.5s})^{1.0}$	1,239	9.5	2,831
A-2-N	$Q = 1{,}543\ (1\text{-}e^{-3.5s})^{2.0}$	1,543	4.9	2,143

b) Type A connectors with small concrete blocks

Fig. 5.4 Effect of steel block thickness

5.4.3 Effect of concrete block size

The load-slippage curves of the tests with Types A and B shear connections with different concrete block sizes are compared, and the main observations are listed below.

a) Type A connectors with 30 mm thick steel block

i. All these tests failed in concrete fracture, i.e. Mode CF. As shown in Fig. 5.5a), all the load-slippage curves of Tests A-1-W and A-1-N exhibit a fairly ductile behaviour at large deformation. The shear resistances of Tests A-1-W and A-1-N are 1,457 and 1,239 kN, respectively, the corresponding ultimate slippages are 7.5 and 9.5 mm, respectively, and their initial stiffnesses are 2,614 and 2,831 kN/mm, respectively.

ii. Hence, when compared with the result of Test A-1-W, the shear resistance of Test A-1-N is decreased with a factor of 0.85. The ultimate slippage is increased by 2.0 mm, and the initial stiffness is increased with a factor of 1.08.

b) Type A connectors with 50 mm thick steel block

i. All these tests failed in concrete fracture, i.e. Mode CF. As shown in Fig. 5.5b), all the load-slippage curves of Tests A-2-W and A-2-N exhibit a non-ductile behaviour with small reductions in their resistance at large deformation. The shear resistances of Tests A-2-W

and A-2-N are 1,857 and 1,543 kN, respectively, the corresponding ultimate slippages are 5.7 and 4.9 mm, respectively, and their initial stiffnesses are 2,146 and 2,143 kN/mm, respectively.

ii. Similar to the findings given in Point a) above, when compared with the result of Test A-2-W, the shear resistance of Test A-2-N is decreased with a factor of 0.83. The corresponding ultimate slippage is decreased by 0.8 mm, while the initial stiffnesses are almost the same.

c) Type B connectors with 30 mm thick steel block

i. All these tests failed in concrete fracture, i.e. Mode CF. As shown in Fig. 5.5c), all the load-slippage curves of Tests B-1-W and B-1-N exhibit a non-ductile behaviour with small reductions in their resistance at large deformation. The shear resistances of Tests B-1-W and B-1-N are 1,313 and 1,137 kN, respectively, the corresponding ultimate slippages are 6.8 and 5.5 mm, respectively, and their initial stiffnesses are 2,233 and 2,810 kN/mm, respectively.

ii. Hence, when compared with the result of Test B-1-W, the shear resistance of Test B-1-N is decreased with a factor of 0.87. The ultimate slippage is decrease by 1.3 mm, while the initial stiffness is increased with a factor of 1.26.

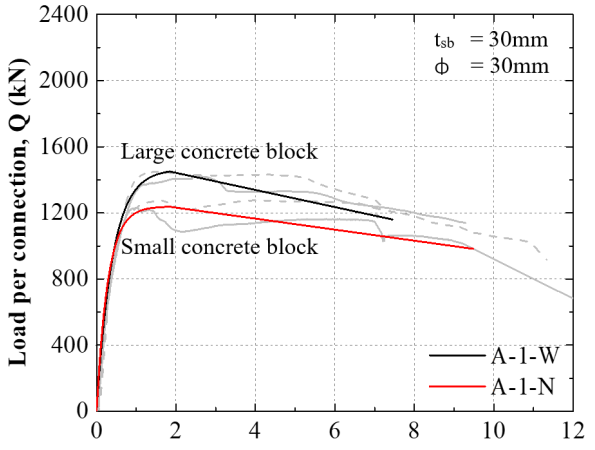

Test	Load-slippage curves $Q = Q_n (1\text{-}e^{-\alpha s})^{\beta}$	Q_m (kN)	s_u (mm)	K (kN/mm)
A-1-W	$Q = 1{,}457\ (1\text{-}e^{-2.5s})^{1.0}$	1,457	7.5	2,614
A-1-N	$Q = 1{,}239\ (1\text{-}e^{-3.5s})^{1.0}$	1,239	9.5	2,831

a) Type A connectors with 30mm thick steel block

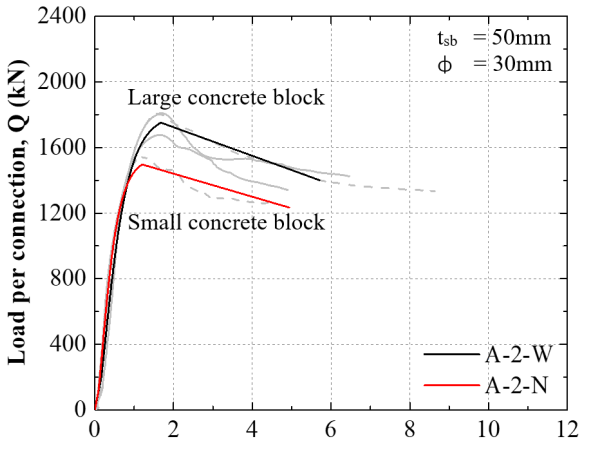

Test	Load-slippage curves $Q = Q_n (1\text{-}e^{-\alpha s})^{\beta}$	Q_m (kN)	s_u (mm)	K (kN/mm)
A-2-W	$Q = 1{,}857\ (1\text{-}e^{-2.5s})^{2.0}$	1,857	5.7	2,146
A-2-N	$Q = 1{,}543\ (1\text{-}e^{-3.5s})^{2.0}$	1,543	4.9	2,143

b) Type A connectors with 50mm thick steel block

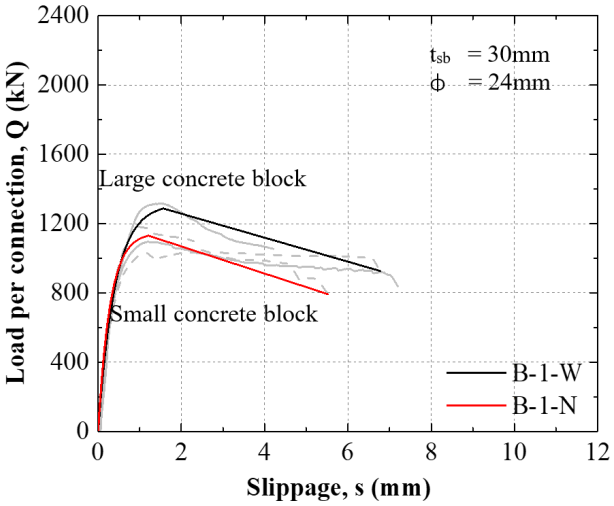

Test	Load-slippage curves $Q = Q_n (1\text{-}e^{-\alpha s})^{\beta}$	Q_m (kN)	s_u (mm)	K (kN/mm)
B-1-W	$Q = 1{,}313\ (1\text{-}e^{-2.5s})^{1.0}$	1,313	6.8	2,233
B-1-N	$Q = 1{,}137\ (1\text{-}e^{-3.5s})^{1.0}$	1,137	5.5	2,810

Fig. 5.5 Effect of concrete block size

5.4.4 Effect of bolt diameter

The load-slippage curves of the tests with Types A and B shear connections with different bolt diameters are compared, and the main observations are listed below.

a) Connections with large concrete blocks

i. All these tests failed in concrete fracture, i.e. Mode CF. As shown in Fig. 5.6a), the load-slippage curves of Test A-1-W exhibits a ductile behaviour while that of Test B-1-W indicates a non-ductile behaviour with small reduction in resistance at large deformation. The shear resistances of Tests A-1-W and B-1-W are 1,457 and 1,313 kN, respectively, the corresponding ultimate slippages are 7.5 and 6.8 mm, respectively, and their initial stiffnesses are 2,614 and 2,233 kN/mm, respectively.

ii. Hence, when compared with the result of Test A-1-W, the shear resistance of Test B-1-W is decreased with a factor of 0.90, the corresponding ultimate slippage is decreased by 0.7 mm, and the initial stiffness is decreased with a factor of 0.85. Despite the use of bolts with 24 mm diameters, when compared with those of 30 mm diameters in Test A-1-W, i.e. a reduction in the bolt cross-sectional area of 0.64, the shear resistance of Test B-1-W is only 0.90 that of Test A-1-W due to the presence of the same steel blocks which resist the applied forces through bearing.

b) Connections with small concrete blocks

i. All these tests failed in concrete fracture, i.e. Mode CF. As shown in Fig. 5.6b), the load-slippage curves of Test A-1-N exhibits a ductile behaviour while that of Test B-1-N indicates a non-ductile behaviour with small reductions in resistance at large deformation. The shear resistances of Tests A-1-N and B-1-N are 1,239 and 1,137 kN, respectively, the corresponding ultimate slippages are 9.5 and 5.5 mm, respectively, and their initial stiffnesses are 2,831 and 2,810 kN/mm, respectively.

ii. Hence, when compared with the result of Test A-1-N, the shear resistance of Test B-1-N is decreased with a factor of 0.92, the corresponding ultimate slippage is decreased by 4.0 mm. The initial stiffnesses are almost the same. Similar findings noted in Point a) above are also applicable in this case.

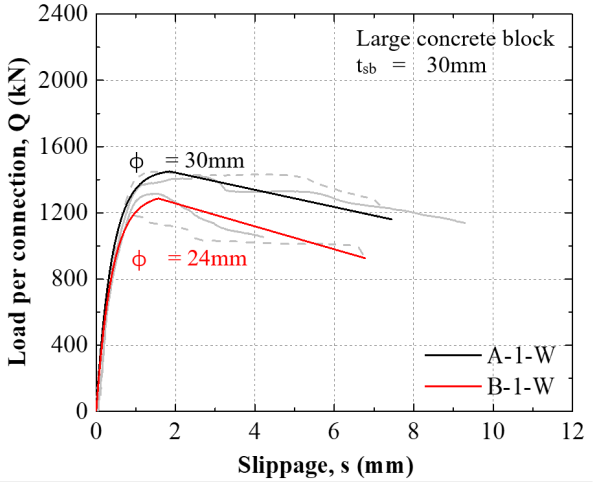

Test	Load-slippage curves $Q = Q_n (1\text{-}e^{-\alpha s})^{\beta}$	Q_m (kN)	s_u (mm)	K (kN/mm)
A-1-W	$Q = 1{,}457\ (1\text{-}e^{-2.5s})^{1.0}$	1,457	7.5	2,614
B-1-W	$Q = 1{,}313\ (1\text{-}e^{-2.5s})^{1.0}$	1,313	6.8	2,233

a) Connections with large concrete blocks

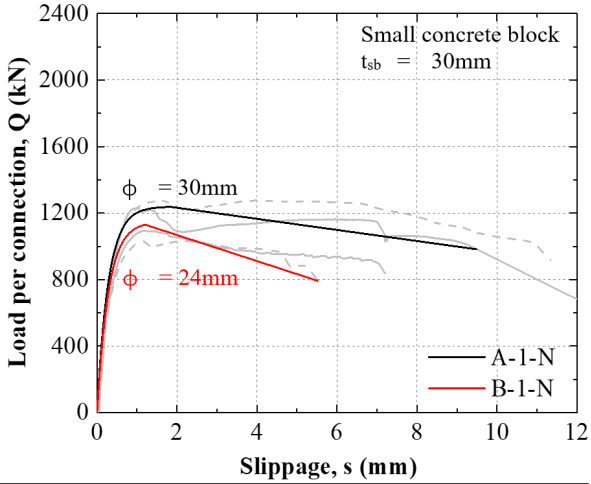

Test	Load-slippage curves $Q = Q_n (1\text{-}e^{-\alpha s})^{\beta}$	Q_m (kN)	s_u (mm)	K (kN/mm)
A-1-N	$Q = 1{,}239\ (1\text{-}e^{-3.5s})^{1.0}$	1,239	9.5	2,831
B-1-N	$Q = 1{,}137\ (1\text{-}e^{-3.5s})^{1.0}$	1,137	5.5	2,810

b) Connections with large concrete blocks

Fig. 5.6 Effect of bolt diameter

5.4.5 Effect of strength of concrete block

The load-slippage curves of the tests with Types A and B shear connections with different strengths of concrete blocks are compared, and the main observations are listed below.

a) Type A connectors with 30 mm thick steel block

i. All these tests failed in concrete fracture, i.e. Mode CF. As shown in Fig. 5.7a), all the load-slippage curves of Tests A-1-W and A-3-W exhibit a fairly ductile behaviour at large

deformation. The shear resistances of Tests A-1-W and A-3-W are 1,457 and 1,215 kN, respectively, the corresponding ultimate slippages are 7.4 and 8.8 mm, respectively, and their initial stiffnesses are 2,614 and 2,077 kN/mm, respectively.

ii. Hence, when compared with the result of Test A-1-W, the shear resistance of Test A-3-W is decreased with a factor of 0.83, owing to the use of C80 concrete blocks in Test A-3-W, i.e. a reduction in the concrete strength of 0.80. The ultimate slippage is increased by 1.4 mm, and the initial stiffness is decreased with a factor of 0.79. Hence, the shear resistance of Type A connector with 30 mm thick steel block is almost proportional to the strength of the concrete block.

b) Type B connectors with 30 mm thick steel block

i. All these tests failed in concrete fracture, i.e. Mode CF. As shown in Fig. 5.7b), all the load-slippage curves of Tests B-1-W and B-3-W exhibit a fairly ductile behaviour at large deformation. The shear resistances of Tests B-1-W and B-3-W are 1,313 and 1,130 kN, respectively, the corresponding ultimate slippages are 6.8 and 7.4 mm, respectively, and their initial stiffnesses are 2,233 and 2,018 kN/mm, respectively.

ii. Hence, when compared with the result of Test B-1-W, the shear resistance of Test B-3-W is decreased with a factor of 0.86. The ultimate slippage is increased by 0.6 mm, and the initial stiffness is decreased with a factor of 0.90. Hence, in tests with a bolt diameter of 24 mm, the increase of the strength of the concrete block has a certain influence on the structural behaviour of the shear connections.

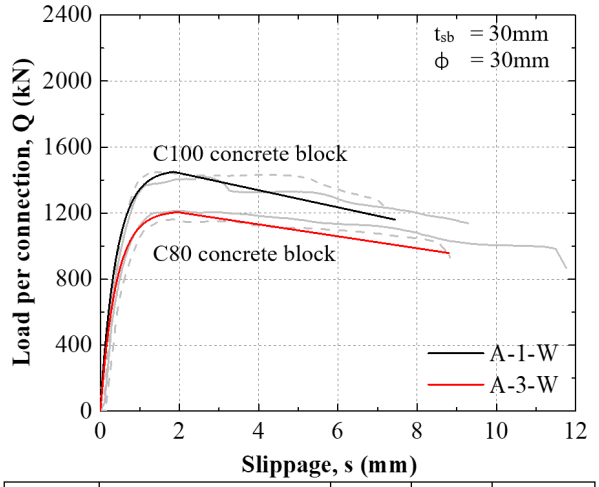

Test	Load-slippage curves $Q = Q_n (1\text{-}e^{-\alpha s})^{\beta}$	Q_m (kN)	s_u (mm)	K (kN/mm)
A-1-W	Q = 1,457 $(1\text{-}e^{-2.5s})^{1.0}$	1,457	7.4	2,614
A-3-W	Q = 1,215 $(1\text{-}e^{-2.5s})^{1.0}$	1,215	8.8	2,077

a) Type A connectors with 30mm thick steel block

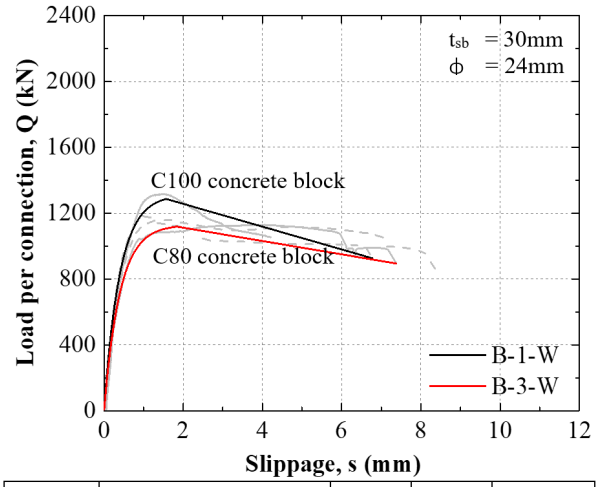

Test	Load-slippage curves $Q = Q_n (1\text{-}e^{-\alpha s})^{\beta}$	Q_m (kN)	s_u (mm)	K (kN/mm)
B-1-W	Q = 1,313 $(1\text{-}e^{-2.5s})^{1.0}$	1,313	6.8	2,233
B-3-W	Q = 1,130 $(1\text{-}e^{-2.5s})^{1.0}$	1,130	7.4	2,018

b) Type B connectors with 30mm thick steel block

Fig. 5.7 Effect of strength of concrete block

5.5 Comparison with single-sided push-out tests

The load-slippage curves of those tests with Connection RBN and 30 mm diameter bolts obtained from standard push-out tests and single-sided push-out tests, i.e. Tests A-1-W and A-C1-p, are compared in Fig. 5.8a), and the load-slippage curves of those tests with Connection RBN and 24 mm diameter bolts obtained from standard push-out tests and single-sided push-out tests, i.e. Tests B-1-W and B-C1-p, are compared in Fig. 5.8b). It should be noted that the structural behaviour of Tests A-1-W and B-1-W under standard push-out tests is presented in Chapter 4. Due to different steel block sizes in the standard and the single-sided push-out test, the shear resistances of the connections in single-sided push-out tests are linearly normalized according to the increased projected area as follows:

$$Q_m = Q_1 * 200 / 120 \tag{5.3}$$

where,

Q_1 is the shear resistance of the connections in single-sided push-out tests; and

Q_m is the shear resistance of the connections in standard push-out tests.

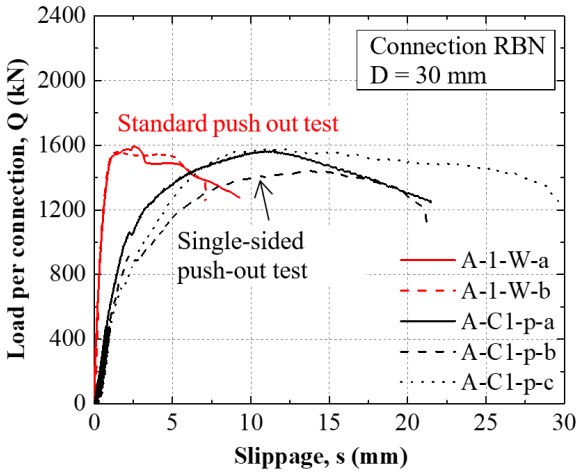

Test	$f_{cu,150}$ (N/mm^2)	Q_m (kN)	s_m (mm)	s_u (mm)	K (kN/mm)
A-1-W	108.1	1,578.9	2.0	8.4	2,498
A-C1-p	111.2	1,528.2	11.9	24.1	528

a) Type A connectors

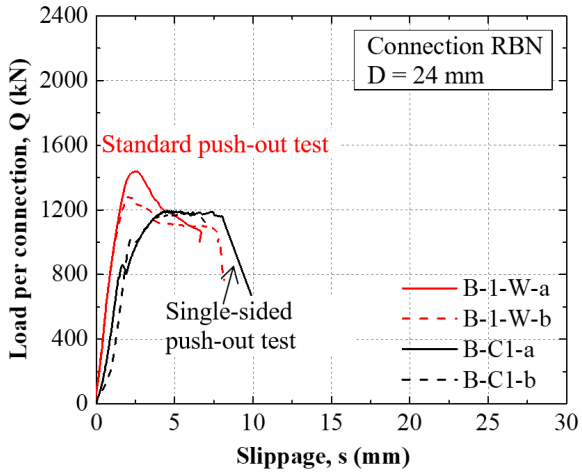

Test	$f_{cu,150}$ (N/mm^2)	Q_m (kN)	s_m (mm)	s_u (mm)	K (kN/mm)
B-1-W	101.8	1,361.0	1.3	5.5	2,516
B-C1-p	118.4	1,187.0	4.9	9.0	450

b) Type B connectors

Fig. 5.8 Comparison with single-sided push-out tests

5.5.1 Tests with Type A connections

In general, Mode CF is found in all these tests. It is found that:

i) The average shear resistances Q_m of Tests A-1-W and A-C1-p are 1,578.9 and 1,528.2 kN respectively, and the corresponding slippage limits s_u are 8.4 and 24.1 mm respectively. The initial stiffnesses are 2,498 and 528 kN/mm respectively. It is worth noting that the shear resistances of these two tests are almost the same. Compared with Test A-C1-p, the initial stiffness of Test A-1-W is increased with a factor of 4.73, while the slippage limit is decreased by 15.7 mm.

ii) Hence, the shear resistance of Test A-C1-p is comparable to that of Test A-1-W, while the slippage limit of Test A-C1-p is larger. In the single-sided push-out test, the infilled concrete block is susceptible to tilting as the applied load increases, and hence, this leads to an increase in the slippage, and a reduction in the initial stiffness.

5.5.2 Tests with Type B connectors

In general, Mode CF is found in all these tests, and all the bolts are fractured after tests. It is found that:

i) The average shear resistances Q_m of Tests B-1-W and B-C1-p are 1,361.0 and 1,187.0 kN

respectively, and the corresponding slippage limits s_u are 5.5 and 9.0 mm respectively. The initial stiffnesses are 2,516 and 450 kN/mm respectively. It is worth noting that compared with Test B-C1-p, the shear resistances of Test B-1-W is increased with a factor of 1.14, and the initial stiffness is increased with a factor of 5.59. The slippage limit is decreased by 3.5 mm.

ii) Similar to those found in Type A connectors, in the single-sided push-out test, the infilled concrete block is susceptible to tilting as the applied load increases, and hence, this leads to an increase in the slippage, and a reduction in the initial stiffness.

5.6 Comparison with the tests reported in the literature

5.6.1 Comparison with the tests on stud / bolted shear connectors

Key results of the present study and the other studies on bolted / stud shear connectors are compared in Table 5.4 and Fig. 5.9. It should be noted that the shear resistance Q_m denotes the resistance of a pair of studs / bolts.

a) In those tests on a group of studs in precast concrete slabs (Wang *et al*., 2018), the stud diameter is 30 mm, and the tensile strength of the stud steel is 436 N/mm^2. The shear resistances of Tests PGNSC2 and PGNSC3 are 579.0 and 671.2 kN respectively. It is shown that when compared with Test PGNSC2, the strength of the concrete block in Test PGNSC3 is increased with a factor of 2.19, and the shear resistance is increased with a factor of 1.16. The shear resistance obtained in Test PGUHPC2 is 676.6 kN. When compared with Test PGNSC3, the strength of the precast concrete slab in Test PGUHPC2 is increased with a factor of 2.53, while the shear resistance remains almost unchanged. As a result, the strength of the concrete block has a great influence on the shear resistance of the connections, while the strength of the precast concrete slab has minor influence. In the present study, the nominal bolt diameter in Test C-0-W is 30 mm, and the average shear resistance is 717.3 kN. When compared with Test PGNSC3, the shear resistance is increased with a factor of 1.07 due to an

increase in the tensile strength of the bolt.

b) In the tests on bolted shear connectors with precast concrete slabs and cast-in-situ concrete slabs (Du *et al*., 2020), the bolt diameter is 16 mm, and the tensile strength of the bolt steel is 886 N/mm^2. The shear resistances of Tests DBC2 and DBC4 are 212.8 and 179.8 kN respectively. It is found that when compared with Test DBC4, the resistance of Test DBC2 with a precast concrete slab is increased with a factor of 1.18, owing to an increase in the strength of the concrete block. When compared with Test DBC2, the bolt diameter in Test C-0-W is increased with a factor of 1.88, and hence, the shear resistance is increased with a factor of 3.37, which is almost proportional to the square of the bolt diameter.

c) In the tests on HSFGB shear connectors with NC and SFRC slabs (Zhang *et al*., 2020), the shear resistances of Tests NC-M27-γ1-G8.8 and SFRC-M27-γ1-G8.8 are 611.0 and 740.4 kN respectively. It is shown that when compared with Test NC-M27-γ1-G8.8, the shear resistance of Test SFRC-M27-γ1-G8.8 is increased with a factor of 1.21, owing to the provision of steel fibres in the concrete slab. When compared with Test SFRC-M27-γ1-G8.8, the concrete strength of Test C-0-W is increased with a factor of 1.54, while the shear resistance remains almost the same, and hence, when the critical failure mode is shear fracture of bolts, the strength of the concrete slab has only minor influence on the shear resistance of the shear connections.

In general, the shear resistance of bolted / stud shear connectors is primarily influenced by the stud / bolt diameters, concrete strengths and types, and tensile strength of the studs / bolts. It should be noted that the strength of the concrete block in the vicinity of the studs / bolts has a great influence on the shear resistance, while the strength of the concrete slab has only minor influence on the shear resistance when the critical failure mode is concrete failure. When steel fibres are provided

in the concrete block, the shear resistance of the connection is increased due to the improvement of the tensile strength of the concrete. Moreover, the shear resistance of stud / bolted shear connectors is proportional to the square of the bolt diameter.

Table 5.4 Comparison with stud / bolted shear connectors in the literature

Connector type	Test	Concrete	Bolt / stud		Q_m
		f_c (N/mm^2)	d (mm)	f_u (N/mm^2)	(kN)
Bolts (Present study)	C-0-W-a	61.9 (98.4)	30	912	708.8
	C-0-W-b	65.9 (93.6)			725.8
Grouped studs (Wang *et al.*, 2018)	PGNSC2	49.0 (56.7)	30	436	579.0
	PGNSC3	49.0 (124.2)			**671.2**
	PGUHPC2	124.0 (125.0)			676.6
Single nut embedded bolts (Du *et al.*, 2020)	DBC1	29.8 (30.9)	16	886	171.2
	DBC2	29.4 (40.3)			**212.8**
	DBC3	30.7 (28.8)			160.0
	DBC4	30.9			179.8
HSFGB connector (Zhang *et al.*, 2020)	NC-M22-γ1-G8.8	58.8	22	800	483.6
	NC-M27-γ1-G8.8		27		611.0
	SFRC-M22-γ1-G8.8	62.2	22		496.4
	SFRC-M27-γ1-G8.8		27		**740.4**
	SFRC-M24-γ1-G8.8		24		589.0
	SFRC-M24-γ1-G10.9		24	1,000	709.2

Note:
For concrete strengths, the values are the strengths of the precast concrete slabs. Those values in the brackets are the strengths of the infilled concrete blocks.

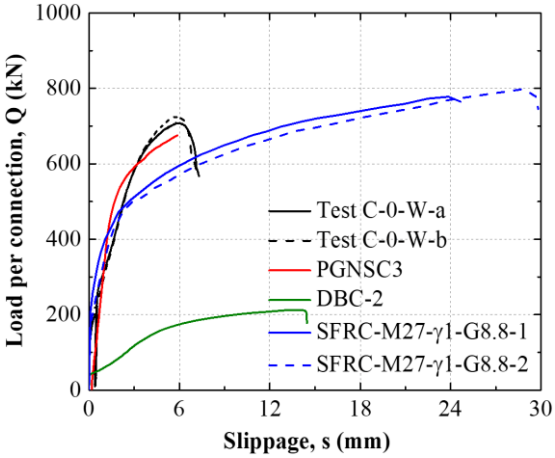

Fig. 5.9 Comparison with stud / bolted shear connections (Vianna *et al.*, 2008; 2009; Shim et al., 2004)

5.6.2 Comparison with the tests on block shear connectors

Key results of the present study and the other studies on block shear connectors are compared in Table 5.5 and Fig. 5.10.

a) In those tests on SBSC with precast concrete slabs (Wang *et al*., 2019), the dimensions of the steel blocks are 140 × 60 mm ($l \times h$). The shear resistance of Test PRM is 958.1 kN, and the shear resistance of Test A-1-W in the present study is 1,578.9 kN. When compared with Test PRM, the bearing area of the steel block in Test A-1-W is reduced with a factor of 0.71, while the strength of the concrete block is increased with a factor of 2.02, and hence, the shear resistance is increased with a factor of 1.65. It is shown that the shear resistance is almost proportional to the multiplication of the bearing area of the steel block and the strength of the concrete block.

b) In those tests on B-S connectors with precast concrete slabs (Zou *et al*., 2021), the length of the bearing plate is 80 mm, and the heights are 70, 80, 120, and 160 mm respectively. The shear resistances of Tests SB-r20-h80 and SB-r20-h160 are 1,138.9 and 1,184.2 kN respectively. It is shown that when compared with Test SB-r20-h80, although the area of the bearing plate in Test SB-r20-h160 is increased with a factor of 2.0, the shear resistance is merely increased with a factor of 1.04. When compared with Test SB-r20-h160, the bearing area of the steel block in Test A-1-W is reduced with a factor of 0.47, while the strength of the concrete block is increased with a factor of 2.47, and the shear resistance of Test A-1-W is increased with a factor of 1.33.

c) In the tests on headed stud-steel block connectors with precast concrete slabs (Liu *et al*., 2023), the length of the bearing plate is 200 mm, and the heights are found to be 35, 50, and 65 mm respectively. The shear resistances of Tests T2-U-550-I, T1-U-550-I, and T3-U-550-I are 1,387.7, 1,754.5, and 1,821.2 kN respectively. It is shown that when compared with Test T2-U-550-I, the bearing area of the steel block in Test T3-U-550-I is increased with a factor 1.86, and the shear resistance is increased with a factor of 1.31. When compared with Test T1-U-550-I, the bearing area of the steel block in Test A-1-W is decreased with a factor of 0.60,

while the strength of the concrete block is increased with a factor of 1.42, and hence, the shear resistance of Test A-1-W is decreased with a factor of 0.90. Hence, the shear resistance of the block shear connector is almost proportional to the multiplication of the bearing area and the strength of the concrete block.

In general, the shear resistance of the block shear connector is primarily influenced by the strength of the concrete block and the bearing area of the steel block against the surrounding concrete. The shear resistance of the block shear connector is almost proportional to the multiplication of the bearing area and the strength of the concrete block. It should be noted that B-S connector exhibits large ultimate slippage due to large deformations of the shear plate.

Table 5.5 Comparison with block shear connectors in the literature

Connector type	Test	Concrete	Bolt/ stud/ rebar/ plate		Steel	Q_m (kN)
		f_c (N/mm^2)	d / t (mm)	f_u (N/mm^2)	$l \times h$ (mm)	
Bolts with welded steel block (Present study)	A-1-W-a	71.2 (108.8)	30	828	200 × 30	1,594.0
	A-1-W-b	71.2 (107.3)				1,563.8
SBSC (Wang *et al*., 2019)	**PRM**	34.0 (53.5)	20	(465)	140 × 60	**958.1**
B-S connector (Zou *et al*., 2021)	SB-r20-h120	36.7 (43.6)	16	(361 / 450)	80 × 120	1,200.9
	SB-r20-h80				80 × 80	1,138.9
	SB-r20-h160				80 × 160	**1,184.2**
	SB-r0-h120				80 × 120	1,121.4
	SB-r20-h50d				80 × 70	1,207.9
Headed stud-steel block connector (Liu *et al*., 2023)	**T1-U-550-I**	40.6 (76.1)	19	498	200 × 50	**1,754.5**
	T1-U-550-N	40.6 (76.1)				1,597.7
	T1-C-550-I	40.6 (50.9)				1,387.7
	T1-U-350-N	40.6 (76.1)				1,146.7
	T1-U-750-I	40.6 (76.1)				1,565.1
	T2-U-550-I	40.6 (76.1)			200 × 35	**1,387.7**
	T3-U-550-I	40.6 (76.1)			200 × 65	**1,821.2**

Notes:

i) For concrete strengths, the values are the strengths of the precast concrete slabs. Those values in the brackets are the strengths of the infilled concrete blocks.

ii) For the tensile strengths of bolts, studs, and rebars, the values in the bracket denote their yield strengths.

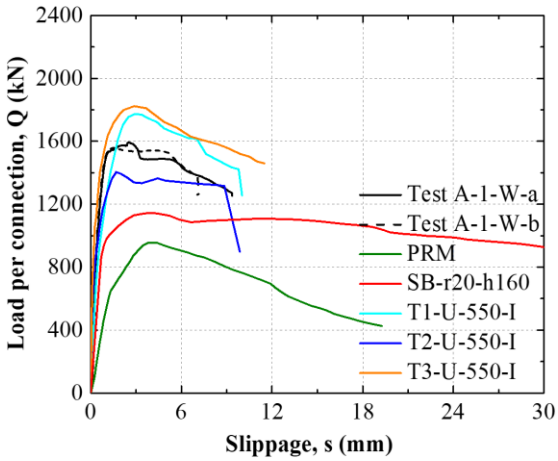

Fig. 5.10 Comparison with block shear connections

5.6.3 Comparison with the tests on perfobond rib shear connectors

Key results of the present study and the other studies on perfobond rib shear connectors are compared in Table 5.6 and Fig. 5.11.

a) In those tests on perfobond rib shear connectors conducted by Ahn *et al*. (2010), the dimensions of the perfobond rib are 500 × 129 × 6 mm , and the yield strength of the perfobond rib is 352 N/mm^2. The shear resistances of Tests PF-S-C30 and PF-S-C50 are 590.7 and 692.2 kN respectively. It is shown that when compared with Test PF-S-C30, the strength of the concrete in Test PF-S-C50 is increased with a factor of 1.61, and the shear resistance is increased with a factor of 1.17. In the present study, the average shear resistance of Test D-0-W is 1,330.4 kN. When compared with Test PF-S-C50, the strength of the concrete block in Test D-0-W is increased with a factor of 2.10, and the shear resistance is increased with a factor of 1.92.

b) In those tests on perfobond rib shear connectors conducted by Vianna *et al*. (2009), the dimensions of the perfobond rib are 180×150 ×12.5 mm, and the yield strength of the perfobond rib is 500 N/mm^2. The shear resistance of Test P-4F_200-28 is 433.8 kN. When compared with Test P-4F_200-28, the strength of the concrete block in Test D-0-W is increased with a factor of 4.10, and the shear resistance is increased with a factor of 3.07.

c) In the tests on T-perfobond rib connectors (Vianna *et al*., 2008), the dimensions of the bearing plate are 137×150×18.3 mm , and the yield strength of the perfobond rib is 500 N/mm^2. The shear resistances of Tests TP_4F_200-28 and TP_4F_200-44 are 691.2 and 770.3 kN respectively. It is shown that when compared with Test TP_4F_200-44, the strength of the concrete block in Test D-0-W is increased with a factor of 2.51, while the bearing area of the bearing plate is decreased with a factor of 0.70, and hence, the shear resistance is increased with a factor of 1.73. It is shown that the shear resistance of the T-perfobond rib shear connection is almost proportional to the multiplication of the concrete block strength and the bearing area of the bearing plate.

In general, the shear resistances of the perfobond and the T-perfobond rib shear connections are significantly influenced by the strength of the infilled concrete block. The shear resistance of the T-perfobond rib shear connection is almost proportional to the multiplication of the bearing area of the bearing plate and the strength of the concrete block. However, the ductility of the T-perfobond rib shear connection is smaller than that of the perfobond rib shear connection. Both the shear resistance and the ductility of the T-perfobond rib shear connection are increased when SFRC is used in concrete blocks.

Table 5.6 Comparison with perfobond shear connectors in the literature

Connector type	Test	Concrete	Rebar		Steel plate	Q_m
		f_c (N/mm^2)	d / t (mm)	f_u (N/mm^2)	$l \times h \times t_s$ (mm)	(kN)
Modified T-perfobond rib connector (Present study)	D-0-W-a	60.2 (106.9)	16	593 (421)	120 × 120 × 12	1,266.8
	D-0-W-b	61.0 (113.9)				1,394.0
Perfobond rib connector (Ahn *et al*., 2010)	PF-S-C27	28.1	16	450 (352)	500 × 129 × 6	539.5
	PF-S-C30	**32.7**				**590.7**
	PF-S-C40	41.5				620.5
	PF-S-C50	52.6				692.2
Perfobond rib connector (Vianna *et al*., 2009)	P_2F_200-28	26.7	10	(500)	180 × 150 × 12.5	447.1
	P_4F_200-28	**26.9**				**433.8**
T-perfobond rib connector (Vianna *et al*., 2008)	TP_2F_200-28	28.3	10	(500)	137 × 150 × 18.3 (Bearing plate)	682.8
	TP_4F_200-28	**28.3**				**691.2**
	TP_2F_200-44	43.9				792.2
	TP_4F_200-44	**43.9**				**770.3**

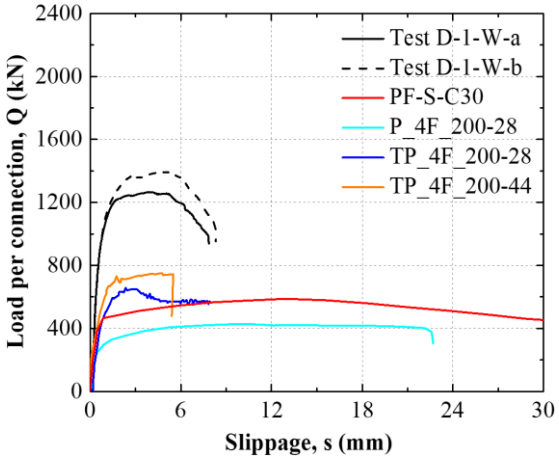

Fig. 5.11 Comparison with perfobond rib shear connections

5.7 Design approach

Considering the design rules for headed stud, bolted shear connectors and block shear connectors, it is desirable to adopt these design rules for the bolted shear connections and modified T-perfobond rib shear connections after calibration against the test results, as the load transfer mechanism and the failure modes of these connections are broadly similar. Accordingly, the shear connections should be checked against the following failure modes:

- Concrete failure; and
- Shear fracture of bolts.

Hence, the design shear resistance of the proposed shear connections, Q_{Rd}, can be determined by:

$$Q_{Rd} = Q_{c1} + \min \{Q_{c2} , Q_{sfb}\} \quad (5.4)$$

where Q_{c1} is the concrete bearing resistance against the steel block;

Q_{c2} is the concrete bearing resistance against the two bolts; and

Q_{sfb} is the shear resistance against shear fracture of bolts.

It should be noted that:

a) The design shear resistances against concrete failure of the proposed shear connection Q_{c1} and Q_{c2} are given by:

$$Q_{c1} = \alpha_1 f_{ck} A_{c1} \quad (5.5a)$$

where

f_{ck} is the characteristic concrete cylinder strength in compression;

α_1 $= \sqrt{A_{cp1}/A_{c1}}$

A_{c1} is the bearing area of concrete in the vicinity of the steel block;

$= l_s\, h_s$; and

A_{cp1} is the projected bearing area of the concrete in the direction of loading, which is amplified by an inclination rate of 1:5 from the basic bearing area.

$= (l_s + 2e_1/5)\,(h_s + e_1/5)$.

e_1 is the distance between the steel block and the concrete block, as shown in Fig. 5.12.

$$Q_{c2} = 2\,\alpha_2 f_{ck} A_{c2} \qquad (5.5b)$$

where

α_2 $= \sqrt{A_{cp2}/A_{c2}}$

A_{c2} is the bearing area of concrete in the vicinity of a bolt;

$= l_{sb}\, h_{sb}$; and

A_{cp2} is the projected bearing area of the concrete in the direction of loading, which is amplified by an inclination rate of 1:5 from the basic bearing area;

$= (l_{sb} + 2e_2/5)\,(h_{sb} + e_2/5)$

e_2 is the distance between the steel bolt and the concrete block, as shown in Fig. 5.12.

The schematic diagram of the bearing areas of both the steel block and the pair of bolts is shown in Fig. 5.12. Eqs. (5.5a) and (5.5b) were adopted to predict the bearing resistances of the steel block and the pair of bolts through the use of α_1 and α_2 which are empirical factors to allow for the presence of multi-axial stresses in the concrete in front of the shear connectors as recommended in Vianna *et al*. (2009) and Hicks (2017). It should be noted that in calculating both the basic and the projected bearing areas, the bolt shank is simplified as a rectangular section while an effective bolt diameter is used. Any overlapping of these projected areas should be subtracted. When calculating the design shear resistance of connections with Type D connectors, the bearing area is taken as the sum of the web thickness and six times the flange thickness of the T-perfobond rib.

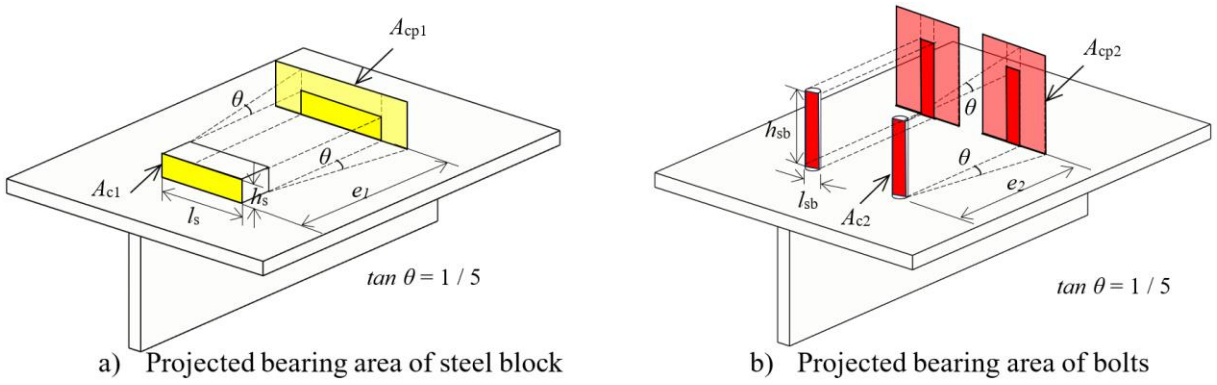

Fig. 5.12 Schematic diagram of the design method

b) According to Cl. 3.6.1 of EN 1993:1-8 (EC3, 2005), the shear resistance Q_{sfb} is given by:

$$Q_{sfb} = 0.7 \times 2A_b f_{ub} \quad (5.5c)$$

where

A_b is the effective cross-sectional area of a bolt or a steel reinforcement; and

f_{ub} is the tensile strength of the bolt or the steel reinforcement.

A calibration of the proposed design method against measured test data of the proposed shear connection was conducted. In order to improve predictability, the effective bolt diameters should be used to calculate both the bearing areas, A_{c2} , and the projected bearing areas A_{cp2} of the bolts. The comparison between the measured and the design shear resistances of these proposed shear connections reported in the present study is shown in Table 5.7a).

In order to assess the structural adequacy and efficiency of this design rule, a model factor η is established, which is defined as follows:

$$\eta = Q_{Rt} / Q_{Rd}$$

The values of η for these shear connections are also presented in Table 5.7a), and it is shown that:

a) For tests with Type A connectors, the values of η range from 1.04 to 1.18, indicating a high effectiveness of the design rule for this type of shear connection.

b) For tests with Type B connectors, the values of η range from 1.06 to 1.15, indicating some a

high effectiveness of the design rule for this type of shear connection.

c) For tests with Type C connectors, the values of η are found to be 1.01 and 1.03, and hence, the existing formula is applicable to this type of shear connection.

d) For tests with Type D connectors, the values of η are found to be 1.02 and 1.06, and hence, the existing formula is applicable to this type of shear connection.

Standard push-out tests on similar high strength stud connections were conducted and reported by Liu *et al*. (2023) and Wang *et al*. (2019), and hence, a total of eight sets of test data were adopted to demonstrate accuracy of the proposed design method. Refer to the literature for details of the connection configurations of these stud connections. The comparison between the measured and the design shear resistances of these shear connections is shown in Table 5.7b). The model ratios of the proposed design method are found to range from 1.00 to 1.21. Hence, the proposed design method is demonstrated to be able to predict the shear resistances of these shear connections in a conservative manner.

Table 5.7 Calibration of the proposed design method

a) Standard push-out tests reported in the present study

Test	Q_{Rt} (kN)	Concrete failure							Shear fracture of bolts				**Q_{Rd} (kN)**	η
		$f_{cu,150}$ (N/mm^2)	f_{ck} (N/mm^2)	A_{c1} (mm^2)	A_{cp1} (mm^2)	Q_{c1} (kN)	A_{c2} (mm^2)	A_{cp2} (mm^2)	Q_{c2} (kN)	A_b (mm^2)	f_{ub} (N/mm^2)	Q_{sfb} (kN)		
A-1-W-a	1,594.0	108.8	**87.0**	6,000	10,672	**696**	3,047	7,634	840	707	828	**819**	**1,515**	**1.05**
A-1-W-b	1,563.8	107.3	**85.8**	6,000	10,672	**687**	3,047	7,634	828	707	828	**819**	**1,506**	**1.04**
A-1-N-a	1,295.0	104.5	**83.6**	6,000	7,632	**566**	3,314	5,034	**683**	707	828	819	**1,249**	**1.04**
A-1-N-b	1,329.8	101.8	**81.4**	6,000	7,632	**551**	3,314	5,034	**665**	707	828	819	**1,216**	**1.09**
A-2-W-a	1,999.8	107.7	**86.2**	10,000	15,312	**1,066**	2,512	6,460	**694**	707	770	762	**1,760**	**1.14**
A-2-W-b	1,989.8	104.9	**83.9**	10,000	15,312	**1,038**	2,512	6,460	**676**	707	770	762	**1,714**	**1.16**
A-2-N-a	1,829.5	109.1	**87.3**	10,000	11,872	**951**	2,779	4,260	**601**	707	770	762	**1,552**	**1.18**
A-2-N-b	1,562.8	101.3	**81.0**	10,000	11,872	**883**	2,779	4,260	**558**	707	770	762	**1,441**	**1.08**
A-3-W-a	1,507.0	99.2	**79.4**	6,000	10,672	**635**	3,047	7,634	**766**	707	828	819	**1,401**	**1.08**
A-3-W-b	1,393.8	89.9	**71.9**	6,000	10,672	**576**	3,047	7,634	**694**	707	828	819	**1,270**	**1.10**
B-1-W-a	1,439.5	105.8	**84.6**	6,000	10,672	**677**	2,417	6,916	692	452	929	**588**	**1,265**	**1.14**
B-1-W-b	1,282.5	97.7	**78.1**	6,000	10,672	**625**	2,417	6,916	639	452	929	**588**	**1,213**	**1.06**
B-1-N-a	1,259.3	110.8	**88.6**	6,000	7,632	**600**	2,629	4,316	597	452	929	**588**	**1,188**	**1.06**

B-1-N-b	1,187.0	103.5	**82.8**	6,000	7,632	**560**	2,629	4,316	**558**	452	929	588	**1,118**	**1.06**
B-3-W-a	1,254.0	88.8	**71.0**	6,000	10,672	**569**	2,417	6,916	**581**	452	929	588	**1,150**	**1.09**
B-3-W-b	1,373.5	94.7	**75.8**	6,000	10,672	**606**	2,417	6,916	620	452	929	**588**	**1,194**	**1.15**
C-0-W-a	708.8	98.4	**78.7**	-	-	**-**	4,240	10,296	**1,040**	552	912	**705**	**705**	**1.01**
C-0-W-b	725.8	93.6	**74.9**	-	-	**-**	4,240	10,296	**989**	552	912	**705**	**705**	**1.03**
D-0-W-a	1,266.8	106.9	**85.5**	10,080	15,776	**1,078**	-	-	**-**	201	593	**167**	**1,245**	**1.02**
D-0-W-b	1,394.0	113.9	**91.1**	10,080	15,776	**1,149**	-	-	**-**	201	593	**167**	**1,316**	**1.06**

b) Standard push-out tests reported in the literature

Test	Q_{Rt} (kN)	Concrete failure								Shear fracture of bolts			Q_{Rd} (kN)	η
		$f_{cu,150}$ (N/mm^2)	f_{ck} (N/mm^2)	A_{c1} (mm^2)	A_{cp1} (mm^2)	Q_{c1} (kN)	A_{c2} (mm^2)	A_{cp2} (mm^2)	Q_{c2} (kN)	A_b (mm^2)	f_{ub} (N/mm^2)	Q_{sfb} (kN)		
T1-U-550-I	1,754.5	76.1	**60.9**	10,000	29,502	**1,046**	1,349	14,040	1,060	284	498	**452**	**1,498**	**1.17**
T1-U-550-N	1,597.7	76.1	**60.9**	10,000	27,072	**1,002**	1,444	12,840	1,049	284	498	**452**	**1,454**	**1.10**
T1-C-550-I	1,387.7	50.9	**40.7**	10,000	30,000	**705**	1,330	14,280	710	284	498	**452**	**1,157**	**1.20**
T1-U-350-N	1,146.7	76.1	**60.9**	10,000	13,200	**699**	2,090	4,680	762	284	498	**452**	**1,151**	**1.00**
T1-U-750-I	1,565.1	76.1	**60.9**	10,000	25,200	**966**	1,520	11,880	1,035	284	498	**452**	**1,418**	**1.10**
T2-U-550-I	1,387.7	76.1	**60.9**	7,000	18,695	**696**	1,814	11,440	1,109	284	498	**452**	**1,148**	**1.21**
T3-U-550-I	1,821.2	76.1	**60.9**	13,000	26,765	**1,136**	1,244	8,800	806	284	498	**452**	**1,588**	**1.15**
PRM	918.1	53.5	**42.8**	8,400	31,200	**693**	-	-	-	314	465	**205**	**898**	**1.02**

Notes:

f_{ck} is the characteristic compressive strength of concrete cylinders $f_{ck} = f_{cm}$ for back analysis

f_{cm} is the average compressive strength of concrete cylinders $f_{cm} = 0.8 \times f_{cu,150}$

$f_{cu,150}$ is the minimum value of measured compressive strengths of 150 mm concrete cubes

Q_{Rd} is the design shear resistance of the shear connection;

Q_{Rt} is the measured shear resistance of the shear connection, Q_m; and

η is the model factor which is defined as the ratio Q_{Rt} / Q_{Rd} .

5.8 Applicability

Based on the test data of the present investigation and those of Liu *et al*. (2023) and Wang et al. (2019), applicability of the proposed design method for both bolted and stud shear connections is summarised as follows:

a) Steel bolts and studs

- Diameter of bolts = 19 to 30 mm
- Yield strength of steel = 350 to 630 N/mm^2
- Tensile strength of steel = 450 to 930 N/mm^2

b) Steel blocks

- Dimension L = 120 to 200 mm
- Dimension W = 60 to 80 mm
- Dimension T_b = 30 to 50 mm

c) Concrete blocks

- Compressive cube strength, $f_{cu,150}$ = 50 to 120 N/mm^2

d) Concrete slabs

- Compressive cube strength, $f_{cu,150}$ = 40 to 72 N/mm^2

5.9 Conclusions

In this chapter, a comprehensive data analysis is conducted on the test results of the proposed shear connections and their deformation characteristics are compared to investigate the effects of connection configuration, steel block thickness, concrete block size, bolt diameter, and strength of the concrete block on the structural behaviour of the shear connections. The load-slippage curves of these shear connections are compared with the results of the standard push-out tests on stud / bolted shear connectors, block shear connectors and perfobond rib shear connectors reported in the literature. Based on the data analysis, a design method for the shear resistances of the proposed shear connections was proposed and calibrated against the test data. Key findings are summarised as follows:

i) The provision of the welded steel blocks is shown to be efficient to increase both the shear resistances and the initial stiffness of the bolted shear connections. It is demonstrated that Type A connection with a 30 mm thick steel block and a large concrete block is highly effective. Moreover, the load-slippage curves of a pair of headed shear studs and bolted shear connections are fairly similar at large deformations though that of the bolted shear connection exhibits a smaller initial stiffness, when compared with that of the stud shear connection.

ii) Increasing the thickness of the steel plate in the proposed shear connection to 50 mm offers only minimal benefit to the overall connection behaviour. Although there is a substantial increase in the shear resistance of the connection, a reduction in its resistance at large deformation is also evident. The size of the concrete block is also shown to have a limited

effect on the structural behaviour of the shear connections. When the diameter of the pair of bolts is decreased from 30 to 24 mm, the bearing area of the bolts is decreased, and the shear resistance of the connection is also decreased. The slippage limit of the connection with a bolt diameter of 24 mm is smaller than that with a bolt diameter of 30 mm due to the premature fracture of the bolts. In connections with a bolt diameter of 30 mm, with an increase in the strength of the concrete block, the shear resistance is increased proportionally.

iii) The shear resistances of those connections in the single-sided push-out tests are comparable to those of the connections in the standard push-out tests, while the initial stiffnesses of the connections in the single-sided push-out tests are smaller due to tilting of the infilled concrete blocks. Moreover, slippage limits of the shear connections in the single-sided push-out tests are larger than those in the standard push-out tests. Hence, the single-sided push-out test is able to obtain the lower bound solutions of these shear connections.

iv) Compared with the test results of stud / bolted shear connectors, block shear connectors, and perfobond rib shear connectors, the proposed shear connections reported in the present study are demonstrated to have favourable shear resistances, initial stiffnesses, and ductility when similar connection configurations are adopted.

v) A semi-empirical design approach, supported by the test results, was shown to be effective in predicting the shear resistances of the proposed shear connections for practical applications. The shear resistances of these connections against specific failure modes are predicted with adequate accuracy.

CHAPTER 6

NUMERICAL SIMULATIONS OF STANDARD PUSH-OUT TESTS

6.1 Introduction

This chapter presents non-linear numerical simulations on the structural responses of four types of shear connections presented in Chapter 4. A total of ten numerical models were developed to examine and quantify the "stress and damage" distributions, and the deformation characteristics of these shear connections. In addition, the internal force distributions along the height of the shear connectors, and the distributions of the concrete bearing forces are analysed to establish understanding on the structural behaviour of these shear connections. The numerical simulations include the following parts:

i) Development of finite element models

   The Standard/Static module of an advanced finite element software, namely, ABAQUS, is used to simulate the structural responses of the shear connections under standard push-out tests. Detailed modelling techniques, including element types, mesh sizes, boundary conditions and element interactions as well as constitutive models for steel and concrete, are presented.

ii) Calibration against test results

   The numerical models are calibrated against the experimental results in terms of typical failure modes, load-slippage curves, and deformation characteristics.

iii) Analyses of the modelling results

   The internal force distributions along the height of the shear connectors together with the distributions of the concrete bearing forces acting onto the shear connectors are plotted and analysed to provide insights into the structural behaviour of the shear connections.

6.2 Static analysis of the shear connections

The structural behaviour of the shear connections is numerically investigated using the Standard/Static module of an advanced finite element software, namely, ABAQUS 2020 (ABAQUS User Manual, 2020). Compared to the Dynamic analysis module, the static analysis module is able to simulate the static behaviour of the shear connection in which time-dependent effects such as inertia and transient effects are negligible. However, the convergence problem of the static model should be carefully solved due to potential non-linearities and contact complexities. Both material and geometric non-linearities are incorporated into the numerical models through an iterative process that accounts for changes in the stiffness matrix at large deformations. The numerical analysis involves the following key steps:

i) Model discretisation: The structure is divided into finite elements, where displacement fields within each element are approximated using shape functions.

ii) Stress/ strain evaluation: At integration points within each element, stresses and strains are computed based on the material constitutive model and the current deformation state.

iii) Non-linear solver: The Newton-Raphson iterative method is employed to solve the non-linear equilibrium equations. The stiffness matrix is updated at each iteration to reflect material non-linearity and geometric non-linearity.

iv) Convergence criteria: Residual forces and displacements are monitored to ensure equilibrium is satisfied within a specified tolerance.

It should be noted that boundary conditions, contact interactions, material constitutive models, and mesh sizes have a great influence on the convergence and accuracy of the model, and hence, these parameters have been carefully calibrated during modelling phase to avoid numerical instabilities, and to ensure physically meaningful results.

6.3 Modelling procedures

To illustrate the modelling procedures for the shear connections, overall geometry of the models is firstly presented in this section, followed by choice of element types, boundary conditions and element interactions as well as constitutive models for steel and concrete. Moreover, a mesh convergence study is conducted to determine the appropriate mesh sizes for the concrete blocks and the shear connectors. Detailed modelling procedures are presented as follows:

6.3.1 Overall geometry

Due to double symmetry, only a quarter of the shear connection is modelled for simplicity and computational efficiency. The models of four typical test specimens of the shear connections are shown in Fig. 6.1. It should be noted that the recess at the end of the concrete slab was established for load transfer between the concrete slab and the reaction frame of the testing machine in tests.

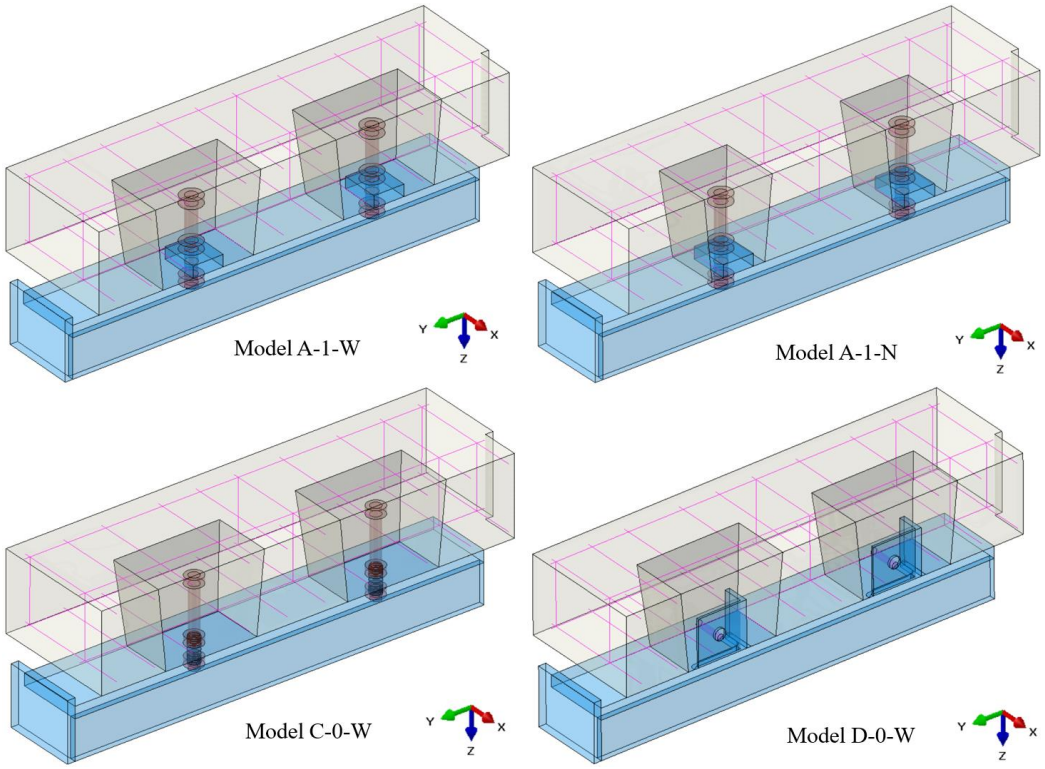

Fig. 6.1 Overall geometry of typical models

6.3.2 Element types

As shown in Fig. 6.2, the following element types are employed in the models:

a) Element C3D8R

Three-dimensional solid element C3D8R is employed to model concrete slabs, concrete blocks, steel bolts, steel blocks, and welded H-sections. It should be noted that the solid element with reduced-integration are employed to avoid shear and volumetric locking.

b) Element T3D2

Truss element T3D2 is employed to model the steel rebars in the concrete slabs as they are primarily designed to resist the tensile forces induced by the surrounding concrete.

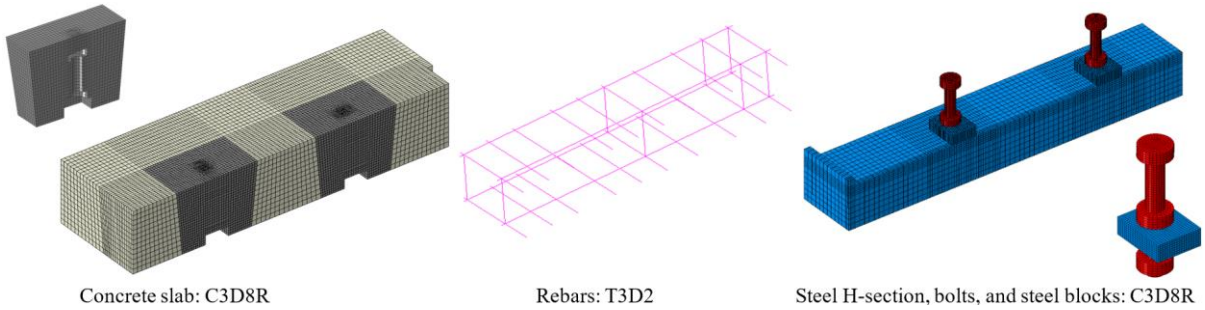

Fig. 6.2 Element types in three-dimensional finite element model

6.3.3 Boundary conditions and interactions

Boundary conditions of the numerical models are illustrated in Fig. 6.3. The specimen is symmetrical about Surfaces 1 and 2. Hence, on Surface 1, displacement along the Z-axis and rotations about both the X- and the Y- axes are constrained to zero. On Surface 2, displacement along the X- axis and rotations about both the Y- and the Z- axes are also constrained to zero. On Surface 3, all translational displacements are fully fixed. All nodal deformations of the upper surface of the top steel plate are coupled on a reference point (RP) to act as a displacement control.

The loading procedure in models with Connections RBN and R is divided into two steps: i) pre-tensioning forces are applied onto the bolt shanks, and ii) a vertical displacement is applied to the RP. However, in models with Connection MTP, a load step is defined, in which only a vertical

displacement is applied to the RP.

In order to establish proper contact conditions for non-linear analysis of the shear connection, it is essential to provide contact surfaces among various components in the model. Two distinct contact properties are established for different actions at a contact surface: i) a hard contact acting in a normal direction of the surface, and hence, separation between any two surfaces is permitted, and ii) a coulomb friction acting in a tangential direction of the surface. The friction coefficients between various components are assigned as follows:

- 0.6 between two concrete components (Wang *et al*., 2021);
- 0.3 between a concrete and a steel component (Xu *et al*., 2017); and
- 0.14 between two steel components (Pavlović *et al*., 2013).

In addition, tied contact pairs are established between the following components:

- the flanges and the web of the H-section;
- the steel blocks and the flanges of the H-section; and
- the T-perfobond ribs and the flanges of the H-section.

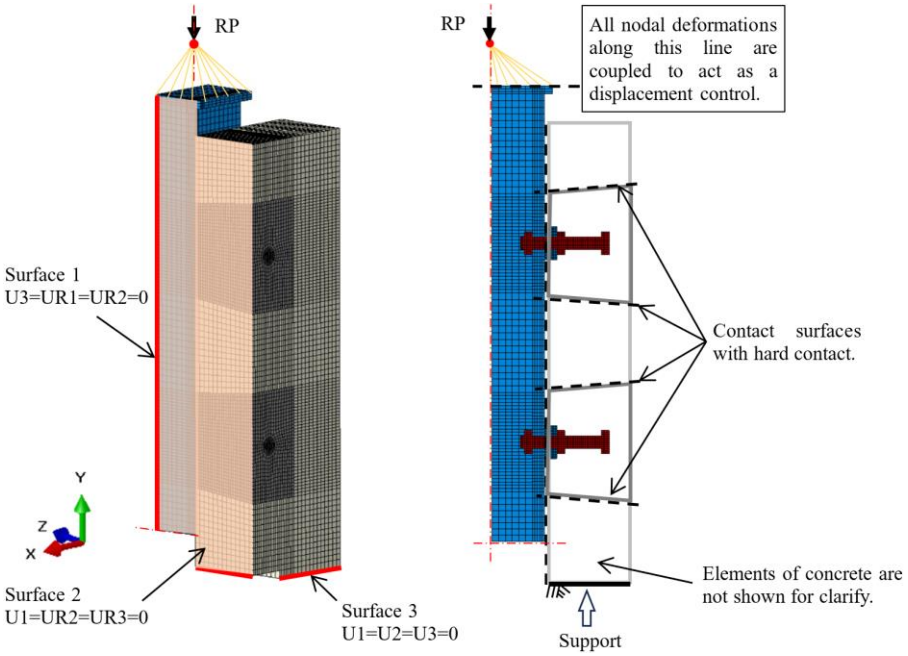

Fig. 6.3 Boundary conditions and interactions

6.3.4 Material models for steel

Three coupons were extracted from the shanks of M30 and M24 bolts as well as from the steel plates for standard tensile tests to attain their mechanical properties. The measured stress-strain curves of the bolts, as shown in Fig. 6.4a), are converted to true stress-strain curves, and then, they are input into the numerical models. Both the damage initiation and the damage evolution parameters are incorporated into the models to simulate the ductile fracture of the bolts. Moreover, bi-linear stress-strain curves are used to simulate the mechanical properties of the steel plates and the steel reinforcement. The elastic modulus of the steel is taken as 210 kN/mm^2, and the Poisson's ratio is taken as 0.3.

a) Undamaged stress-strain curves for bolt steel

Measured engineering stress-strain curves of the bolt steel are converted into true stress-strain curves using traditional integration method, as shown in Eq. (6.1).

$$\sigma_t = \sigma_e (1 + \varepsilon_e) \quad (6.1a)$$

$$\varepsilon_t = \ln (1 + \varepsilon_e) \quad (6.1b)$$

where

σ_t is true stress;
σ_e is engineering stress;
ε_t is true strain; and
ε_e is engineering strain.

b) Damage initiation and evolution criterions

After obtaining the undamaged behaviour of the bolt steel, the damaged behaviour is described by i) damage initiation criterion, which identifies the material state at the onset of ductile damage; and ii) damage evolution, which identifies stiffness degradations in the region of strain localization (ABAQUS User Manual, 2020) as follows:

i) Continuous damage mechanics (CDM) approach was proposed by Lemaitre (1985), and it was successfully applied by Pavlović *et al*. (2013) to simulate mechanical properties of the bolts. Damage initiation criterion is defined as an exponential relationship between equivalent plastic strain $\bar{\varepsilon}_0^{pl}$ and stress triaxiality θ, as shown in Fig. 6.4b) and Eq. (6.2).

$$\bar{\varepsilon}_0^{pl}(\theta) = \varepsilon_n^{pl} \exp[-1.5(\theta - 1/3)] \quad (6.2)$$

where

$\bar{\varepsilon}_0^{pl}$ is the equivalent plastic strain at the onset of damage;

ε_n^{pl} is the uniaxial plastic strain at the onset of necking; and

θ is the stress triaxiality, which is the ratio of hydrostatic stress σ_m to von Mises equivalent stress σ_{eq}, ranging from 0 to 2.0.

ii) Damage evolution is defined as a relationship between damage variable d_t and equivalent plastic displacement $\bar{u}^{pl}$, as shown in Eq. (6.3).

$$d_t = \frac{1 - e^{-\alpha(\bar{u}^{pl}/\bar{u}_f^{pl})}}{1 - e^{-\alpha}} \quad (6.3)$$

where

d_t is the damage variable of bolt steel;

$\bar{u}^{pl}$ is the equivalent plastic displacement after necking;

$\bar{u}_f^{pl}$ is the equivalent plastic displacement at fracture; and

α is the exponent, $\alpha = 0.7$ (Pavlović *et al*. 2013).

The damage parameters of the bolt steel are calibrated against the results of the standard tensile tests. The measured and the simulated engineering stress-strain curves of the bolt steel are plotted onto the same graph for direct comparison, as shown in Fig. 6.4a), and a good accuracy is obtained by using the constitutive models described above.

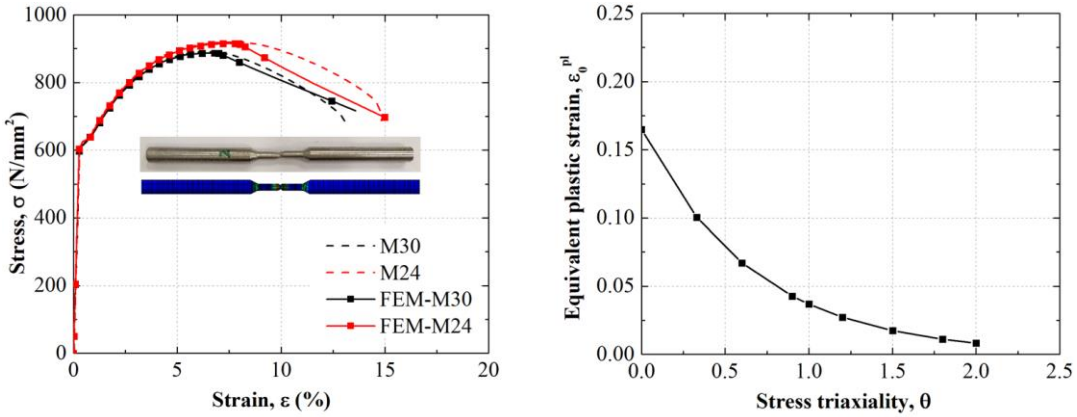

a) Engineering stress-strain curves b) Damage initiation

Fig. 6.4 Constitutive model for bolt steel

6.3.5 Material models for concrete

Based on the investigations into the monotonic and the cyclic behaviour of concrete conducted by Lubliner *et al*. (1988) and Lee *et al*. (1998), a concrete damage plasticity (CDP) model is adopted to simulate the primary failure mechanisms of concrete, namely: i) compressive crushing; and ii) tensile cracking. Hence, the evolution of the failure surface of the concrete in the CDP model is controlled by both the compressive and the tensile equivalent plastic strains, i.e. PEEQ and PEEQT, respectively. Typical plastic parameters in the CDP model are presented in Table 6.1. The Poisson's ratio of the concrete is taken as 0.2. The uniaxial stress-strain curves and various damage parameters of the concrete in compression and in tension are illustrated in Figs. 6.5 and 6.6 respectively. Detailed constitutive models of concrete are described as follows:

a) Undamaged behaviour of SFRC

A constitutive model of SFRC has been developed by Lu *et al*. (2017) and Zhang *et al*. (2017), and Jiao *et al*. (2004) based on Chinese code GB50010 (2010), and it is applied successfully by Wang *et al*. (2021). Owing to the presence of steel fibres, both the elastic modulus and the stress-strain curves of SFRC are modified as follows:

The elastic modulus of SFRC (Lu *et al*., 2017) is given by:

$$E_{cf} = \frac{10^5}{2.2 + (34.7 / f_{cu,f})}(1 - 0.0006\,\lambda_f) \tag{6.4}$$

where

$f_{cu,f}$ is the cube compressive strength of SFRC;

λ_f is a characteristic parameter for steel fibre content;

$= V_f\, l_f / d_f$; and it should be noted that λ_f is taken as 1.31 in the present study;

V_f is the volumetric percentage of steel fibre; and

l_f / d_f is the length-to-diameter ratio of steel fibre.

The stress-strain curve of SFRC in compression (Jiao *et al*. 2004; Wang *et al*., 2021) is given

by:

$$\sigma = \begin{cases} \dfrac{Ax - x^2}{1 + (A\text{-}2)\,x} f_{cf}, & 0 \le x \le 1 \\ \dfrac{Bx}{1 + (B\text{-}2)\,x + x^2} f_{cf}, & 1 < x \end{cases} \tag{6.5}$$

where

f_{cf} is the characteristic cylinder compressive strength of SFRC;

x is strain ratio;

$= \varepsilon / \varepsilon_{cf}$; when $x = 1$, the strain is equal to the peak compressive strain;

A & B are the parameters for the ascending and the descending segments of the curve respectively, which are based on back analysis on related test data (Jiao *et al*., 2004).

The corresponding stress-strain curve of SFRC in tension (Zhang *et al*., 2017) is given by:

$$\sigma = (1 - d_{tf})\, E_{cf}\, \varepsilon \tag{6.6a}$$

$$d_{tf} = \begin{cases} 1 - \rho_{tf}(1.2 - 0.2\, x^5), & x \le 1 \\ 1 - \dfrac{\rho_{tf}}{\alpha_{tf}\,(x - 1)^{1.7} + x}, & x > 1 \end{cases} \tag{6.6b}$$

$$\alpha_{tf} = 0.312\, f_{tf}^{\,2} / (1 + 36\, \lambda_f) \qquad \& \qquad \rho_{tf} = \frac{f_{tf}}{E_{cf}\, \varepsilon_{tf}} \tag{6.6c}$$

where

d_{tf} is the coefficient for the tensile damage evolution;

x $= \varepsilon / \varepsilon_{tf}$; when $x = 1$, the strain is equal to the peak tensile strain;

f_{tf} is the tensile strength of SFRC;

$= f_{cf} / (10.13 + 0.05\, f_{cf} - 0.5\, \lambda_f)$;

ε_{tf} is the peak tensile strain;

$= f_{tf}^{\,0.54} \times 65 \times (1 + 0.2\, \lambda_f) \times 10^{-6}$; and

α_{tf} is the shape parameter of the descending part of the tensile stress-strain curve of SFRC.

b) Damaged behaviour of SFRC

The concrete damage variable D is determined from the perspective of energy loss (Wang *et*

al., 2004), which is given by:

$$D = 1 - \frac{W_\varepsilon}{W_0} \tag{6.7a}$$

$$W_\varepsilon = \int \sigma \, d\varepsilon \tag{6.7b}$$

where

W_ε is the strain energy density of damaged material; and

W_0 is the strain energy density of undamaged material. For one-dimensional stress state of concrete subjected to uniaxial compression, $W_0 = 0.5 E_0 \varepsilon^2$.

c) Constitutive model of NC

According to the Hong Kong Code of Practice (COP, 2013), the elastic modulus of NC is given by:

$$E_c = 3.46 \sqrt{f_{cu,k}} + 3.21 \tag{6.8}$$

where

$f_{cu,k}$ is the cube compressive strength of NC.

The compressive stress-strain behaviour of NC is determined based on Eurocode 2 (EC2, 2004), which has been successfully applied by Shen *et al*. (2023) and Nguyen *et al*. (2009). It should be noted that the third part of the compressive stress-strain curve is a descending part, in which the stress decreases from the characteristic cylinder strength f_{ck} to rf_{ck}, where r is taken as 0.5. The ultimate strain ε_{cu} related to rf_{ck} is calibrated to 0.007 in the present study.

The tensile behaviour of NC is simulated as a relationship between the tensile stress and the crack displacement, which is given in Eurocode 2 (EC2, 2004) and fib Model Code (FIB, 2012).

Table 6.1 Plastic parameters in CDP models

Parameter	Dilation angle	Eccentricity	f_{bo}/f_{co}	K	Viscosity
Value	38°	0.1	1.16	0.667	0.5×10^{-3}

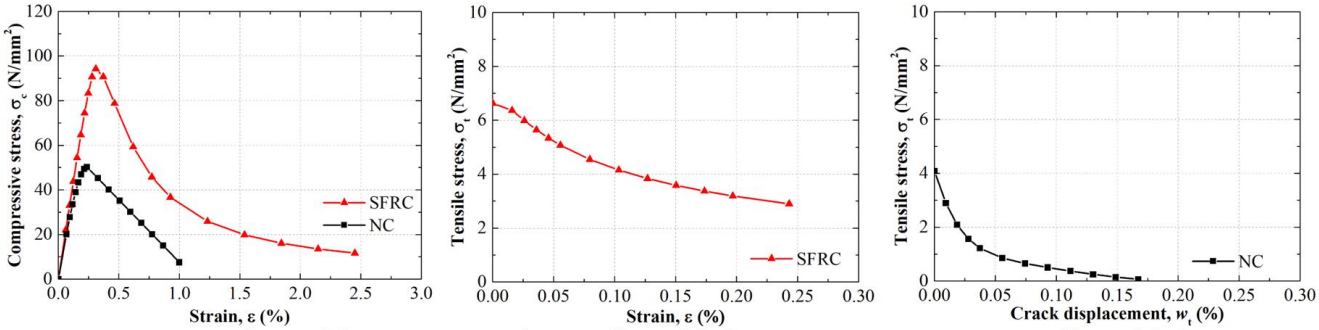

a) Compressive models b) Tensile model of SFRC c) Tensile model of NC

Fig. 6.5 Stress-strain curves for concrete

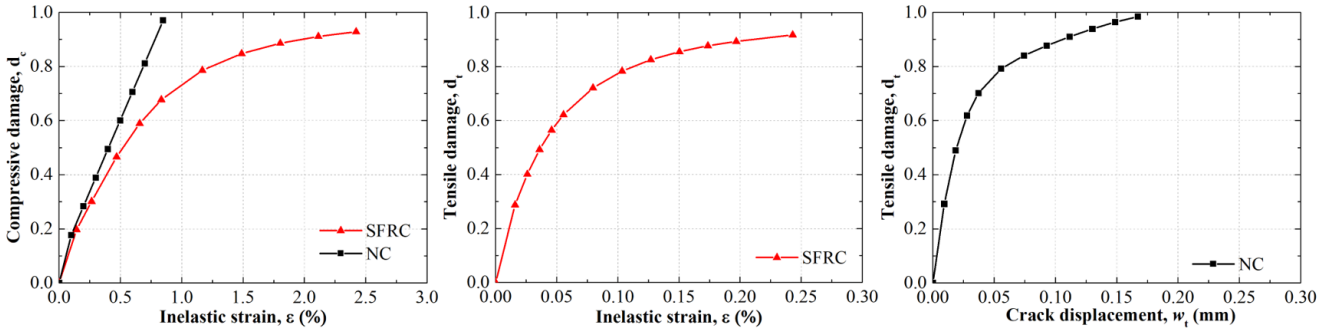

a) Compressive damage models b) Compressive damage model of SFRC c) Tensile damage model of NC

Fig. 6.6 Damage models for concrete

6.3.6 Mesh convergence

Based on the principle of finite element analysis, mesh size has a great influence on the accuracy and computational efficiency of the models. A finer discretisation improves numerical precision at an expense of exponentially increasing solving time. Hence, a convergence study is conducted on Model A-1-W to find out appropriate mesh sizes for the concrete blocks and the shear connectors. In general, the mesh sizes of the precast concrete slabs and the steel beams are taken as 16 mm.

As shown in Fig. 6.7, Meshes C1, C2, and C3, with mesh sizes of 12, 8, and 4 mm, are used in the concrete blocks. Meshes S1, S2, and S3, with mesh sizes of 8, 4, and 2 mm, are used in the steel shear connectors (e.g. bolt shanks, nuts, and steel blocks). The load-slippage curves of Model A-1-W with various mesh sizes are plotted in Fig. 6.8 for comparison. It is shown that the model with Meshes C2 and S2, i.e. with a mesh size of 8 mm in concrete blocks, and 4 mm in shear connectors, is able to predict the results with good numerical accuracy and computational efficiency.

Hence, these element sizes are adopted for subsequent numerical analyses.

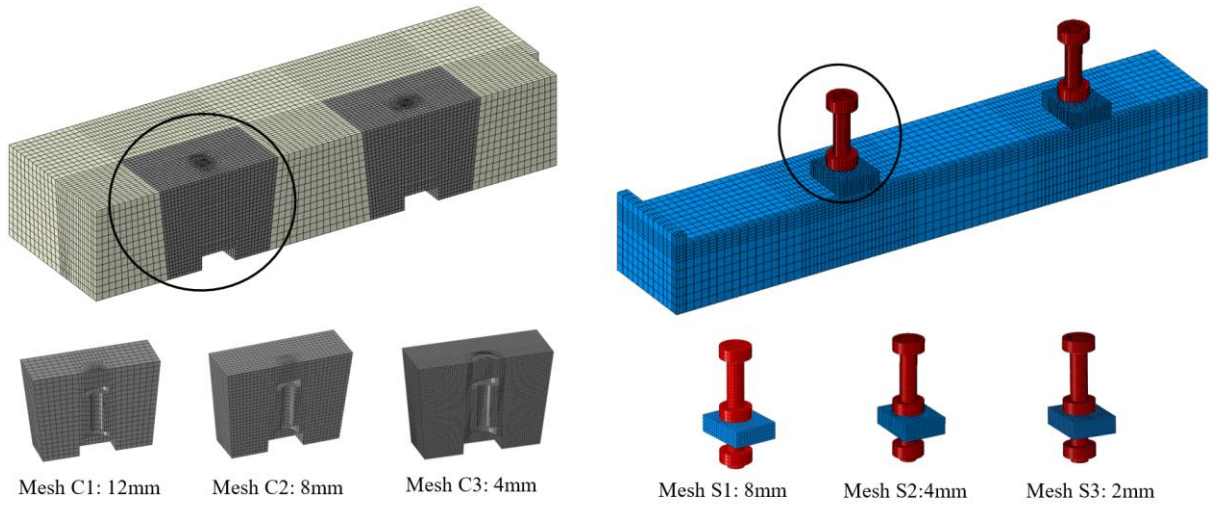

a) Mesh sizes of the infilled concrete blocks b) Mesh sizes of the bolts and the steel blocks

Fig.6.7 Mesh sizes for the concrete blocks and the shear connectors

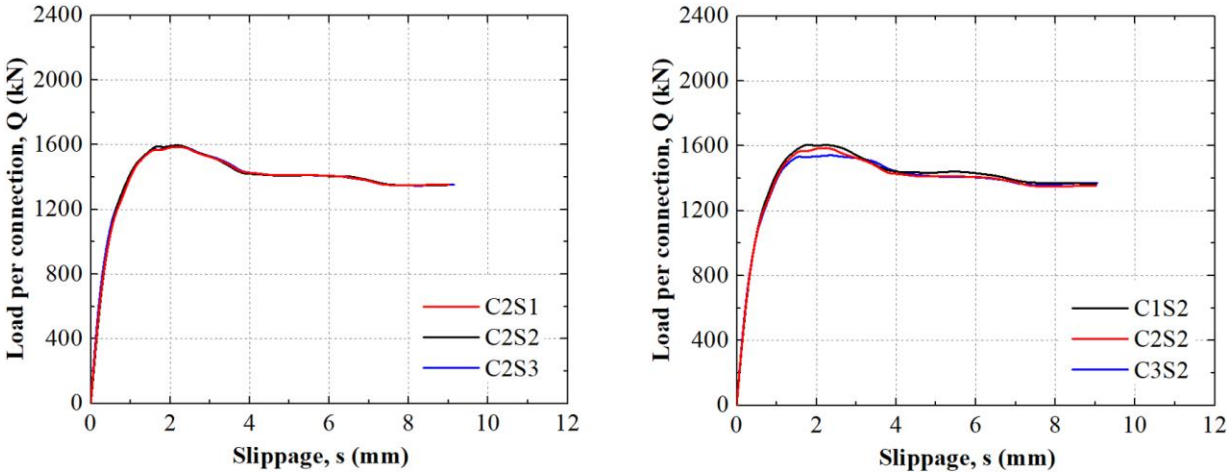

Fig. 6.8 Results of convergence study

6.4 Simulation results of Types A and B connections

Based on the above mentioned modelling techniques and mesh convergence study, a total of eight numerical models for Connection RBN were developed, and the failure patterns and the deformation characteristics of the models were calibrated against the test results. Both the simulated and the measured load-slippage curves are plotted onto the same graph for direct comparison. The internal force distributions along the height of the shear connector and the distributions of the concrete bearing force acting onto the shear connectors are extracted from the models for further understanding of the structural behaviour of the shear connections.

6.4.1 Finite element modelling of Types A and B connections

The numerical models with Types A and B connections are shown in Fig. 6.9. Since no geometric difference is found between Models A-1-W and A-3-W, as well as between Models B-1-W and B-3-W, both Models A-3-W and B-3-W are not shown in the figure. It should be noted that the nuts of the hexagonal bolts are simplified as cylindrical nuts, and the threads of both the bolt shanks and the nuts are not established as they have negligible effect on the structural behaviour of the connections.

The contact conditions of the models are illustrated in Fig. 6.3, and hard contacts are provided to:

- the surfaces between the precast concrete slab and the concrete blocks;
- the surfaces between the flange of the H-section and the concrete blocks, as well as the surfaces between the flange of the H-section and the precast concrete slab; and
- the surfaces between the concrete block and the shear connector.

It should be noted that the nuts were rigidly connected to the bolt shanks through a tied constraint for simplicity, given that a minor loss of pretension force appeared in connection RBN.

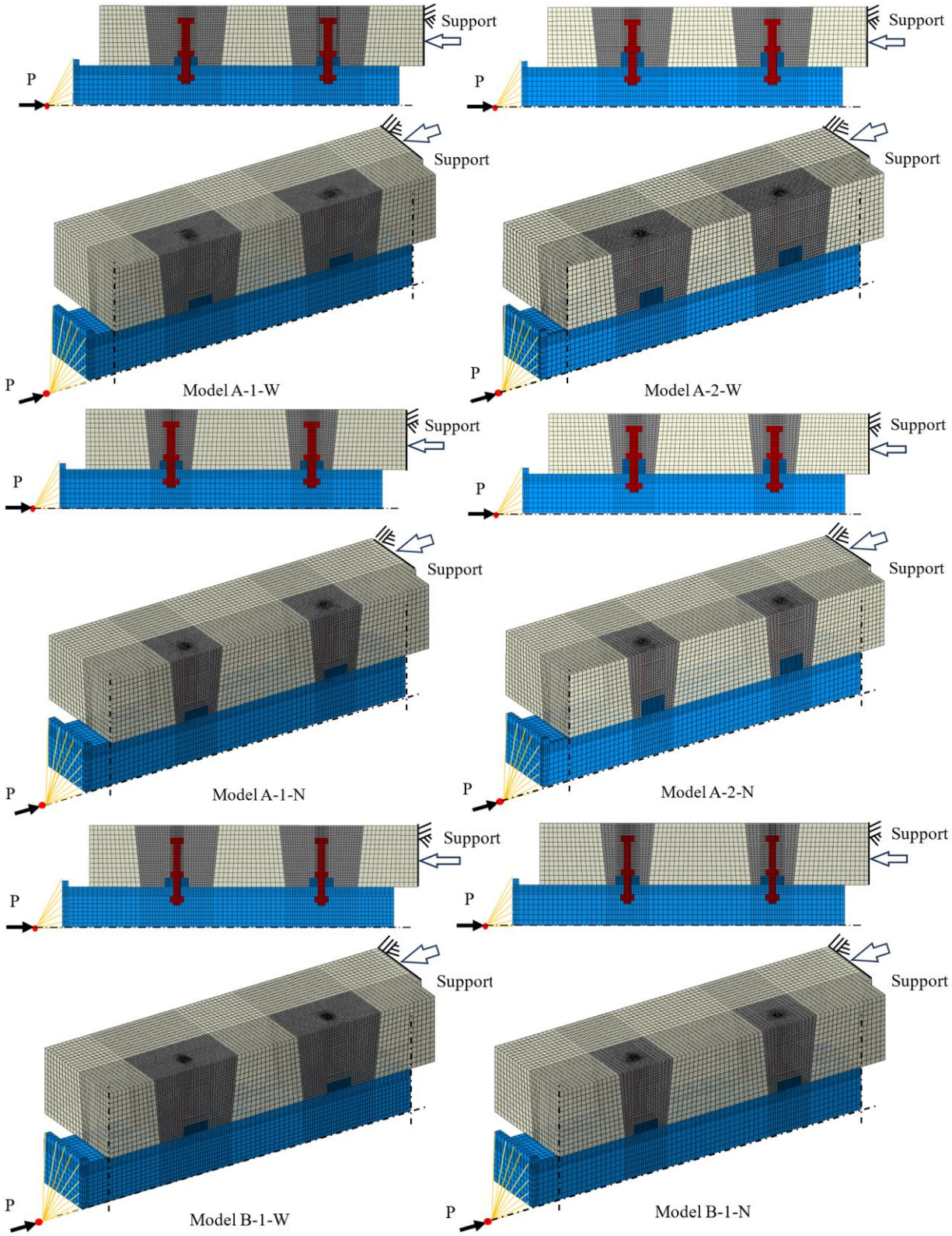

Fig. 6.9 Finite element models of typical models with Types A and B connections

6.4.2 Calibration against test results

The above mentioned modelling techniques are carefully calibrated against the test results in terms of "stress and damage" distributions, load-slippage curves, and deformation characteristics. A detailed comparison between the measured and the simulated results is described as follows:

a) "Stress and damage" distributions

A comparison of the measured and the simulated "stress and damage" distributions in Tests A-2-W and B-1-N at a slippage of 6 mm is illustrated in Figs. 6.10 and 6.11. It should be noted that when the values of the compressive and the tensile damage, i.e. DAMAGEC and DAMAGET, exceed 0.5, the concrete is considered to suffer from compressive and tensile failure. When the bolt stresses exceed the tensile strength, the bolt is considered to have failed. It is shown that:

- In Model A-2-W, severe concrete compressive damage of the precast concrete slab was found in the vicinity of the concrete blocks and at the bottom of the precast concrete slab, which was similar to the failure pattern in the test. Concrete tensile damage was found on the surfaces of the precast concrete slabs, which was comparable to the transverse and the longitudinal cracking pattern of the precast concrete slab. When the thickness of the steel block was 50 mm, the stresses of the bolt shanks were smaller than the tensile strength of the bolt steel, and hence, the bolts had not failed. This pattern was also in agreement with the experimental observation that no bolt fracture was found in those tests with Connector RBN and 50 mm thick steel blocks.
- In Model B-1-N, severe concrete compressive damage of the precast concrete slab was found in the vicinity of the concrete blocks. Concrete tensile damage was found on the surfaces of the precast concrete slabs, which was comparable to both the transverse and the longitudinal cracking patterns of the precast concrete slab. When the bolt diameter was 24 mm, the stresses of the bolt shanks were larger than the tensile strength of the bolt steel, and hence, the bolts had been fractured, as shown in Fig. 6.11.

It is obvious that the numerical models are able to predict the crushing and cracking patterns of the concrete slab, as well as the stress responses of the bolts. It should be noted that more

severe concrete cracking and crushing were found on the precast concrete slab in Model A-2-W when compared with the concrete failure pattern in Model B-1-N.

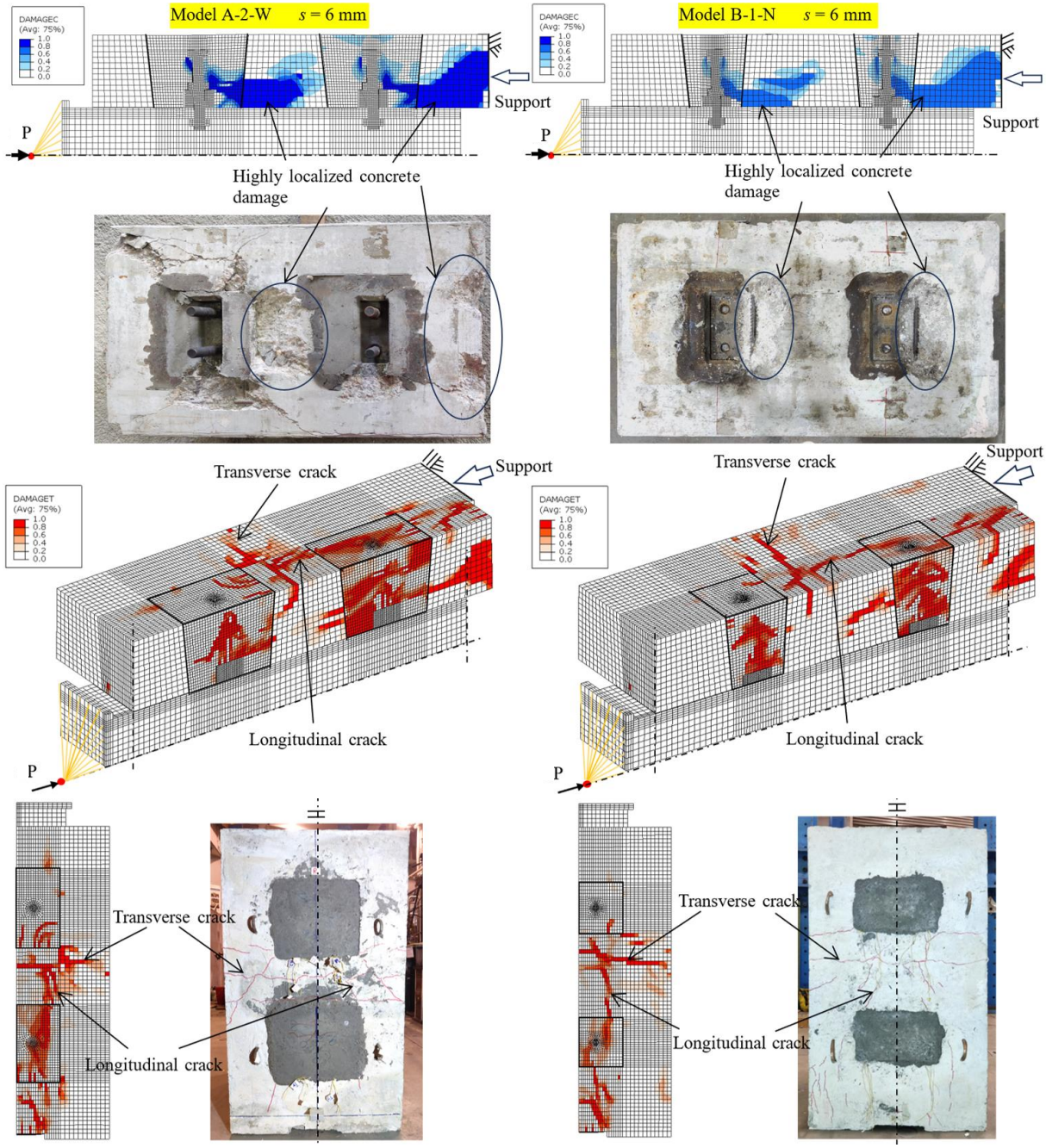

Fig. 6.10 Concrete failure of the concrete slabs in numerical models with Types A and B connections

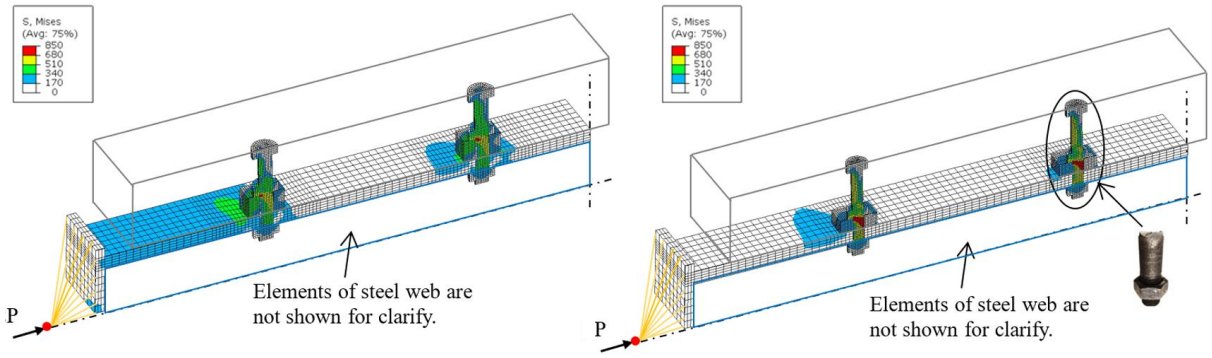

Model A-2-W Model B-1-N

Fig. 6.11 Failure of bolts in models with Types A and B connections

b) Structural behaviour

A comparison of the measured and the simulated load-slippage curves of Types A and B connections is shown in Fig. 6.12 and Table 6.2. It should be noted that the smaller shear resistance of the two nominally identical specimens and the corresponding deformation characteristics are used for comparison. It is shown that:

- The ratios of the measured to the simulated shear resistances range from 0.95 to 1.13, and hence, the models are considered to be able to predict the shear resistances of these connections with a good accuracy.
- The ratios of the measured to the simulated shear resistances at a slippage of 6 mm range from 0.94 to 1.08. It should be noted that the ratio of the measured to the simulated resistances at a slippage of 6 mm in Model B-1-N is 0.78, which is due to the sudden fracture of individual bolts at a slippage of 6 mm. Hence, the models are considered to be able to predict the shear resistances of these shear connections at a slippage of 6 mm with a good accuracy.
- The ratios of the measured to the simulated initial stiffnesses range from 0.70 to 1.29. As the slippages in the initial stages of the tests are in the order of 1.0 to 2.5 mm, any error in the measurements will lead to significant differences in the initial stiffnesses of the shear connections, and hence, the models are able to roughly predict the initial stiffnesses of these connections.

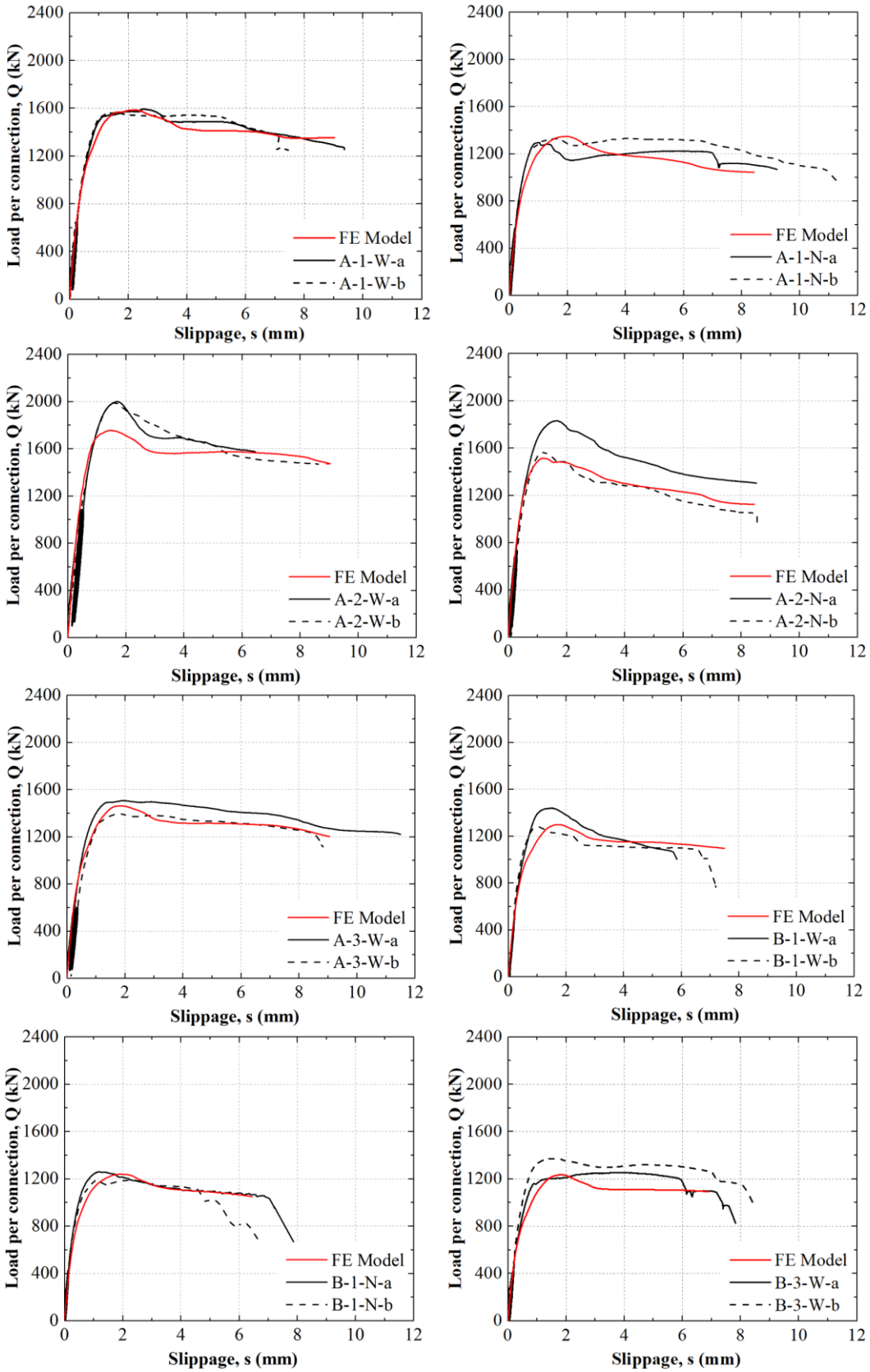

Fig. 6.12 Comparison of measured and simulated load-slippage curves of Types A and B connections

Table 6.2 Comparison between the measured and the simulated results

Test/ Model	Q_m (kN)	**Ratio**	s_m (mm)	**Ratio**	Resistances at 6 mm (kN)	**Ratio**	K (kN/mm)	**Ratio**
A-1-W-a	1,594.0		2.5		1,439.3		2,469	
A-1-W-b	1,563.8		1.5		1,449.0		2,526	
Simulation results	**1,586.1**	**0.98**	**2.2**	**0.68**	**1,406.8**	**1.03**	**2,512**	**1.01**
A-1-N-a	1,295.0		1.0		1,221.0		2,649	
A-1-N-b	1,329.8		1.6		1,316.5		2,576	
Simulation results	**1,346.7**	**0.96**	**2.0**	**0.50**	**1,127.8**	**1.08**	**2,333**	**1.13**
A-2-W-a	1,999.8		1.7		1,588.3		1,937	
A-2-W-b	1,989.8		1.6		1,529.8		2,314	
Simulation results	**1,754.9**	**1.13**	**1.5**	**1.07**	**1,572.8**	**0.97**	**2,953**	**0.78**
A-2-N-a	1,829.5		1.7		1,379.3		2,666	
A-2-N-b	1,562.8		1.2		1,149.5		2,386	
Simulation results	**1,512.5**	**1.03**	**1.2**	**1.00**	**1,228.0**	**0.94**	**2,906**	**0.82**
A-3-W-a	1,507.0		2.0		1,405.8		2,216	
A-3-W-b	1,393.8		1.9		1,313.0		1,686	
Simulation results	**1,461.0**	**0.95**	**1.8**	**1.06**	**1,307.9**	**1.00**	**2,416**	**0.70**
B-1-W-a	1,439.5		1.5		1,002.5		2,303	
B-1-W-b	1,282.5		1.0		1,097.8		2,728	
Simulation results	**1,297.0**	**0.99**	**1.7**	**0.59**	**1,130.1**	**0.97**	**2,317**	**1.18**
B-1-N-a	1,259.3		1.2		1,079.5		2,885	
B-1-N-b	1,187.0		1.1		828.5		2,856	
Simulation results	**1,237.6**	**0.96**	**1.8**	**0.61**	**1,059.3**	**0.78**	**2,207**	**1.29**
B-3-W-a	1,254.0		3.9		1,109.8		2,174	
B-3-W-b	1,373.5		1.4		1,300.5		2,667	
Simulation results	**1,297.0**	**0.97**	**1.7**	**2.29**	**1,130.1**	**0.98**	**2,317**	**0.94**
C-0-W-a	708.8		5.8		707.0		169	
C-0-W-b	725.8		5.7		722.8		147	
Simulation results	**665.5**	**1.07**	**6.0**	**0.97**	**664.9**	**1.06**	**387**	**0.44**
D-0-W-a	1,266.8		3.9		1,195.8		1,598	
D-0-W-b	1,394.0		5.2		1,335.8		1,544	
Simulation results	**1,214.3**	**1.04**	**3.5**	**1.11**	**1,042.9**	**1.15**	**2,213**	**0.72**

Note: Ratio denotes the ratios of the minimum value of the test data to the simulation results.

6.4.3 Distributions of internal forces and concrete bearing forces

In order to examine the distributions of internal forces within the shear connections, the nodal forces at various cross sections of the bolts and the steel blocks are extracted. The sum of the nodal forces at each cross section is determined as the internal forces, i.e. shear force F_{vi}, tension force

F_{ti}, and internal moment M_i . The differences of the nodal forces between planes i and i-1 are determined as the concrete bearing forces F_{bi} acting within this range. It should be noted that the internal forces within both the bolt and the steel block as well as within the bolt are plotted onto the same graph, as shown in Fig. 6.13, for comparison. Moreover, the concrete bearing forces are plotted in Fig. 6.14. Since only the strengths of the concrete blocks are different in Models A-1-W and A-3-W, as well as in Models B-1-W and B-3-W, the distributions of internal forces and concrete bearing forces in Models A-3-W and B-3-W are not presented for simplicity. It should be noted that:

a) After analysing the internal force distributions along the height of the shear connectors, it is shown that:

- In all the models with Types A and B shear connections, the maximum shear force appears at the root of the steel block, while the maximum shear force appears at the root of the embedded nut in the absence of the steel block. At the root of the steel block, the steel block takes up about 85% of the shear resistance.
- In all the models with Types A and B shear connections, the maximum moment of the shear connector also appears at the root of the steel block. The moment is decreased in a quadratic manner along the bolt height.
- In all the models with Types A and B connections, the tension force at the root of the steel block remains almost unchanged, which is almost the same as the pretension force. The tension force is decreased rapidly, and then increased with an increase in the bolt height. The ratios of the maximum tension force to the shear resistance in models with 30 mm thick steel blocks range from 0.21 to 0.23, and the maximum tension forces are located at 73 to 97 mm up from the top surface of the beam flange. The ratios of the maximum tension forces to the shear resistances in those models with 50 mm thick steel blocks are found to be 0.17 and 0.18, and the maximum tension forces are located at 105 to 113 mm up from the top surface of the beam flange.

b) The distributions of the concrete bearing force acting on the shear connectors are presented in Fig. 6.14. It is shown that in all the models with Types A and B shear connections, the

maximum concrete bearing force acts on the steel block, while the force is decreased significantly at the top of the steel block. The steel block takes up 60% to 69% of the applied shear force. Moreover, the ratios of the maximum concrete bearing forces in models with wide concrete blocks to those with narrow concrete blocks range from 1.11 to 1.17.

It is considered that the maximum shear forces and moments within Types A and B shear connections are located at the roots of the steel blocks. The magnitudes of the maximum tension forces are found to be about 20% of the shear resistances of the shear connections. The maximum tension forces in those models with 30 mm thick steel blocks are located at about 85 mm up from the top surface of the beam flange, while those in the models with 50 mm thick steel blocks are located at about 110 mm up from the top surface of the beam flange. The maximum concrete bearing forces act on the steel blocks, and they are influenced by the concrete block width and the bolt diameter.

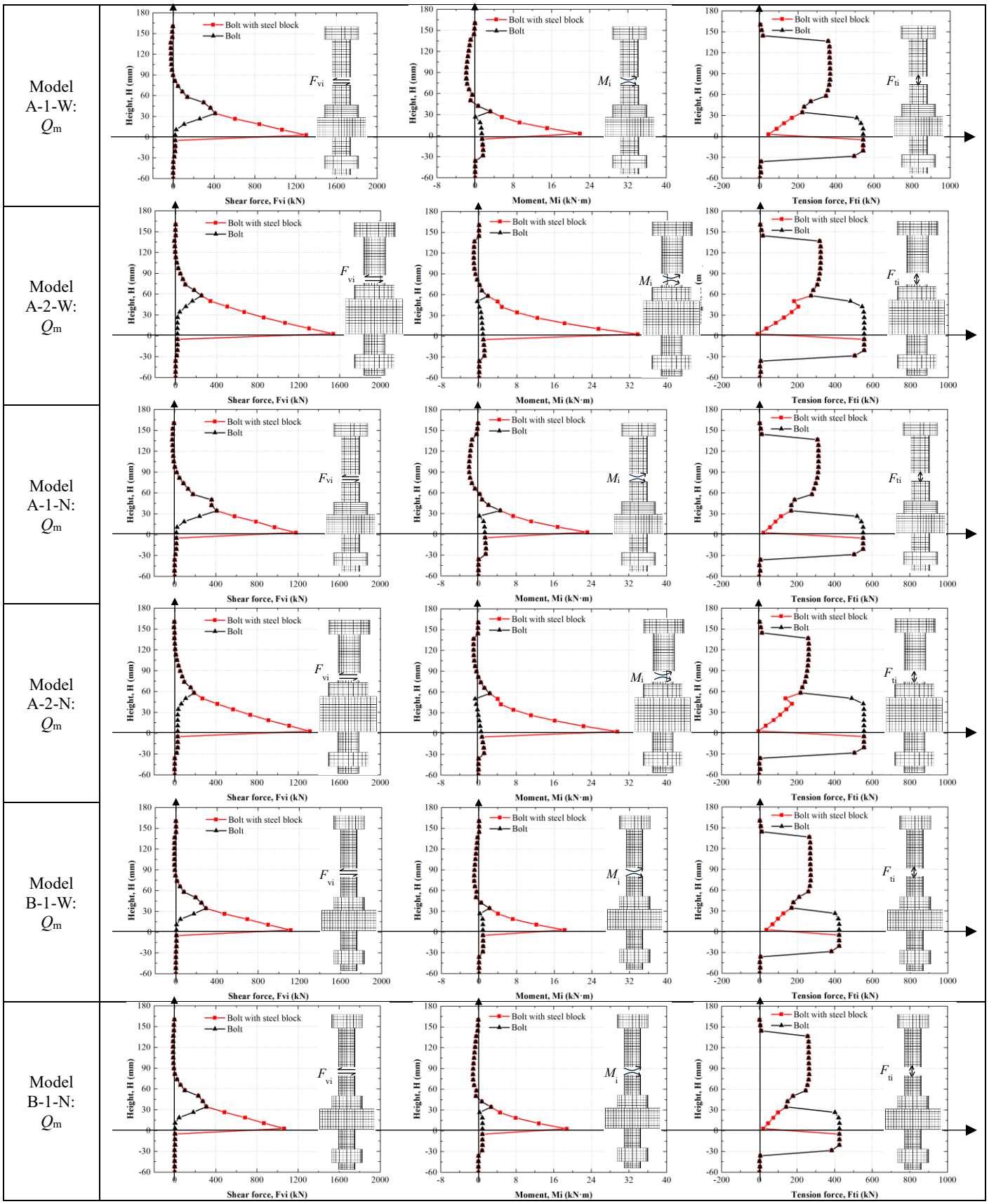

Fig. 6.13 Internal forces and moments within the bolts and steel blocks in models with Types A and B connections

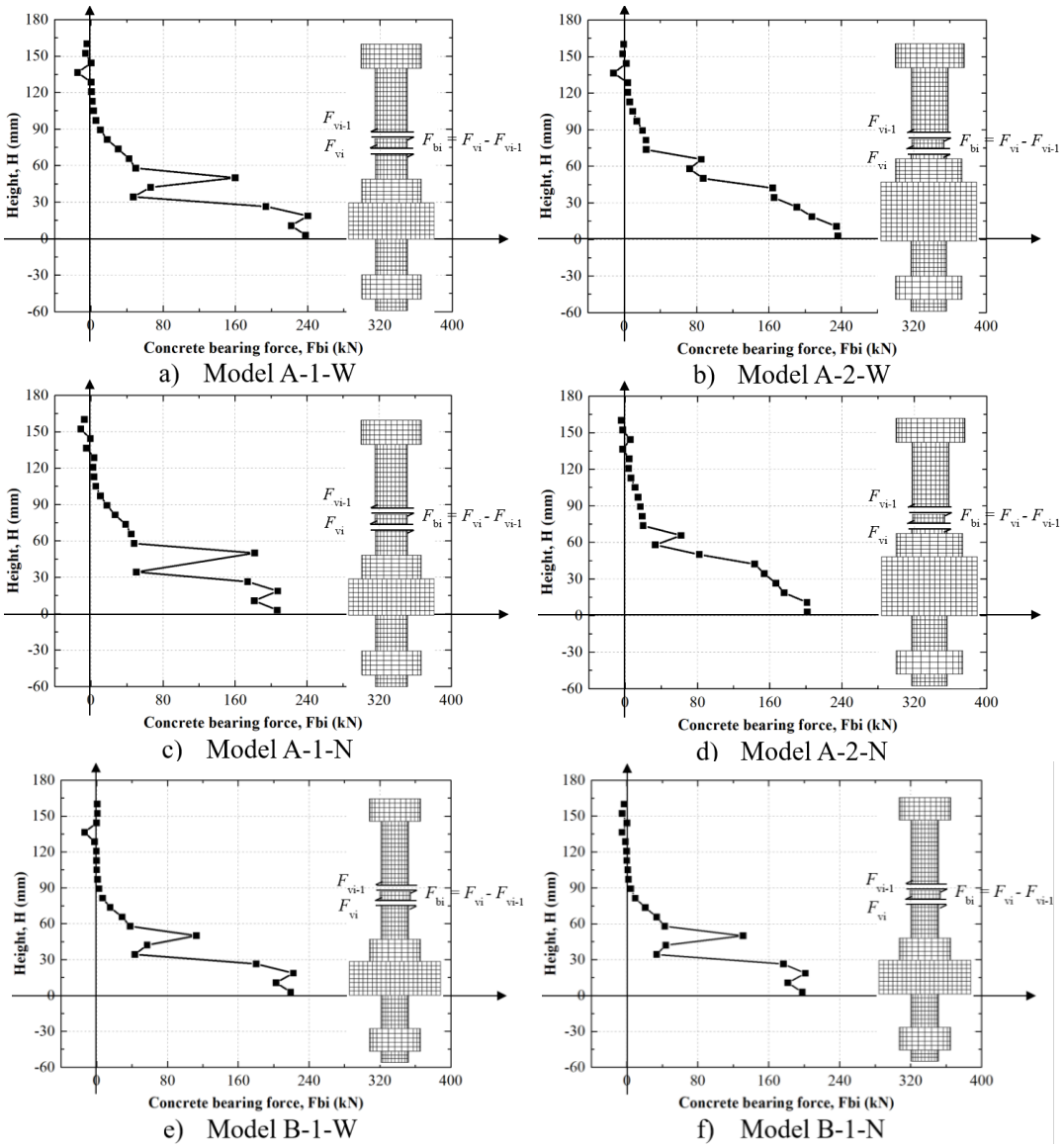

Fig. 6.14 Concrete bearing forces in models with Types A and B connections

6.5 Simulation results of Type C connection

Based on the above mentioned modelling techniques and mesh convergence study, a numerical model for Connection R was developed, and the failure patterns and the deformation characteristics of the model were calibrated against the test results. Both the simulated and the measured load-slippage curves are plotted onto the same graph for direct comparison. The internal force distributions along the height of the shear connector and the distributions of the concrete

bearing force acting onto the shear connectors are extracted from the models for further understanding of the structural behaviour of the shear connection.

6.5.1 Finite element modelling of Type C connection

The numerical model with Type C connection is shown in Fig. 6.15. It should be noted that the nuts of the hexagonal bolts were simplified as cylindrical nuts. The threads of the bolt shanks and the nuts were carefully modelled as they have a significant influence on the initial stiffness of Connection R.

The contact conditions of the models are established, and hard contacts are provided to:

- the surfaces between the precast concrete slab and the concrete blocks;
- the surfaces between the flange of the H-section and the concrete blocks, as well as the surfaces between the flange of the H-section and the precast concrete slab;
- the surfaces between the concrete block and the shear connector; and
- the surfaces between the bolt shank and the nuts.

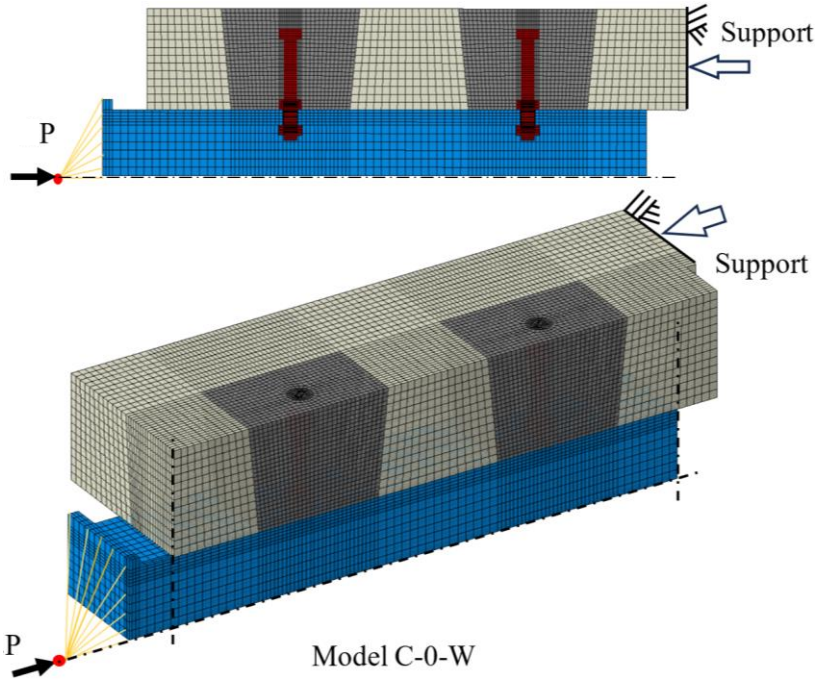

Fig. 6.15 Finite element model of Model C-0-W

6.5.2 Calibration against test results

The above mentioned modelling techniques are carefully calibrated against the test results in terms of "stress and damage" distributions, load-slippage curves, and deformation characteristics. A detailed comparison between the measured and the simulated results is described as follows:

a) "Stress and damage" distributions

A comparison of the measured and the simulated "stress and damage" distributions in Test C-0-W at a slippage of 6 mm is shown in Figs. 6.16 and 6.17. It should be noted that when the values of the compressive and the tensile damage, i.e. DAMAGEC and DAMAGET, exceed 0.5, the concrete is considered to have suffered from compressive and tensile failure. When the bolt stresses exceed the tensile strength, the bolt is considered to have failed. It is shown that no concrete tensile damage is found on the surfaces of the precast concrete slabs, which is similar to the failure pattern observed in the test. Small concrete compressive damage was found in the vicinity of the bolt nut, which was similar to local concrete crushing observed in the test. The stresses of the bolt shanks were larger than the tensile strength of the bolt steel, and hence, all the bolts in the test have fractured.

It is obvious that the numerical model is able to accurately predict the crushing and cracking patterns of the concrete, as well as the stress responses of the bolts.

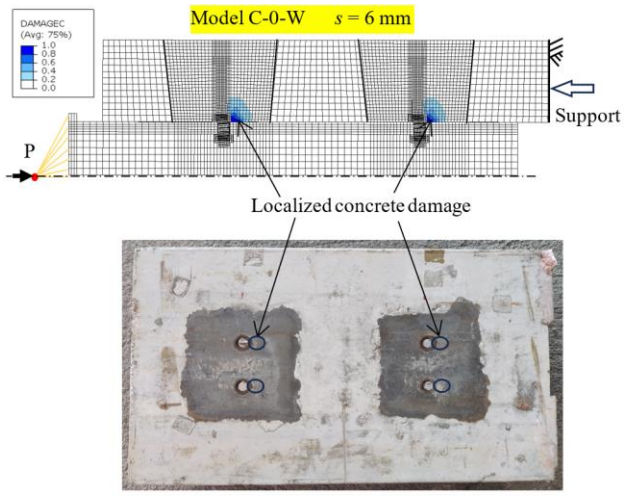

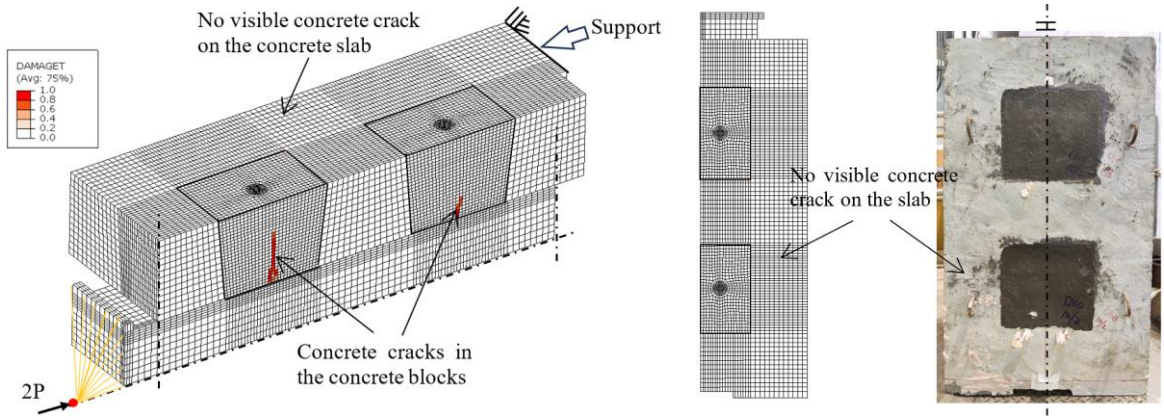

Fig. 6.16 Concrete failure of the concrete blocks in Model C-0-W

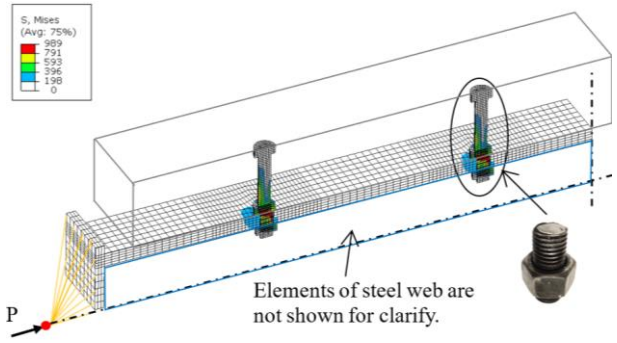

Fig. 6.17 Failure of bolts in Model C-0-W

b) Structural behaviour

A comparison of the measured and the simulated load-slippage curves of Type C connection is shown in Fig. 6.18 and Table 6.2. It should be noted that the smaller shear resistance of the two nominally identical specimens and the corresponding deformation characteristics are used for comparison. It is shown that:

- The ratio of the measured to the simulated shear resistances is found to be 1.07, and hence, the model is considered to be able to predict the shear resistance of Connection R with a good accuracy.
- The ratio of the measured to the simulated shear resistances at a slippage of 6 mm is found to be 1.06, and hence, the model is considered to be able to predict the shear resistance of Connection R at a slippage of 6 mm with a good accuracy.
- The ratio of the measured to the simulated initial stiffnesses is found to be 0.44, and the overestimation of the initial stiffness in the numerical model may be due to some dimensional errors in the bolts during installation.

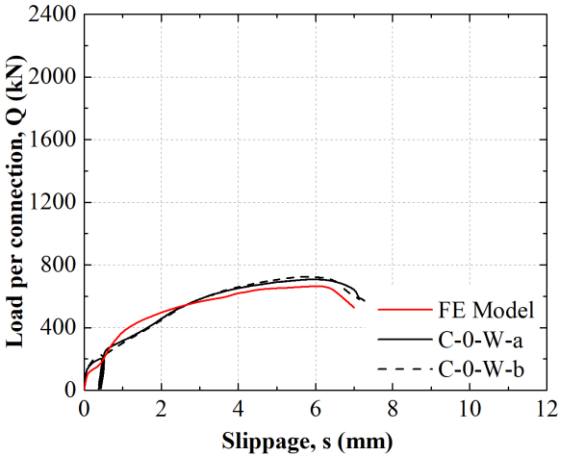

Fig. 6.18 Comparison of measured and simulated load-slippage curves of Model C-0-W

6.5.3 Distributions of internal forces and concrete bearing forces

In order to examine the distributions of internal forces within the shear connection, the nodal forces at various cross sections of the bolts are extracted. The sum of the nodal forces at each cross section is determined as the internal forces, i.e. shear force F_{vi} , tension force F_{ti} , and internal moment M_i . The differences of the nodal forces between planes i and i-1 are determined as the concrete bearing forces F_{bi} acting within this range. The internal forces in Model C-0-W are shown in Fig. 6.19, and the concrete bearing forces are shown in Fig. 6.20. It should be noted that:

a) After analysing the internal force distributions along the height of the shear connectors, it is shown that:

- The maximum shear force appears at the root of the embedded nut. The bolts take up about 98% of the shear resistance while the frictional force on the interface between the bolt nut and the beam flange contributes to the 2% of the shear resistance.
- The maximum moment of the shear connector appears in the proximity of the bottom nut.
- The tension force at the top of the bottom nut takes up only 38% of the pretension force. It is considered that the loss of the pretension force is due to deformation of the threads on the bolt shanks and the nuts. The maximum tension force is located at 60 mm up from the top surface of the beam flange.

b) The distributions of the concrete bearing force acting on the shear connectors are presented in

Fig. 6.20. It is shown that in Model C-0-W, the bearing force acting at the root of the embedded nut is 150 kN. The bearing force is increased to 212 kN and then decreased significantly along the bolt height.

It is considered that the maximum shear force within Type C connection is located at the root of the embedded nut. The maximum tension force is located at 60 mm up from the top surface of the beam flange, and the magnitude of maximum tension force is found to be about 25% of the shear resistance. The maximum concrete bearing force acts at the top of the embedded nut.

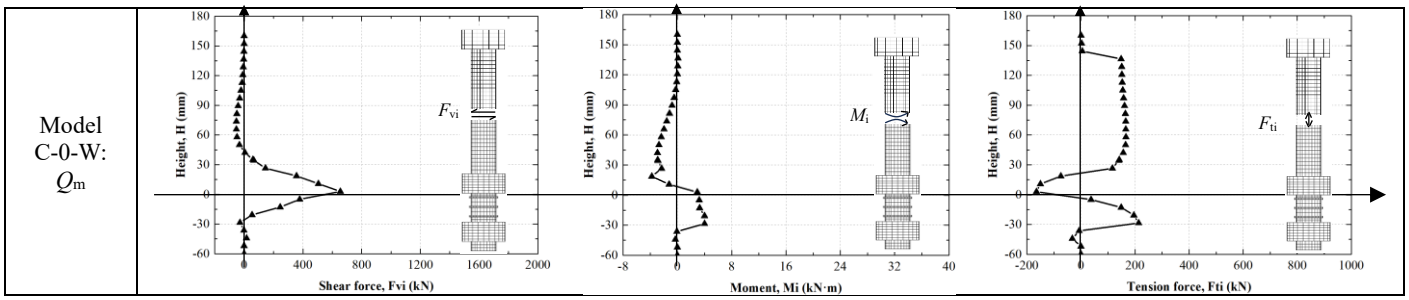

Fig. 6.19 Internal forces and moments within the bolts in Model C-0-W

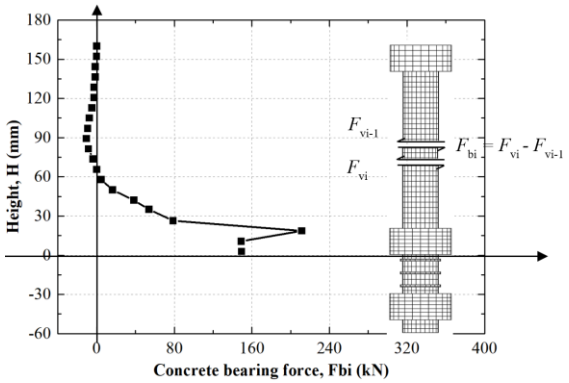

Fig. 6.20 Concrete bearing forces of Model C-0-W

6.6 Simulation results of Type D connection

Based on the above mentioned modelling techniques and mesh convergence study, a numerical model for Connection MTP was developed, and the failure patterns and the deformation characteristics of the model were calibrated against the test results. Both the simulated and the measured load-slippage curves are plotted onto the same graph for direct comparison. The internal force distributions along the height of the shear connector and the distributions of the concrete

bearing force acting onto the shear connectors are extracted from the models to establish understanding on the structural behaviour of the shear connections.

6.6.1 Finite element modelling of Type D connection

The numerical model of Type D connection is shown in Fig. 6.21. It should be noted that the weldment between the T-perfobond rib and the steel section is carefully modelled as it has a significant influence on the shear resistance. Element C3D8R is used to model the steel reinforcements in the perforation of the T-perfobond rib.

Due to the complex contact conditions in Model MTP, the overall mesh sizes of the precast concrete slab and the H section are set as 8 mm to ensure convergence and accuracy.

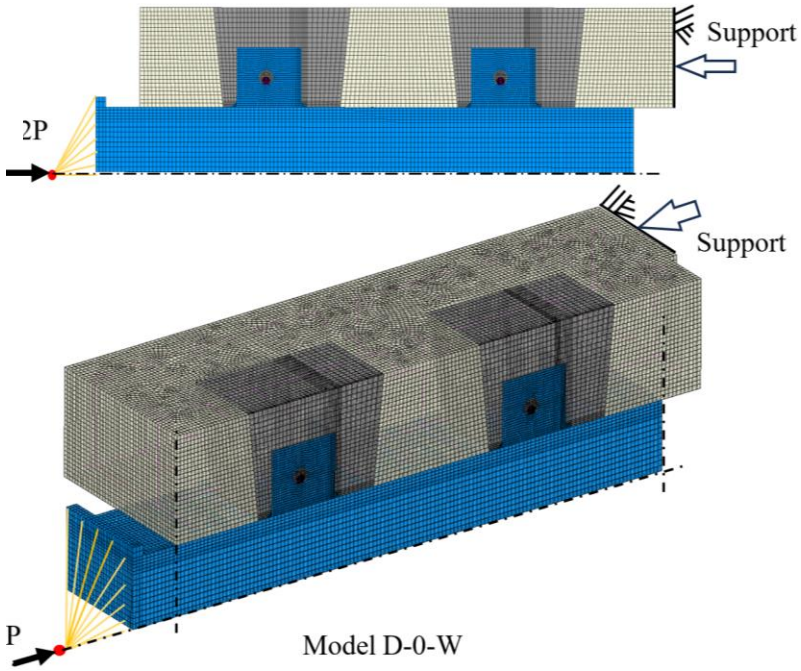

Fig. 6.21 Finite element model of Model D-0-W

6.6.2 Calibration against test results

The above mentioned modelling techniques are carefully calibrated against the test results in terms of “stress and damage” distributions, load-slippage curves, and deformation characteristics. A detailed comparison between the measured and the simulated results is described as follows:

a) “Stress and damage” distributions

A comparison of the measured and the simulated “stress and damage” distributions in Test D-0-W at a slippage of 6 mm is shown in Fig. 6.22. It should be noted that when the values of the compressive and tensile damage, i.e. DAMAGEC and DAMAGET, exceed 0.5, the concrete is considered to have suffered from compressive and tensile failure. It is also shown that concrete tensile damage was found on the surfaces of the precast concrete slab, which is in agreement with the diagonal cracking pattern of the precast concrete slab observed in the tests. Local concrete compressive damage was also found at the roots of the T-perfobond ribs, which was comparable to the concrete crushing pattern in the test.

It is obvious that the numerical model is able to accurately predict the concrete crushing and cracking patterns of the concrete slab.

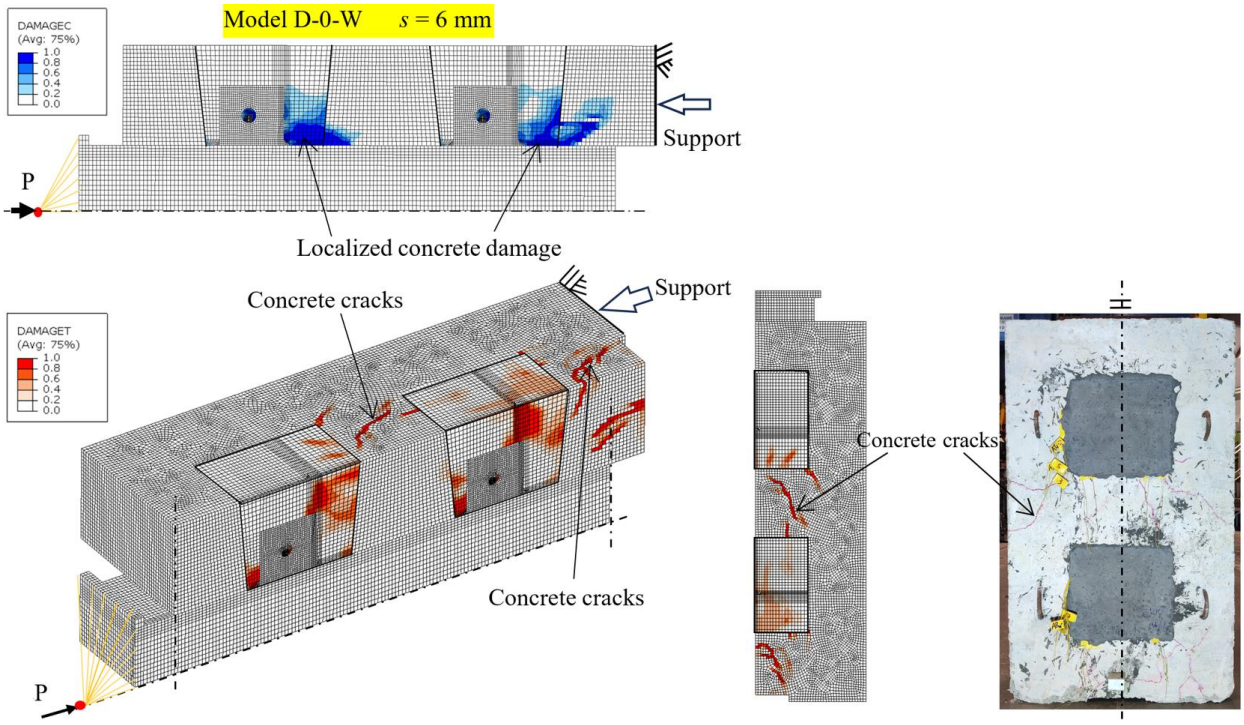

Fig. 6.22 Concrete failure of the concrete slabs in Model D-0-W

b) Structural behaviour

A comparison on the measured and the simulated load-slippage curves of Type D connection

is shown in Fig. 6.23 and Table 6.2. It should be noted that the smaller shear resistance of the two nominally identical specimens and the corresponding deformation characteristics are used for comparison. It is shown that:

- The ratio of the measured to the simulated shear resistances is found to be 1.04, and hence, the models are considered to be able to predict the shear resistances of Connection MTP with a good accuracy.
- The ratio of the measured to the simulated shear resistances at a slippage of 6 mm is found to be 1.15. Hence, the model is considered to be able to predict the shear resistance of Connection MTP at a slippage of 6 mm conservatively.
- The ratio of the measured to the simulated initial stiffnesses is found to be 0.72, and the overestimation of the initial stiffness in the numerical model may be due to the presence of initial defects in the concrete.

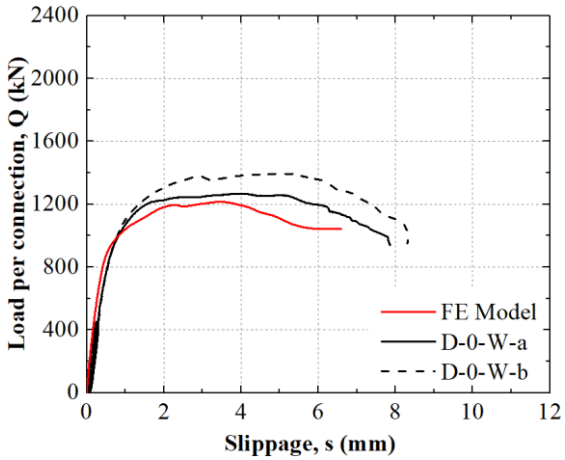

Fig. 6.23 Comparison of measured and simulated load-slippage curves of Model D-0-W

6.6.3 Distributions of internal forces and concrete bearing forces

In order to examine the distributions of internal forces within the shear connection, the nodal forces at various cross sections of the perfobond ribs are extracted. The sum of the nodal forces at each cross section is determined as the internal forces, i.e. shear force F_{vi}, tension force F_{ti}, and internal moment M_i . The differences of the nodal forces between planes i and i-1 are determined as the concrete bearing forces F_{bi} acting within this range. The internal forces in Model D-0-W are shown in Fig. 6.24, and the concrete bearing forces are shown in Fig. 6.25. It should be noted that:

a) After analysing the internal force distributions along the height of the shear connectors, it is shown that:

- The maximum shear force appears at the root of the weldment, and the shear force decreases rapidly along the cross-sectional height.
- The maximum moment of the shear connector appears at the root of the weldment, and the moment decreases rapidly at the perforated hole due to an abrupt change in cross-sectional shape.
- The tension force appears at 30 mm up from the top surface of the steel beam. It increases first and then decreases along the height of the connector due to a provision of the steel reinforcement.

b) The distributions of the concrete bearing force acting onto the shear connectors are presented in Fig. 6.25. It is shown that in Model D-0-W, the bearing force acting onto the weldment is 306 kN. The bearing force decreases rapidly to 56 kN at 15 mm up from the top surface of the beam flange.

It is considered that both the maximum shear force and the maximum moment within Type D connection are located at the root of the weldment. The maximum concrete bearing force acts onto the weldment, and it decreases rapidly due to an abrupt change in the cross-sectional shape.

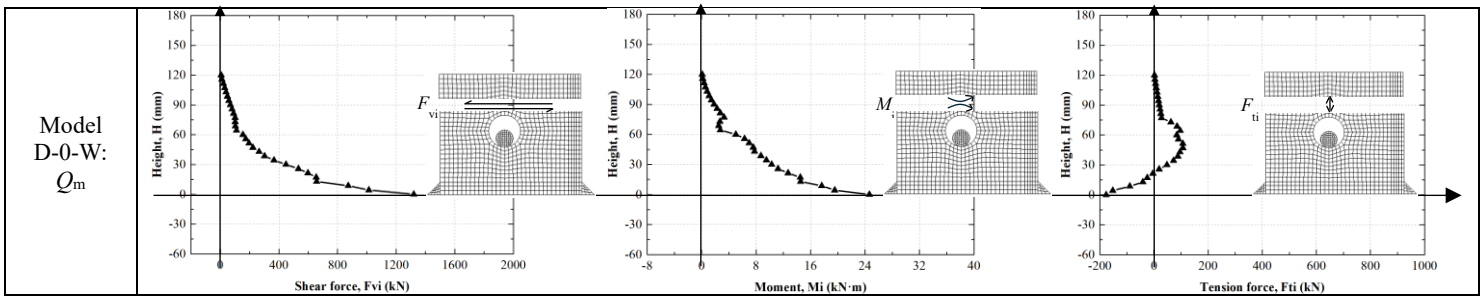

Fig. 6.24 Internal forces and moments within the steel section in Model D-0-W

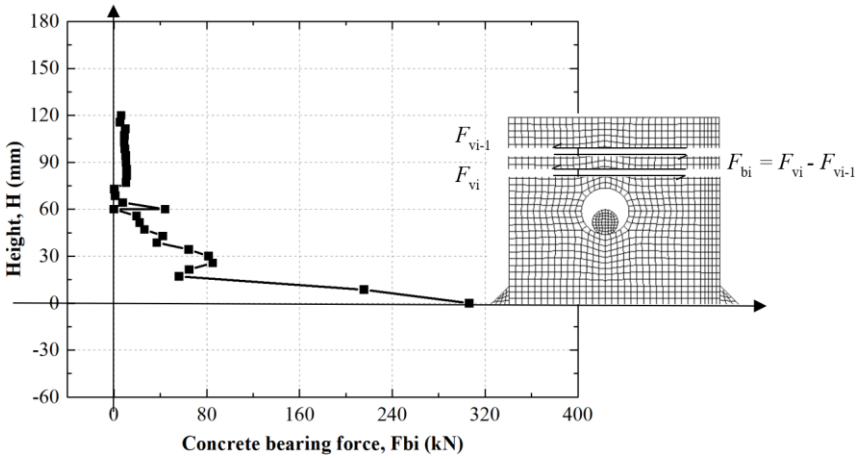

Fig. 6.25 Concrete bearing forces of Model D-0-W

6.7 Conclusions

In this chapter, advanced non-linear numerical simulations were conducted to investigate the structural behaviour of four types of shear connections. A total of ten numerical models were developed, and their "stress and damage" distributions, load-slippage curves, and deformation characteristics were carefully calibrated against test results. After validation of the modelling techniques, the distributions of the internal forces and the concrete bearing forces along the height of the shear connectors were extracted, and insights into the structural behaviour of the shear connections were obtained. Key findings are summarised as follows:

a) The proposed constitutive models for concrete are able to simulate the mechanical properties of both the SFRC and the NC. Owing to the provision of steel fibres, the elastic modulus, the peak strain, the compressive strength, and the tensile strength of SFRC are significantly improved. By incorporating the compressive and the tensile damage parameters into the material models, the concrete damage distribution is comparable to the concrete crushing and cracking pattern observed in the tests. By incorporating the damage initiation and evolution parameters into the constitutive model for bolt steel, the ductile fracture of the bolt is successfully simulated. It should be noted that the threads of both the bolt shanks and the nuts

were carefully modelled in Model C-0-W since they have a great influence on the initial stiffness of Connection R. A mesh size of 8 mm in the concrete blocks and a mesh size of 4 mm in the shear connectors are shown to be appropriate to simulate the structural behaviour of the shear connections.

b) The concrete compressive and tensile damage patterns in the concrete slabs predicted by the models are in close agreement with those concrete cracking and crushing patterns observed in the tests. Moreover, the simulated load-slippage curves are shown to correlate well with the test results in terms of shear resistance, initial stiffness and resistance corresponding to a slippage of 6 mm. Hence, the modelling techniques are considered to be able to simulate the structural behaviour of the shear connections accurately.

c) The internal force distributions along the height of the shear connectors and the concrete bearing forces acting onto the shear connectors are effective to understand the load transfer mechanisms within the shear connections. For models with Types A and B connections, both the maximum shear forces and the maximum moments are located at the roots of the steel blocks, and hence, typical failure mode in these connections is concrete crushing in the vicinity of the steel blocks. The magnitudes of the maximum tension forces are found to be about 20% of the shear resistance. The locations of the maximum tension forces in those models with 30 mm thick steel blocks are about 25 mm lower than those in the models with 50 mm thick steel blocks, and hence, the bolts in those models with 50 mm thick steel blocks do not suffer from fracture failure. The maximum concrete bearing forces act onto the steel blocks, and they are influenced by both the widths of the concrete blocks and the bolt diameters. In general, the steel block takes up 60% to 69% of the applied shear forces. Hence, the applied forces are primarily resisted by the steel blocks through bearing while a small portion of the applied force is resisted by the two bolts through bearing. In addition, the two

bolts play an important role in resisting pull-out forces which are induced during slippage of the shear connection.

d) For those models with Type C connection, the maximum shear force is located at the roots of the embedded nuts. The maximum tension force is located at 60 mm up from the top surface of the beam flange, and the magnitude of the maximum shear force is found to be about 25% of the shear resistance. The maximum concrete bearing force acts onto the top of the embedded nuts.

e) For those models with Type D connection, the maximum shear force and the maximum moment are located at the roots of the weldment. The maximum concrete bearing force acts onto the weldment, and it decreases rapidly along the cross-sectional height due to an abrupt change in the cross-sectional shape.

CHAPTER 7

PARAMETRIC STUDY AND DESIGN RULES

7.1 Introduction

This chapter presents a comprehensive parametric study on the structural behaviour of shear connections with Connectors RBN and R employing the validated modelling techniques presented in Chapter 6. The effects of various parameters on the load-slippage curves, the deformation characteristics, the "stress and damage" distributions, as well as the internal force distributions of the shear connectors are analysed. For those shear connections with Connector RBN, key parameters include bolt diameter, steel block thickness, concrete block width, concrete block strength, concrete slab strength, fibre content in concrete block and longitudinal spacing of shear connections.

It should be noted that Test A-1-W presented in Chapter 4 is modelled as a reference model for the parametric study, in which the bolt diameter and the steel block thickness are both 30 mm, the width of the concrete block is 240 mm, and the strengths of the concrete block and the precast concrete slab are 100 and 50 N/mm^2, respectively. For shear connections with Connector R, key parameters include bolt diameter, bolt strength, concrete block strength and concrete slab strength. It should be noted that Test C-0-W presented in Chapter 4 is modelled as a reference model for the parametric study, in which the bolt diameter is 30 mm, the width of the concrete block is 240 mm, and the strengths of the concrete block and the precast concrete slab are 100 and 50 N/mm^2, respectively.

Based on data analysis of the parametric results, the contributions of each component in the

connection are identified, and hence, the load transfer mechanisms within the shear connections with Connectors RBN and R are readily identified.

Then, a complementary design rule is proposed to determine the shear resistances of the connections, considering influence of various key parameters. Simplified load-slippage curves of the shear connections are also developed for practical design of prefabricated composite beams.

In addition, finite element models of three practical composite beams with similar shear connections are developed, and validated against the experimental data to assess feasibility of the proposed load-slippage curves for the shear connections.

7.2 Parametric studies on Connection RBN

A total of 38 parametric models with Connection RBN were developed to investigate the structural behaviour of Connection RBN. The effects of bolt diameter, steel block thickness, concrete block width, strengths of concrete block and concrete slab, fibre content in concrete block and longitudinal spacing of shear connections on the structural behaviour of the shear connections were investigated. Load-slippage curves, shear resistances, and "stress and damage" distributions are analyzed in detail. The parameters and their values in parametric studies on Connection RBN are summarised in Table 7.1. Key results of the models with Connection RBN are summarised in Table 7.2. It should be noted that Model A-1-W with Connection RBN is selected as a reference model for easy comparison. In Figs. 7.4 a), 7.8 a), 7.12 a), 7.15 a), 7.18 a), 7.21 a), and 7.24 a), those lines with different markers represent the shear forces in the bolts while those lines without markers represent the shear forces in bolts with steel blocks.

Table 7.1 Parameters and their values in parametric studies on Connection RBN

Connector configuration	Parameter	Range	Values
RBN	Bolt diameter, d (mm)	18 ~ 36	18, 24, **30**, 36
	Thickness of steel block, T_b (mm)	20 ~ 100	20, **30**, 40, 50, 60, 70, 80, 90, 100
	Width of concrete block, W_c (mm)	80 ~ 320	80, 160, **240**, 320
	Infilled concrete block strength, f_{ci} (N/mm^2)	40 ~ 120	40, 50, 60, 70, 80, 90, **100**, 110, 120
	Precast concrete slab strength, f_{cp} (N/mm^2)	40 ~ 120	40, **50**, 60, 70, 80, 90, 100, 110, 120
	Fibre content in concrete block, w (%)	0.0 ~ 2.0	0.0, 0.5, 1.0, **1.5**, 2.0
	Longitudinal spacing of shear connections, L_s (mm)	360 ~ 840	360, **480**, 600, 720, 840

7.2.1 Effect of bolt diameter

Models with bolt diameters of 18, 24, 30, and 36 mm were developed to investigate the effect of bolt diameter on the structural behaviour of Connection RBN. A total of four models were developed, as shown in Fig. 7.1.

Key deformation characteristics are presented as follows:

a) Load-slippage curves of those models with various bolt diameters are plotted in Fig. 7.2. It is shown that when the bolt diameter is increased from 18 to 36 mm, the shear resistance is increased with a factor of 1.23. When the load-slippage curves enter the non-linear stage, the shear resistances at the same slippage increase with an increase in the bolt diameter. Hence, the bolts play a significant role in the non-linear behaviour of the shear connection.

b) The concrete damage distributions in those models with bolt diameters of 18, 24, and 36 mm are shown in Fig. 7.3. It is shown that no apparent compressive damage appears in the three models when the applied load is increased to 0.5 Q_m. When the slippage is increased to 6 mm, the concrete damage within the concrete block and the precast concrete slab in those

models with bolts of 36 mm diameter is shown to be more severe than the damage in those models with bolts of 18 mm diameter. The von Mises stresses of the bolt shanks in the models with bolt of 18 and 24 mm diameters reach the tensile strength while the stresses in the model with bolts of 36 mm diameter are smaller than the tensile strength, and hence, bolt fracture is not found in this model. The von Mises stresses of the bolt shanks in the model with bolts of 30 mm diameter reach the tensile strength, and hence, the shear connection with a bolt diameter of 30 mm is considered to be effective as the full bolt strength is readily utilised.

c) The distributions of shear forces and concrete bearing forces in those models with bolt diameters of 18, 24, 30, and 36 mm are shown in Fig. 7.4. When the bolt diameter increases from 18 to 36 mm, the shear force at the root of the steel block is increased with a factor of 1.26, and the shear force at the top of the steel block is increased with a factor of 3.28. The concrete bearing force acting onto the steel block is decreased from 75% to 59% of the applied shear force while the bearing force acting onto the bolt is significantly increased. Hence, when the bolt diameter is increased, the applied force taken by the bolt is increased correspondingly.

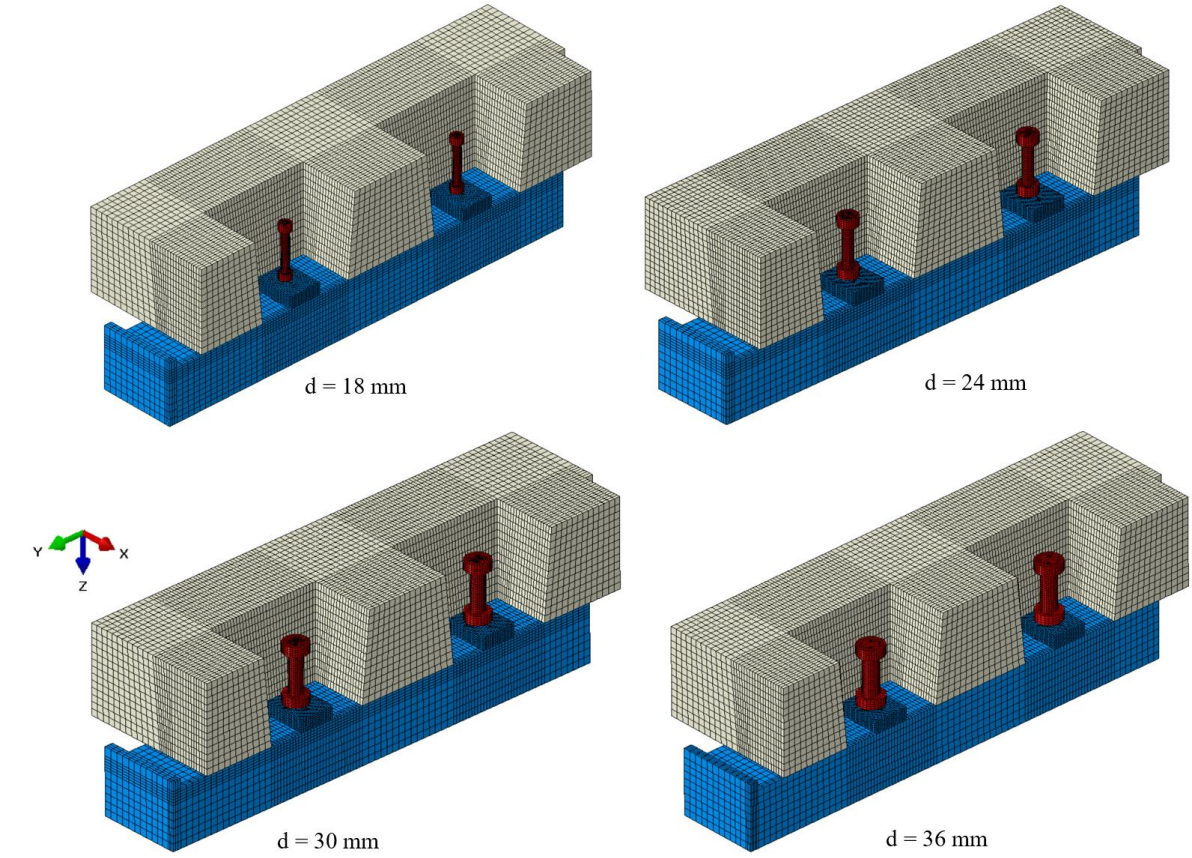

Note: Concrete blocks and steel reinforcements are omitted for clarity.

Fig. 7.1 Models with Connection RBN and various bolt diameters

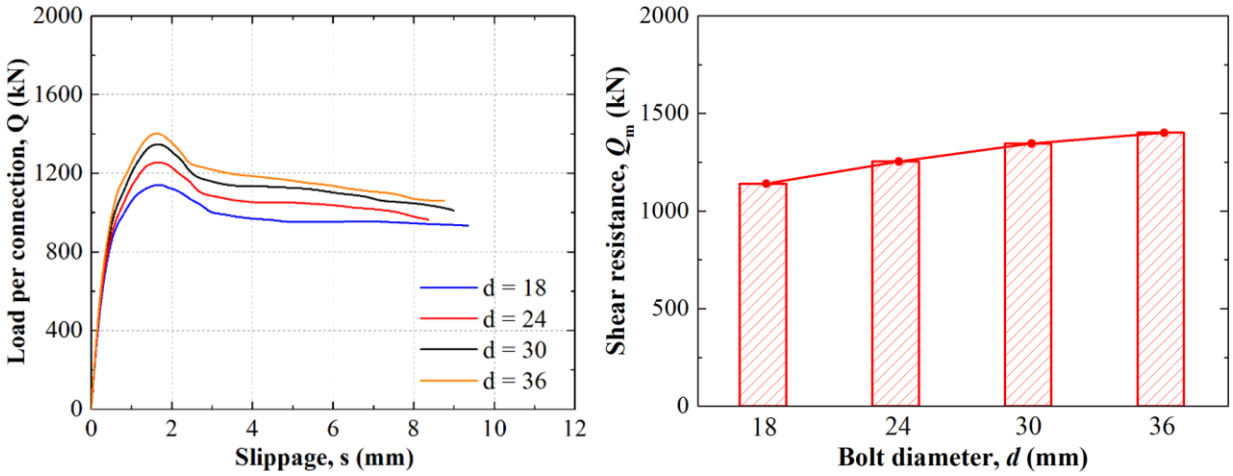

Fig. 7.2 Load-slippage curves of models with Connection RBN and various bolt diameters

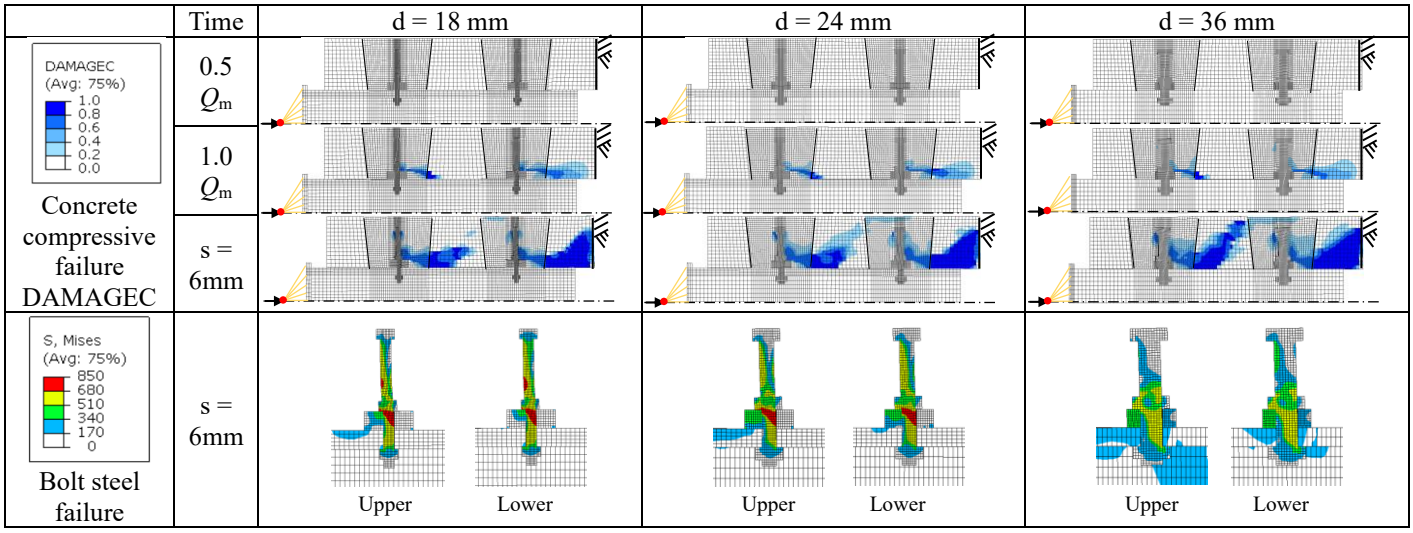

Fig. 7.3 Damage in models with Connection RBN and various bolt diameters

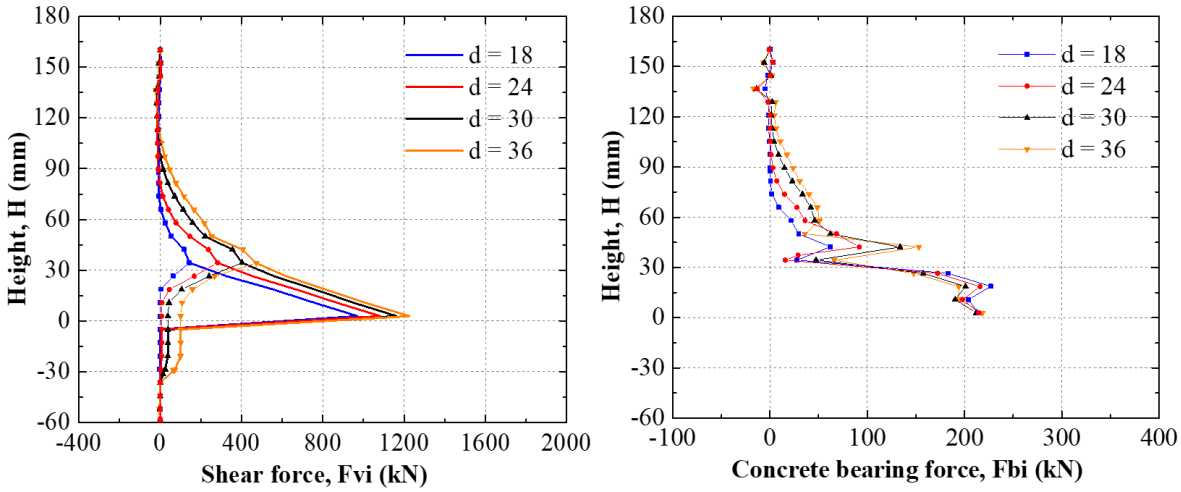

a) Distribution of shear force b) Distribution of concrete bearing force

Fig. 7.4 Internal force distributions in models with Connection RBN and various bolt diameters

7.2.2 Effect of steel block thickness

Those models with steel block thicknesses of 20 to 100 mm at 10 mm intervals were developed to investigate the effect of steel block thickness onto the structural behaviour of Connection RBN. A total of nine models were developed, and the models with steel block thicknesses of 40, 60, 80, and 100 mm are shown in Fig. 7.5.

Key deformation characteristics are presented as follows:

a) Load-slippage curves of those models with various steel block thicknesses are plotted in Fig. 7.6. It is shown that when the steel block thickness is increased from 20 to 90 mm, the shear resistance is increased with a factor of 1.26. When the steel block thickness is increased from 90 to 100 mm, the shear resistance is decreased with a factor of 0.99. However, with an increase in the steel block thickness, the slippage s_m corresponding to the peak load is decreased.

b) The concrete damage distributions in those models with steel block thicknesses of 20, 60, and 100 mm are shown in Fig. 7.7. It is shown that no apparent compressive damage appears in these three models when the applied load is increased to 0.5 Q_m. When the slippage is increased to 6 mm, the concrete damage in the models with steel block thicknesses of 60 and 100 mm is more severe than the damage in the model with a steel block thickness of 20 mm. The von Mises stresses of the bolt shanks in the model with the steel block thickness of 20 mm reach the tensile strength while most of the stresses in the models with steel block thicknesses of 60 and 100 mm are smaller than the tensile strength. Moreover, the stresses in the model with the steel block thickness of 40 mm are smaller than the tensile strength. Hence, when the bolt diameter is 30 mm, the connection with a steel block thickness of 30 mm is considered to be effective as the full bolt strength is readily mobilized, and favourable

ductility of the shear connection is obtained.

c) The distributions of shear forces and concrete bearing forces in those models with steel block thicknesses of 20, 60, and 100 mm are shown in Fig. 7.8. When the steel block thickness is increased from 20 to 90 mm, the shear force at the root of the steel block is increased with a factor of 1.40, and the concrete bearing force acting onto the steel block is increased from 55% to 91% of the applied shear force while the force change at the top of the steel block is less abrupt.

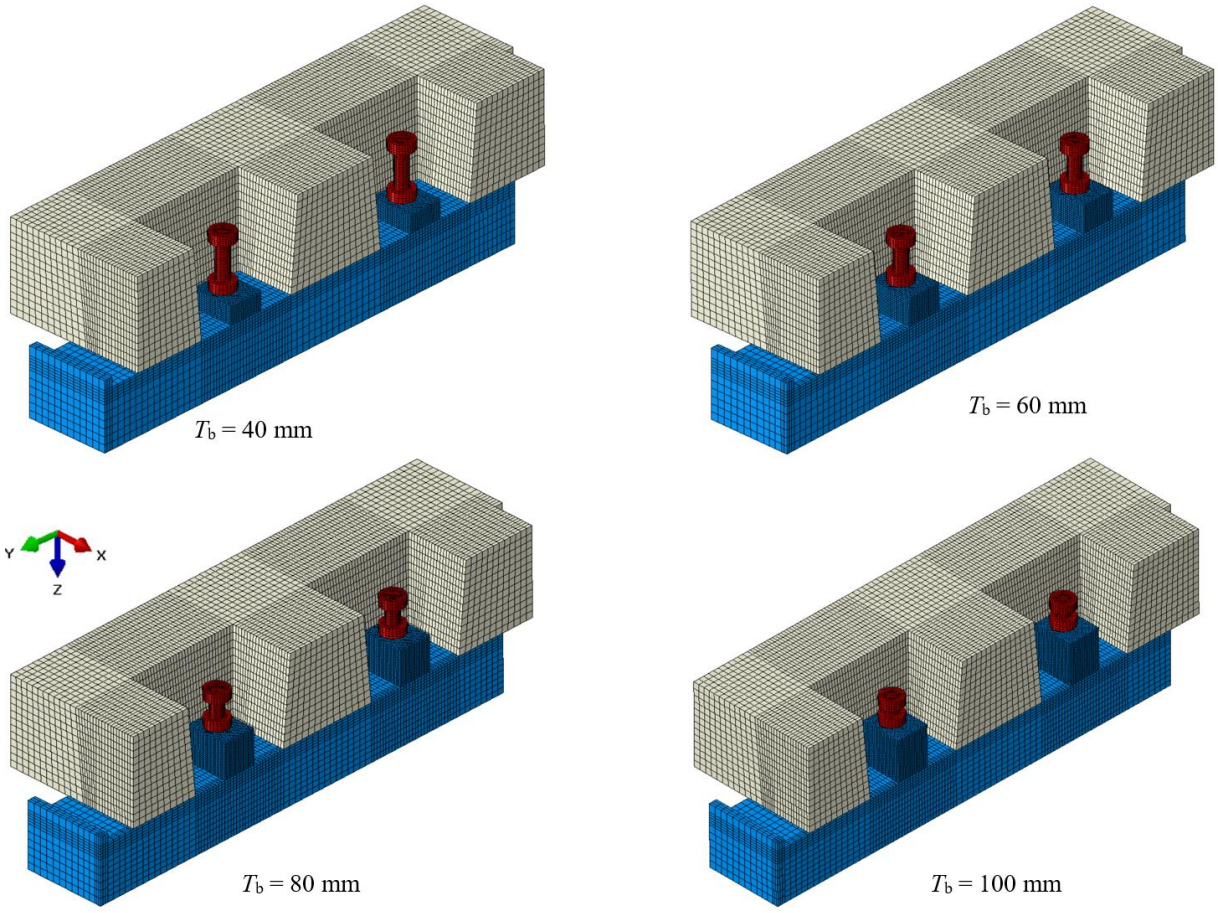

Note: Concrete blocks and steel reinforcements are omitted for clarity.

Fig. 7.5 Models with Connection RBN and various steel block thicknesses

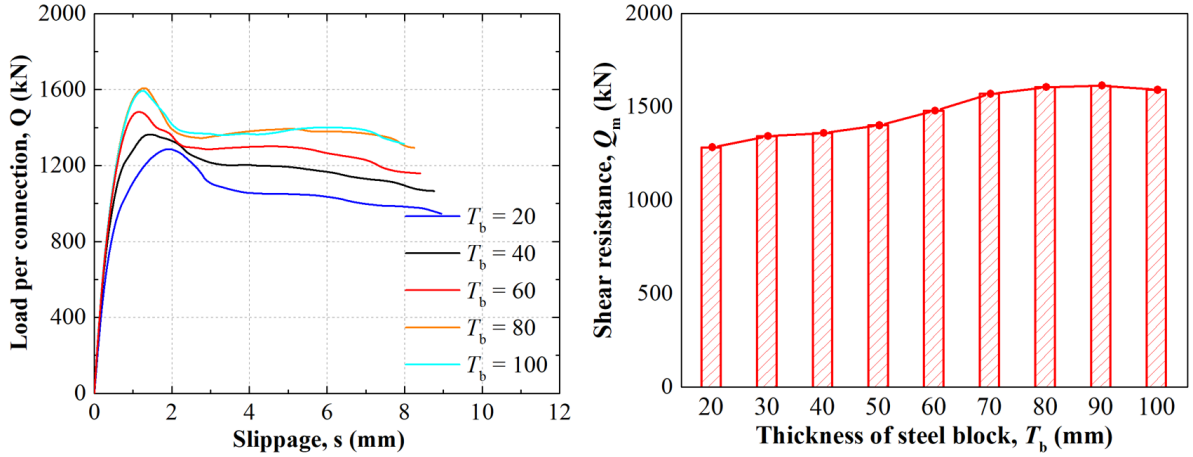

Fig. 7.6 Load-slippage curves of models with Connection RBN and various steel block thicknesses

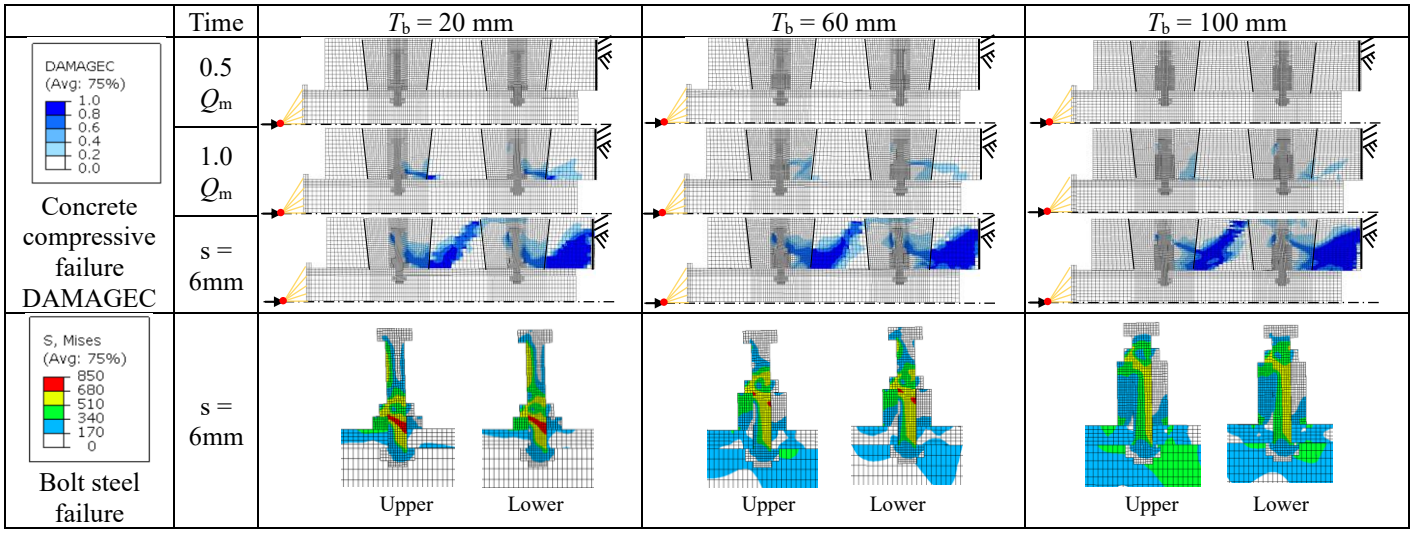

Fig. 7.7 Damage in models with Connection RBN and various steel block thicknesses

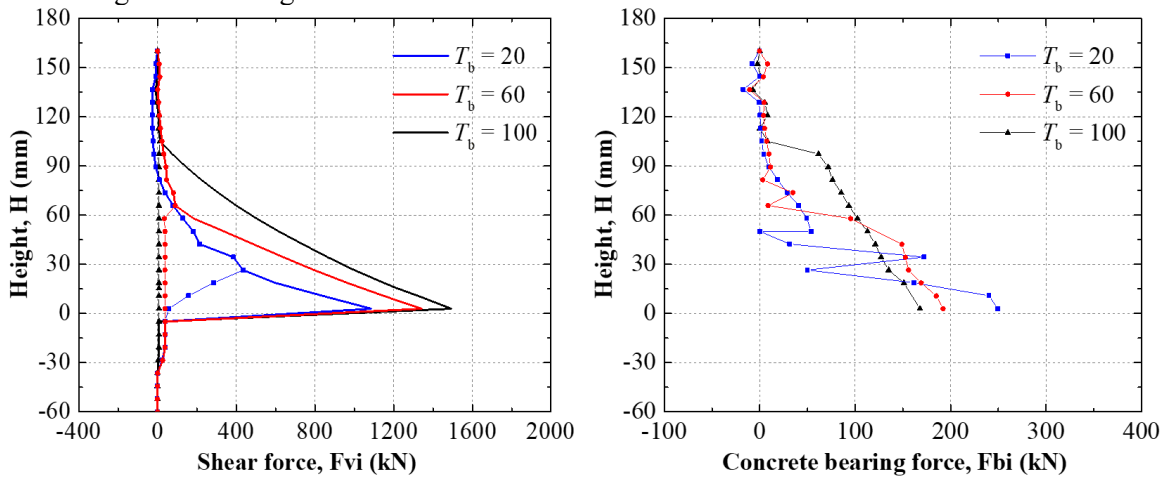

a) Distribution of shear force b) Distribution of concrete bearing force

Fig. 7.8 Internal force distributions in models with Connection RBN and various steel block thicknesses

7.2.3 Effect of concrete block width

Those models with concrete block widths of 80, 160, 240, and 320 mm were developed to investigate the effect of concrete block width onto the structural behaviour of Connection RBN. A total of four models were developed, as shown in Fig. 7.9.

Key deformation characteristics are presented as follows:

a) Load-slippage curves of those models with various concrete block widths are plotted in Fig. 7.10. It is shown that when the concrete block width is increased from 80 to 160 mm, the shear resistance is increased with a factor of 1.07. When the concrete block width is increased from 160 to 240 mm, the shear resistance is increased with a factor of 1.02. Hence, when the concrete block width exceeds 160 mm, any increase in the shear resistance is insignificant by increasing the concrete block width.

b) The concrete damage distributions in those models with concrete block widths of 160, 240, and 320 mm are shown in Fig. 7.11. It is shown that no apparent compressive damage appears in these three models when the applied load is increased to 0.5 Q_m. When the slippage is increased to 6 mm, the concrete damage in the model with the concrete block width of 320 mm is less severe than the damage in the model with the concrete block width of 160 mm. The von Mises stresses of the bolt shanks in these three models reach the tensile strength.

c) The distributions of shear forces and concrete bearing forces in those models with concrete block widths of 80, 160, 240, and 320 mm are shown in Fig. 7.12. When the concrete block width is increased from 80 to 160 mm, the shear force at the root of the steel block is increased with a factor of 1.11, while the shear force at the top of the steel block is decreased with a factor of 0.91. When the concrete block width is increased from 80 to 320 mm, the concrete bearing force acting on the steel block is increased from 53% to 63% of the shear

force.

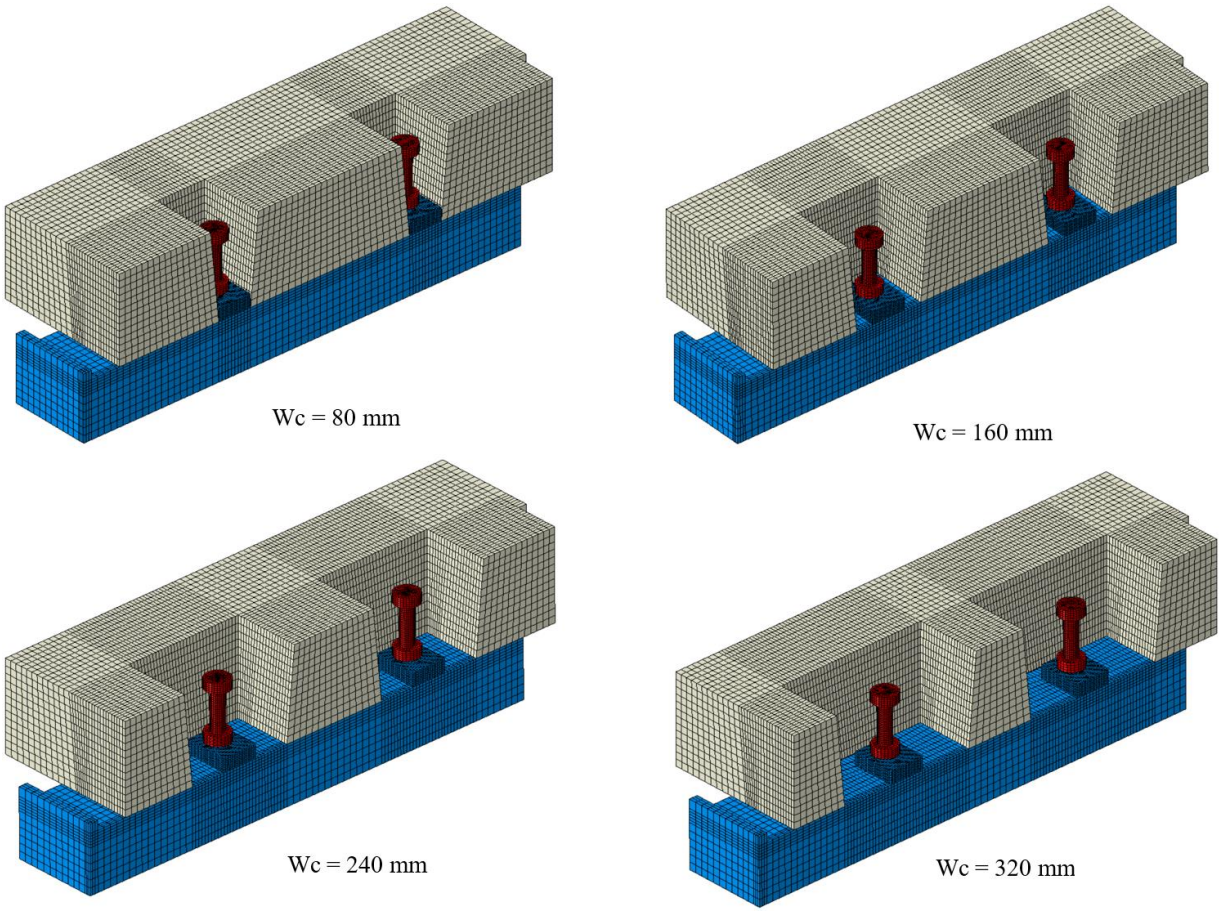

Note: Concrete blocks and steel reinforcements are omitted for clarity.

Fig. 7.9 Models RBN with various concrete block widths

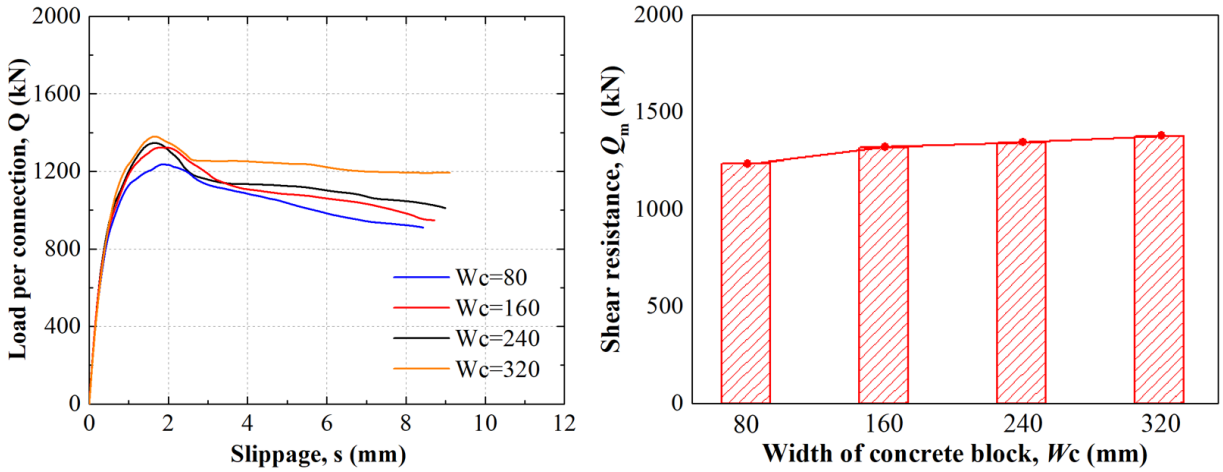

Fig. 7.10 Load-slippage curves of models with Connection RBN and various concrete block widths

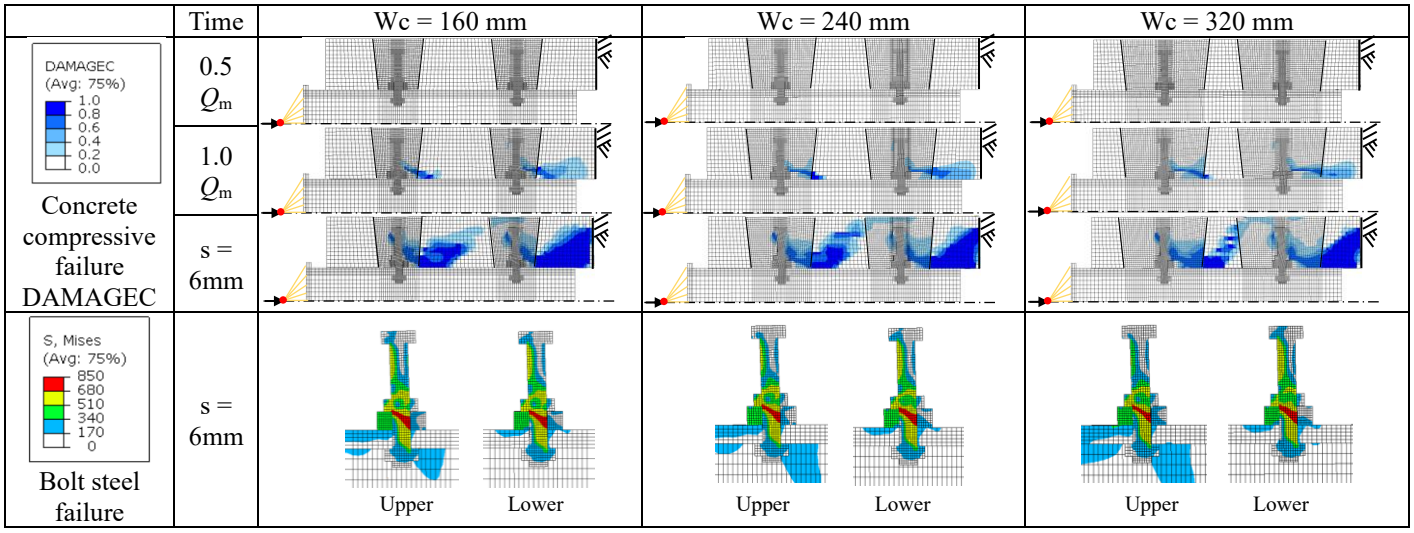

Fig. 7.11 Damage in models with Connection RBN and various concrete block widths

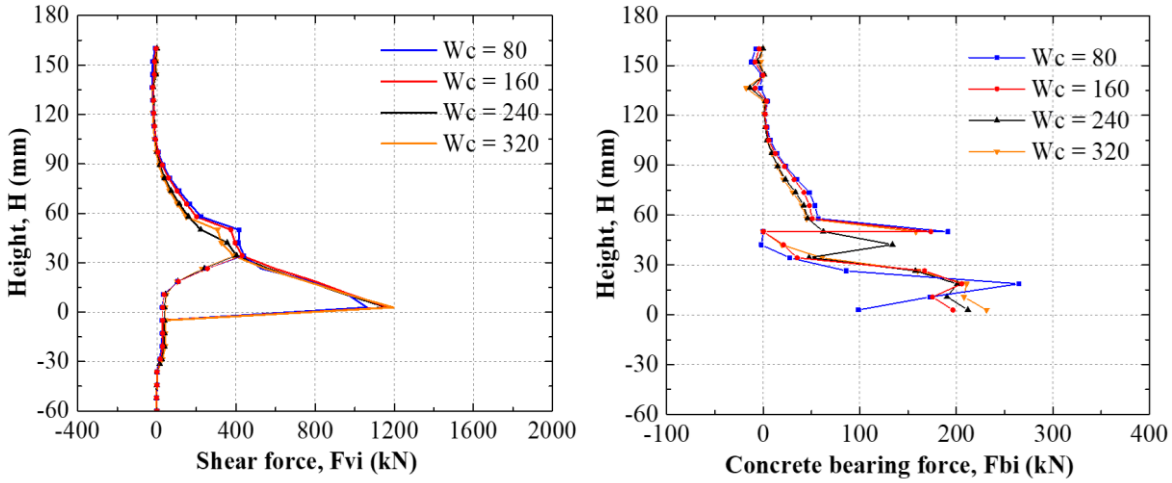

a) Distribution of shear force b) Distribution of concrete bearing force

Fig. 7.12 Internal force distributions in models with Connection RBN and various concrete block widths

7.2.4 Effect of concrete block strength

Those models with compressive strengths of the concrete blocks ranging from 40 to 120 N/mm^2 at 10 N/mm^2 intervals were developed to investigate the effect of concrete block strength onto the structural behaviour of Connection RBN. A total of nine models were developed.

Key deformation characteristics are presented as follows:

a) Load-slippage curves of those models with various strengths of concrete blocks are plotted in Fig. 7.13. It is shown that when the strength of the concrete block is increased from 40 to

100 N/mm^2, the shear resistance of the connection is increased with a factor of 1.21, while the slippage corresponding to the peak load is decreased. However, when the strength of the concrete block is increased from 100 to 120 N/mm^2, the shear resistance is decreased with a factor of 0.98. Hence, the shear connection with the strength of the concrete block of 100 N/mm^2 and the steel fibre content of 1.5% is considered to be effective when the strength of the precast concrete slab is 50 N/mm^2.

b) The concrete damage distributions in those models with strengths of concrete blocks of 40, 80, and 120 N/mm^2 are shown in Fig. 7.14. It is shown that when the applied load is increased to 0.5 Q_m, a small portion of compressive damage appears in the concrete blocks of the models with concrete block strengths of 40 and 80 N/mm^2 while no apparent damage appears in the concrete blocks of the model with the concrete block strength of 120 N/mm^2. With an increase in the strength of the concrete block, the damage area in the concrete block is decreased correspondingly. When the slippage is increased to 6 mm, the von Mises stresses of the bolt shanks in the models with compressive strengths of 80 and 120 N/mm^2 reach the tensile strength, while most of the stresses of the bolt shanks in the model with the compressive strength of 40 N/mm^2 are smaller than the tensile strength.

c) The distributions of shear forces and concrete bearing forces in those models with strengths of concrete blocks of 40, 80, and 120 N/mm^2 are shown in Fig. 7.15. With an increase in the concrete block strength, the shear force at the root of the steel block is increased, while the shear force in the vicinity of the embedded shank is decreased. With an increase in the compressive strength of the concrete block, the concrete bearing force acting onto the root of the steel block is increased.

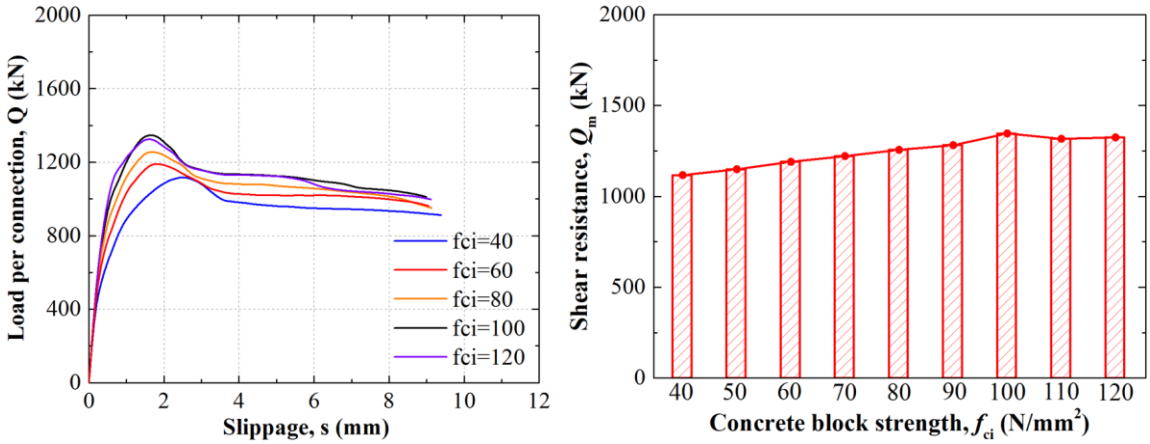

Fig. 7.13 Load-slippage curves of models with Connection RBN and various strengths of concrete blocks

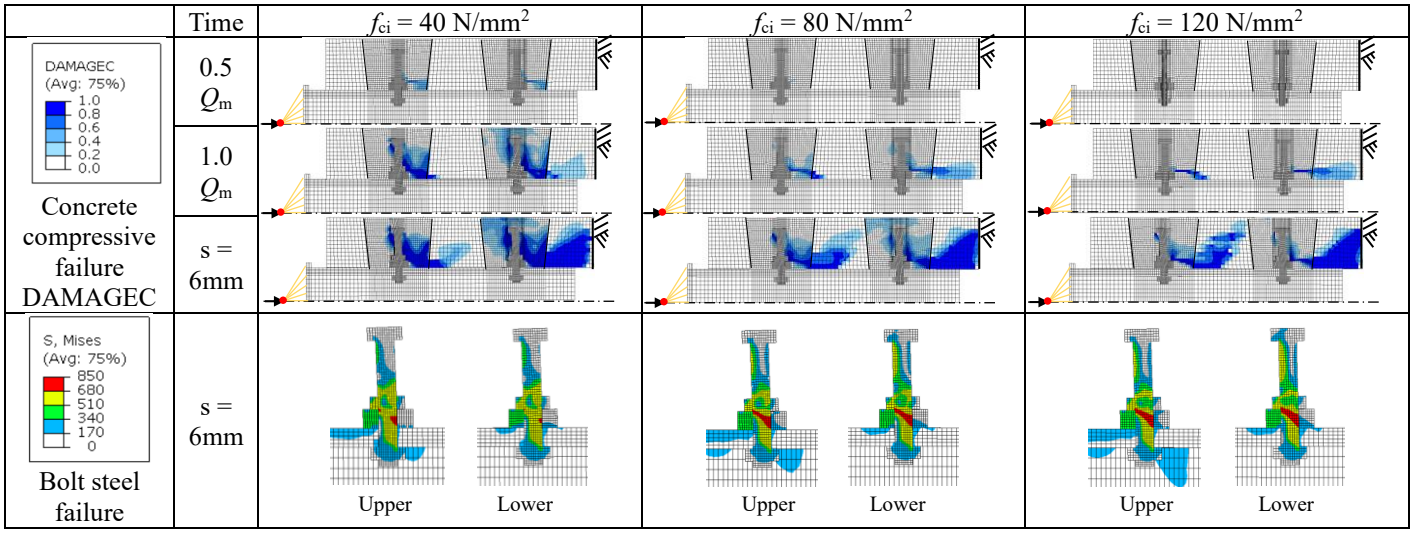

Fig. 7.14 Damage in models with Connection RBN and various strengths of concrete blocks

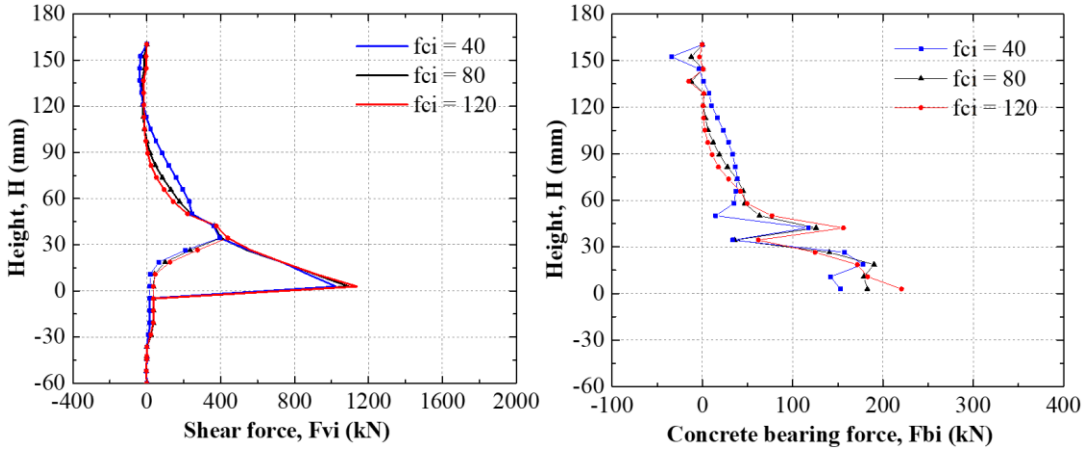

Fig. 7.15 Internal force distributions in models with Connection RBN and various strengths of concrete blocks

7.2.5 Effect of precast concrete slab strength

Those models with compressive strengths of the precast concrete slabs ranging from 40 to 120 N/mm^2 at 10 N/mm^2 intervals were developed to investigate the effect of precast concrete slab strength on the structural behaviour of Connection RBN. A total of nine models were developed. Key deformation characteristics are presented as follows:

a) The load-slippage curves of those models with various strengths of precast concrete slabs are plotted in Fig. 7.16. It is shown that when the strength of the precast concrete slab is increased from 40 to 120 N/mm^2, the shear resistance is increased with a factor of 1.55, and the slippage corresponding to the peak load is increased. Hence, the shear connection is strong enough when the precast concrete slab with a compressive strength of 120 N/mm^2 is used. However, as there is no steel fibre, concrete failure becomes critical.

b) The concrete damage distributions in those models with strengths of precast concrete slabs of 40, 80, and 120 N/mm^2 are shown in Fig. 7.17. It is shown that when the applied load is increased to 0.5 Q_m, no apparent compressive damage appears in the models with concrete strengths of 40 and 80 N/mm^2 while slight damage appears in the concrete blocks of the model with the concrete strength of 120 N/mm^2. When the slippage is increased to 6 mm, the von Mises stresses of the bolt shanks in these three models reach the tensile strength.

c) The distributions of shear forces and concrete bearing forces in those models with strengths of the concrete slabs of 40, 80, and 120 N/mm^2 are shown in Fig. 7.18. When the compressive strength of the concrete slab is increased from 40 to 120 N/mm^2, the shear force at the root of the steel block is increased with a factor of 1.52, and the shear force at the top of the steel block is increased with a factor of 1.31. With an increase in the compressive strength of the concrete slab, the concrete bearing force acting onto the steel block is increased.

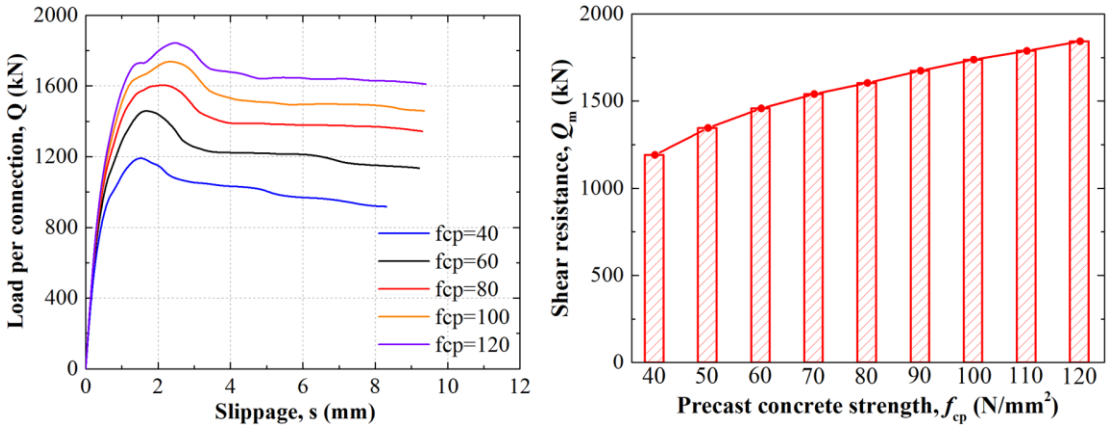

Fig. 7.16 Load-slippage curves of those models with Connection RBN and various strengths of concrete slabs

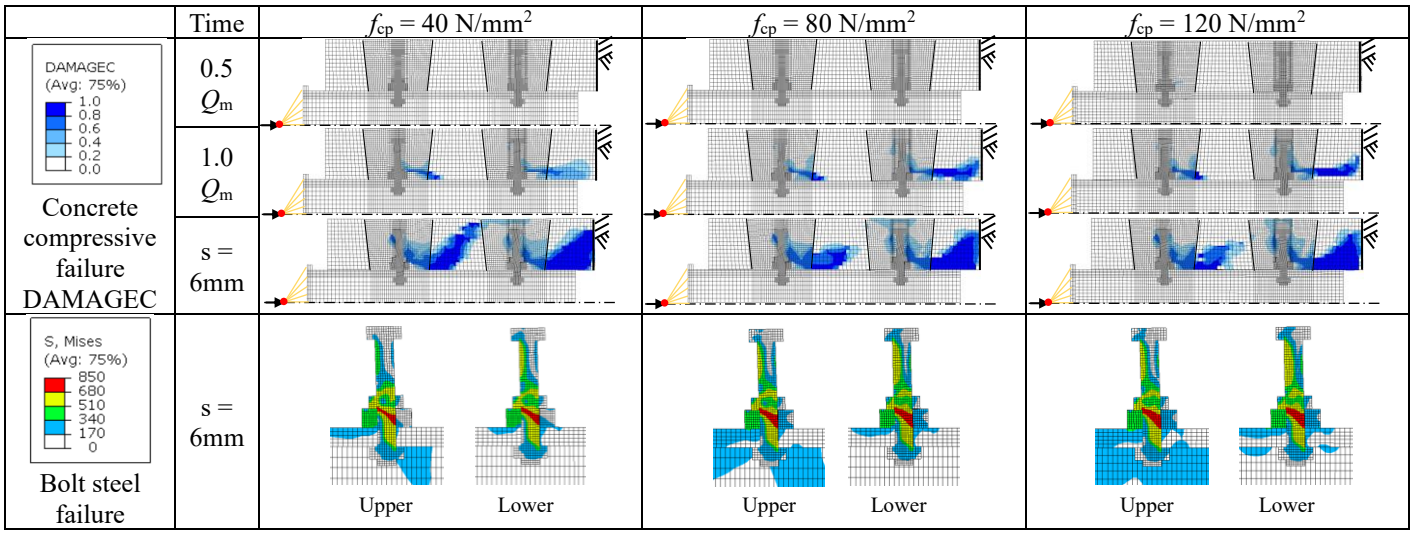

Fig. 7.17 Damage in those models with Connection RBN and various strengths of concrete slabs

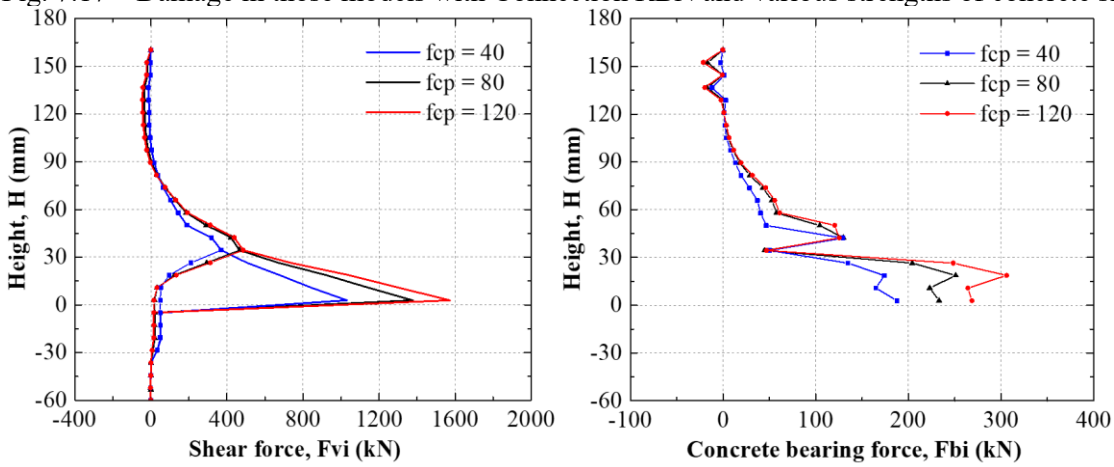

a) Distribution of shear force b) Distribution of concrete bearing force

Fig. 7.18 Internal force distributions in those models with Connection RBN and various strengths of concrete slabs

7.2.6 Effect of fibre content in concrete block

Those models with fibre content of 0%, 0.5%, 1.0%, 1.5%, and 2.0% in the concrete blocks were developed to investigate the effect of fibre content on the structural behaviour of Connection RBN. It should be noted that the strength of the concrete block with various fibre content remains at 100 N/mm^2 for easy comparison. A total of five models were developed.

Key deformation characteristics are presented as follows:

a) Load-slippage curves of those models with various fibre content are plotted in Fig. 7.19. It is shown that when the fibre content in the concrete block is increased from 0.0 % to 1.5 %, the shear resistance is increased with a factor of 1.17. When the fibre content is increased from 1.5 % to 2.0 %, the shear resistance is decreased with a factor of 0.95. Hence, the shear connection with the fibre content in the concrete block of 1.5 % and the strength of concrete block of 100 N/mm^2 is considered to be effective when the strength of the precast concrete slab is 50 N/mm^2.

b) The concrete damage distributions in those models with fibre content of 0.0%, 1.0%, and 2.0% are shown in Fig. 7.20. It is shown that no apparent compressive damage appears in these three models when the applied load is increased to 0.5 Q_m. When the slippage is increased to 6 mm, the von Mises stresses of the bolt shanks in the models with fibre content of 1.0% and 2.0% reach the tensile strength.

c) The distributions of shear forces and concrete bearing forces in those models with fibre content of 0.0%, 1.0%, and 2.0% are shown in Fig. 7.21. When the fibre content is increased from 0.0% to 1.5%, the shear force at the root of the steel block is increased with a factor of 1.12. With an increase in the fibre content, the concrete bearing force acting on the steel block remains almost unchanged.

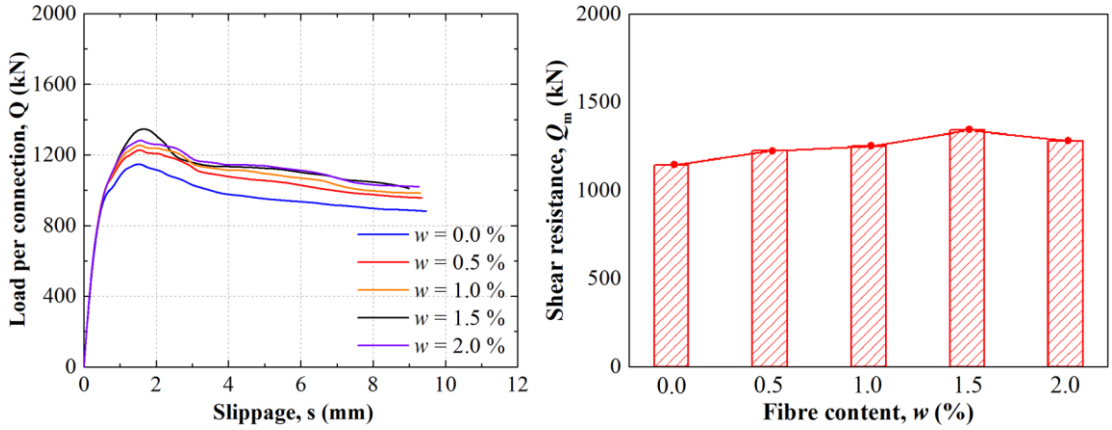

Fig. 7.19 Load-slippage curves of those models with Connection RBN and various fibre content

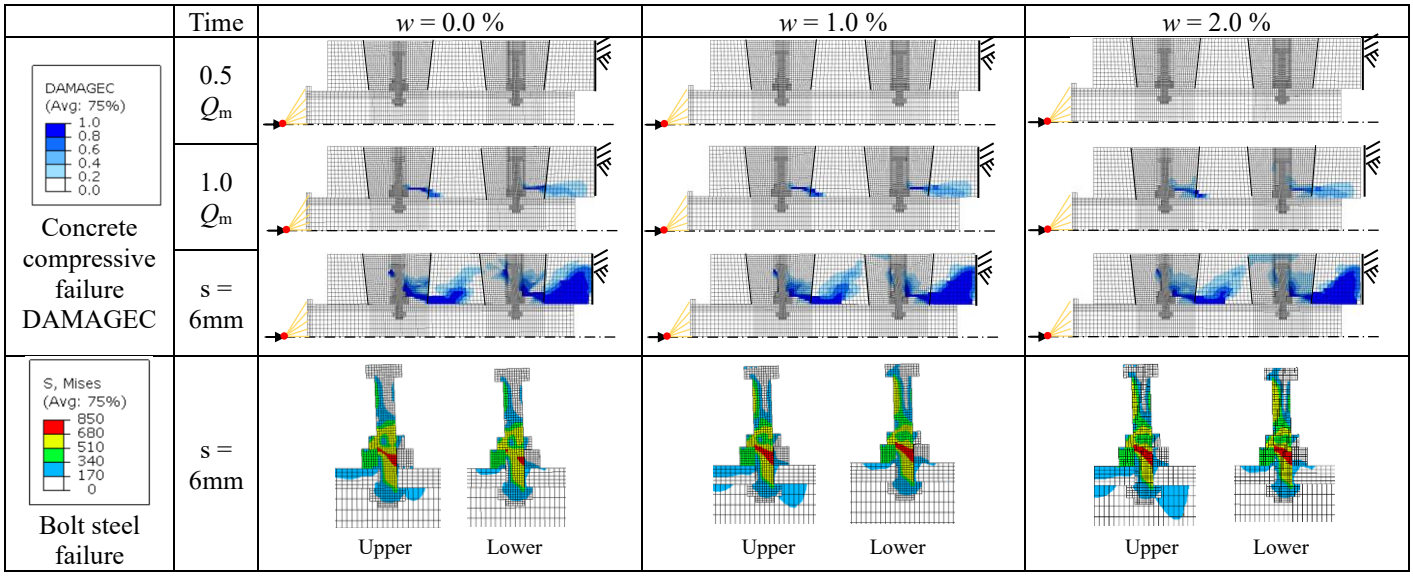

Fig. 7.20 Damage in models with Connection RBN and various fibre content

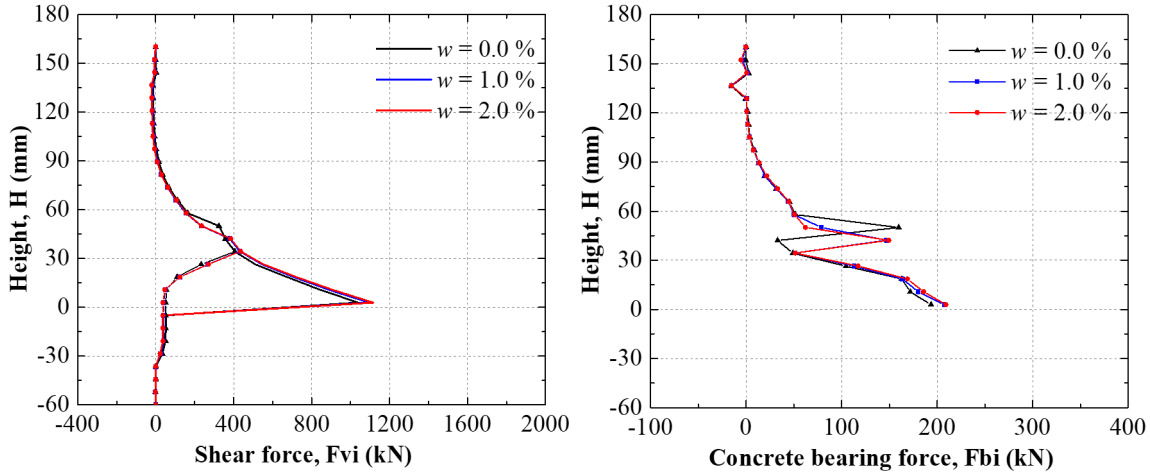

a) Distribution of shear force b) Distribution of concrete bearing force

Fig. 7.21 Internal force distributions in models with Connection RBN and various fibre content

7.2.7 Effect of longitudinal spacing of shear connections

Those models with longitudinal spacings of shear connections of 360, 480, 600 and 720 mm were developed to investigate the effect of longitudinal spacing of shear connections on the structural behaviour of Connection RBN. A total of four models were developed. It should be noted that the distance between the top surface of the precast concrete slab and the upper side of the preformed hole in the parametric model is either larger than or at least the same as the distance in the reference model.

Key deformation characteristics are presented as follows:

a) Load-slippage curves of those models with various longitudinal spacings of shear connections are plotted in Fig. 7.22. It is shown that when the longitudinal spacing is increased from 360 to 720 mm, the shear resistance is increased with a factor of 1.03, while the shear resistance is decreased with a factor of 0.99 when the longitudinal spacing is increased from 720 to 840 mm. Hence, the longitudinal spacing between two shear connections should be smaller than 720 mm.

b) The concrete damage distributions in those models with longitudinal spacings of 360, 600, and 840 mm are shown in Fig. 7.23. It is shown that no apparent compressive damage appears in these three models when the applied load is increased to 0.5 Q_m. With an increase in the longitudinal spacing, the damage area of the concrete slab between the two shear connections is decreased due to the increased volume of the concrete. When the slippage is increased to 6 mm, the concrete damage of the precast concrete slab in models with the longitudinal spacing of 360 and 480 mm extends to the adjacent concrete block, and hence, the longitudinal spacing between two shear connections should be larger than 480 mm to provide sufficient precast concrete for bearing. The von Mises stresses of the bolt shanks in these

three models reach the tensile strength.

c) The distributions of shear forces and concrete bearing forces in those models with longitudinal spacings of 360, 480, 720, and 840 mm are shown in Fig. 7.24. With an increase in the longitudinal spacing, the shear forces at both the root and the top of the steel block are marginally increased. With an increase in the longitudinal spacing, the concrete bearing force acting onto the steel block is decreased.

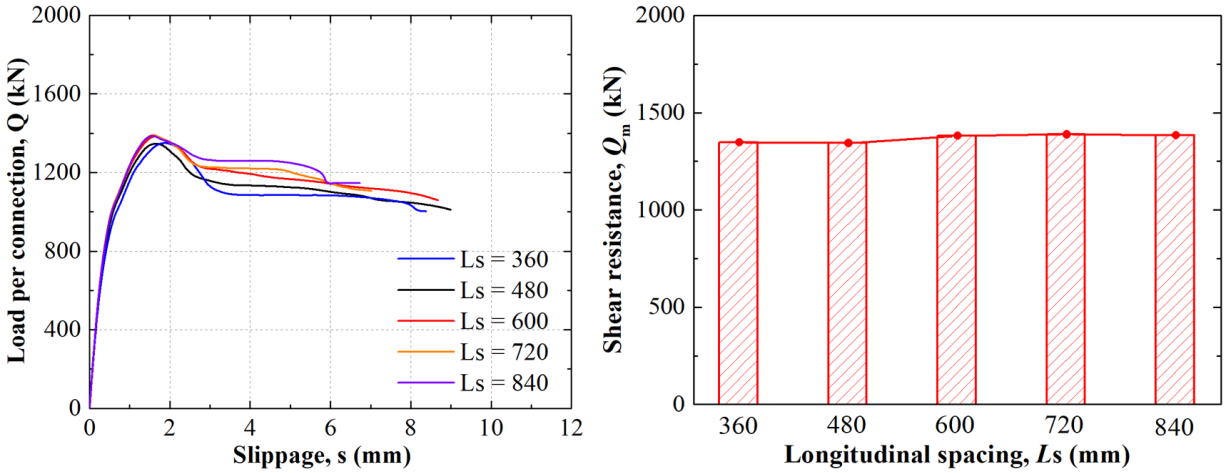

Fig. 7.22 Load-slippage curves of those models with Connection RBN and various longitudinal spacings

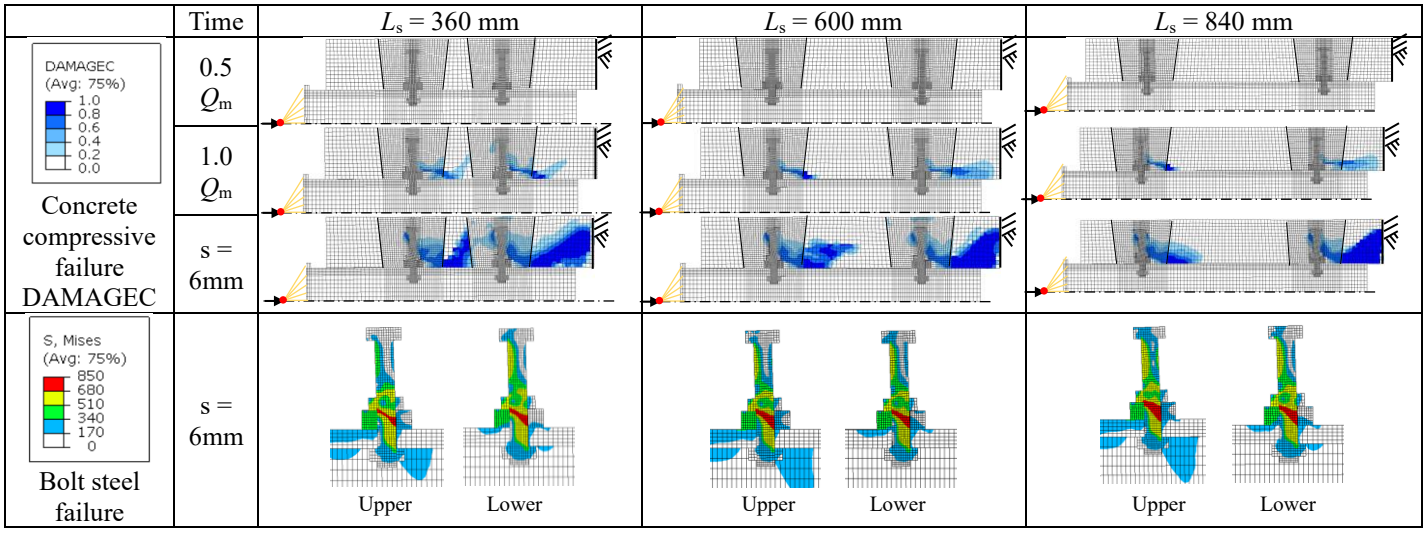

Fig. 7.23 Damage in those models with Connection RBN and various longitudinal spacings

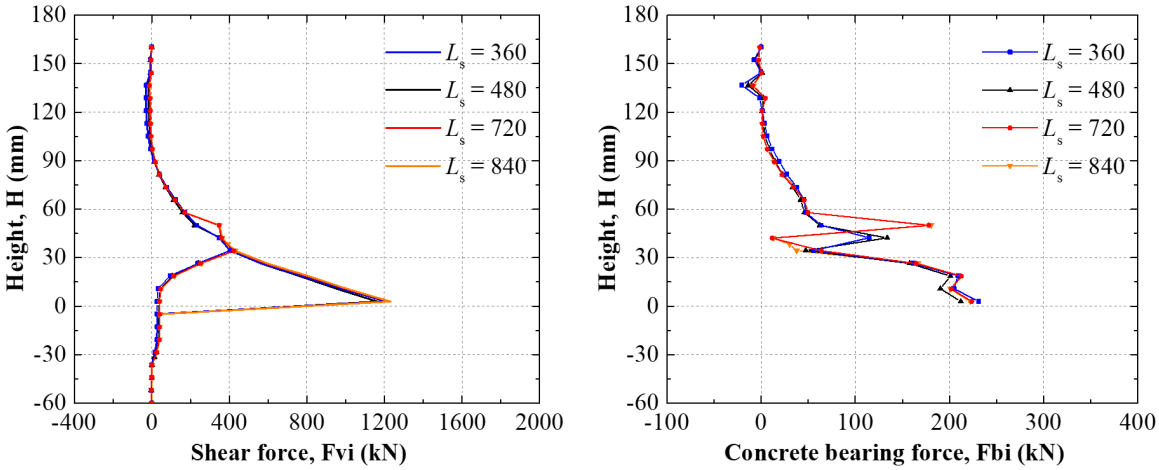

a) Distribution of shear force b) Distribution of concrete bearing force

Fig. 7.24 Internal force distributions in those models with Connection RBN and various longitudinal spacings

Key results of the models with Connection RBN are summarised in Table 7.2. In general, with increases in bolt diameter, steel block thickness, concrete block width, concrete block strength, precast concrete slab strength, and fibre content in concrete block, shear resistances of the connections are increased, while when the concrete block strength exceeds 100 N/mm^2, and the steel fibre content in concrete block exceeds 1.5%, the shear resistance is decreased slightly. Hence, the connection with the concrete block strength of 100 N/mm^2, and the steel fibre content of 1.5% is highly effective. When the applied load is increased to 1.0 Q_m, compressive damage appears in both the concrete blocks and the precast concrete slabs. It should be noted that the shear forces taken by the bolts in the upper row are larger than those taken by the bolts in the lower row according to the stresses in the H-sections.

7.2.8 Key findings of parametric studies

Based on the results of various parameters over practical ranges of values, it is found that:

- Among all these parameters, the most effective one is the thickness of the steel blocks, T_b . By increasing their values from 30 to 80 mm, the shear resistances of the shear connections are

readily increased from 1,346.6 kN to 1,607.9 kN, i.e. by a factor of 1.20. Since the steel plates are small in sizes, the increase in material costs is minimal.

- By increasing the strengths of both the infilled concrete block, f_{ci} and the precast concrete slab f_{cp}, and also the fibre content in the concrete block w to their respective practical limits, there are only minimal increases, i.e. ≤ 5 to 10 %, in the shear resistances of the shear connections.
- For other geometrical parameters such as bolt diameter d, and the width of the concrete block W_c, any increase from their basic values to their practical limits is found to be ineffective to increase the shear resistances of the shear connections.

Table 7.2 Key results of the models with Connection RBN

Parameters							Influence of various parameters					
	s_m (mm)	Q_m (kN)	***Ratio***	Q_{Rd} (kN)	η	von Mises stresses in bolt shanks	$F_{v,max}$ (kN)	***Ratio***	F_{bs} (kN)	λ (%)	Changing pattern of shear resistance
Bolt diameter, d (mm)	**18**	**1.7**	**1,140.8**	**1.00**	1,045.8	1.13	≥ f_{ub}	**972.2**	**1.00**	856.1	75	Increase
	24	1.6	1,254.1	1.10	1,259.6	1.00	≥ f_{ub}	1,083.2	1.11	817.0	65	
	30	1.7	1,346.6	1.18	1,332.8	1.01	≥ f_{ub}	1,163.6	1.20	808.4	60	
	36	1.6	1,401.5	1.23	1,332.8	1.05	< f_{ub}	1,227.4	1.26	821.4	59	
Thickness of steel block T_b (mm)	**20**	**1.9**	**1,286.2**	**1.00**	1,257.2	1.02	≥ f_{ub}	**1,086.4**	**1.00**	701.2	55	Increase
	30	1.7	1,346.6	1.05	1,332.8	1.01	≥ f_{ub}	1,163.6	1.07	808.4	60	
	40	1.5	1,362.7	1.06	1,390.7	0.98	< f_{ub}	1,186.0	1.09	842.6	62	
	50	1.3	1,403.9	1.09	1,448.7	0.97	< f_{ub}	1,245.2	1.15	1,011.6	72	
	60	1.2	1,482.5	1.15	1,506.6	0.98	< f_{ub}	1,342.6	1.24	1,107.9	75	
	70	1.2	1,572.2	1.22	1,564.6	1.00	< f_{ub}	1,429.2	1.32	1,338.0	85	
	80	1.3	1,607.9	1.25	1,622.5	0.99	< f_{ub}	1,507.2	1.39	1,445.3	90	
	90	1.3	1,616.8	1.26	1,680.5	0.96	< f_{ub}	1,519.6	1.40	1,473.6	91	
	100	1.3	1,593.6	1.24	1,738.4	0.92	< f_{ub}	1,493.4	1.37	1,314.1	82	Decrease
Width of concrete block W_c (mm)	**80**	**1.9**	**1,237.2**	**1.00**	1,022.3	1.21	≥ f_{ub}	**1,062.6**	**1.00**	649.6	53	Increase
	160	1.8	1,322.7	1.07	1,223.6	1.08	≥ f_{ub}	1,174.8	1.11	780.0	59	
	240	1.7	1,346.6	1.09	1,332.8	1.01	≥ f_{ub}	1,163.6	1.10	808.4	60	
	320	1.6	1,380.1	1.12	1,332.8	1.04	≥ f_{ub}	1,196.8	1.13	870.8	63	
Infilled concrete block strength, f_{ci} (N/mm^2)	**40**	**2.5**	**1,117.5**	**1.00**	1,110.7	1.01	< f_{ub}	**1,024.8**	**1.00**	663.2	59	Increase
	50	2.0	1,149.5	1.03	1,100.9	1.04	< f_{ub}	1,035.8	1.01	680.0	59	
	60	1.8	1,190.4	1.07	1,106.6	1.08	< f_{ub}	1,059.8	1.03	700.6	59	
	70	1.7	1,221.9	1.09	1,139.3	1.07	< f_{ub}	1,077.0	1.05	716.8	59	
	80	1.7	1,256.2	1.12	1,200.1	1.05	≥ f_{ub}	1,193.8	1.07	727.8	58	
	90	1.7	1,282.0	1.15	1,285.5	1.00	≥ f_{ub}	1,106.0	1.08	725.8	57	

	100	1.7	1,346.6	1.21	1,332.8	1.01	$\geq f_{ub}$	1,163.6	1.14	808.4	60	
	110	1.6	1,317.3	1.18	1,332.8	0.99	$\geq f_{ub}$	1,130.0	1.10	745.4	57	Decrease
	120	1.6	1,325.0	1.19	1,332.8	0.99	$\geq f_{ub}$	1,138.8	1.11	762.0	58	
Precast concrete slab strength, f_{cp} (N/mm^2)	**40**	**1.5**	**1,191.5**	**1.00**	1,162.5	1.02	$\geq f_{ub}$	**1,031.0**	**1.00**	711.6	60	
	50	1.7	1,346.6	1.13	1,332.8	1.01	$\geq f_{ub}$	1,163.6	1.13	808.4	60	
	60	1.7	1,458.7	1.22	1,459.3	1.00	$\geq f_{ub}$	1,260.6	1.22	889.6	61	
	70	1.9	1,540.6	1.29	1,522.2	1.01	$\geq f_{ub}$	1,329.4	1.29	929.4	60	
	80	2.1	1,604.7	1.38	1,580.9	1.02	$\geq f_{ub}$	1,376.8	1.34	956.2	60	Increase
	90	2.3	1,674.8	1.41	1,636.1	1.02	$\geq f_{ub}$	1,442.0	1.40	1,006.8	60	
	100	2.3	1,738.4	1.46	1,688.3	1.03	$\geq f_{ub}$	1,496.0	1.45	1,055.4	61	
	110	2.4	1,788.8	1.50	1,738.1	1.03	$\geq f_{ub}$	1,533.6	1.49	1,092.0	61	
	120	2.5	1,843.6	1.55	1,785.7	1.03	$\geq f_{ub}$	1,572.2	1.52	1,134.2	62	
Fibre content in concrete block, w (%)	**0.0**	**1.5**	**1,147.8**	**1.00**	**-**	**-**	$< f_{ub}$	**1,039.2**	**1.00**	**681.8**	**59**	
	0.5	1.5	1,227.0	1.07	-	-	$< f_{ub}$	1,081.0	1.04	652.0	53	Increase
	1.0	1.5	1,254.9	1.09	-	-	$\geq f_{ub}$	1,095.6	1.05	715.2	57	
	1.5	1.7	1,346.6	1.17	1,332.8	1.01	$\geq f_{ub}$	1,163.6	1.12	808.4	60	
	2.0	1.6	1,282.5	1.12	-	-	$\geq f_{ub}$	1,116.2	1.07	732.4	57	Decrease
Longitudinal spacing of shear connections, L_s (mm)	**360**	**1.9**	**1,350.4**	**1.00**	1,332.8	1.01	$\geq f_{ub}$	**1,210.0**	**1.00**	**861.8**	**64**	
	480	1.7	1,346.6	1.00	1,332.8	1.01	$\geq f_{ub}$	1,163.6	0.96	808.4	60	Increase
	600	1.6	1,383.6	1.02	1,332.8	1.04	$\geq f_{ub}$	1,221.2	1.01	860.0	62	
	720	1.6	1,391.1	1.03	1,332.8	1.04	$\geq f_{ub}$	1,226.4	1.01	866.8	62	
	840	1.6	1,386.7	1.03	1332.8	1.04	$\geq f_{ub}$	1,232.6	1.02	838.8	60	Unchanged

Notes:

Q_m denotes shear resistances predicted by numerical models;

s_m denotes slippages corresponding to the predicted shear resistances;

Ratio denotes the ratio of shear resistances of connections with various parameters to those of the reference connection;

Q_{Rd} denotes the design shear resistance predicted by the design method presented in Section 7.5.1 of this chapter;

η denotes a model factor,
$= Q_m / Q_{Rd}$;

f_{ub} denotes the tensile strength of the bolt steel;

$F_{v,max}$ denotes the maximum shear force;

F_{bs} denotes the concrete bearing force acting onto the steel block; and

λ denotes proportion of shear force taken by the steel block,
$= F_{bs} / Q_m$.

7.3 Parametric studies on Connection R

A total of 24 parametric models with Connection R were developed to investigate the structural behaviour of Connection R. The effects of bolt diameter, bolt strength, strengths of concrete block and concrete slab on the structural behaviour of the shear connections were investigated. The load-slippage curves, shear resistances, and "stress and damage" distributions at key increments are analysed in detail. The parameters and their values in parametric studies on Connection R are summarised in Table 7.3. Key results of the models with Connection R are summarised in Table 7.4. It should be noted that Model C-0-W with Connection R is considered as a reference model for easy comparison.

Table 7.3 Parameters and their values in parametric studies on Connection R

Connector configuration	Parameter	Range	Values
R	Bolt diameter, d (mm)	18 ~ 36	18, 24, **30**, 36
	Bolt strength, f_{ub} (N/mm^2)	400 ~ 1,200	400, 500, **800**, 1,000, 1,200
	Infilled concrete block strength, f_{ci} (N/mm^2)	40 ~ 120	40, 50, 60, 70, 80, 90, **100**, 110, 120
	Precast concrete slab strength, f_{cp} (N/mm^2)	40 ~ 120	40, **50**, 60, 70, 80, 90, 100, 110, 120

7.3.1 Effect of bolt diameter

Models with bolt diameters of 18, 24, 30, and 36 mm were developed to investigate the effect of bolt diameter on the structural behaviour of Connection R. A total of four models were developed, as shown in Fig. 7.25.

Key deformation characteristics are presented as follows:

a) Load-slippage curves of those models with various bolt diameters are plotted in Fig. 7.26. It is shown that when the bolt diameter is increased from 18 to 36 mm, i.e. an increase in the bolt diameter with a factor of 2.00, the shear resistance is increased with a factor of 4.04.

Hence, the shear resistance is in proportion of the square of the bolt diameter. Moreover, with an increase in the bolt diameter, the slippage corresponding to the shear resistance is increased, and the ultimate slippage is also increased.

b) The concrete damage distributions in those models with bolt diameters of 18, 24, and 36 mm are shown in Fig. 7.27. It is shown that slight compressive damage appears in the concrete blocks of the three models when the applied load is increased to 0.5 Q_m. With an increase in the bolt diameter, the damage area in the concrete block is increased proportionally.

c) The distributions of shear forces and concrete bearing forces in those models with bolt diameters of 18, 24, 30, and 36 mm are shown in Fig. 7.28. When the bolt diameter increases from 18 to 36 mm, the shear force at the root of the embedded nut is increased with a factor of 3.88, and the concrete bearing force acting onto the embedded bolt nut is decreased from 98% to 66% of the applied shear force.

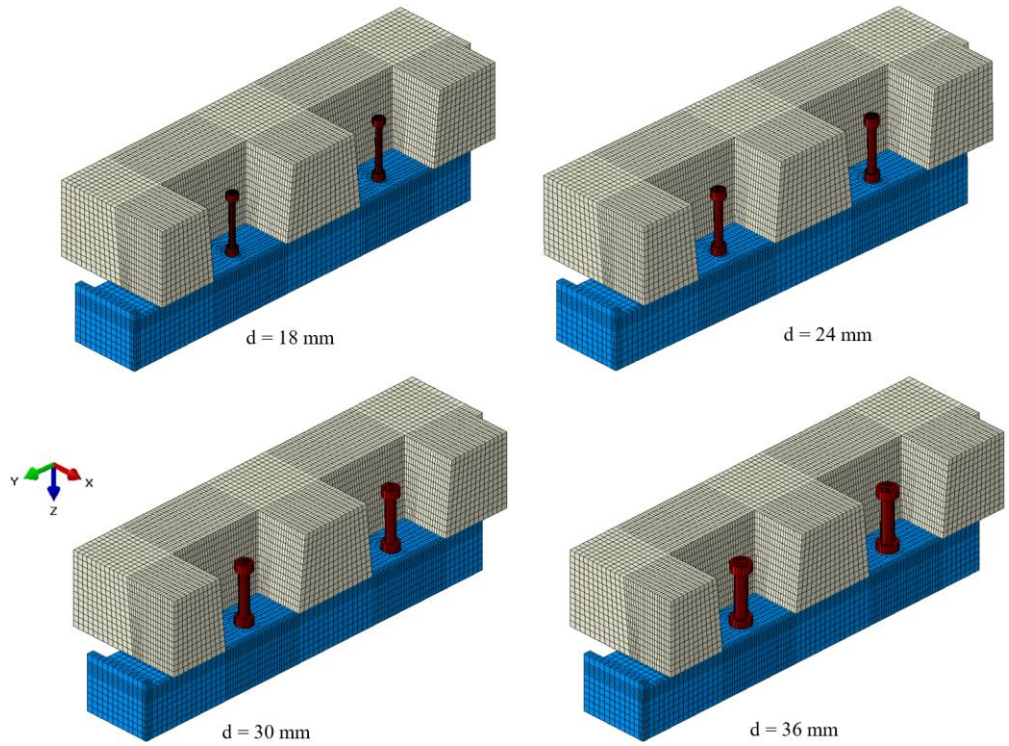

Note: Concrete blocks and steel reinforcements are omitted for clarity.

Fig. 7.25 Models with Connection R with various bolt diameters

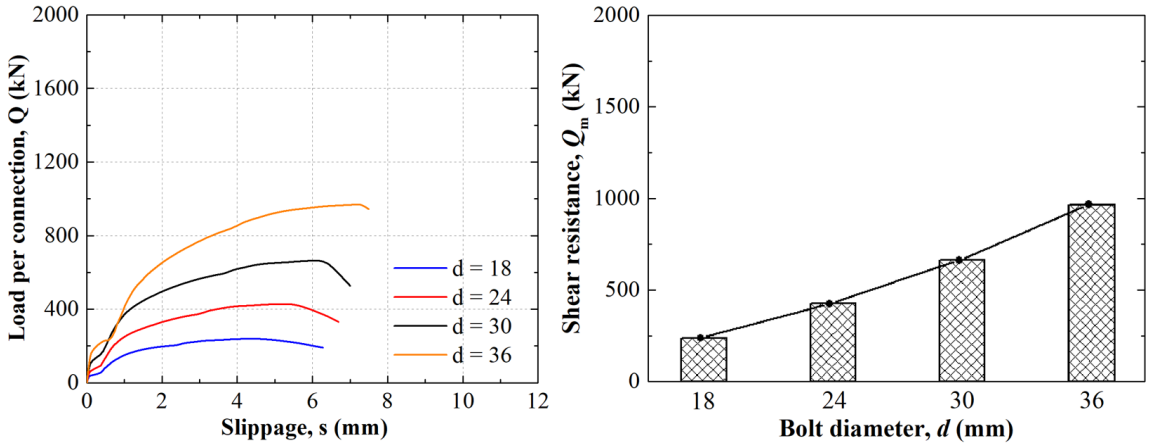

Fig. 7.26 Load-slippage curves of models with Connection R and various bolt diameters

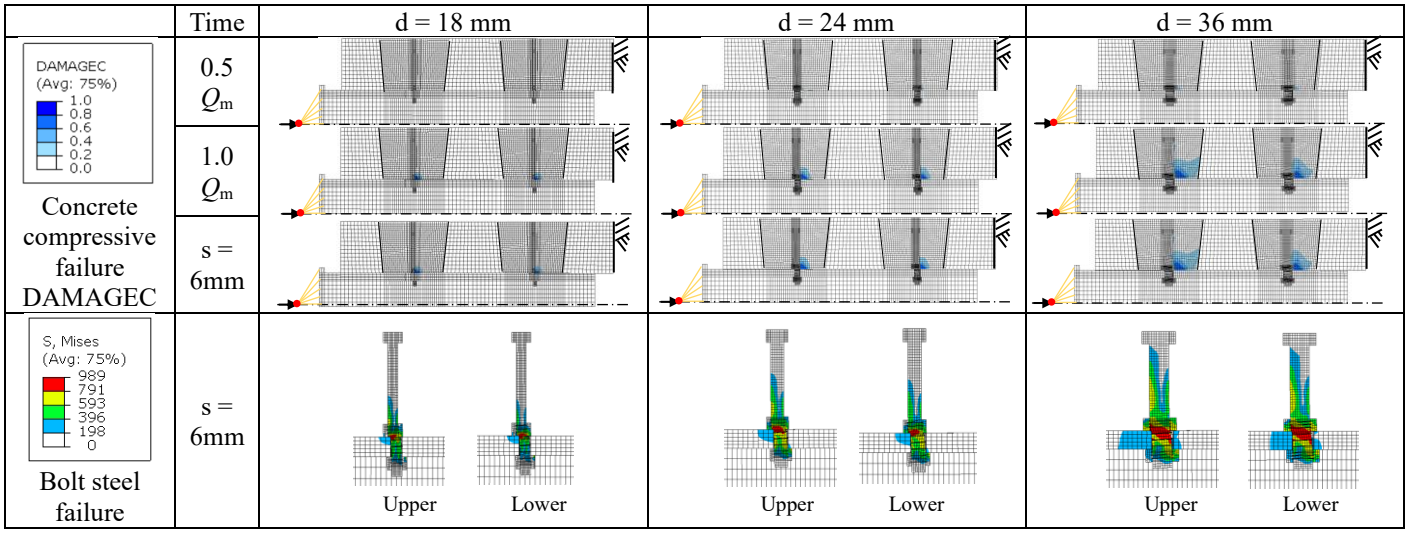

Fig. 7.27 Damage in models with Connection R and various bolt diameters

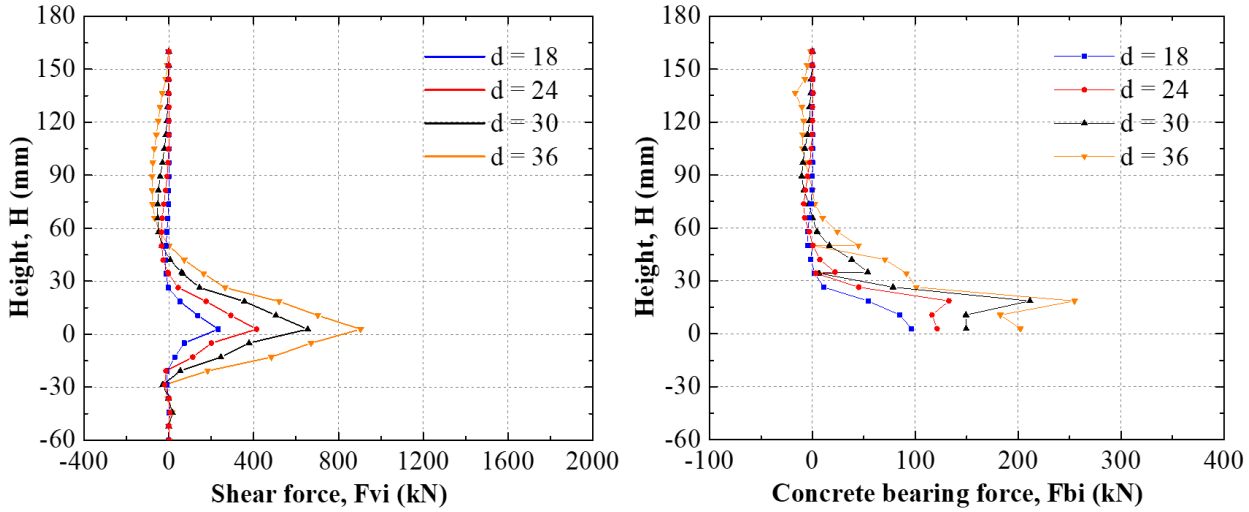

a) Distribution of shear force b) Distribution of concrete bearing force

Fig. 7.28 Internal force distributions in models with Connection R and various bolt diameters

7.3.2 Effect of bolt strength

Those models with bolt tensile strengths of 400, 500, 800, 1,000, and 1,200 N/mm^2, were developed to investigate the effect of bolt strength on the structural behaviour of Connection R. A total of five models were developed.

Key deformation characteristics are presented as follows:

a) Load-slippage curves of those models with various bolt strengths are plotted in Fig. 7.29. It is shown that when the tensile strength of the bolt is increased from 400 to 1200 N/mm^2, i.e. an increase in the bolt tensile strength with a factor of 3.00, the shear resistance is increased with a factor of 2.90. Hence, the shear resistance is approximately proportional to the tensile strength of the bolt. Moreover, with an increase in the bolt strength, the slippage corresponding to the shear resistance is increased, and the ultimate slippage is also increased.

b) The concrete damage distributions in those models with bolt tensile strengths of 400, 800, and 1200 N/mm^2 are shown in Fig. 7.30. It is shown that when the applied load is increased to 0.5 Q_m , slight compressive damage appears in those models with bolt tensile strengths of 800 and 1200 N/mm^2. With an increase in the bolt tensile strength, the damage area in the concrete block is increased proportionally.

c) The distributions of shear forces and concrete bearing forces in those models with bolt tensile strengths of 400, 800, and 1200 N/mm^2 are shown in Fig. 7.31. When the bolt tensile strength increases from 400 to 1200 N/mm^2, the shear force at the root of the embedded nut is increased with a factor of 3.00, and the concrete bearing force acting onto the bolt nut is decreased from 83% to 63% of the applied shear force.

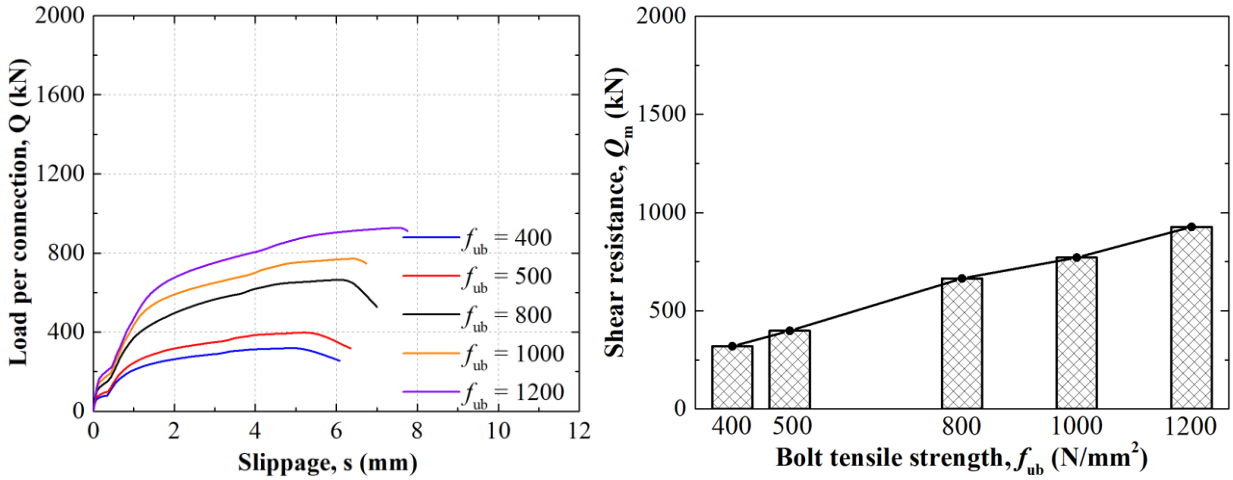

Fig. 7.29 Load-slippage curves of models with Connection R and various bolt strengths

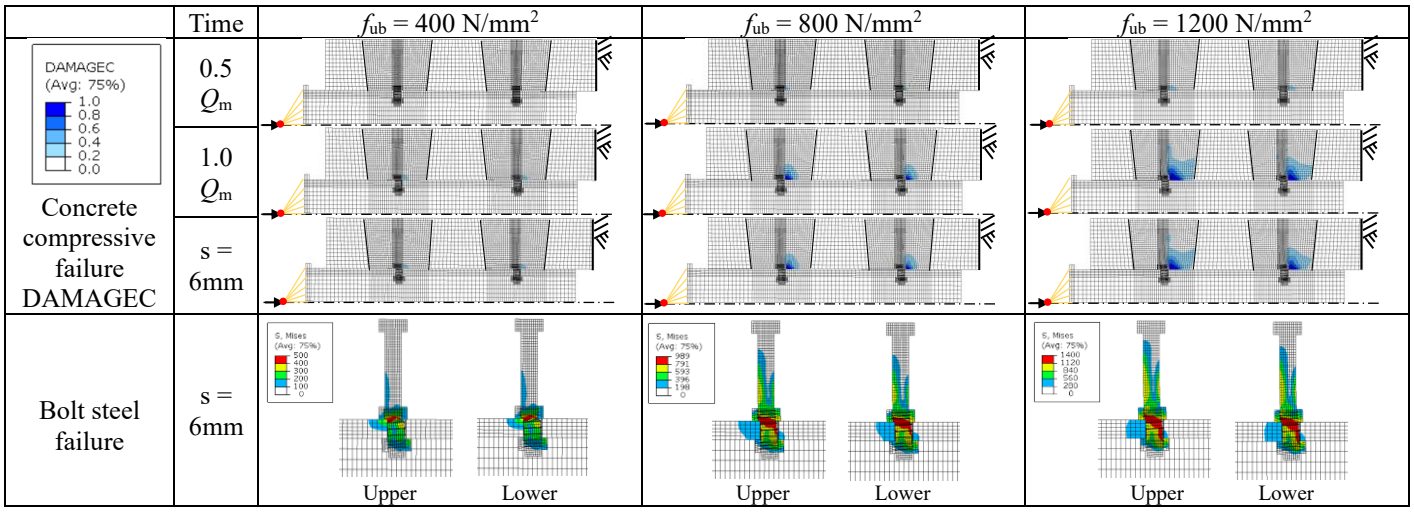

Fig. 7.30 Damage in models with Connection R and various bolt strengths

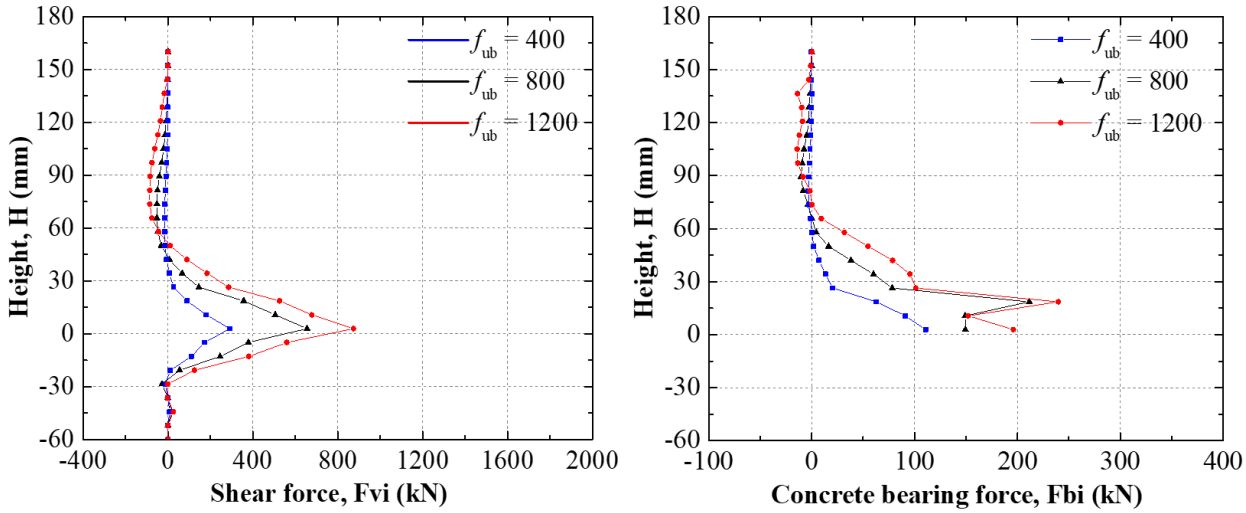

a) Distribution of shear force b) Distribution of concrete bearing force

Fig. 7.31 Internal force distributions in models with Connection R and various bolt strengths

7.3.3 Effect of concrete block strength

Those models with compressive strengths of the concrete blocks ranging from 40 to 120 N/mm^2 at 10 N/mm^2 intervals were developed to investigate the effect of concrete block strength on the structural behaviour of Connection R. A total of nine models were developed.

Key deformation characteristics are presented as follows:

a) Load-slippage curves of those models with various strengths of concrete blocks are plotted in Fig. 7.32. It is shown that when the strength of the concrete block is increased from 40 to 60 N/mm^2, the shear resistance is increased with a factor of 1.10, while when the strength of the concrete block is increased from 60 to 120 N/mm^2, the shear resistance is decreased with a factor of 0.98. Hence, the shear connection with the strength of the concrete block of 60 N/mm^2 and the steel fibre content of 1.5% is considered to be effective when the strength of the precast concrete slab is 50 N/mm^2.

b) The concrete damage distributions in those models with strengths of concrete blocks of 40, 80, and 120 N/mm^2 are shown in Fig. 7.33. It is shown that when the applied load is increased to 0.5 Q_m, concrete compressive damage appears in the concrete blocks of the models with concrete block strengths of 40 and 80 N/mm^2, while no apparent damage appears in the model with the concrete block strength of 120 N/mm^2. With an increase in the concrete block strength, the damage area in the concrete block is decreased correspondingly.

c) The distributions of shear forces and concrete bearing forces in those models with strengths of concrete blocks of 40, 80, and 120 N/mm^2 are shown in Fig. 7.34. With an increase in the concrete block strength, the shear force at the root of the embedded nut is increased, and the concrete bearing force acting onto the bolt nut is increased.

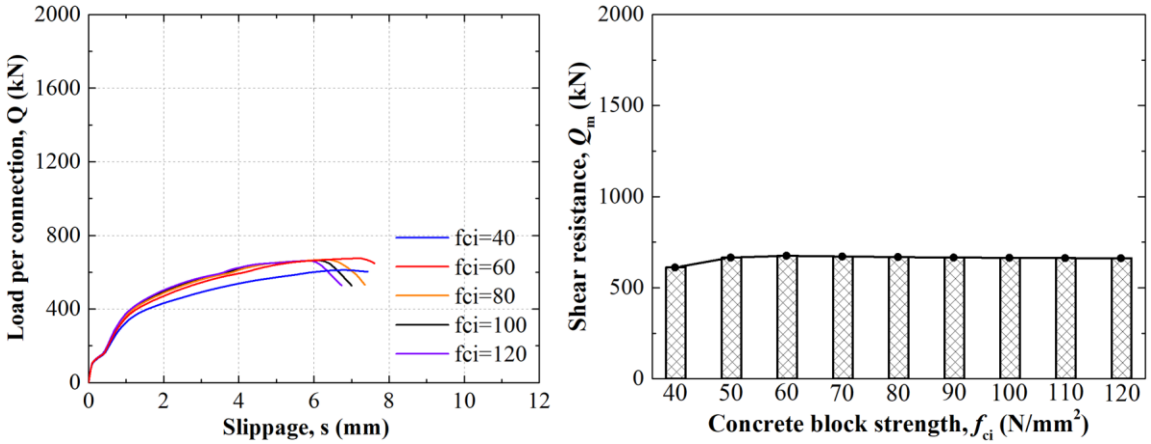

Fig. 7.32 Load-slippage curves of models with Connection R and various strengths of concrete blocks

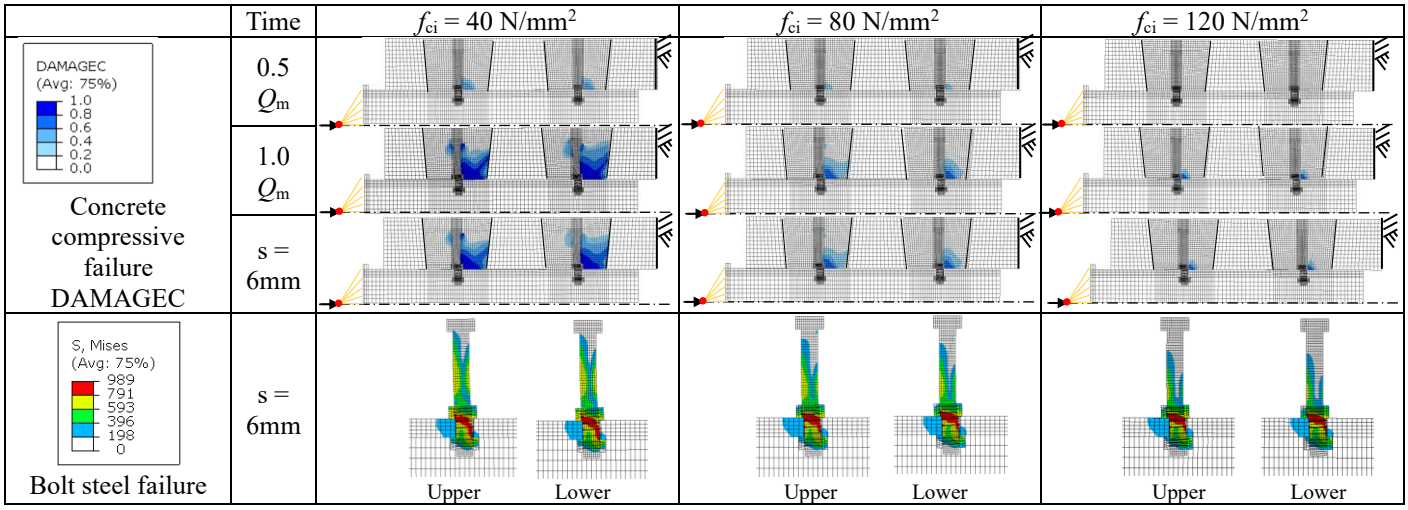

Fig. 7.33 Damage in models with Connection R and various strengths of concrete blocks

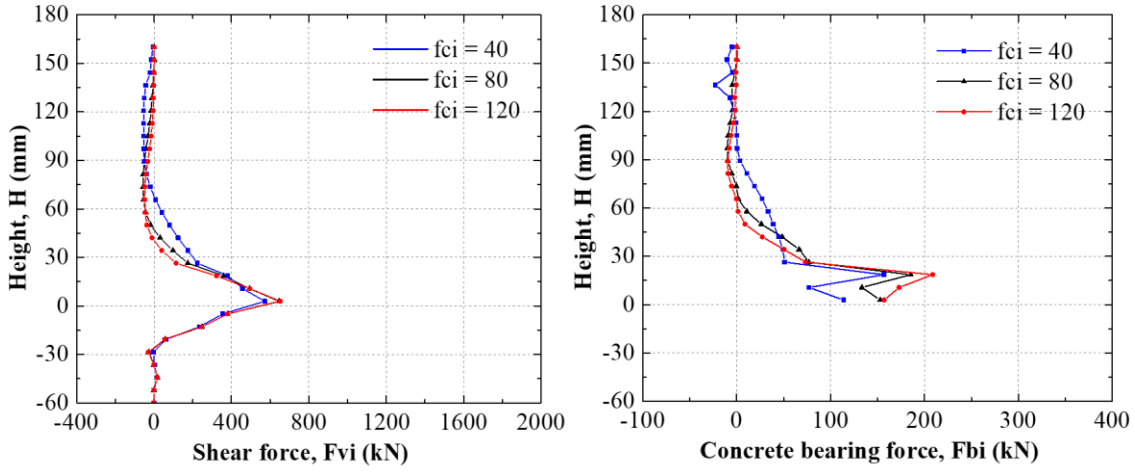

a) Distribution of shear force b) Distribution of concrete bearing force

Fig. 7.34 Internal force distributions in models with Connection R and various strengths of concrete blocks

7.3.4 Effect of concrete slab strength

Those models with compressive strengths of the precast concrete slabs ranging from 40 to 120 N/mm^2 at 10 N/mm^2 intervals were developed to investigate the effect of precast concrete slab strength on the structural behaviour of Connection R. A total of nine models were developed.

Key deformation characteristics are presented as follows:

a) Load-slippage curves of those models with various strengths of precast concrete slabs are plotted in Fig. 7.35. It is shown that when the strength of the precast concrete slab is increased from 40 to 120 N/mm^2, the shear resistance remains almost unchanged.

b) The concrete damage distributions in those models with strengths of precast concrete slabs of 40, 80, and 120 N/mm^2 are shown in Fig. 7.36. No apparent difference is found among the "stress and damage" distributions of the three models as the concrete damage appears primarily in the concrete blocks.

c) The distributions of shear forces and concrete bearing forces in those models with strengths of the concrete slabs of 40, 80, and 120 N/mm^2 are shown in Fig. 7.37. With an increase in the compressive strength of the precast concrete slab, the shear force at the root of the embedded nut as well as the concrete bearing force acting onto the bolt nut remain almost unchanged. Hence, the compressive strength of the precast concrete slab has minor influence on the structural behaviour of Connection R.

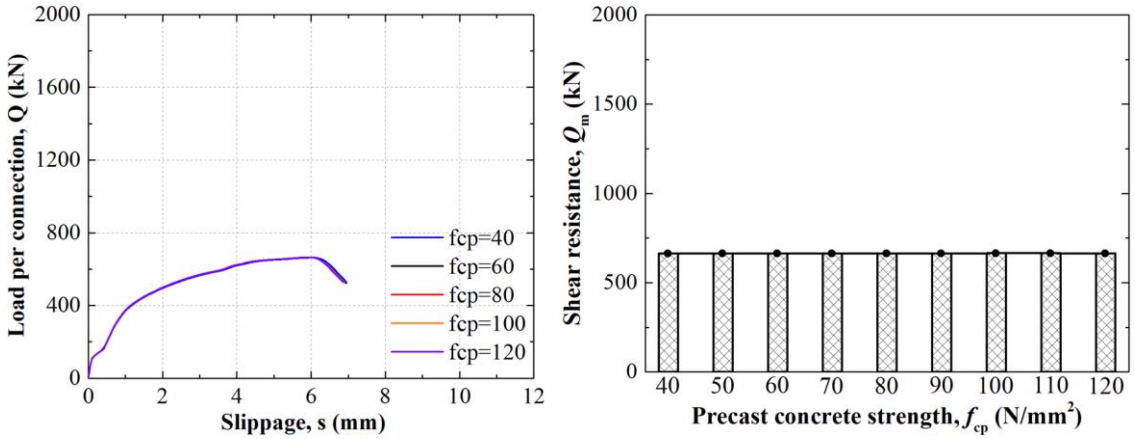

Fig. 7.35 Load-slippage curves of models with Connection R and various strengths of precast slabs

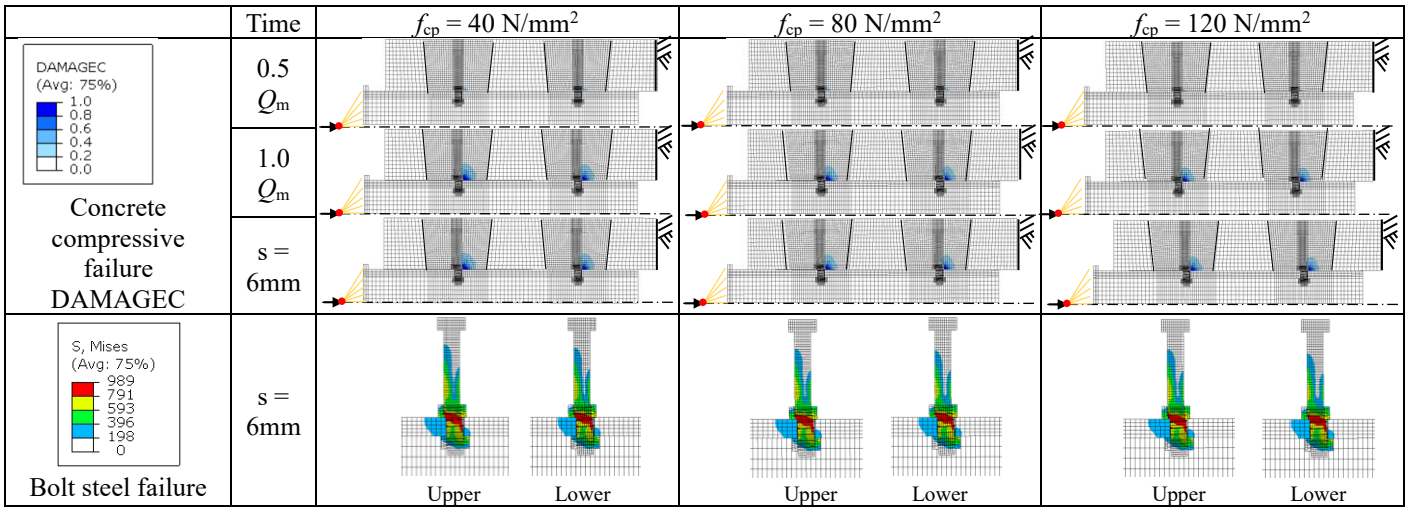

Fig. 7.36 Damage in models with Connection R and various strengths of precast slabs

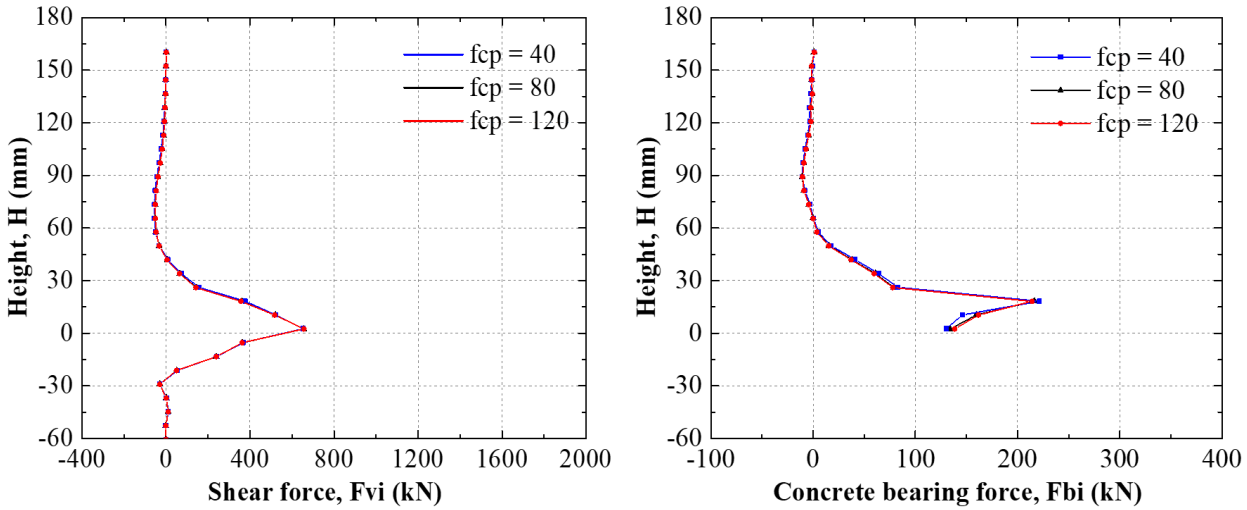

a) Distribution of shear force b) Distribution of concrete bearing force

Fig. 7.37 Internal force distributions in models with Connection R and various strengths of concrete slabs

Key results of the models with Connection R are summarised in Table 7.4. In general, with increases in bolt diameter, bolt strength, and concrete block strength, shear resistances of the shear connections are increased significantly, while when the concrete block strength exceeds 60 N/mm^2, the shear resistance is decreased slightly. Hence, the connection with a concrete block strength of 60 N/mm^2 is found to be effective when the bolt diameter is 30 mm. When the applied load is increased to 1.0 Q_m, compressive damage appears in the concrete blocks while no compressive damage appears in the precast concrete slabs. When the slippage is increased to 6 mm, the von Mises stresses of the bolt shanks in all the models reach the tensile strength.

7.3.5 Key findings of parametric studies

Based on the results of various parameters over practical ranges of values, it is found that:

- Among all these parameters, the most effective one is the diameter of the steel bolts, d . By increasing their values from 30 to 36 mm, the shear resistances of the shear connections are readily increased from 664.7 kN to 968.6 kN, i.e. by a factor of 1.46. Since the steel bolts are small in quantities, the increase in material costs is minimal. It should also be noted that a similar increase in shear resistances of the shear connections may be attained with an increase in their bolt strengths f_{ub} , i.e. from 800 to 1,200 N/mm^2, and the corresponding increase is from 664.7 to 927.5 kN though this depends heavily on availability of such a high strength bolt steel.
- By increasing the strengths of both the infilled concrete block, f_{ci} and the precast concrete slab f_{cp}, to their respective practical limits, there are only minimal increases, i.e. ≤ 5 % , in the shear resistances of the shear connections.

Table 7.4 Key results of the models with Connection R

Parameters		s_m (mm)	Q_m (kN)	***Ratio***	Q_{Rd} (kN)	η	Influence of various parameters: $F_{v,max}$ (kN)	***Ratio***	F_{bn} (kN)	λ (%)	Changing pattern of shear resistance
Bolt diameter, d (mm)	**18**	**4.3**	**239.6**	**1.00**	215.0	1.11	**233.0**	**1.00**	**235.2**	**98**	Increase
	24	5.2	428.4	1.79	395.4	1.08	414.0	1.78	370.1	86	
	30	6.1	664.7	2.77	628.3	1.06	655.0	2.81	510.1	77	
	36	7.2	968.6	4.04	893.2	1.08	905.0	3.88	639.6	66	
Bolt strength, f_{ub} (N/mm^2)	**400**	**4.9**	**319.8**	**1.00**	314.2	1.02	291.2	1.00	264.7	83	Increase
	500	5.2	398.2	1.25	392.7	1.01	383.2	1.32	341.1	86	
	800	6.1	664.7	2.08	628.3	1.06	655.0	2.25	510.1	77	
	1,000	6.4	771.3	2.41	777.3	0.99	756.8	2.60	551.0	71	
	1,200	7.5	927.5	2.90	777.3	1.19	873.6	3.00	588.0	63	
Infilled concrete block strength, f_{ci} (N/mm^2)	**40**	**6.81**	**611.8**	**1.00**	608.8	1.00	572.0	1.00	347.6	57	Increase
	50	7.94	665.8	1.09	628.3	1.06	-	-	-	-	
	60	7.18	675.9	1.10	628.3	1.08	640.2	1.12	452.4	67	
	70	6.68	671.6	1.10	628.3	1.07	-	-	-	-	
	80	6.37	668.7	1.09	628.3	1.06	646.0	1.13	471.6	71	
	90	6.15	666.1	1.09	628.3	1.06	-	-	-	-	Decrease
	100	6.09	664.7	1.09	628.3	1.06	655.0	1.15	510.1	77	
	110	5.92	663.1	1.08	628.3	1.06	-	-	-	-	
	120	5.92	662.1	1.08	628.3	1.05	652.0	1.14	538.7	81	
Precast concrete slab strength, f_{cp} (N/mm^2)	**40**	**6.05**	**664.0**	**1.00**	628.3	1.06	653.2	1.00	497.4	75	Unchanged
	50	6.09	664.7	1.00	628.3	1.06	655.0	1.00	510.1	77	
	60	6.03	664.6	1.00	628.3	1.06	-	-	-	-	
	70	6.04	664.8	1.00	628.3	1.06	-	-	-	-	
	80	6.03	664.9	1.00	628.3	1.06	655.6	1.00	510.2	77	
	90	6.01	665.0	1.00	628.3	1.06	-	-	-	-	
	100	5.99	665.1	1.00	628.3	1.06	-	-	-	-	
	110	5.99	665.2	1.00	628.3	1.06	-	-	-	-	
	120	5.94	665.0	1.00	628.3	1.06	656.8	1.01	514.4	77	

Notes:

Q_m denotes shear resistances predicted by numerical models;

s_m denotes slippages corresponding to the predicted shear resistances;

Ratio denotes the ratio of shear resistances of connections with various parameters to those of the reference connection;

Q_{Rd} denotes the design shear resistance predicted by the design method presented in Section 7.5.1 of this chapter;

η denotes a model factor,
$= Q_m / Q_{Rd}$;

f_{ub} denotes the tensile strength of the bolt steel; and

$F_{v,max}$ denotes the maximum shear force.

F_{bn} denotes the concrete bearing force acting onto the bolt nut; and

λ denotes proportion of shear force taken by the bolt nut,
$= F_{bn} / Q_m$.

7.4 Load transfer mechanisms

Based on the parametric analyses presented above, the load transfer mechanisms within Connections RBN and R are illustrated in Fig. 7.38. It is shown that:

a) For Connection RBN, the shear resistance is primarily provided by the welded steel block through bearing while a certain portion of the shear resistance is provided by the bolts through bearing and shear actions. It should be noted that based on the test data and the parametric results, the steel blocks are ready to take up about 50% to 90% of the applied shear forces, and these forces are highly related to the thickness T_b of the steel block, the bolt diameter d , and the width W_c of the concrete block.

   More specifically, as the bolts deform during slippage, large shear forces are induced in the two bolts which are then transferred to cause large bearing forces within the infilled concrete block in the vicinity of both the steel blocks and the steel nuts of the bolts. Local concrete crushing may take place at the bottom parts of the concrete blocks due to stress concentration. It should also be noted that tension forces are also induced in the bolt shanks of the two bolts due to a dowel action. Then, the applied shear forces are subsequently transferred from the concrete block through the action of the "***twin shear connection***" onto the precast concrete slab. Failure at the bottom parts of the precast concrete slab in the vicinity of the concrete block due to low concrete strengths is found to be typical.

b) For Connection R, the shear resistance is primarily provided by the bolts through bearing and shear actions. As the bolts deform during slippage, both shear and tension forces are induced in the bolt shanks of the two bolts due to a dowel action due to their limited stiffnesses. Large shear forces are then transferred to cause bearing forces at the bottom

parts of the infilled concrete block in the vicinity of the steel nuts of the bolts, and local concrete crushing may take place at the bottom parts of the concrete blocks due to stress concentration. Then, the applied shear forces are subsequently transferred from the concrete block through the action of the "twin shear connection" onto the precast concrete slab. Typical failure is the shear fracture of the bolts.

It should be noted that failure at the bottom parts of the precast concrete slab does not normally take place in the vicinity of the concrete block because of the low shear resistances of the shear connections, when compared with those of Connection RBN. Hence, the concrete strength of the precast concrete slab is found to have minimal effects on the shear resistances of the shear connections.

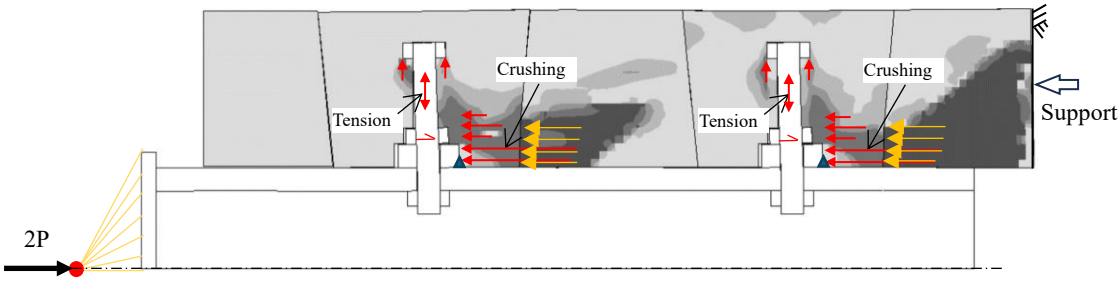

a) Connection RBN – ***Twin shear connection***
Typical shear connection = 1,300 kN

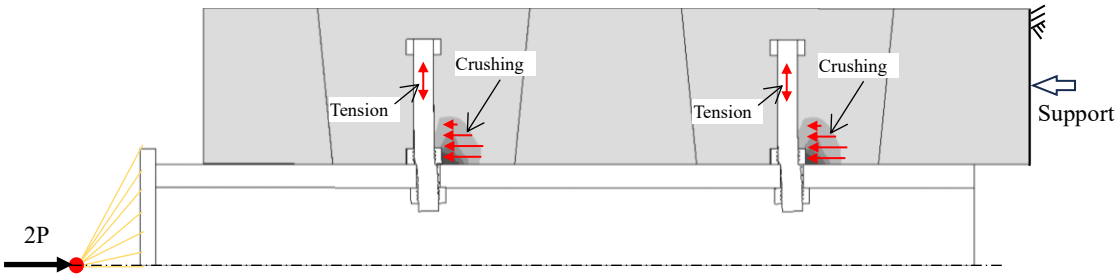

b) Connection R
Typical shear connection = 650 kN

Fig. 7.38 Load transfer mechanisms of Connections RBN and R

7.5 Development of design method

7.5.1 Shear resistances

Based on the numerical analyses and the parametric investigations into the structural behaviour of the bolted shear connections, a complementary design method is proposed for the shear resistance of the shear connections according to the load transfer mechanisms of the "***twin shear connections***" as described in Section 7.4. The shear connections should be checked against following:

- Concrete failure of concrete blocks;
- Shear fracture of bolts; and
- Concrete failure of precast concrete slabs.

The design shear resistances of the connections are denoted as Q_{Rd} , and determined as follows:

$$Q_{c12} = \eta_1 \bullet \eta_2 \bullet \min \{ Q_{c2}, Q_{sfb} \} \quad (7.1a)$$

$$Q_{Rd} = \min \{ Q_{c1} + Q_{c12}, Q_{c3} \} \quad (7.1b)$$

where

Q_{c1} is the concrete bearing resistance against a steel block;
Q_{c2} is the concrete bearing resistance against the two bolts;
Q_{sfb} is the shear resistance against shear fracture of the two bolts;
Q_{c3} is the bearing resistance of the precast concrete slab;
η_1 is a factor considering the effect of concrete block strength;
$= 23\ e^{-f_{cu,f}/20} + 0.97$
$f_{cu,f}$ is the cube compressive strength of the concrete block;
η_2 is a factor considering the effect of precast concrete strength;
$= (f_{cu}/50)^{0.51}$; and
f_{cu} is the cube compressive strength of the precast concrete slab.

a) The design shear resistances against concrete block failure of the proposed shear connection Q_{c1} and Q_{c2} are given by:

$$Q_{c1} = \alpha_1 f_{ck1} A_{c1} \quad (7.2a)$$

where

f_{ck1} is the characteristic concrete cylinder strength of concrete block;

α_1 $= \sqrt{A_{cp1}/A_{c1}}$

A_{c1} is the bearing area of the concrete in the vicinity of the steel block;

$= l_s\, h_s$; and

A_{cp1} is the projected bearing area of the concrete in the direction of loading, which is amplified by an inclination rate of 1:5 from the basic bearing area;

$= (l_s + 2e/5)\,(h_s + e/5)$

e_1 is the distance between the steel block and the concrete block, as shown in Fig. 7.39a).

$$Q_{c2} = 2\,\alpha_2\, f_{ck1}\, A_{c2}\, \eta_b \qquad (7.2b)$$

where

α_2 $= \sqrt{A_{cp2}/A_{c2}}$

A_{c2} is the bearing area of the concrete in the vicinity of a bolt;

$= l_{sb}\, h_{sb}$; and

A_{cp2} is the projected bearing area of the concrete in the direction of loading, which is amplified by an inclination rate of 1:5 from the basic bearing area;

$= (l_{sb} + 2e/5)\,(h_{sb} + e/5)$

e_2 is the distance between the steel bolt and the concrete block, as shown in Fig. 7.39b).

η_b is a factor considering the effective bolt length for bearing against the surrounding concrete, which is taken as 0.75 through regression analysis.

The schematic diagram of the bearing areas of both the steel block and the pair of bolts is shown in Fig. 7.39.

b) The design shear resistance of a pair of bolts Q_{sfb} is given by:

$$Q_{sfb} = 2\,A_b \times 0.7\, f_{ub} \qquad (7.3)$$

where:

A_b is the effective cross-sectional area of a bolt; and

f_{ub} is the tensile strength of the bolt.

c) The design shear resistance against the precast concrete slab failure Q_{c3} is given by:

$$Q_{c3} = \eta_3 l_s f_{ck2} [h_s + \int_0^{h_{sl}} (1 - \frac{x}{h_{s1}}) dx] \qquad h_{s1} = h_{slab} - h_s \qquad (7.4)$$

where

f_{ck2} is the characteristic concrete cylinder strength of the precast concrete slab;

l_s is the length of the steel block;

h_s is the thickness of the steel block;

h_{slab} is the thickness of the precast concrete slab; and

η_3 is a factor considering the effect of precast concrete strength on the resistance against the precast concrete slab failure.

$= 5.1 - 0.89 \text{ Ln } (1.13 f_{cu})$

The schematic diagram of the design resistance against the precast concrete slab failure is shown in Fig. 7.39 c). It is assumed that on the critical failure section of the precast concrete slab, the stress of the concrete remains at f_{ck2} within the heigh of the steel block and then decreases linearly to 0 at the top surface of the concrete slab.

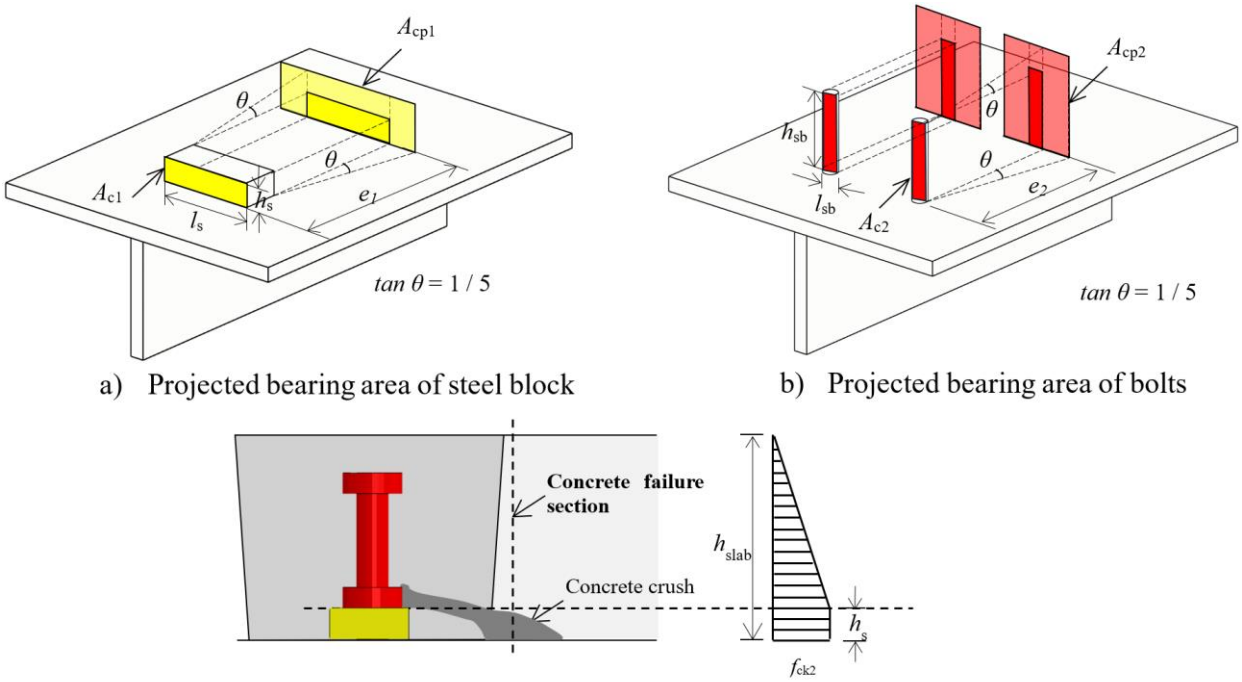

a) Projected bearing area of steel block

b) Projected bearing area of bolts

c) Failure of concrete slab

Fig. 7.39 Schematic diagram of the design method

In order to assess structural adequacy and efficiency of this design method, a model factor η is established, which is defined as follows:

$$\eta = Q_{Rt} / Q_{Rd}$$

The values of η for these shear connections are presented in Table 7.5. It should be noted that all the test data and results of the standard push-out tests are presented in Chapter 4. The values of η range from 1.00 to 1.12. The average variation is 1.04, and the standard deviation coefficient is 0.038. It is demonstrated that the proposed design method is able to predict the shear resistances of the test specimens with good accuracy.

Table 7.5 Comparison of the design and the measured shear resistances

Model	Q_{Rt} (kN)	Concrete failure of concrete block							Shear fracture of bolts			Concrete failure of concrete slab		Q_{Rd} (kN)	η
		f_{ck1} (N/mm^2)	A_{c1} (mm^2)	A_{cp1} (mm^2)	Q_{c1} (kN)	A_{c2} (mm^2)	A_{cp2} (mm^2)	Q_{c2} (kN)	A_b (mm^2)	f_{ub} (N/mm^2)	Q_{sfb} (kN)	f_{ck2} (N/mm^2)	Q_{c3} (kN)		
A-1-W-a	1,594.0	95.1	6,000	10,672	761	3,047	7,634	688	707	828	819	58.0	**1,593**	**1,593**	1.00
A-1-W-b	1,563.8	93.6	6,000	10,672	749	3,047	7,634	677	707	828	819	55.0	**1,563**	**1,563**	1.00
A-1-N-a	1,295.0	90.7	6,000	7,632	**614**	3,314	5,034	**556**	707	828	819	51.7	1,525	**1,306**	0.99
A-1-N-b	1,329.8	88.0	6,000	7,632	**595**	3,314	5,034	**539**	707	828	819	51.2	1,519	**1,275**	1.04
A-2-W-a	1,999.8	94.0	10,000	15,312	1,163	2,512	6,460	568	707	770	762	64.6	**1,797**	**1,797**	1.11
A-2-W-b	1,989.8	91.1	10,000	15,312	1,038	2,512	6,460	676	707	770	762	64.4	**1,795**	**1,795**	1.11
A-2-N-a	1,829.5	95.4	10,000	11,872	**1,039**	2,780	4,260	**492**	707	770	762	50.7	1,645	**1,634**	1.12
A-2-N-b	1,562.8	87.5	10,000	11,872	**953**	2,780	4,260	**452**	707	770	762	50.4	1,640	**1,520**	1.03
A-3-W-a	1,507.0	85.4	6,000	10,672	**683**	3,047	7,634	**618**	707	828	819	55.0	1,563	**1,501**	1.00
A-3-W-b	1,393.8	76.1	6,000	10,672	**609**	3,047	7,634	**551**	707	828	819	55.0	1,563	**1,400**	1.00
B-1-W-a	1,439.5	92.0	6,000	10,672	**737**	2,417	6,916	**564**	452	929	588	40.1	1,361	**1,361**	1.06
B-1-W-b	1,282.5	83.9	6,000	10,672	**671**	2,417	6,916	**514**	452	929	588	40.1	1,361	**1,271**	1.01
B-1-N-a	1,259.3	97.1	6,000	7,632	**657**	2,629	4,316	**491**	452	929	588	47.1	1,467	**1,226**	1.03
B-1-N-b	1,187.0	89.7	6,000	7,632	**607**	2,629	4,316	**453**	452	929	588	49.0	1,491	**1,162**	1.02
B-3-W-a	1,254.0	75.0	6,000	10,672	**600**	2,417	6,916	**460**	452	929	588	42.4	1,397	**1,197**	1.05
B-3-W-b	1,373.5	80.9	6,000	10,672	**647**	2,417	6,916	**496**	452	929	588	42.4	1,397	**1,254**	1.10
C-0-W-a	708.8	84.6	-	-	-	4,242	10,298	851	552	912	**705**	49.2	1,300	**705**	1.01
C-0-W-b	725.8	79.8	-	-	-	4,242	10,298	839	552	912	**705**	53.0	1,339	**705**	1.03

In order to further demonstrate accuracy of the proposed design method for the connections with various bolt diameters, steel block thicknesses, concrete block strengths and precast concrete strengths, the parametric results presented in Sections 7.2 and 7.3 are plotted onto Fig. 7.40

together with the design resistances obtained with the proposed design method. A model factor η is defined as the ratio of the predicted to the design shear resistance to assess structural efficiency of the proposed design method, and the values of η are summarised in Tables 7.1 and 7.2. It is shown that:

- In models with Connection RBN, the average value of η is 1.02, and the standard deviation coefficient is 0.04.
- In models with Connection R, the average value of η is 1.06, and the standard deviation coefficient is 0.03.

Hence, it is demonstrated that the proposed design method is applicable to both Connections RBN and R for accurate prediction of their shear resistances.

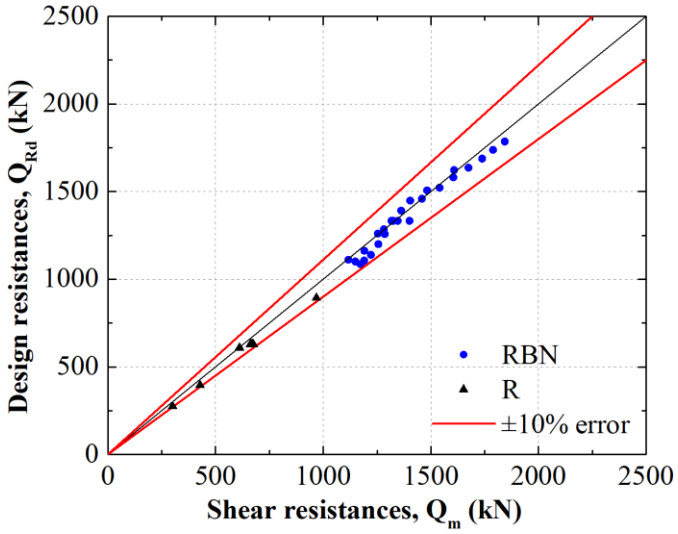

Fig. 7.40 Evaluation of the proposed design method

7.5.2 A work example for the shear resistance of a shear connection

Work example:

Please predict the shear resistance of a shear connection with Connector RBN. The dimensions and strengths of the shear connection are presented as follows:

Dimensions of the steel block: $200 \times 80 \times 35$ mm

Diameter of the Grade 8.8 bolt, d:	36	mm
Bolt height, h_b:	160	mm
Thickness of the precast concrete slab, h_{slab}	200	mm
Dimensions of the infilled concrete block:	270×200×200	mm
Compressive strength of the concrete block, $f_{cu,f}$:	120	N/mm^2
Compressive strength of the precast concrete slab, f_{cu} :	60	N/mm^2

Solution:

According to Section 7.5.1, the design shear resistance Q_{Rd} is determined as follows:

$$Q_{c12} = \eta_1 \bullet \eta_2 \bullet \min \{ Q_{c2}, Q_{sfb} \} \quad (7.1a)$$

$$Q_{Rd} = \min \{ Q_{c1} + Q_{c12}, Q_{c3} \} \quad (7.1b)$$

Dimensions:

Length of the steel block, l_s :	200	mm
Height of the steel block, h_s :	35	mm
Distance between the steel and the concrete block, e_1:	60	mm
Bolt height excluding the steel block thickness, h_{sb} :	125	mm
Effective cross-sectional area of a bolt, A_b :	817	mm^2
Effective bolt diameter, d_e / l_{sb} :	32.3	mm

Concrete strengths:

Characteristic strength of the concrete block, f_{ck1}:	106.6	N/mm^2
Characteristic strength of the precast concrete slab, f_{ck2}	47.5	N/mm^2
Tensile strength of the bolt, f_{ub}	800	N/mm^2

Bearing area of the concrete block against steel block, A_{c1}:

$A_{c1} = l_s h_s = 200 \times 35 = 7{,}000$ mm^2

Projected area of the concrete in the direction of loading, A_{cp1}:

$A_{cp1} = (200 + 2 \times 60 / 5) \times (35 + 60 / 5) = 10{,}528$ mm^2

$\alpha_1 = \sqrt{A_{cp1}/A_{c1}} = 1.23$

$Q_{c1} = \alpha_1 f_{ck1} A_{c1}$ = 917.8 kN

η_1 = 23 $e^{-f_{cu,f}/20}$ + 0.97 = 1.03

η_2 = $(f_{cu}/50)^{0.51}$ = 1.10

A_{c2} = 3,645 mm^2

A_{cp2} = 7,032 mm^2

α_2 = 1.39

$Q_{c2} = 2\ \alpha_2 f_{ck1} A_{c2} \eta_b$ = 810.1 kN

$Q_{sfb} = 2\ A_b \times 0.7 f_{ub}$ = 915.0 kN

$Q_{c12} = \eta_1 \cdot \eta_2 \cdot \min \{ Q_{c2}, Q_{sfb} \} = 1.03 \times 1.10 \times \min \{810.1, 915.0\}$ = 917.8 kN

$\eta_3 = 5.1 - 0.89\ \mathrm{Ln}\ (1.13 f_{cu})$ = 1.35

$h_{s1} = h_{slab} - h_s = 200 - 35 = 165$ mm

$Q_{c3} = \eta_3 l_s f_{ck2} [\ h_s + \int_0^{h_{sl}} (1 - \frac{x}{h_{s1}}) dx\ ]$ = 1,506.9 kN

Q_{Rd} = min { $Q_{c1} + Q_{c12}, Q_{c3}$} = min {917.8 +917.8, 1,506.9 } = 1,506.9 kN

Hence, the shear resistance of this shear connection is 1,506.9 kN.

7.5.3 Simplified load-slippage curves

As shown in Chapter 5.3, the simplified load-slippage curves are readily applicable to those shear connections within the following parameter range:

a) Steel bolts and studs
   - Diameter of bolts = 19 to 30 mm
   - Yield strength of steel = 350 to 630 N/mm^2
   - Tensile strength of steel = 450 to 930 N/mm^2

b) Steel blocks

- Dimension L = 120 to 200 mm
- Dimension W = 60 to 80 mm
- Dimension T_b = 30 to 50 mm

c) Concrete blocks

- Compressive cube strength, $f_{cu,150}$ = 50 to 120 N/mm^2

d) Concrete slabs

- Compressive cube strength, $f_{cu,150}$ = 40 to 72 N/mm^2

In order to extend applicability of the proposed load-slippage curves of Connections RBN and R, the parametric results presented in Sections 7.2 and 7.3 are used for regression analysis on the values of α, β and k, and they are improved as follows:

e) Connection RBN

- $\alpha = 2.5*(f_{cu,f}/100)^{0.5}*(50/f_{cu})^{0.3}$, $\beta = 1.0$ and $k = -0.03$

where

$f_{cu,f}$ is the cube compressive strength of the concrete block; and

f_{cu} is the cube compressive strength of the precast concrete slab.

f) Connection R

- $\alpha = 0.9$, $\beta = 1.0$ and $k = -0.05$, when bolt diameter is smaller than 30 mm, and the bolt grade is lower than G8.8; and
- $\alpha = 0.6$, $\beta = 1.0$ and $k = -0.05$, for the other cases.

After a rigorous regression analysis on all the parametric results presented in Sections 7.2 and 7.3, the value of Ψ is found to be 0.99. The simulated curves are plotted as dotted lines, and the simplified load-slippage curves of the corresponding shear connections are plotted onto the same graphs for comparison, as shown in Fig. 7.41. It is shown that the simplified representation matches reasonably well with the simulated curves in both the ascending and the descending parts.

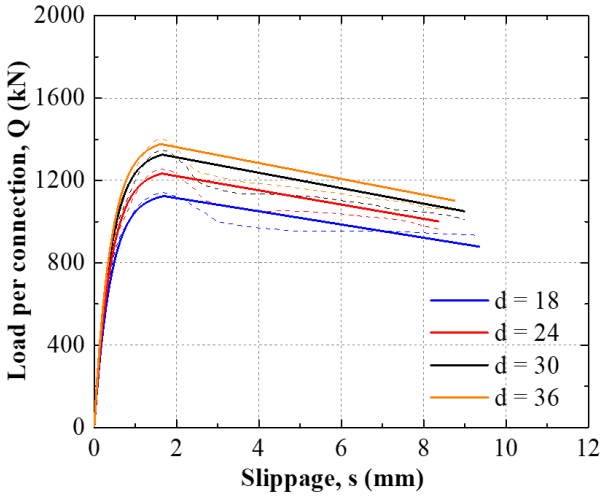

a) Connection RBN with various bolt diameters

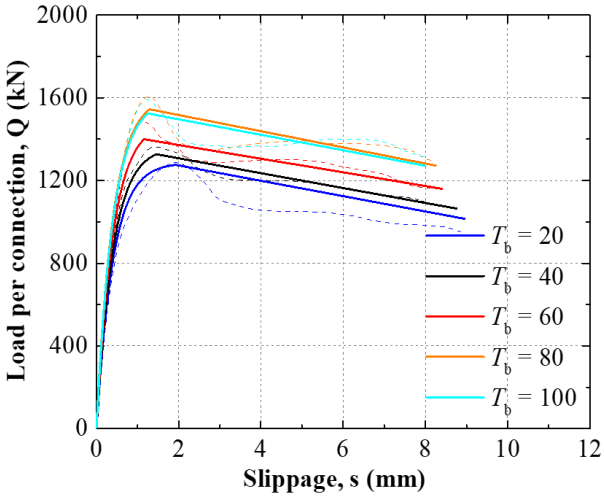

b) Connection RBN with various thicknesses of steel blocks

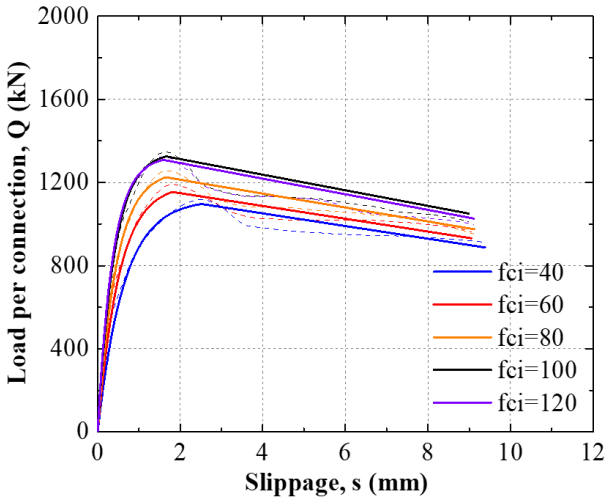

c) Connection RBN with various strengths of concrete blocks

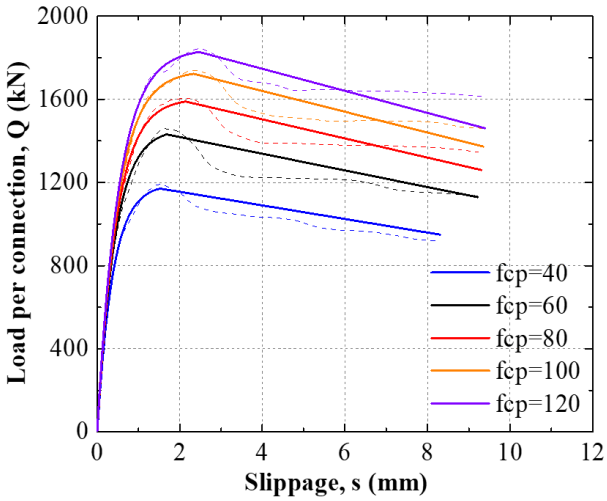

d) Connection RBN with various strengths of concrete slabs

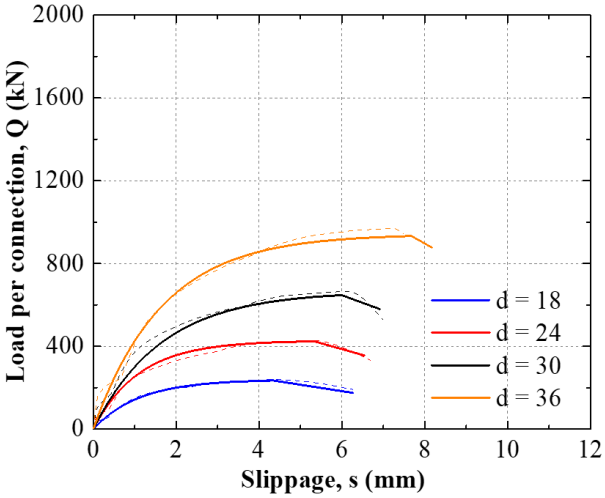

e) Connection R with various bolt diameters

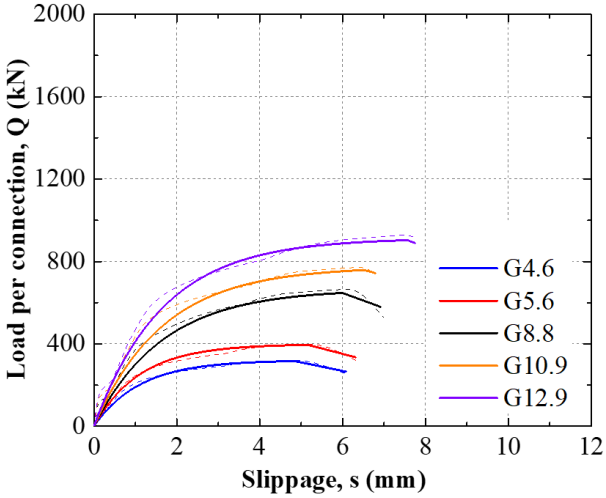

f) Connection R with various bolt strengths

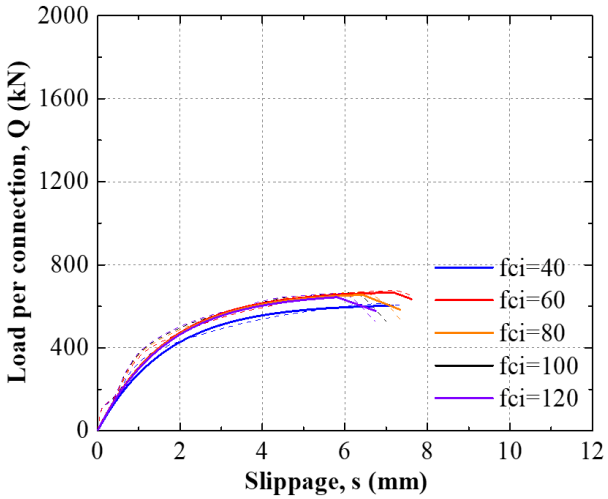

g) Connection R with various strengths of concrete blocks

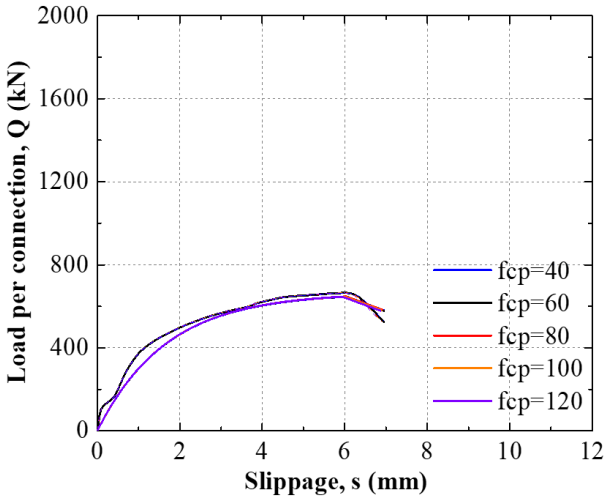

h) Connection R with various strengths of concrete slabs

Fig. 7.41 Comparison of simulated and simplified load-slippage curves

Consequently, the simplified load-slippage curves are considered to be effective for those connections with the following parameters:

a) Steel bolts

- Diameter of bolts = 18 to 36 mm
- Yield strength of steel = 240 to 1,080 N/mm^2
- Tensile strength of steel = 400 to 1,200 N/mm^2

b) Steel blocks

- Dimension L = 120 to 200 mm
- Dimension W = 60 to 80 mm
- Dimension T_b = 20 to 100 mm

c) Concrete blocks

- Compressive cube strength, $f_{cu,150}$ = 40 to 120 N/mm^2

d) Concrete slabs

- Compressive cube strength, $f_{cu,150}$ = 40 to 120 N/mm^2

7.6 Calibration of the simplified load-slippage curves

In order to access effectiveness of the proposed simplified load-slippage curves for applications

to high-strength steel-concrete composite beams, a total of three practical composite beams with full and partial shear connections are numerically simulated. Beam tests on the bending behaviour of these high-strength steel-concrete composite beams with various degrees of shear connectors conducted by Xiong *et al*. (2022) are used for numerical analyses. Both the measured and the simulated "stress and damage" distributions, the load-deflection curves, and the deformation characteristics of the composite beams are compared for validation of the proposed load-slippage curves. After that, the load-slippage curves of two pairs of shear connections are analysed to illustrate the structural behaviour of these connections.

Key areas of interest are described as follows:

i) To assess feasibility of using connector elements to simulate the structural behaviour of the shear connections in composite beams;

ii) To assess effectiveness of the proposed load-slippage curves for the shear connections.

iii) To investigate the structural behaviour of the shear connections along the beam span.

7.6.1 Brief introduction of the practical beam tests

The bending behaviour of high strength steel-precast concrete slab composite beams (HSS-PCS) with steel block shear connections (SBSCs) were tested under a concentrated load. The dimensions of the HSS-PCS are shown in Fig. 7.42. The loading and support conditions of the HSS-PCS are shown in Fig. 7.43. The dimensions of the SBSC are 160×60×60 (L×W×H), and they are provided at regular spacings *s* along the steel beams. The dimensions of the concrete blocks in the precast concrete slabs are 230×160×120 (L×W×H). The Q690 steel with yield and tensile strengths of 695 and 725 N/mm^2 was used in all the three steel beams. C50 concrete with a cube compressive strength of 55.7 N/mm^2 was used in the precast concrete slabs. High strength steel fibre reinforced concrete with a cube compressive strength of 91.4 N/mm^2 was used in the

concrete blocks. Table 7.6 summarises the test programme of the beam tests.

Table 7.6 Test programme of the beam tests

Test	Spacing of shear connections s (mm)	Degree of shear connection η	Panel width x_1 (mm)	Panel width x_2 (mm)
L50-690-350	350	1.0	1,425	1,050
L50-690-560	560	0.71	1,040	1,120
L50-690-700	700	0.61	1,250	1,400

Two typical failure modes were identified in the tests: i) Concrete crushing at the mid-span; and ii) Failure of shear connectors. In Test L50-690-350 with full shear connections, when the applied load reached the peak load, extensive concrete crushing was found at the mid-span of the concrete slab, and then, the applied load was reduced slowly. In Tests L50-690-560 and L50-690-700 with partial shear connections, when the applied load reached about 0.9 times the peak load, the concrete at the bottom of the concrete slabs near the concrete blocks spalled. Oblique concrete cracks with an angle of 45° were found on the surfaces of the precast concrete slabs. When the applied load reached peak load, the concrete block was crushed and the studs in the SBSCs were sheared off. The load-deflection curves of the beams are shown in Fig. 7.44. When the connection degree is decreased from 1.0 to 0.71, the moment resistance is decreased correspondingly with a factor of 0.81 while its flexural rigidity remains unchanged. When the connection degree is decreased from 0.71 to 0.61, the moment resistance remains approximately unchanged while the flexural rigidity is decreased with a factor of 0.92.

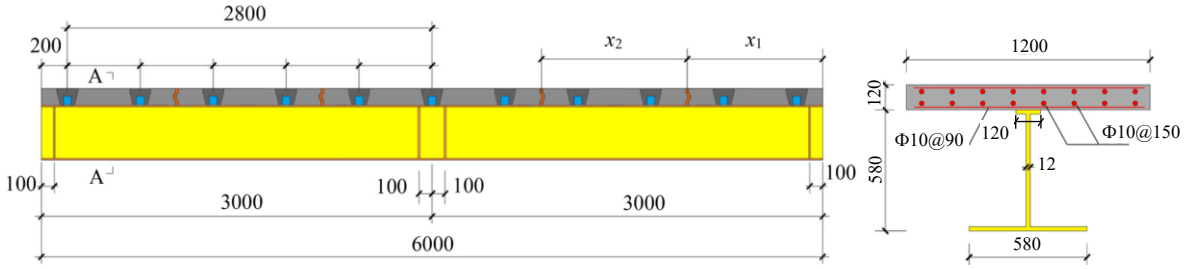

Fig. 7.42 Typical dimensions of Beams HSS-PCS

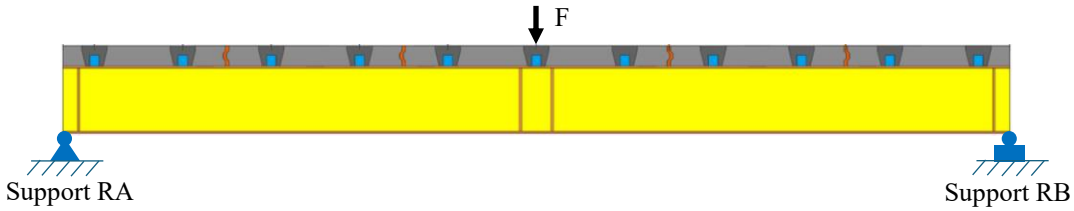

Fig. 7.43 Loading and support conditions of Beams HSS-PCS

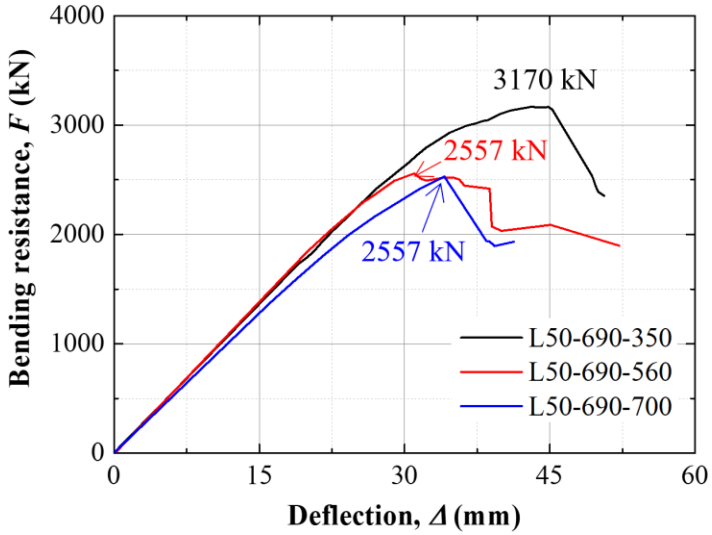

Fig. 7.44 Load-deflection curves of the composite beams

7.6.2 Development of numerical models

Numerical models of the three composite beams are illustrated in Fig. 7.45. The concrete slab, the steel beam, as well as the stiffeners are modelled with solid elements C3D8R, while the steel reinforcements in the concrete slab are modelled with truss element T3D2.

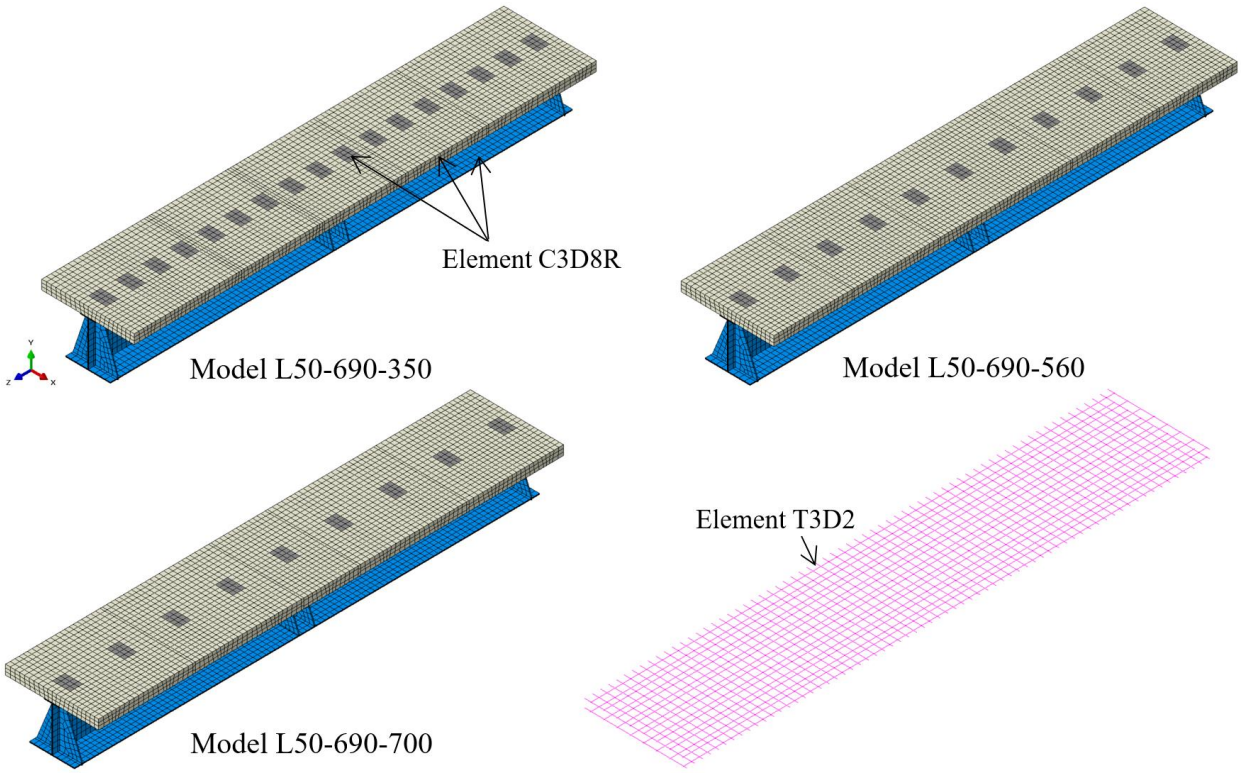

Fig. 7.45 Three-dimensional numerical models of the composite beams

a) Boundary conditions and interactions

The boundary conditions of typical model are illustrated in Fig. 7.46. A loading jack is used for application of the concentrated load, and all the nodes along the top surface of the loading plate are coupled as a reference point to apply a vertical load onto the composite beam. The supports at both beam ends are modelled as rollers, and they are connected to the steel beam using surface-to-surface contacts. All translational displacements of Support RA are fully fixed, while the displacements along the X- and Y- axes of Support RB are constrained to zero, and its displacement along the Z-axis is free to move.

Steel stiffeners are connected to the flanges and the web of the steel beams through tied constraints, and the nodal deformations of the stiffener surfaces and the beam surfaces are assigned to be the same. The bottom surface of the concrete slabs and the concrete blocks are connected to the top surface of the steel beam using hard contacts, and the friction coefficient is taken as 0.4. The surfaces of the concrete blocks are also connected to those of the concrete slabs with hard contacts, and the friction coefficient is also taken as 0.4. Steel reinforcements are fully embedded into the concrete slab, and they are required to deform together with the surrounding concrete elements through constrained deformations of specific nodes of their meshes.

To simulate the structural behaviour of the shear connectors between the concrete slab and the steel beam, the bottom surfaces of the concrete blocks and the corresponding top surfaces of the beam flange are linked up using connector elements at regular spacings in Abaqus.

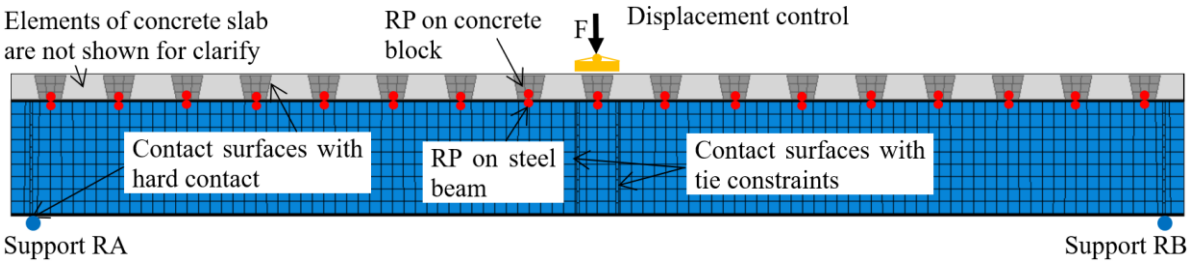

Fig. 7.46 Boundary conditions and interactions

b) Material properties

- Steel beams and reinforcements

  A tri-linear stress-strain model is adopted to simulate the mechanical properties of the steel beams, and a bi-linear model is adopted to simulate the mechanical properties of the steel reinforcements. The elastic modulus E_s is taken as 210 kN/mm^2 while the strain hardening modulus is taken as 0.01 E_s.

- Concrete materials

  The concrete constitutive models presented in Chapter 6 are adopted to simulate the

mechanical properties of NC in the precast concrete slabs and SFRC in the concrete blocks.

c) Connection models

Element CONN3D2 is used to simulate the structural behaviour of the shear connections in the composite beams. Basic connection components are adopted, and all the three rotational displacements of the connections are restrained to zero. The translational displacements along the X- and Y- axes are restrained, and the simplified load-slippage curves proposed in Section 7.5 are used to describe the non-linear behaviour of the shear connections along the Z-axis. It should be noted that the shear resistance of the connection is determined by Eq. (5.6) while the input load-slippage curve of the connection derived according to the proposed simplified load-slippage described in Section 7.5.2 is shown in Fig. 7.47.

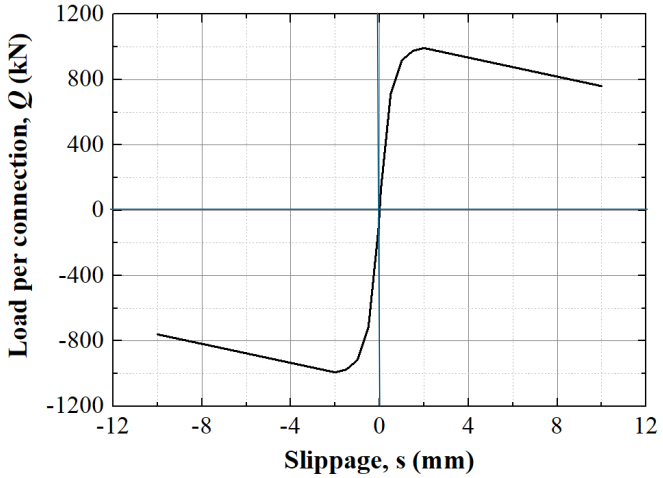

Fig. 7.47 Non-linear behaviour of shear connections

7.6.3 Assessment of the simulation results

The simulation results are used to provide further insights into the structural behaviour of the composite beams and the failure modes, and both the load-deflection curves and the deformation characteristics are compared with the test results. It should be noted that

a) Stress and damage conditions of the concrete slabs and the shear connections

Fig. 7.48 illustrates the contour plots of the von Mises stresses of the steel beams, the principal stresses of the concrete slabs, and the tensile damage within the concrete blocks at peak loads. It should be noted that when the von Mises stress exceeds 698 N/mm^2, the steel is considered to have yielded. When the normal stresses of the precast concrete slabs exceed 50 N/mm^2, the concrete is conservatively considered to have crushed. Moreover, when the normal stresses of the infilled concrete blocks exceed 90 N/mm^2, the concrete is conservatively considered to have crushed. When its tensile damage reaches 1.0, the concrete is also considered to have failed.

It should also be noted that in Model L50-690-350, the normal stresses of the concrete at the mid-span of the precast slab exceeds 50 N/mm^2, which correlates well with the concrete crushing under large compression due to global bending action in the test. However, owing to partial shear connection in Model L50-690-700, only slight local concrete crushing is found at the mid-span of the model. In addition, extensive concrete cracking under tension actions is found in the concrete blocks of both Models L50-690-350 and L50-690-700, and this failure pattern is similar to the concrete cracking observed in the tests.

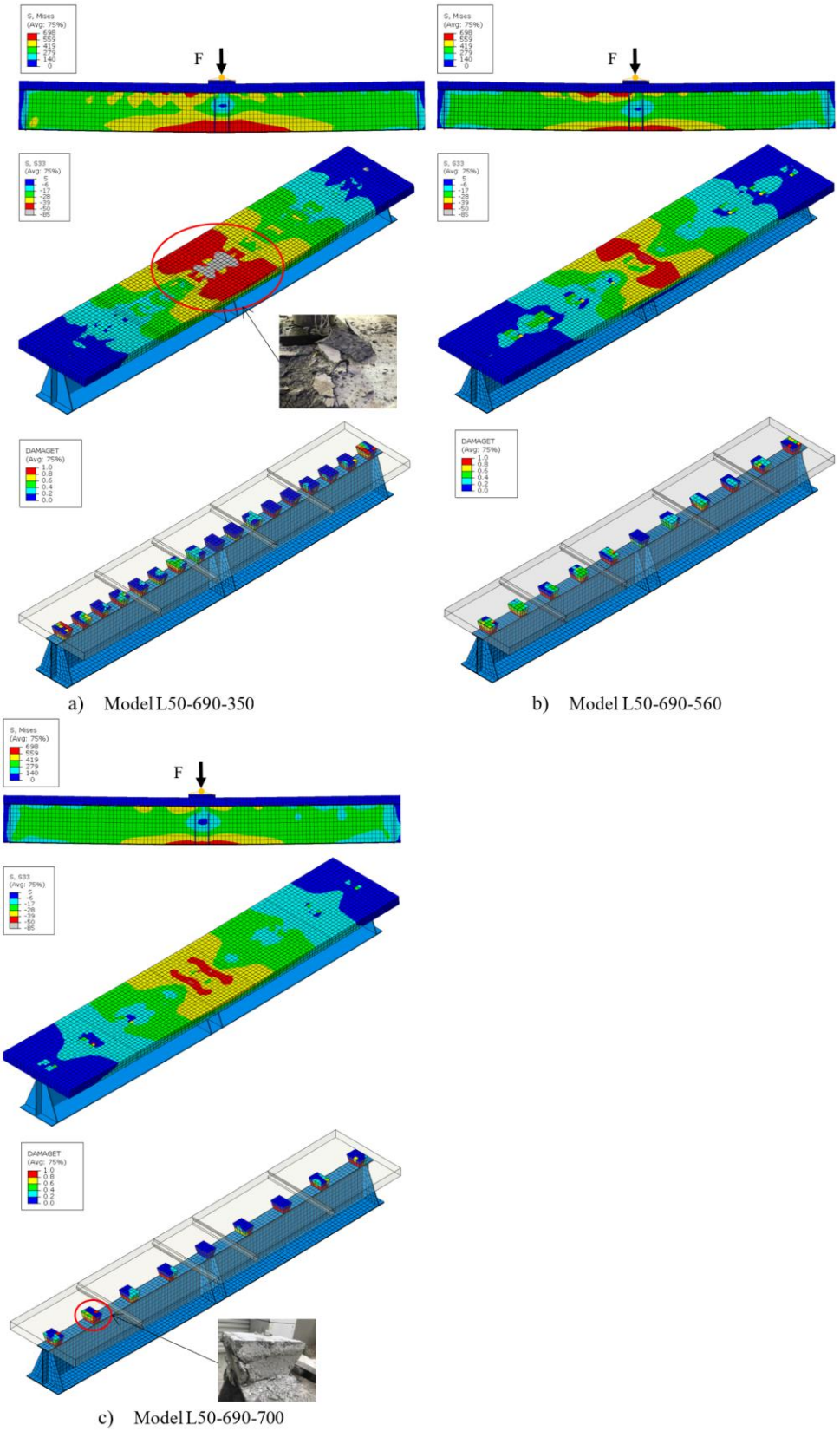

a) Model L50-690-350 b) Model L50-690-560

c) Model L50-690-700

Fig. 7.48 Three dimensional plots of “stress and strain” distributions

b) Load-deflection curves

The measured and the predicted load-deflection curves of the composite beams are plotted in Fig. 7.49. It is evident that the predicted load-deflection curves follow closely the measured ones in both the linear and the non-linear stages up to the peak loads, and hence, the finite element results are considered to be representative for practical applications. A comparison between the measured and the predicted data of these composite beams is shown in Table 7.7. It is shown that the ratios of the measured to the predicted moment resistances range from 0.98 to 1.02, and the ratios of the measured to the predicted flexural rigidities range from 0.94 to 1.01. The ratios of the measured to the predicted deflections at peak loads range from 0.97 to 1.12. Hence, the models are considered to be able to predict the moment resistances, flexural rigidities, and the mid-span deflections of the composite beams with good accuracy.

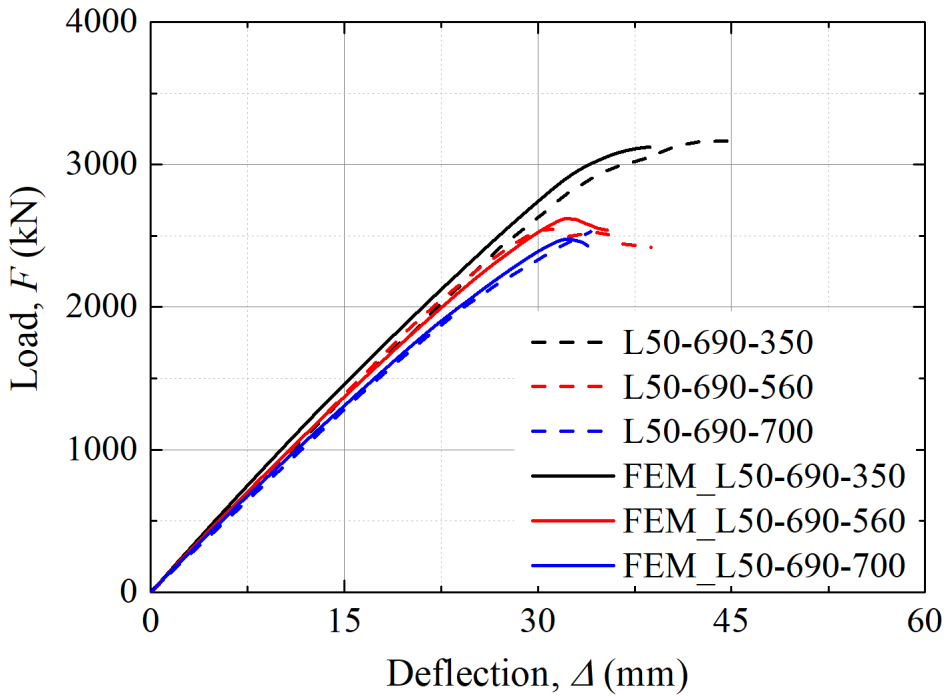

Fig. 7.49 Load-mid-span deflection curves of composite beams

Table 7.7 Comparison of the measured and the predicted results

Test		Load resistance F (kN)	Moment resistance M (kN•m)	Flexural Rigidity K_r (kN/mm)	Mid-span deflection at peak load Δ_m (mm)
L50-690-350	Measured	3,169.9	4,754.9	90.7	43.3
	Predicted	3,121.4	4,682.1	96.6	38.7
	Ratio	**1.02**	**1.02**	**0.94**	**1.12**
L50-690-560	Measured	2,557.4	3,836.1	92.8	31.0
	Predicted	2,621.1	3,931.7	91.7	32.1
	Ratio	**0.98**	**0.98**	**1.01**	**0.97**
L50-690-700	Measured	2,529.5	3,794.3	85.0	34.1
	Predicted	2,475.8	3,713.7	87.5	32.5
	Ratio	**1.02**	**1.02**	**0.97**	**1.05**

Note:
K_r denotes the flexural rigidity of the composite beam, which is defined as the ratio of $0.5F$ to the corresponding mid-span deflection.

c) Load-slippage curves of shear connections

In order to investigate the structural behaviour of the shear connections in composite beams, the load-slippage curves and load-deflection curves of the shear connections at the beam ends and near the mid-span of the composite beams are presented in Figs. 7.50 and 7.51. It is shown that in Model L50-690-350 with full shear connection, the resistances of the shear connections are increased linearly with an increase in slippage. However, in Models L50-690-560 and L50-690-700, the resistances of the shear connections are increased and then decreased with the increases in the slippage and the mid-span deflection. Hence, before reaching the peak load, the structural behaviour of the shear connections within the composite beams is similar to their linear elastic behaviour observed in standard push-out tests. The simplified load-slippage curves proposed in the present study are able to effectively simulate the structural behaviour of the shear connections with steel blocks.

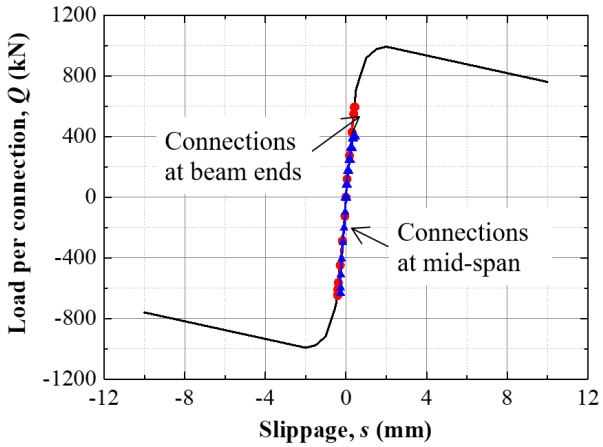

a) Model L50-690-350

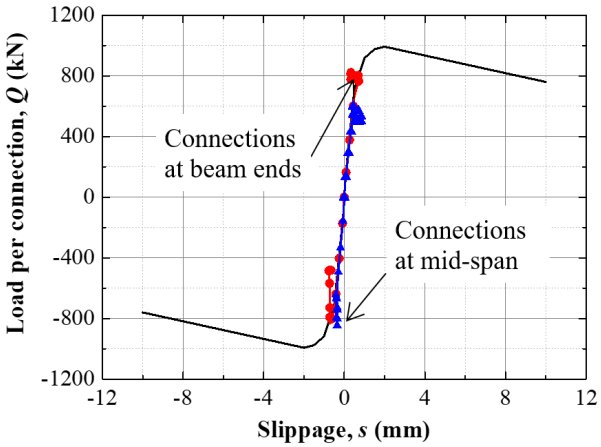

b) Model L50-690-560

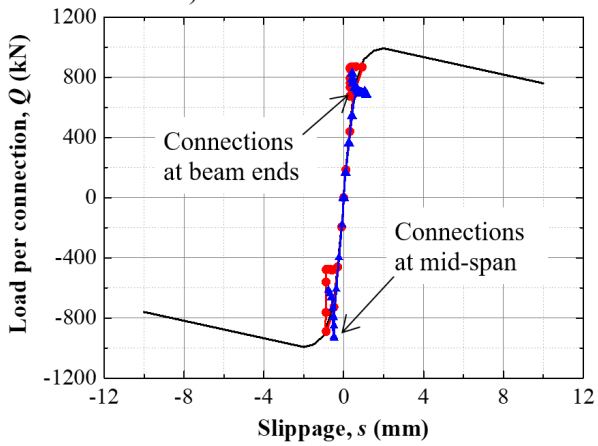

c) Model L50-690-700

Fig. 7.50 Load-slippage curves of shear connections at beam ends and mid-spans

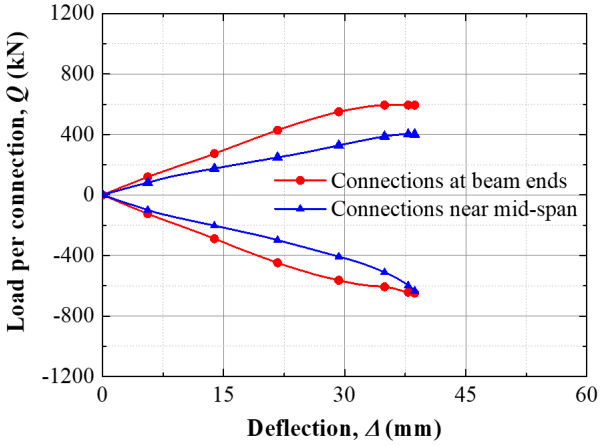

a) Model L50-690-350

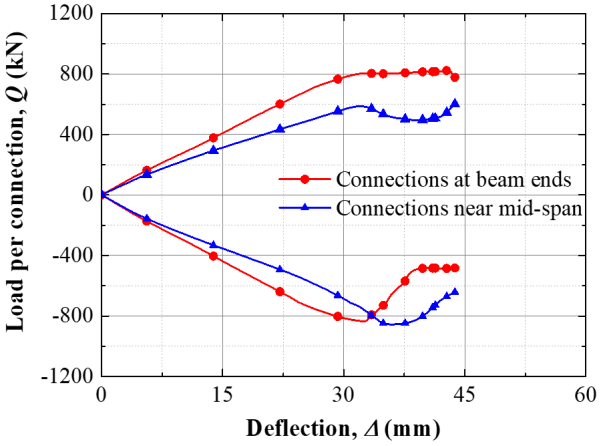

b) Model L50-690-560

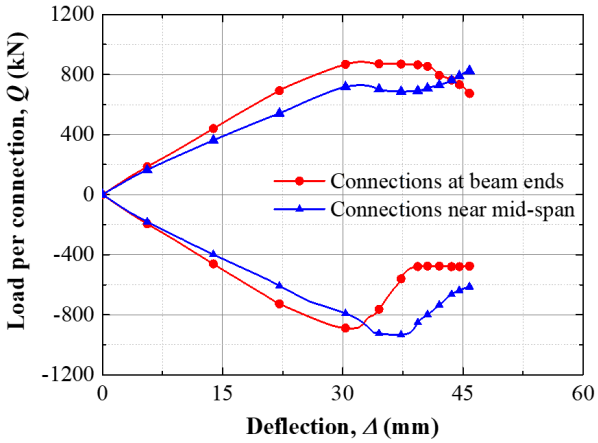

c) Model L50-690-700

Fig. 7.51 Load-deflection curves of shear connections at beam ends and mid-spans

7.7 Conclusions and design recommendations

Based on the numerical investigations into the structural behaviour of the bolted shear connections presented in Chapter 6, a comprehensive parametric study was conducted to investigate the effects of various parameters onto the structural behaviour of Connections RBN and R. A total of 62 numerical models were developed and the shear resistances, the load-slippage curves, the "stress and damage" distributions as well as the internal force distributions of the models were analysed. The load-transfer mechanisms of Connections RBN and R were identified according to the internal force distributions within the shear connections. A complementary design method for the shear resistances and the simplified load-slippage curves of the connections were proposed. Key findings are summarised as follows:

i) For Connection RBN, bolt diameter, steel block thickness, strength of the concrete block, and strength of the precast concrete slab each have a significant influence on the deformation characteristics and the "stress and damage" distributions of the shear connections. With an increase in the bolt diameter, the shear resistance of the model with Connection RBN is increased significantly due to the increase in the cross-sectional area of the bolt, and hence,

the damage area of the concrete block is increased correspondingly. Among all these parameters, the most effective one is the thickness of the steel blocks. By increasing their values from 30 to 80 mm, the shear resistances of the shear connections are readily increased from 1,346.6 kN to 1,607.9 kN, i.e. by a factor of 1.20.

ii) For Connection R, bolt diameter, bolt strength, and concrete block strength have a great influence on the deformation characteristics and the "stress and damage" distributions of the shear connections despite of a reduced stiffness when compared with those of Connection RBN. Among all these parameters, the most effective one is the diameter of the steel bolts. By increasing their values from 30 to 36 mm, the shear resistances of the shear connections are readily increased from 664.7 kN to 968.6 kN, i.e. by a factor of 1.46.

iii) For Connection RBN, the applied shear force is resisted primarily by the welded steel block through bearing while a certain portion of the shear force is resisted by the bolts. It should be noted that based on the test data and the parametric results, the steel block takes up about 50% to 90% of the applied shear force, and the proportion is directly related to the bolt diameter, the steel block thickness and the concrete block width. As the bolt deforms under the applied shear force, a tension force is also induced in the bolt shank during the slippage due to a dowel action.

iv) A complementary design method for the shear resistances of the shear connections with Connectors RBN and R was proposed, and it was highly effective to deal with a) concrete failure of the concrete blocks; b) shear failure of the bolts; and c) concrete failure of the precast concrete slabs. The proposed design method is considered to be able to predict the shear resistances of Connections RBN and R with good accuracy. Moreover, the proposed simplified load-slippage curves are readily adopted for numerical modelling to simulate the

structural behaviour of composite beams using Connections RBN and R.

v) For design of the shear connection with Connector RBN in composite beams, the following material strengths and connection configurations are recommended to be adopted:

   a) Concrete C100 with a compressive cube strength of 100 N/mm^2 and a steel fibre content of 1.5% should be adopted in the concrete block when Concrete C50 with a compressive cube strength of at least 50 N/mm^2 is adopted in the precast concrete slab.

   b) For the bolt steel, its yield and tensile strengths should be 640 and 800 N/mm^2 respectively, and the bolt diameter should be at least 30 mm.

   c) For the steel blocks, their yield and tensile strengths should be at least 355 and 430 N/mm^2, and their thickness should be at least 30 mm.

   c) The dimensions of the concrete blocks should be at least 270 (Length) × 160 (Width) mm.

   d) The longitudinal spacing between two shear connections is at least 480 mm, but not larger than 720 mm.

CHAPTER 8

CONCLUSIONS AND FUTURE WORK

8.1 Introduction

This chapter presents key findings obtained from both the experimental investigations and the numerical simulations of the proposed shear connections. The significance of the present study is also identified. To facilitate practical applications of the proposed shear connections for simple on-site assembly of prefabricated composite beams, a complementary design method is provided after careful calibration. A number of research work for future development is also outlined.

8.2 Experimental investigations

i) Single-sided push-out tests

A total of 39 single-sided push-out tests were conducted to investigate the structural behaviour of shear connections with three types of bolted shear connectors, i.e. Types A, B, and C, and three types of welded connectors, i.e. Types SC, BC, and PC. After analysing the deformation characteristics of these shear connections, four effective shear connections, i.e. Tests SC-C1-h3, BC-C1-a, PC-r-C1, and A-C1-p, were identified as effective based on their favourable combination of shear resistance, initial stiffness, and ductility, coupled with their "simple on-site assembly" in large scale composite beams. Key findings are summarised as follows:

a) The tests clearly indicated two distinct failure modes for the connections, namely, i) failure of concrete blocks with severe crushing and cracking (Mode CF), and ii) shear yielding of the steel box, the steel profiled connectors and the bolt shanks (Mode SFS).

b) Addition of steel fibres to C100 concrete blocks is shown to be efficient to increase the shear resistance, the initial stiffness and the slippage limits of the connections with Type A

connector. It is obvious that the steel fibres are able to improve both tensile strength and ductility of the high strength concrete, and to contribute to crack control by bridging microcracks and preventing their propagation. When the fibre content is 1.5%, the structural behaviour of the shear connection with Type A connector and C100 concrete is demonstrated to be highly effective.

ii) Standard push-out tests

As the shear connections with concrete blocks were loaded directly in the absence of the concrete slabs, many of these concrete blocks were found to have significant tilting, especially towards the end of the tests. In order to obtain reliable deformation characteristics of the effective bolted shear connections with Connectors RBN and R, a series of standard push-out tests were carried out. A total of eighteen large-scale push-out tests with extensive instrumentation were conducted to investigate the structural behaviour of large-diameter bolted shear connections with Connectors RBN and R in terms of shear resistance, initial stiffness, and ductility. In addition, a total of two standard push-out tests were conducted on the shear connections with Connector MTP for comparison. Key findings are summarised as follows:

a) As shown in Fig. 8.1, compared with a pair of headed studs, Connections R and MTP, the connection with a 30 mm thick steel block and a pair of specially designed high-strength bolts, each with a diameter of 30 mm, i.e. Connector RBN, is found to be highly effective in terms of resistance, stiffness, and ductility. This connection is demonstrated to meet all the structural requirements for prefabricated composite beams in highway bridges.

b) In general, two typical failure modes are identified in these standard push-out tests. Concrete failure, i.e. Mode CF, primarily appears in those tests with Connections RBN and MTP, while

shear fracture of bolts, i.e. Mode SFB, primarily appears in those tests with Connection R. **It should be noted that the proposed shear connection acts effectively as a twin connection due to the provision of a steel connector fully embedded into an infilled steel fibre reinforced concrete block, and hence, concrete failure appears in both the concrete blocks and the precast concrete slabs.** Moreover, in most of the tests with Connector RBN and a pair of 24 mm diameter bolts, fracture of bolts became evident when the applied load was decreased to 80% ~ 93% of the peak loads, and hence, small slippage limits are found in these tests.

c) It is shown that increasing the thickness of the steel block from 30 to 50 mm offers only minimal benefits to the overall connection behaviour. Although there is a substantial increase in the shear resistance of the connection, a reduction in its resistance at large deformations is also evident. When the diameter of the pair of bolts is decreased from 30 to 24 mm, the bearing area of the bolts is decreased, and the shear resistance of the connection is decreased with a factor of about 0.9. As **the concrete block acts as a "concrete shear connector"**, it should be made of high-performance concrete reinforced with steel fibres, and **the size of the concrete block together with the strength of the concrete block** are shown to have considerable effects on the structural behaviour of the shear connections in both ultimate and serviceability limit states.

d) Typical failure mode in Test D-0-W is Mode CF. Although there was a loud sound of concrete crushing when the applied load was decreased to about 90% of the peak load, the slippage limit was still larger than 6.0 mm, which was mainly attributed to the excellent ductility of SFRC.

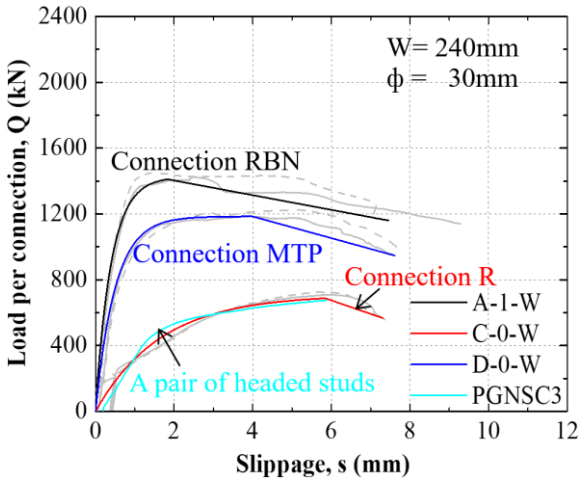

Test	Load-slippage curves $Q = Q_n (1\text{-}e^{-\alpha s})^{\beta}$	Q_m (kN)	s_u (mm)	K (kN/mm)
A-1-W	$Q = 1{,}457\ (1\text{-}e^{-2.5s})^{1.0}$	1,457	7.4	2,614
C-0-W	$Q = 709\ (1\text{-}e^{-0.6s})^{1.0}$	709	7.4	301
D-0-W	$Q = 1{,}185\ (1\text{-}e^{-2.0s})^{1.0}$	1,185	7.6	1,693
PGNSC3	-	675	5.9	327

Fig. 8.1 Load-slippage curves of connections with various configurations

8.3 Numerical simulations

In order to establish the load transfer mechanism of the proposed shear connection, advanced non-linear numerical simulations were conducted to numerically investigate the structural behaviour of shear connections with Connectors RBN, R, and MTP. A total of ten models with the shear connections were developed to examine typical failure modes, deformation characteristics as well as the internal force distributions within the shear connections. After calibration and validation against the test results, the modelling techniques were used for subsequent parametric study. The key findings are summarised as follows:

a) The proposed constitutive models for concrete are able to simulate the mechanical properties of both the SFRC and the NC. Owing to the presence of steel fibres, the elastic modulus, the peak strains, the compressive and the tensile strengths are improved in SFRC. By incorporating the compressive and the tensile damage parameters into the material models, the concrete damage distribution is comparable to the concrete crushing and cracking pattern in the tests. By incorporating various damage initiation and evolution parameters into the constitutive model for the bolt steel, ductile fracture of the bolt is successfully simulated. It should be noted that the threads of the bolt shanks and the nuts have been carefully modelled

in Model C-0-W since they have a great influence on the initial stiffness of Connection R. Mesh sizes of 8 mm in the concrete blocks and 4 mm in the shear connectors are demonstrated to be appropriate to simulate the structural behaviour of the shear connections.

b) The locations of various concrete compressive and tensile damage are in close agreement with the concrete cracking and crushing failure observed in the precast concrete slabs. Moreover, the simulated load-slippage curves correlate well with the test results in terms of shear resistance, initial stiffness and ductility corresponding to a slippage of 6 mm. Hence, the proposed modelling techniques are able to simulate the structural behaviour of the proposed shear connections accurately, and they are considered to be reliable for subsequent parametric studies.

c) As shown in Fig. 8.2, for those models with Types A and B connections, the maximum shear forces and moments are located at the roots of the steel block, and hence, typical failure mode in these connections is concrete crushing in the vicinity of the steel block. The magnitudes of the maximum tension forces are found to be about 20% of the shear resistances of the shear connections. The locations of the maximum tension forces in those models with 30 mm thick steel blocks are about 25 mm lower than that in those models with 50 mm thick steel blocks, and hence, the bolts in models with 50 mm thick steel blocks do not suffer from fracture failure. For models with Connection Type C, the maximum shear force is located at the root of the embedded nut. The maximum tension force is located at 60 mm up from the bottom of the nuts, and the magnitudes of the maximum tension forces are found to be about 25% of the shear resistances of the shear connections. The maximum concrete bearing force acts at the top of the embedded nut. For those models with Connection Type D, the maximum shear force and moment are located at the root of the weldment. The maximum concrete

bearing force acts on the weldment, and it is decreased rapidly with an increase in the cross-sectional height due to the abrupt change in the cross-sectional shape.

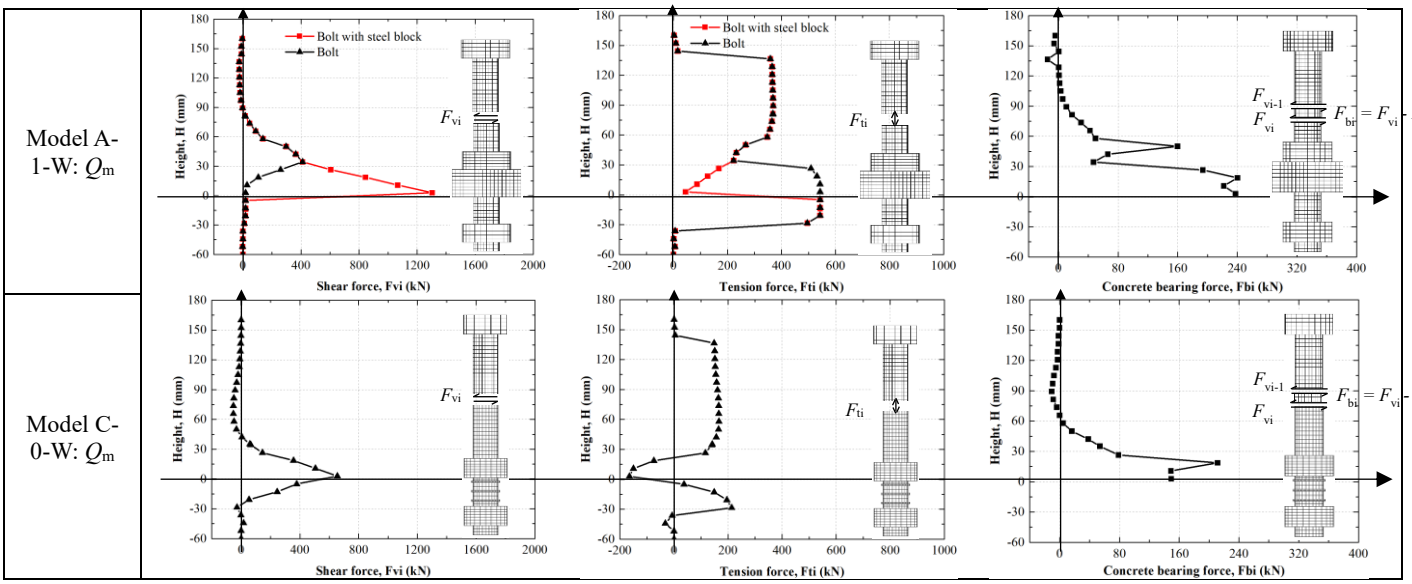

Fig. 8.2 Distributions of internal forces and concrete bearing forces along the height of the shear connectors

A comprehensive parametric study was conducted to investigate the effects of various parameters on the structural behaviour of the shear connections with Connectors RBN and R. A total of 62 FE models were developed and the load-slippage curves, the deformation characteristics, the "stress and damage" distributions, as well as the internal force distributions of the shear connectors were analysed. The load-transfer mechanisms of Connections RBN and R were identified based on the internal force distributions within the shear connections. Key findings are summarised as follows:

i) For Connection RBN, bolt diameter, steel block thickness, strengths of the concrete block and the precast concrete slab have a great influence on the deformation characteristics and the "stress and damage" distributions of the shear connections. With an increase in the bolt diameter, the shear resistance of the model with Connection RBN is increased significantly due to the increase in the cross-sectional area of the bolt, and the damage area of the concrete

block is increased correspondingly. Among all these parameters, the most effective one is the thickness of the steel blocks. By increasing their values from 30 to 80 mm, the shear resistances of the shear connections are readily increased from 1,346.6 kN to 1,607.9 kN, i.e. by a factor of 1.20.

ii) For Connection R, bolt diameter, bolt strength, and concrete block strength have a great influence on the deformation characteristics and the "stress and damage" distributions of the shear connections despite of a reduced stiffness when compared with those of Connection RBN. Among all these parameters, the most effective one is the diameter of the steel bolts. By increasing their values from 30 to 36 mm, the shear resistances of the shear connections are readily increased from 664.7 kN to 968.6 kN, i.e. by a factor of 1.46.

iii) As shown in Fig. 8.3, the load transfer mechanisms within Connections RBN and R were identified based on the internal force distributions within the shear connections. The applied shear force is resisted primarily by the welded steel block through bearing while a relatively small portion of the shear force is resisted by the bolts. It should be noted that based on the tests and parametric models, the steel block takes up 50% to 90% of the applied shear force, and the proportion is highly related to the bolt diameter, steel block thickness and the concrete block width. As the bolt deforms during slippage, the resulting pull-out force is resisted by the two bolts.

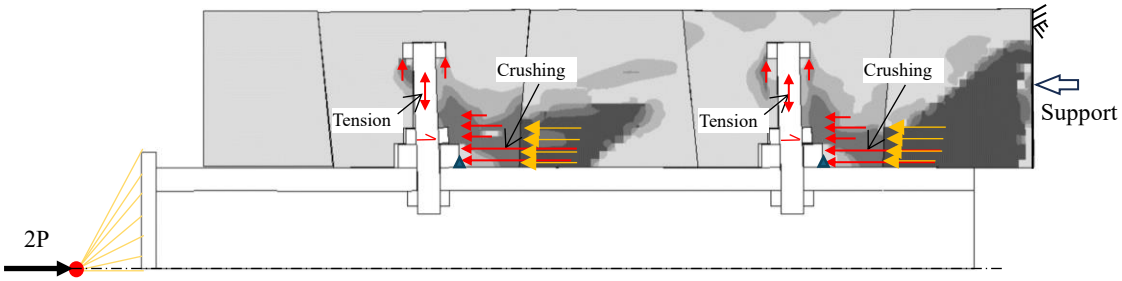

a) Connection RBN – ***Twin shear connection***
Typical shear connection = 1,300 kN

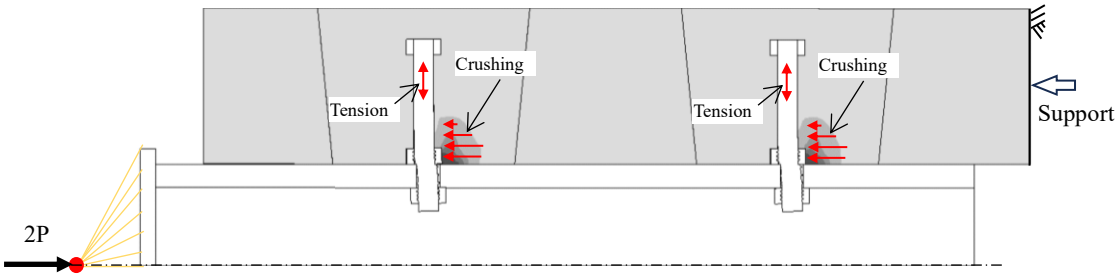

b) Connection R
Typical shear connection = 650 kN

Fig. 8.3 Load transfer mechanisms within shear connections of Connectors RBN and R

8.4 Design recommendations

i) Design methods for the shear resistances of these shear connections were developed based on experimental and numerical investigations, considering i) concrete failure of the concrete blocks; ii) shear failure of the bolts; and iii) concrete failure of the precast concrete slabs. The proposed design rule is considered to be able to predict the shear resistances of Connections RBN and R with high accuracy.

ii) To enable practical applications of the proposed shear connections to composite beams, simplified load-slippage curves for the connections with Connectors RBN and R were proposed. The simplified load-slippage models were then applied to three practical high-strength steel-concrete composite beams to predict the bending behaviour of the beams. It is shown that the proposed simplified load-slippage curves are readily adopted for numerical modelling to simulate the structural behaviour of the composite beams.

iii) The proposed design rules for the shear resistances and the simplified load-slippage curves of the proposed bolted shear connections are considered to be effective within the following parametric range:

a) Steel bolts

- Diameter of bolts = 18 to 36 mm
- Yield strength of steel = 240 to 1,080 N/mm^2
- Tensile strength of steel = 400 to 1,200 N/mm^2

b) Steel blocks

- Dimension L = 120 to 200 mm
- Dimension W = 60 to 80 mm
- Dimension T_b = 20 to 100 mm

e) Concrete blocks

- Compressive cube strength, $f_{cu,150}$ = 40 to 120 N/mm^2

f) Concrete slabs

- Compressive cube strength, $f_{cu,150}$ = 40 to 120 N/mm^2

8.5 Significance of the present study

i) In the present study, four effective large resistance shear connections are identified through a systematic experimental investigation using single-sided push-out tests. The structural behaviour of large resistance bolted shear connections are further investigated through standard push-out tests and numerical simulations, and the twin shear connection with a 30 mm thick steel block, and a pair of specially designed high-strength bolts, each with a diameter of 30 mm, i.e. Connector RBN, and fully embedded into steel fibre reinforced concrete block is found to be highly effective in terms of resistance, stiffness, and ductility. In addition, using a combination of normal concrete with a strength of 50 N/mm^2 in the precast concrete slab and steel fibre reinforced concrete with a strength of 100 N/mm^2 and a fibre content of 1.5% in the concrete block is considered to be highly effective. The connection with a pair of Grade 8.8 bolts, each with a diameter of 30 mm and a bolt grade of G8.8, i.e. Connector R, fully embedded into steel fibre reinforced concrete with a strength of

60 N/mm^2 is considered to be effective.

ii) This study presents a detailed account on the measured deformation characteristics, in particular, the load-slippage curves, of the shear connections with Connectors RBN, R, and MTP. The test data are readily to be used in practical design of the composite beams with similar shear connections.

iii) The shear resistances of those connections with Connector RBN in the single-sided push-out tests are demonstrated to be comparable to those of the connections in the standard push-out tests, while the initial stiffnesses of the connections in the single-sided push-out tests are shown to be smaller due to uplifting of the concrete blocks. Moreover, the slippage limits of the connections in the single-sided push-out tests are significantly larger than those in the standard push-out tests. Hence, the single-sided push-out tests on those shear connections encased by the concrete blocks are able to provide the lower bound solutions on the shear resistances.

iv) The modelling techniques are demonstrated to be able to accurately simulate the structural behaviour of the proposed shear connections, and they are ready to be used for subsequent parametric studies to expand the database of the deformation characteristics of the shear connections with Connections RBN and R. Constitutive models incorporating damage parameters for concrete are considered to be able to simulate the crushing and cracking the NC and the SFRC. Moreover, the proposed constitutive models incorporating the damage initiation and evaluation parameters for the bolt steel are demonstrated to be able to simulate the ductile fracture of the bolts. The threads on the bolt shanks and the bolt nuts have a significant influence on the stiffnesses of the shear connections, and it is necessary to establish the threads when simulating the structural behaviour of Connection R.

v) The present study provides a deep understanding of the structural behaviour of Connections RBN, R, and MTP. The proposed design rule for the shear resistances and the load-slippage curves are ready to be used for practical design and simulations of the shear connections for easy applications to prefabricated composite beams. For practical design of these shear connections with Connector RBN, the following material strengths and connection configurations are recommended to be adopted: a) Concrete C100 with a cube strength of 100 N/mm^2 and a steel fibre content of 1.5% is adopted in the concrete block when concrete C50 with a cube strength of at least 50 N/mm^2 is adopted in the precast concrete slab; b) the width of the concrete block is larger than 160 mm; c) the bolt diameter of 30 mm is compatible with the steel block thickness of 30 mm; and d) the longitudinal spacing between two connections is at least 480 mm, but not larger than 720 mm.

8.6 Practical implications and limitations

Practical implications of the present study are shown as follows:

i) A shear connection with a high shear resistance, a large stiffness, and a good ductility is developed, and it is also easily assembled on site. It is ready to be used in prefabricated composite beams.

ii) An optimized connection design is achieved, and the shear resistance and ductility of Connection RBN are related rationally to the dimensions of the steel block thickness and the bolt diameter. An optimal behaviour of the shear connection is obtained when the combination of the steel block thickness and the bolt dimeter is appropriate, i.e. a bolt diameter of 30 mm and a steel block thickness of 30 mm.

iii) A design method is also proposed to predict shear resistances and load-slippage curves of the

bolted shear connections.

Limitations of the present study are shown as follows:

i) Limited loading conditions. This research focused on the structural behaviour of shear connections under static loading. In bridges, the structural behaviour of shear connections under fatigue and dynamic loads is critical.

ii) Limited ranges of parameters. The proposed design rules for the shear resistances and the simplified load-slippage curves of the proposed bolted shear connections are considered to be effective within a limited range of parameters.

iii) Constructability. Constructional details of the shear connections should be further investigated using beam tests for applications in practical composite beams.

8.7 Future work

a) Experimental investigations

Standard push-out tests and non-linear numerical simulations were conducted to investigate the structural behaviour of the large diameter bolted shear connections. The influence of a wide range of parameters on the structural behaviour of the connection was investigated, and the design rule for the shear resistance and load-slippage curve of the connections with Connectors RBN and R was also developed. For practical applications of the shear connections to prefabricated composite beams, it is necessary to conduct half-scale or even full-scale beam tests to investigate the structural behaviour of these shear connections in prefabricated composite beams under i) sagging moment; and ii) hogging moment.

Since the proposed shear connections are expected to be used in bridges, the fatigue loads appear commonly in these bridges, and hence, it is necessary to investigate the fatigue behaviour of the proposed shear connections over a practical ranges of traffic loads and stress ranges.

In the present study, only two standard push-out tests were conducted to investigate the structural behaviour of shear connections with Connector MTP for comparison with Connection RBN, and it is found that Connection MTP meets all the structural requirements proposed in Chapter 1. Additional standard push-out tests should be conducted to investigate the influence of i) thickness of the perfobond rib; ii) height of the end plate; iii) width of the end plate; iv) diameter of the perforated hole; and v) diameter of the passing reinforcement, on the structural behaviour of the connections with Connector MTP for their applications to prefabricated composite beams.

b) Numerical simulations

The structural behaviour of the connections with Connectors RBN, R, and MTP have been successfully simulated using advanced FE software Abaqus. A comprehensive parametric study is conducted numerically to investigate the structural behaviour of these shear connections with Connectors RBN and R. Hence, a complementary parametric study should be conducted to investigate the structural behaviour of Connection MTP, and the ductile fracture of steel plates as well as interactions between the steel plates and the surrounding concrete should also be carefully created.

The FE models of three practical high-strength steel-concrete composite beams were established for validation of the simplified load-slippage curves, in which the shear connections are simulated using connector elements. Detailed numerical models of the composite beams should be further developed with actual geometry of the shear connections, and interactions between the connectors and the surrounding concrete incorporated should also be examined. The modelling results using these modelling techniques in simulating composite beams should be compared for subsequent numerical investigations and parametric studies.

c) Design rules

The design rules for the shear connections with Connector MTP should be proposed in accordance with additional test and numerical data. The existing design rules in GB 50936 and EN 1994-1-1 for composite beams with the proposed shear connections should be further developed according to experimental and numerical results.

REFERENCES

Ahn J-H, Lee C-G, Won J-H, & Kim S-H. (2010). Shear resistance of the perfobond-rib shear connector depending on concrete strength and rib arrangement. Journal of Constructional Steel Research, 66(10), 1295–1307.

Ataei A., Bradford M.A., & Liu X. (2016). Experimental study of composite beams having a precast geopolymer concrete slab and deconstructable bolted shear connectors. Engineering Structures, 114, 1–13.

ABAQUS User Manual, Version 2020. (2020). Abaqus: Dassault Systemes Simulia Corp.

Ataei A., & Zeynalian M. (2021). A study on structural performance of deconstructable bolted shear connectors in composite beams. Structures, 29, 519–533.

American Institute of Steel Construction. (2022). Specification for Structural Steel Buildings.

Brussels: CEN-European Committee for Standardization. (1992). EC4. ENV 1994. Design of Composite Steel and Concrete Structures. Part 1.1: general rules and rules for buildings.

British Standards Institution. (2005). BS EN 1994-1-1. Eurocode 4: Design of composite steel and concrete structures. Part 1-1: General rules and rules for buildings.

British Standards Institution. (2004). BS EN 1992-1-1. Eurocode 2: Design of Concrete Structures. Part 1-1: General rules and rules for buildings.

British Standards Institution. (2005). BS EN 1993-1-8: Design of Steel Structures. Part 1-8: Design of joints.

Badie S.S., Morgan Girgis A.F., Tadros M.K., & Nguyen N.T. (2010). Relaxing the stud spacing limit for full-depth precast concrete deck panels supported on steel girders (Phase I). Journal of Bridge Engineering, 15(5), 482–492.

Badie S.S., Morgan Girgis A.F., Tadros M.K., & Sriboonma K. (2011). Full-scale testing for composite slab/beam systems made with extended stud spacing. Journal of Bridge Engineering, 16(5), 653–661.

Buildings Department of the Government of Hong Kong SAR. (2011). Code of Practice for the Structural Use of Steel.

Baran E., & Topkaya C. (2012). An experimental study on channel type shear connectors. Journal of Constructional Steel Research, 74, 108–117.

Buildings Department of the Government of Hong Kong SAR. (2013). Code of Practice for the Structural Use of Concrete.

Du H., Hu X., Meng Y., Han G., & Guo K. (2020). Study on composite beams with prefabricated steel bar truss concrete slabs and demountable shear connectors. Engineering Structures, 210, 110419.

Ding Y., Wang X.D., Shen M.H., Chung K.F., Zhou X.H., & Elghazouli A.Y. (2024). Deformation characteristics of ductile large resistance shear connections for practical composite beams. Engineering Structures, 320, 118838.

Ding Y., Chung K.F., Tong C.C., Wang X.D., Zhou X.H., & Elghazouli A.Y. (2024). Behaviour of large-diameter high-strength bolted shear connections for prefabricated composite beams. Engineering Structures, 322, 119002.

Ellobody E., & Young B. (2006). Performance of shear connection in composite beams with profiled steel sheeting. Journal of Constructional Steel Research, 62(7), 682–694.

Ernst S. (2006). Factors affecting the behavior of the shear connection of steel-concrete composite beams. PhD thesis. The University of Western Sydney.

Fang Z., Jiang H., Chen G., Dong X., & Shao T. (2020). Behavior of grouped stud shear connectors between precast high-strength concrete slabs and steel beams. Steel and Composite Structures, 34(6), 837–851.

Fang Z. , Liang W., Fang H., Jiang H., & Wang S. (2021). Experimental investigation on shear behavior of high-strength friction-grip bolt shear connectors in steel-precast UHPC composite structures subjected to static loading. Engineering Structures, 244, 112777.

Hicks S.J. (2017). Design shear resistance of headed studs embedded in solid slabs and encasements. Journal of Constructional Steel Research, 139, 339–352.

Hu Y., Qiu M., Chen L., Zhong R., & Wang J. (2021). Experimental and analytical study of the shear strength and stiffness of studs embedded in high strength concrete. Engineering Structures, 236, 111792.

He J., Suwaed A. S. H., Vasdravellis G., & Wang S. (2022). Behaviour and design of the 'lockbolt' demountable shear connector for sustainable steel-concrete composite structures. Structures, 44, 988–1010.

ISO 6892-1:2019. Metallic materials - Tensile testing - Part 1: Method of test at room temperature. International Organization for Standardization.

Jiao C., Sun W., Qin H., Zhang Y., & Jiang J. (2004). Constitutive equation of SFRHSC under uniaxial compression. Journal of Southeast University (Natural Science Edition), 34, 366-9. [In Chinese]

Jung D.S., Park S.H., Kim T.H., Han J. & Kim C. (2022). Demountable bolted shear connector for easy deconstruction and reconstruction of concrete slabs in steel–concrete bridges. Applied Sciences, 12(3), 1508.

Lemaitre J. (1985). A continuous damage mechanics model for ductile fracture. Journal of Engineering Materials and Technology, 107, 83-9.

Lubliner J., Üliver J., Üller S., & Ünate E. (1988). A plastic-damage model for concrete. International Journal of Solids and Structures, 25, 299–326.

Lee J., & Fenves G.L. (1998). Plastic-damage model for cyclic loading of concrete structures. Journal of Engineering Mechanics, 124, 892–900.

Lee P-G, Shim C-S, & Chang S-P. (2005). Static and fatigue behavior of large stud shear connectors for steel–concrete composite bridges. Journal of Constructional Steel Research, 61(9), 1270–1285.

Lam D., & El-Lobody E. (2005). Behavior of headed stud shear connectors in composite beam. Journal of Structural Engineering, 131(1), 96–107.

Lee M.S.S., & Bradford M.A. (2013). Sustainable composite beam behaviour with deconstructable bolted shear connectors. Composite Construction in Steel and Concrete VII, 445–455.

Liu X., Bradford M.A., & Lee M.S.S. (2015). Behavior of high-strength friction-grip bolted shear connectors in sustainable composite beams. Journal of Structural Engineering, 141(6), 04014149.

Luo Y., Hoki K., Hayashi K., & Nakashima M. (2016). Behavior and strength of headed stud–SFRCC shear connection. I: Experimental study. Journal of Structural Engineering, 142(2), 04015112.

Luo Y., Hoki K., Hayashi K., & Nakashima M. (2016). Behavior and strength of headed stud–SFRCC shear connection. II: Strength evaluation. Journal of Structural Engineering, 142(2).

Liu X., Bradford M.A., Chen Q.J., & Ban H. (2016). Finite element modelling of steel–concrete composite beams with high-strength friction-grip bolt shear connectors. Finite Elements in Analysis and Design, 108, 54–65.

Liu X., Bradford M.A., & Ataei A. (2017). Flexural performance of innovative sustainable composite steel-concrete beams. Engineering Structures, 130, 282–296.

Lu X., Zhang Y., & Nian X. (2017). Experimental study on stress-strain curves for high-strength steel fiber reinforced concrete under monotonic and repeated compressive loadings. Journal of Building Structures, 38, 135-43. [In Chinese]

Luo Y.B., & Yan J.B. (2022). Developments of prefabricated steel-concrete composite beams with novel steel-yielding demountable bolt connectors. Journal of Constructional Steel Research, 190, 107123.

Liu J., Xie J., Xiong G., Wang X., Zou Y., Shu R., & Chen Y.F. (2023). Full-scale push-out testing of headed stud-steel block connectors in prefabricated steel-concrete composite beams. Engineering Structures, 285, 116020.

Ministry of Housing and Urban-Rural Development of the People's Republic of China. (2010). Chinese Code for Design of Concrete Structures.

Ministry of Housing and Urban-Rural Development of the People's Republic of China. (2017). Chinese Standard for Design of Steel Structures.

Nguyen H.T., & Kim S.E. (2009). Finite element modeling of push-out tests for large stud shear connectors. Journal of Constructional Steel Research, 65(10), 1909–1920.

Ollgaard J. G., Slutter R.G., & Fisher J.W. (1971). Shear strength of stud connectors in lightweight and normal weight concrete. American Institute of Steel Construction Engineering Journal, 8(2), 55-62.

Pavlović M., Marković Z., Veljković M., & Buđevac D. (2013). Bolted shear connectors vs. headed studs behaviour in push-out tests. Journal of Constructional Steel Research, 88, 134–149.

Pavlović, M., Spremić, M., Marković, Z., & Veljković, M. (2016). Headed shear studs versus high-strength bolts in prefabricated composite decks. Composite Construction in Steel and Concrete, 7, 687-702.

Shim C-S, Lee P-G, & Yoon T-Y. (2004). Static behavior of large stud shear connectors. Engineering Structures, 26(12), 1853–1860.

Spremic M., Markovic Z., Veljkovic M., & Buđevac D. (2013). Push-out experiments of headed shear studs in group arrangements. Advanced Steel Construction, 9(2), 139-160.

Spremić M., Gluhović N., Marković Z., Dobrić J., & Filipović A. (2017). Comparison of headed studs with perfobond shear connectors – experimental and numerical analysis. Eurosteel, 1(2–3), 2237–2246.

Shen M.H., & Chung K.F. (2017). Experimental investigation into stud shear connections under combined shear and tension forces. Journal of Constructional Steel Research, 133, 434–447.

Shen M.H., & Chung K.F. (2017). Structural Behaviour of Stud Shear Connections with Solid and Composite Slabs Under Co-Existing Shear and Tension Forces. Structures, 9, 79–90.

Shen M.H., Chung K.F., Elghazouli A.Y., & Tong J. (2020). Structural behaviour of stud shear connections in composite floors with various connector arrangements and profiled deck configurations. Engineering Structures, 210, 110370.

Shen M.H., Chung K.F., & Elghazouli A.Y. (2023). Performance of stud shear connections under combined shear and pull-out forces. Structures, 51, 415–434.

The International Federation for Structural Concrete. (2012). fib Model Code 2010.

Tong L., Chen L., Wen M., & Xu C. (2020). Static behavior of stud shear connectors in high-strength-steel–UHPC composite beams. Engineering Structures, 218, 110827.

US Department of Transportation. (2011). Accelerated bridge construction: experience in design, fabrication and erection of prefabricated bridge elements and systems: final manual.

Vianna J. da.C., Costa-Neves L. F., Vellasco P.C.G. da S., & de Andrade S.A.L. (2008). Structural behaviour of T-Perfobond shear connectors in composite girders: An experimental approach. Engineering Structures, 30(9), 2381-2391.

Vianna J. da.C., Costa-Neves L. F., Vellasco P.C.G. da S., & de Andrade S.A.L. (2009). Experimental assessment of Perfobond and T-Perfobond shear connectors' structural response. Journal of Constructional Steel Research, 65(2), 408–421.

Vianna J. da.C., de Andrade S.A.L., Vellasco P.C.G. da S., & Costa-Neves L.F. (2013). Experimental study of Perfobond shear connectors in composite construction. Journal of Constructional Steel Research, 81, 62–75.

Wang Z. & Yu Z. (2004). Concrete damage model based on energy loss. Journal of Building Materials, 7(4), 365-369. [in Chinese]

Wang J. , Xu Q., Yao Y., Qi J., & Xiu H. (2018). Static behavior of grouped large headed stud-UHPC shear connectors in composite structures. Composite Structures, 206, 202–214.

Wang Y.H., Yu J., Liu J., & Chen Y.F. (2019). Experimental and Numerical Analysis of Steel-Block Shear Connectors in Assembled Monolithic Steel–Concrete Composite Beams. Journal of Bridge Engineering, 24(5), 04019024.

Wang S., Fang Z., Chen G., Jiang H., & Teng S. (2021). Numerical analysis on shear behavior of grouped head stud shear connectors between steel girders and precast concrete slabs with high-strength concrete-filled shear pockets. Journal of Bridge Engineering, 26(6), 04021030.

Wang X.D., Shen M.H., Chung K.F., Liu J.P., Liao Y., & Jin Z.Z. (2021). Study on shear behavior of shear connectors with large diameter-high strength bolts. Journal of Building Structures, 42, 8. [in Chinese]

Wang X.D., Shen M.H., Chung K.F., Zhou X.H., & Liao Y. (2022). Experimental investigation into high strength bolted shear connections for simple on-site assembly of composite beams. Engineering Structures, 257, 113980.

Xue W., Ding M., Wang H., & Luo Z. (2008). Static behavior and theoretical model of stud shear Connectors. Journal of Bridge Engineering, 13(6), 623–634.

Xu C., Su Q., & Masuya H. (2017). Static and fatigue performance of stud shear connector in steel fiber reinforced concrete. Steel and Composite Structures, 24(4), 467–479.

Xu Q., Lu K., Wang J., & Yao Y. (2021). Performance of large-diameter studs in thin ultra-high performance concrete slab. Structures, 34, 4936–4951.

Xu Q., Sebastian W., Lu K., Yao Y., & Wang J. (2022). Parametric experimental study of ultra-short stud connections for lightweight steel–UHPC composite bridges. Journal of Bridge Engineering, American Society of Civil Engineers, 27(2), 04021108.

Xu Q., Sebastian W., Lu K., Yao Y., & Wang J. (2022). Shear behaviour and calculation model for stud-UHPC connections: Finite element and theoretical analyses. Engineering Structures, 254, 113838.

Xiong G., Li W., Wang X., Liu J., Bai Y., & Chen Y.F. (2022). Flexural behavior of prefabricated high-strength steel-concrete composite beams with steel block connectors. Journal of Constructional Steel Research, 197, 107507.

Zhang Y., Lu X., & Nian X. (2017). Stress-strain behaviour for high-strength steel fibre reinforced concrete under tensile loading. Structural Engineers, 33(01), 107-113+200. [In Chinese]

Zhao C. , Li Z., Deng K., & Wang W. (2018). Experimental investigation on the bearing mechanism of Perfobond rib shear connectors. Engineering Structures, 159, 172–184.

Zhang Y., Chen B., Liu A., Pi Y., Zhang J., Wang Y., & Zhong L. (2019). Experimental study on shear behavior of high strength bolt connection in prefabricated steel-concrete composite beam. Composites Part B: Engineering, 159, 481–489.

Zhao W., Lu S., & Jing X. (2020). Shear performance of high-strength bolt connector considering different pad and bolt hole. Structures, 28, 1291–1300.

Zhang Y., Liu A., Chen B., Zhang J., Pi Y., & Bradford M.A. (2020). Experimental and numerical study of shear connection in composite beams of steel and steel-fibre reinforced concrete. Engineering Structures, 215, 110707.

Zou Y., Qin F., Zhou J., Zheng Z., Huang Z., & Zhang Z. (2021). Shear behavior of a novel bearing-shear connector for prefabricated concrete decks. Construction and Building Materials, 268, 121090.